Structure Function Analysis of Turbulent Flows

Strukturfunktionsanalyse Turbulenter Strömungen

Von der Fakultät für Maschinenwesen der Rheinisch-Westfälischen Technischen Hochschule Aachen zur Erlangung des akademischen Grades eines Doktors der Ingenieurwissenschaften genehmigte Dissertation

vorgelegt von

Jonas Peter Maria Boschung

Berichter: Univ.-Prof. Dr.-Ing. Heinz Pitsch
Univ.-Prof. Dr.-Ing. Wolfgang Schröder

Tag der mündlichen Prüfung: 26. Juni 2017

Diese Dissertation ist auf den Internetseiten der Universitätsbibliothek online verfügbar.

Berichte aus der Strömungstechnik

Jonas Boschung

Structure Function Analysis of Turbulent Flows

Shaker Verlag
Aachen 2017

Bibliographic information published by the Deutsche Nationalbibliothek
The Deutsche Nationalbibliothek lists this publication in the Deutsche Nationalbibliografie; detailed bibliographic data are available in the Internet at http://dnb.d-nb.de.

Zugl.: D 82 (Diss. RWTH Aachen University, 2017)

Printed in Germany.

ISBN 978-3-8440-5449-1
ISSN 0945-2230

Shaker Verlag GmbH • P.O. BOX 101818 • D-52018 Aachen
Phone: 0049/2407/9596-0 • Telefax: 0049/2407/9596-9
Internet: www.shaker.de • e-mail: info@shaker.de

Für meine Eltern

Vorwort

Die vorliegende Arbeit entstand während meiner Tätigkeit als wissenschaftlicher Mitarbeiter am Institut für Technische Verbrennung der RWTH Aachen und wurde teilweise durch die NRW-Forschungsschule BrenaRo (Brennstoffgewinnung aus nachwachsenden Rohstoffen) sowie den Europäischen Forschungsrat (ERC) unter dem Advanced Grant "MILESTONE" (Multi-Scale Description of Non-Univesal Behavior in Turbulent Combustion) unterstützt. Ein Großteil der numerischen Auswertungen und Berechnungen wurden auf dem Supercomputer Juqueen des Forschungszentrums Jülich durchgeführt; für die zur Verfügung gestellte Rechenzeit möchte ich dem Forschungszentrum danken.

In weiten Teilen geht diese Arbeit auf eine sehr enge Zusammenarbeit mit Prof. Norbert Peters zurück. Für die große Unterstützung, die stets offene Tür, die vielen Freiheiten sowie die vielen Diskussionen bin ich sehr dankbar; durch die intensive Betreuung durfte ich sehr viel lernen. Seine Begeisterung für die Wissenschaft, die Neugierde kombiniert mit einem scharfen Blick auf das Wesentliche bei gleichzeitiger Bescheidenheit, Freundlichkeit und Offenheit für andere Sichtweisen haben mich sehr beeindruckt. Die etwas mehr als zweieinhalb Jahre unserer Zusammenarbeit werden mir deshalb äußerst positiv in dauerhafter Erinnerung bleiben und es betrübt mich zutiefst, dass Norbert Peters die vorliegende Arbeit nicht mehr begutachten konnte.

Sehr dankbar bin ich auch Prof. Heinz Pitsch, der die Betreuung dieser Arbeit anschließend übernommen sowie weiterhin begleitet und damit einen aus meiner Sicht sehr zufriedenstellenden Abschluss ermöglicht hat. Bedanken möchte ich mich auch bei Prof. Wolfgang Schröder für die Berichterstattung sowie Prof. Marek Behr für die Übernahme des Vorsitzes der Promotionskommission.

Für viele anregende Diskussionen (nicht nur) über Strukturfunktionen, kritisches Korrekturlesen und viele Anmerkungen bin ich Reginald J. Hill sehr dankbar. Prof. Charles Meneveau danke ich herzlich für die Möglichkeit eines halbjährigen Aufenthalts an der Johns Hopkins University in Baltimore, für die Unterstützung und immer offene Tür sowie viele Diskussionen und Gespräche. Prof. Christos Vassilicos und Sylvain Laizet bin ich für viele Diskussionen über Stromlinien dankbar, ebenso Prof. Lipo Wang. Günther Pazko danke ich für die Hilfe bezüglich ODE-Lösern und viele weitere Gespräche über allerlei sonstige

Themen.

Herzlich bedanken möchte ich mich bei meinen Bureaukollegen Fabian Hennig, Dominik Denker, Jens Henrik Göbbert, Philip Schäfer und Markus Gampert für viele fachliche und nicht-fachliche Diskussionen, gemeinsame Abende und Konferenzreisen. Nicht zuletzt Dank einer sehr guten Bureauatmosphäre hatte ich eine sehr schöne Zeit und hat mir meine Arbeit immer viel Spass bereitet; ein großer Dank geht in dieser Hinsicht auch an Michael Gauding.

Für sorgfältiges und kritisches Korrekturlesen dieser Arbeit möchte ich meinem geschätzten Kollegen Fabian Hennig danken, ebenso meinen Hiwis David, Tobias, Björn und Philipp für ihre Arbeit.

Abschließend bin ich meinem Bruder und meinen Eltern sehr dankbar, auf deren Unterstützung ich mich immer verlassen konnte.

Aachen, im Juni 2017

Jonas Boschung

Publications

The present thesis is mostly based on the following articles published in peer-reviewed scientific journals; they were redacted, where some parts have been shortened and others expanded. Furthermore, additional material has been included.

- J. Boschung, "Exact relations between the moments of dissipation and longitudinal velocity derivatives in turbulent flows", *Physical Review E*, **2015**, 92, 043013
- J. Boschung, F. Hennig, M. Gauding, H. Pitsch & N. Peters, "Generalised higher-order Kolmogorov scales", *Journal of Fluid Mechanics*, **2016**, 794, 233-251
- J. Boschung, N. Peters, S. Laizet & J. C. Vassilicos, "Streamlines in stationary homogeneous isotropic turbulence and fractal-generated turbulence", *Fluid Dynamics Research*, **2016**, 48, 021403
- N. Peters, J. Boschung, M. Gauding, J. H. Göbbert, R. J. Hill & H. Pitsch, "Higher-order Dissipation in the Theory of Homogeneous Isotropic Turbulence", *Journal of Fluid Mechanics*, **2016**, 803, 250-274
- J. Boschung, M. Gauding, F. Hennig, D. Denker & H. Pitsch, "Finite Reynolds number corrections to the 4/5-law for decaying turbulence", *Physical Review Fluids*, **2016**, 1, 064403
- J. Boschung, F. Hennig, D. Denker, H. Pitsch & R. J. Hill, "Analysis of structure function equations up to the seventh order", *Journal of Turbulence*, **2017**, 1-32
- J. Boschung, F. Hennig, D. Denker, H. Pitsch & R. J. Hill, "Ratios of same-order moments of dissipation, pseudo-dissipation and dissipation surrogates in homogeneous isotropic turbulence", submitted to *Journal of Turbulence*

Moreover, parts of the supporting material

- N. Peters, J. Boschung, M. Gauding, J. H. Göbbert & H. Pitsch, Exact equations for structure functions and equations for source terms up to the sixth order, *arXive.org*, **2015**, `http://arxiv.org/abs/1504.07490`
- J. Boschung, F. Hennig, D.Denker, H. Pitsch & R. J. Hill, Balances of structure function equations and their traces for the second to seventh order for homogeneous, isotropic turbulence, **2017**, `http://www.tandfonline.com/doi/suppl/10.1080/14685248.2017.1346377`

were used. Additionally, the following papers were prepared during my time at the institute:

- J. Boschung, P. Schaefer, N. Peters & C. Meneveau, "The local topology of stream- and vortex lines in turbulent flows", *Physics of Fluids (1994-present)*, **2014**, 26, 045107
- M. Gampert, J. Boschung, F. Hennig, M. Gauding & N. Peters, "The vorticity versus the scalar criterion for the detection of the turbulent/non-turbulent interface", *Journal of Fluid Mechanics*, **2014**, 750, 578-596
- F. Hennig, J. Boschung & N. Peters, "Statistical Description of Streamline Segments in a Turbulent Channel Flow with a Wavy Wall", *New Results in Numerical and Experimental Fluid Mechanics X*, **2016**, 135-143

Abstract

The present work focuses on structure functions in homogeneous isotropic turbulence. Structure functions are statistics (more precisely, higher-order moments) of the velocity difference evaluated at two points in space, separated by some distance r. While most of the work found in the literature is based on phenomenology and thus requires additional assumptions besides homogeneity and continuity, the present thesis aims at examining structure functions based on the Navier-Stokes equations, the governing equations of motion for incompressible fluids. For that reason, firstly the system of structure function equations is discussed and analysed, with emphasis on their dissipative and pressure source terms. It is found that the dissipative source terms and equations derived thereof contain the higher moments of the (pseudo-)dissipation. Next, the viscous range is examined more closely. It is found that there are exact solutions for even-order longitudinal structure functions, which are determined by the higher moments of the dissipation $\langle \varepsilon^{N/2} \rangle$ and the viscosity ν. These findings are then used to define exact order-dependent dissipative cut-off scales $\eta_{C,N}$ and $u_{C,N}$, which reduce to the well-known Kolmogorov scales η and u_η for the second order $N = 2$. Considering the inertial range, one may use the previous dissipative range results to match both regimes and relate inertial range scaling exponents of longitudinal structure functions to the Reynolds number scaling of the moments of the dissipation when assuming Kolmogorov's refined similarity hypothesis (RSH). Furthermore, the inertial range scaling exponent of the trace of the fifth-order structure functions is examined with regard to the system of equations. It is found that the fifth order is mostly determined by the dissipation source term, which contains the second moment of the (pseudo)-dissipation. In the inertial range, terms acting on the large scales and viscous terms are usually neglected. However at finite Reynolds numbers, these terms contribute to the structure function equation balances. For that reason, their influence is examined for the second-order equations for decaying turbulence. It is found that both the unsteady and the viscous terms contribute significantly to the second-order balances at moderate Reynolds numbers and their influence decreases only slowly. Finally, streamline segment statistics are briefly considered, because the higher conditional moments are conceptually similar to the longitudinal structure functions.

Zusammenfassung

Gegenstand der vorliegenden Arbeit sind Strukturfunktionen in homogen isotroper Turbulenz, die als statistische Momente der Geschwindigkeitsdifferenz zweier Punkte mit Abstand r im Raum aufgefasst werden können. Die meisten in der Literatur vorgelegten Arbeiten basieren auf phänomenologischen Überlegungen, die weitere Annahmen voraussetzen. Hingegen zielt die vorliegende Arbeit auf eine Untersuchung basierend auf Transportgleichungen der Strukturfunktionen ab. Zunächst wird deshalb das resultierende System der Strukturfunktionstransportgleichungen analysiert, mit Schwerpunkt auf den Dissipations- und Druck-Quelltermen. Tatsächlich finden sich die höheren Momente der (Pseudo-) Dissipation in den Dissipations-Quelltermen bzw. weiteren davon abgeleiteten Transportgleichungen. Für den viskosen Bereich kann gezeigt werden, dass longitudinale Strukturfunktionen gerader Ordnung exakt durch höhere Momente der Dissipation $\langle \varepsilon^{N/2} \rangle$ sowie die Viskosität ν bestimmt sind. Damit können eindeutig exakte ordnungsabhängige dissipative Längen- und Geschwindigkeitsskalen $\eta_{C,N}$ und $u_{C,N}$ definiert werden, die sich für die zweite Ordnung $N = 2$ zu den Kolmogorovskalen η und u_η ergeben. Im Hinblick auf den Inertialbereich können diese Ergebnisse genutzt werden, um die Skalierungsexponenten longitudinaler Strukturfunktionen mit der Reynoldszahlskalierung der höheren Momente der Dissipation unter der Annahme von Kolmogorovs verfeinerter Ähnlichkeitshypothese zu verknüpfen. Weiterhin wird der Skalierungsexponent der Spur der Strukturfunktionen fünfter Ordnung in Hinblick auf das Gleichungssystem betrachtet. Es ergibt sich, dass die fünfte Ordnung hauptsächlich durch die dissipativen Quellterme bestimmt ist, deren Transportgleichung das zweite Moment der (Pseudo-)Dissipation beinhaltet. Üblicherweise werden im Inertialbereich großskalige und viskose Terme vernachlässigt, obwohl diese bei endlichen Reynoldszahlen zu der Bilanz der Strukturfunktionsgleichungen beitragen. Aus diesem Grund wird der Einfluss dieser Terme für die zweite Ordnung für abklingende Turbulenz genauer untersucht. Sowohl die instationären als auch die viskosen Terme tragen wesentlich zu den Bilanzen bei; deren Einfluss klingt mit steigender Reynoldszahl nur schwach ab. Schlussendlich werden kurz Statistiken von Stromliniensegmenten untersucht, da die höheren konditionierten Momente konzeptuell ähnlich zu longitudinalen Strukturfunktionen aufgefasst werden können.

Contents

List of Figures

List of Tables

1 Introduction

Most flows in nature and technical applications are turbulent. Examples include winds in the atmosphere, internal flows in combustion engines, the mixing of milk and coffee and many more. Despite their high importance (and consequently much of work on the problem) and besides the fact that the governing equations are known for more than one-hundred years, there are depressingly few exact results. The advent of supercomputers made direct numerical simulations (DNS) of turbulent flows feasible, which fully resolve the flow and allow detailed studies, as one can compute all quantities of interest. However, DNS can only be carried out for very simple flow geometries, and that situation is not likely to change in the foreseeable future. Nevertheless, if there is some universality of turbulence, these simple geometries should suffice to arrive at a deeper understanding. In the present thesis, we look based on DNS at a well-established, but not dated method known as structure function analysis in an effort to examine fundamental properties of turbulence. Structure functions are statistics of the velocity difference evaluated at two points in space, with the separation distance as variable.

In this chapter, we first present the governing equations of motion before we briefly discuss general properties of turbulence. We then review the very successful and celebrated K41 theory by Kolmogorov, which first introduced structure functions; they are the main focus of the present work.

1.1 Governing equations of fluid motion

In the present work, we only consider incompressible fluids with constant material properties which can be treated by means of continuum mechanics. This implies that the smallest scales of the flow are large in comparison to the (average) distance between individual molecules, the so-called mean-free path length. In general, mass conservation then gives

$$\frac{\partial \rho}{\partial t} + \frac{\partial \rho u_i}{\partial x_i} = 0, \tag{1.1}$$

where u_i are the components of the (instantaneous) velocity field. As the density ρ is constant for incompressible flows*, one has

$$\frac{\partial u_i}{\partial x_i} = 0, \tag{1.2}$$

i.e. the velocity field u_i is divergence-free and solenoidal. Physically, this implies that the rate of change of the dilatation along particle paths in the flow vanishes, i.e. that any infinitesimal material element keeps its volume while being moved and distorted by the flow, cf. e.g. p. 82-84 of Aris (1962). Eq. (1.2) will be called continuity equation henceforth and throughout the remainder of this work, Einstein's summation convention is used. That is, any index appearing twice implies a summation over said index†.

Assuming that fluids are continuous media and applying Newton's second law to an infinitesimal small fluid element results in the so-called Navier-Stokes equations

$$\frac{\partial u_i}{\partial t} + u_j \frac{\partial u_i}{\partial x_j} = -\frac{1}{\rho}\frac{\partial \wp}{\partial x_i} + 2\nu \frac{\partial S_{ij}}{\partial x_j} \quad (+f_i)\,, \tag{1.3}$$

where $\wp$ is the pressure, ν the kinematic viscosity and

$$S_{ij} = \frac{1}{2}\left(\frac{\partial u_i}{\partial x_j} + \frac{\partial u_j}{\partial x_i}\right) \tag{1.4}$$

the strain tensor which equals the symmetric part of the velocity gradient tensor $\partial u_i/\partial x_j$. For a detailed derivation of the Navier-Stokes equations, see e.g. Batchelor (1967). Specifically, the viscous forces are assumed to be proportional to the strain tensor. Due to continuity eq. (1.2), the divergence of the strain tensor $\partial S_{ij}/\partial x_j = (\partial^2 u_i/\partial x_j^2)/2$ and the Navier-Stokes equations can also be written as

$$\frac{\partial u_i}{\partial t} + u_j \frac{\partial u_i}{\partial x_j} = -\frac{1}{\rho}\frac{\partial \wp}{\partial x_i} + \nu \frac{\partial^2 u_i}{\partial x_j^2} \quad (+f_i)\,, \tag{1.5}$$

The last term f_i includes all additional forces, e.g. such stemming from a large-scale forcing scheme for forced turbulence and are neglected hereafter; f_i is only included in eq. (1.3) and eq. (1.5) because it is helpful for some of the discussion

*More precisely, $\partial\rho/\partial t + u_i \partial\rho/\partial x_i = 0$.

†E.g.

$$\frac{\partial u_i}{\partial x_i} = \sum_{i=1}^{3} \frac{\partial u_i}{\partial x_i} = \frac{\partial u_1}{\partial x_1} + \frac{\partial u_2}{\partial x_2} + \frac{\partial u_3}{\partial x_3}.$$

below. In the following, because $\rho = const.$, the density is absorbed in a modified pressure $p = \wp/\rho$. While eq (1.3) and eq. (1.5) are equal for incompressible flows, it is more convenient to use the latter eq. (1.5) for the analysis below, as it contains the Laplacian of the velocity field rather than the divergence of the strain tensor.

It can be shown that the Navier-Stokes equations obey several symmetries and transformational invariances such as invariance regarding rotations and reflections of the coordinate system. Specifically, they are also Galilean-invariant, i.e. invariant to a moving (but not accelerated) coordinate system. However due to the viscous forces, the Navier-Stokes equations are not time-reversible in the sense that reversing time does not give the initial state of the system.

Taking the derivative of eq. (1.5) with respect to x_i and using continuity, one can derive an equation for the pressure

$$\frac{\partial^2 p}{\partial x_i^2} = -\frac{\partial u_i}{\partial x_j}\frac{\partial u_j}{\partial x_i}. \tag{1.6}$$

The solution to this Poisson equation can then be given using Green's function, which allows to compute the pressure p given the velocity field,

$$p(x_i, t) = p^h(x_i, t) - \frac{1}{4\pi}\iiint_V \left(\frac{\partial u_i}{\partial x_j}\frac{\partial u_j}{\partial x_i}\right)\frac{\mathrm{d}y_i}{|x_i - y_i|} \tag{1.7}$$

where $p^h(x_i, t)$ is a harmonic function depending on the boundary conditions. Thus for incompressible flows, the pressure at any given point in space depends on all other points in the domain, i.e. the pressure gradient and consequently the Navier-Stokes equations are non-local in space.

The conservation equation for a passive scalar ϕ is given by

$$\frac{\partial \phi}{\partial t} + u_j\frac{\partial \phi}{\partial x_j} = D\frac{\partial^2 \phi}{\partial x_j^2}, \tag{1.8}$$

where D is the diffusivity. As there are no source or sink terms in eq. (1.8), ϕ is conserved and its motion is determined by convection due to the velocity field as well as diffusion. It is also passive, because its value has no influence upon material quantities such as the density, the viscosity or diffusivity and therefore does not influence the velocity field.

Lastly, taking the curl of the Navier-Stokes equation (1.5) yields an equation

for the vorticity $\omega_i = \epsilon_{ijk}\partial u_k/\partial x_j$ where ϵ_{ijk} is the Levi-Civita symbol,

$$\frac{\partial \omega_i}{\partial t} + u_j \frac{\partial \omega_i}{\partial x_j} = \omega_j \frac{\partial u_i}{\partial x_j} + \nu \frac{\partial^2 \omega_i}{\partial x_j^2}. \tag{1.9}$$

The term $\omega_j(\partial u_i/\partial x_j)$ is known as vortex stretching term and acts as a source term; it vanishes for 2D-flows. Therefore, 2D- and 3D-turbulence are fundamentally different.

Further quantities of interest include the enstrophy $\omega^2 = \omega_i^2$ and the kinetic energy,

$$k = \frac{1}{2} u_i^2. \tag{1.10}$$

One obtains a governing equation for k by multiplying eq. (1.3) by u_i,

$$\frac{\partial k}{\partial t} + u_j \frac{\partial k}{\partial x_j} = -\frac{\partial u_j p}{\partial x_j} + \nu \frac{\partial u_i S_{ij}}{\partial x_j} - \varepsilon \quad (+u_i f_i)\,. \tag{1.11}$$

Integrating over some fixed volume $\mathrm{d}V$,

$$\frac{\partial}{\partial t} \int k \mathrm{d}V = -\int n_i u_i k \mathrm{d}A - \int n_i u_i p dA + \int u_i n_j S_{ij} \mathrm{d}A - \int \varepsilon \mathrm{d}V \tag{1.12}$$

where Gauss' divergence theorem has been used and n_i is a unit vector normal to the surface $\mathrm{d}A$, it can be seen that ε defined by

$$\varepsilon = 2\nu S_{ij} S_{ij} = \nu \left(\frac{\partial u_i}{\partial x_j} \frac{\partial u_i}{\partial x_j} + \frac{\partial u_i}{\partial x_j} \frac{\partial u_j}{\partial x_i} \right) \tag{1.13}$$

is always positive and can be interpreted as dissipation of the kinetic energy per unit volume, while the first term on the r.h.s. equals the flux of kinetic energy across the boundary and the second and third term on the r.h.s. can be interpreted as rate of work done on the boundary by the pressure forces and viscous forces, respectively.

Using eq. (1.5), one finds rather*

$$\frac{\partial k}{\partial t} + u_j \frac{\partial k}{\partial x_j} = -\frac{\partial u_j p}{\partial x_j} + \nu \frac{\partial^2 k}{\partial x_j^2} - \epsilon \quad (+u_i f_i) \tag{1.14}$$

where ϵ equals the *pseudo*-dissipation

$$\epsilon = \nu \frac{\partial u_i}{\partial x_j} \frac{\partial u_i}{\partial x_j}. \tag{1.15}$$

Noticeably, the pseudo-dissipation ϵ differs from the dissipation by the additional term $\nu(\partial u_i/\partial x_j)(\partial u_j/\partial x_i)$†. For incompressible flows, this contribution is related to the second invariant Q of the velocity gradient tensor $\partial u_i/\partial x_j$ (cf. e.g. Chong et al. (1990)) as well as the Laplacian of the pressure $\nabla^2 p$. Statistics of ε as well as $\nabla^2 p$ and joint statistics of ε and the enstrophy ω_i^2 were examined by Yeung et al. (2012) for Reynolds numbers up to $Re_\lambda = 1000$. They found that extreme events of dissipation and enstrophy tend to occur together at high Reynolds numbers. Furthermore, they found that the moments of $\nabla^2 p$ increase slower with increasing Reynolds number than the corresponding moments of the dissipation.

1.2 Characteristics of turbulent flows

Non-dimensionalising the Navier-Stokes equations with suitable reference quantities $\widehat{u}$, $\widehat{L}$ results in

$$\frac{\partial \widetilde{u}_i}{\partial \widetilde{t}} + \widetilde{u}_j \frac{\partial \widetilde{u}_i}{\partial \widetilde{x}_j} = \frac{\partial \widetilde{p}}{\partial \widetilde{x}_i} + \frac{1}{Re} \frac{\partial^2 \widetilde{u}_i}{\partial \widetilde{x}_j^2}, \tag{1.16}$$

where $\widetilde{u}_i = u_i/\widehat{u}$, $\widetilde{x}_j = x_j/\widehat{L}$ and $\widetilde{t} = t/(\widehat{L}/\widehat{u})$. The non-dimensional number

$$Re = \frac{\widehat{u}\widehat{L}}{\nu} \tag{1.17}$$

*For homogeneous isotropic turbulence, both equations give

$$\frac{\partial \langle k \rangle}{\partial t} = -\langle \varepsilon \rangle + \langle u_i f_i \rangle ,$$

because under these assumptions also $\langle \varepsilon \rangle = \langle \epsilon \rangle$.

†Of course, these differences are also contained in the term $\nu(\partial u_i S_{ij}/\partial x_j)$, so that eq. (1.11) and eq. (1.14) are equal.

is one of the most important characteristic numbers in fluid mechanics and can be interpreted as the ratio of inertial to viscous forces. It is called Reynolds number, in honour of Osbourne Reynolds and his pioneering work. With increasing Reynolds number, laminar flows become more unstable, until there is a transition to turbulence.

While it is difficult to give an exact definition of the phenomenon called turbulence (see e.g. Tsinober (2009) for a collection of different definitions), there are several properties by which turbulence can be characterised, cf. e.g. the books of Tennekes and Lumley (1972) or Tsinober (2009):

- Intrinsic randomness and irregularity: Turbulence is chaotic. Although the Navier-Stokes equations are deterministic, their solutions are very sensitive to small disturbances (e.g. of initial conditions or boundary conditions). Turbulence is strongly non-linear.
- Many degrees of freedom: Turbulence is a multi-scale problem and the number of degrees of freedom increases with increasing Reynolds number. Due to the non-linear nature of turbulence, the different scales interact.
- Turbulent flows are highly dissipative due to shear stresses. Without a continuous supply of energy, turbulence decays rapidly.
- Three-dimensional and rotational: Turbulent flows are characterised by a non-vanishing vorticity ω_i. Without three-dimensionality, the dominant production term of vorticity, the vortex stretching, would vanish.
- High rates of mixing: Turbulence strongly increases mixing processes of momentum, energy, passive scalars (e.g. temperature) etc. It is this property which makes turbulent flows so important for many applications.

As turbulence is chaotic and there are no known general solutions of the Navier-Stokes equations, nearly all results and analyses are of statistical nature. As the Reynolds number is the only characteristic number found in eq. (1.16), one might expect some (statistical) universality of turbulent flows when scaled with the Reynolds number, i.e. some universal behaviour independent of the flow type and geometry when properly scaled.

1.3 Scales in turbulent flows

Turbulence is a multi-scale problem as mentioned above. The general picture is that kinetic energy is injected at the large, integral scales and then transported

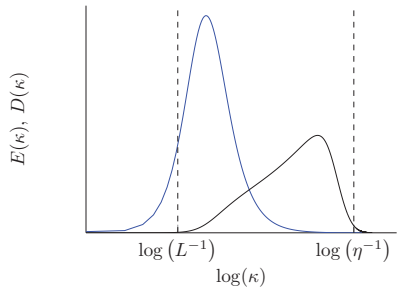

Figure 1.1: (Model)-Spectra of kinetic energy $E(\kappa)$ (blue) and dissipation $D(\kappa)$ (black).

to smaller scales, until it is dissipated at the smallest scales. This can be seen in figure 1.1, where model spectra of the kinetic energy $E(\kappa)$ (cf. pp. 232-234 of Pope (2000)) and dissipation $D(\kappa) = 2\nu\kappa^2 E(\kappa)$ are shown and where the length scale can be thought of as the inverse of the wavenumber κ. The energy and its dissipation in a waveband is then equal to the area under the respective spectrum. It is seen that the bulk of kinetic energy is indeed contained at small wavenumbers (large length scales), while dissipation acts on the smallest scales (large wavenumbers).

2D slices with cross-section $2\pi \times 2\pi$ of the normalised kinetic energy $k/\langle k\rangle$ and dissipation $\ln(\varepsilon/\langle\varepsilon\rangle)$ are shown in figure 1.2 ($Re_\lambda = 88$) and figure 1.3 ($Re_\lambda = 754$), where the black lines in the lower right corner correspond to the integral length L (figure 1.2a and figure 1.3a) and 50η (figure 1.2b and figure 1.3b). Clearly, the dissipation is acting on much smaller scales than the kinetic energy. Furthermore, the smallest scales are much smaller for the higher Reynolds number.

The idea of a cascade of turbulent energy towards smaller scales was first introduced by Richardson (1922). As energy is transported to smaller scales, information about the large scales is more and more lost. One may therefore expect the smallest scales to be isotropic and homogeneous. The assumptions of (statistical) isotropy and homogeneity simplify the analysis of the equations considerably. For that matter, the notion of isotropy was first introduced by Taylor (1935), who considered flows which are isotropic at all scales. Since

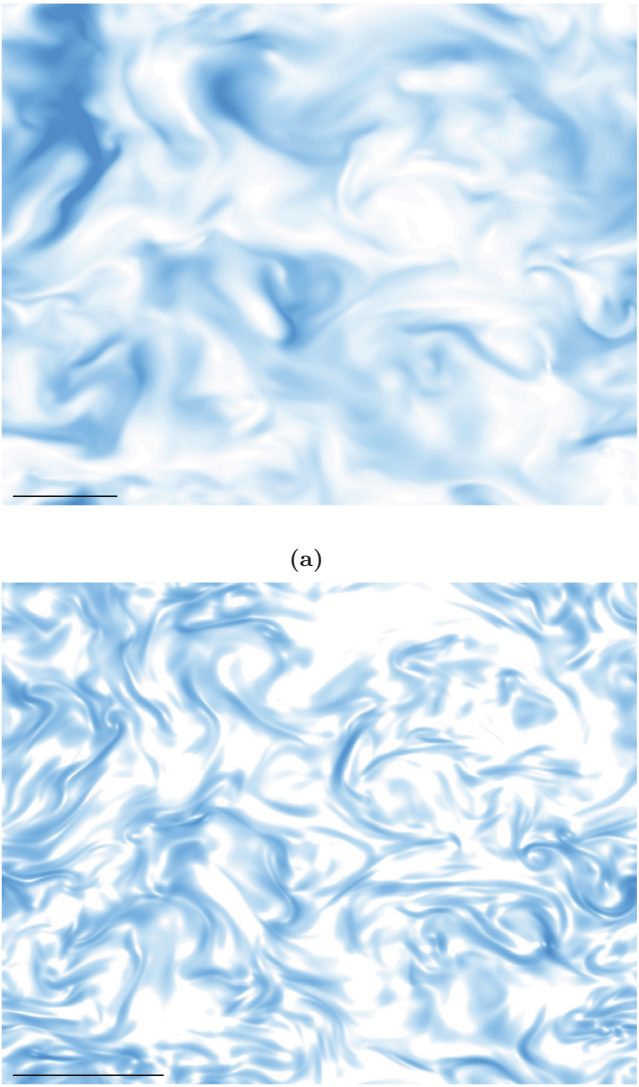

(a)

(b)

Figure 1.2: 2D slices $2\pi \times 2\pi$ of homogeneous isotropic turbulence with $Re_\lambda = 88$ of instantaneous kinetic energy $k/\langle k \rangle$ from 0 (white) to 5 (■) where the black line (lower left corner) corresponds to L (a) and dissipation $\ln(\varepsilon/\langle\varepsilon\rangle)$ from -1 (white) to 3 (■) where the black line (lower left corner) corresponds to 50η (b).

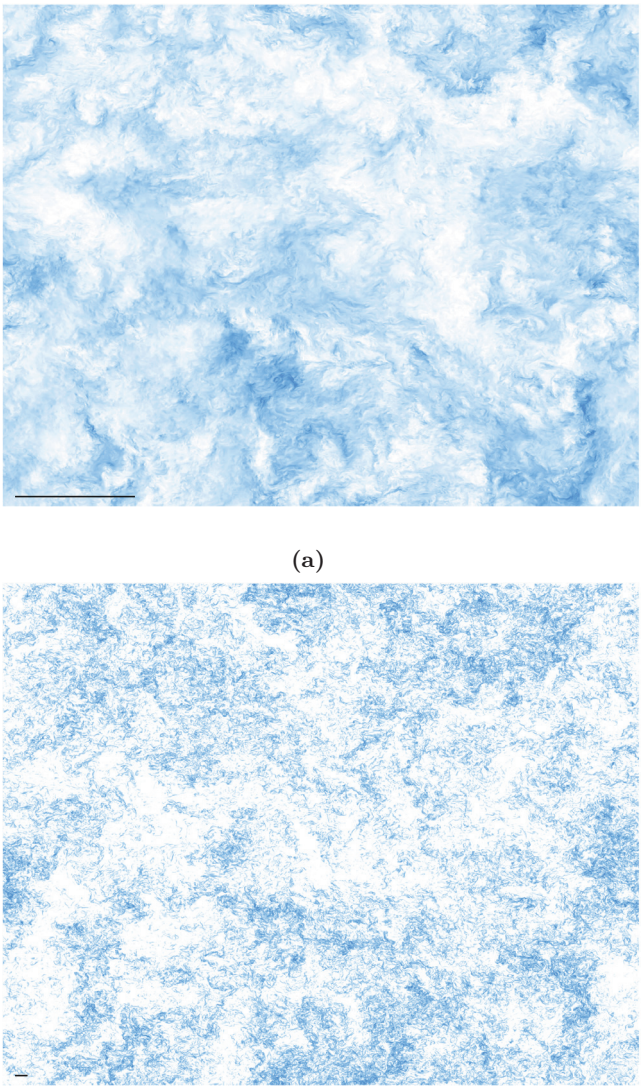

(a)

(b)

Figure 1.3: 2D slices $2\pi \times 2\pi$ of homogeneous isotropic turbulence with $Re_\lambda = 754$ of instantaneous kinetic energy $k/\langle k \rangle$ from 0 (white) to 5 (■) where the black line (lower left corner) corresponds to L (a) and dissipation $\ln(\varepsilon/\langle \varepsilon \rangle)$ from -1 (white) to 3 (■) where the black line (lower left corner) corresponds to 50η (b).

turbulence is a multi-scale problem, it seems reasonable to examine two-point correlations of the velocity field written at positions $\boldsymbol{x} = (x_1, x_2, x_3)$ and $\boldsymbol{x'} = (x'_1, x'_2, x'_3)$ with separation $\boldsymbol{r} = \boldsymbol{x} - \boldsymbol{x'}$ for different flows and Reynolds numbers. Equations for the correlation functions $f = \langle u_1 u'_1 \rangle / \langle u_1^2 \rangle$ and $g = \langle u_2 u'_2 \rangle / \langle u_2^2 \rangle$ were derived by Kármán and Howarth (1938) for isotropic flows (the so-called Kármán-Howarth equation). Hereafter, angle brackets $\langle ... \rangle$ denote averages. Noticeably, f and g fully describe the second-order two-point tensor $\langle u_i u'_j \rangle / \langle u_k^2 \rangle$ under the assumption of isotropy, see e.g. Rotta (1972) for an overview. However, the equations are unclosed due to triple correlations $\langle u_i u_j u_k \rangle$ stemming from the non-linear transport term.

Although there are many different length scales, the following appear frequently in theoretical, numerical and experimental work:

- Integral length scale L: The integral length scale is a large scale, characterised by the flow geometry and boundary conditions. For instance in case of a turbulent jet, a characteristic large length scale is proportional to the nozzle diameter. The corresponding Reynolds number is

$$Re_L = \frac{UL}{\nu} \tag{1.18}$$

  where $U \sim \langle u_i^2 \rangle^{1/2}$ is a large scale velocity. The integral timescale is then defined as $\tau = L/U$.

- Taylor scale λ: The Taylor scale λ is an intermediate length scale, situated between the large and very small scales. It was introduced by Taylor (1935) and is related to the curvature of the velocity correlations f and g for $r \to 0$. It is defined by

$$\lambda = \sqrt{10\nu \frac{\langle k \rangle}{\langle \varepsilon \rangle}} \tag{1.19}$$

  where $\langle k \rangle$ is the (mean) kinetic energy and $\langle \varepsilon \rangle$ the (mean) energy dissipation. The corresponding Reynolds number is

$$Re_\lambda = \frac{u_{\mathrm{rms}} \lambda}{\nu}, \quad Re_\lambda \sim Re_L^{1/2} \tag{1.20}$$

  with $u_{\mathrm{rms}} = \sqrt{\langle u_i^2 \rangle / 3}$*. In numerical studies of isotropic turbulence, the Reynolds number of the simulation reported is usually given as the Taylor

*This gives $Re_\lambda = \sqrt{20/3} Re_L^{1/2}$ if one defines $L \equiv \langle k \rangle^{3/2} / \langle \varepsilon \rangle$ and $U \equiv k^{1/2}$.

based Reynolds number Re_λ. The Taylor scale can be used to scale velocity gradients, $S_{ij} \sim U/\lambda$ and consequently the dissipation, $\langle\varepsilon\rangle \sim \nu U^2/\lambda^2$; however, it is not a small scale but rather an intermediate scale, since $U^2 \sim \langle k\rangle$ is not a small scale.

- Kolmogorov scale η: Introduced by Kolmogorov (1941b) in his seminal paper, the Kolmogorov scale η is usually taken as being proportional to the smallest length scales in turbulent flows. It is defined as

$$\eta = \left(\frac{\nu^3}{\langle\varepsilon\rangle}\right)^{1/4}. \tag{1.21}$$

Together with the Kolmogorov velocity $u_\eta = (\nu\langle\varepsilon\rangle)^{1/4}$, the Reynolds number

$$Re_\eta = \frac{u_\eta \eta}{\nu} = 1, \tag{1.22}$$

indicating that it is truly a dissipative scale. We examine this in more detail in section 4.4 below. A corresponding timescale is $\tau_\eta = (\nu/\langle\varepsilon\rangle)^{1/2}$.

It follows that the ratio of the different scales are determined by the Reynolds number (here the large scale Reynolds number Re_L),

$$\frac{\lambda}{L} \sim Re_L^{-1/2}, \quad \frac{\eta}{L} \sim Re_L^{-3/4}. \tag{1.23}$$

With increasing Reynolds number, these ratios decrease. In other words, η and λ become smaller compared to the integral length L (as does the ratio η/λ) and there is a scale separation. The more turbulent the flow (as characterised by the Reynolds number), the smaller the smallest scales. This is sometimes also referred to as an increase of the degrees of freedom of the flow.

1.4 Kolmogorov's 1941 theory

In the following, let us briefly discuss Kolmogorov's seminal 1941 theory (Kolmogorov (1941a,b)). Rather than examining correlations such as f and g, Kolmogorov proposed to look at so-called structure functions. Structure functions correspond to statistical moments of the velocity difference $\Delta u_i = u_i - u_i'$ of the velocity at positions x_i and x_i' separated by the vector $r_i = x_i - x_i'$ with magnitude $|r_i| = r$. Assuming isotropy, the structure functions can be written in terms of 1- and 2-components only, without loss of generality. Then, the

structure functions are given by

$$D_{m,n} = \langle (\Delta u_1)^m \, (\Delta u_2)^n \rangle \,, \tag{1.24}$$

where angle brackets $\langle \ldots \rangle$ indicate averages. We define $N = m + n$ as the order of the structure function $D_{m,n}$.

By definition,

$$D_{2,0} = 2 \left\langle u_1^2 \right\rangle (1 - f), \quad D_{0,2} = 2 \left\langle u_1^2 \right\rangle (1 - g), \tag{1.25}$$

i.e. the second-order structure functions are related to the correlation functions f and g. Similarly for the third order,

$$D_{3,0} = 6 \left\langle u_1^2 \right\rangle^{3/2} h, \tag{1.26}$$

where h is a third-order correlation function. Using $\partial \langle k \rangle / \partial t = -\langle \varepsilon \rangle$ valid for decaying turbulence as well as using continuity (which relates f and g), Kolmogorov then derived an equation for the longitudinal second-order structure function $D_{2,0}$ from the Kármán-Howarth equation,

$$\left(\frac{\partial D_{3,0}}{\partial r} + \frac{4}{r} D_{3,0} \right) - 6\nu \left(\frac{\partial^2 D_{2,0}}{\partial r^2} + \frac{4}{r} \frac{\partial D_{2,0}}{\partial r} \right) = -4 \langle \varepsilon \rangle \,, \tag{1.27}$$

where isotropy, homogeneity and both $r \ll L$ as well as decaying turbulence have been assumed.

Kolmogorov introduced the notion of an inertial range for asymptotically large Reynolds numbers, located in between the smallest and largest scales, where the influence of the viscosity is negligible. On the other hand, viscous effects dominate the dissipative range (viscous range, $r \to 0$). Therefore, eq. (1.27) reduces to

$$\frac{\partial D_{3,0}}{\partial r} + \frac{4}{r} D_{3,0} = -4 \langle \varepsilon \rangle \tag{1.28}$$

in the inertial range, while for the viscous range

$$-6\nu \left(\frac{\partial^2 D_{2,0}}{\partial r^2} + \frac{4}{r} \frac{\partial D_{2,0}}{\partial r} \right) = -4 \langle \varepsilon \rangle \,. \tag{1.29}$$

Since $\langle \varepsilon \rangle$ is independent of r under the assumption of homogeneity, it can be treated as a flow parameter. This ties into Kolmogorov's similarity hypotheses, which state that structure functions should depend on $\langle \varepsilon \rangle$ in the inertial range

(second similarity hypothesis); in the viscous range, structure functions are postulated to depend on ν and $\langle\varepsilon\rangle$ (first similarity hypothesis). From the first similarity hypothesis, Kolmogorov then defined on dimensional grounds dissipative scales

$$\eta = \left(\frac{\nu^3}{\langle\varepsilon\rangle}\right)^{1/4}, \quad u_\eta = \left(\nu\,\langle\varepsilon\rangle\right)^{1/4}, \quad \tau_\eta = \left(\frac{\nu}{\langle\varepsilon\rangle}\right)^{1/2}, \tag{1.30}$$

where η is the Kolmogorov scale eq. (1.21).

Integration of eq. (1.28) results in

$$D_{3,0} = -\frac{4}{5}\,\langle\varepsilon\rangle\, r, \tag{1.31}$$

valid for the inertial range under the assumptions detailed above*. Similarly, integrating eq. (1.29) yields

$$D_{2,0} = \frac{1}{15}\,\frac{\langle\varepsilon\rangle}{\nu} r^2 \tag{1.32}$$

in the viscous range for $r \to 0$.

Eq. (1.31) is called 4/5-law in the literature and is considered as one of the most important results for fully developed turbulence, since it is exact and non-trivial. Kolmogorov refined the notion of isotropy by introducing local isotropy and local homogeneity, i.e. isotropy and homogeneity are postulated to hold at the small scales for all kinds of flows, while the large scales depend on boundary conditions and may be anisotropic. This implies that eq. (1.27) should hold for all flows in the viscous and inertial range if the Reynolds number is large enough, independent of the boundary and initial conditions. Therefore, the results eq. (1.31) and eq. (1.32) are universal under the given assumptions. It is worth mentioning that the 4/5-law can be derived by solid angle averaging without assuming isotropy, cf. Nie and Tanveer (1999). Consequently, any theory of turbulence needs to reproduce the 4/5-law.

The second similarity hypothesis postulates that any structure function in the inertial range depends only on the mean dissipation $\langle\varepsilon\rangle$ and r, i.e. that $D_{m,n}$ follows a power-law

$$D_{m,n} \sim \left(\langle\varepsilon\rangle\, r\right)^{(m+n)/3}. \tag{1.33}$$

*Technically, this results requires that $D_{3,0}(r_{\text{start}}) = 0$ where r_{start} marks the beginning of the inertial range.

However, it should be stressed that eq. (1.33) is solely based on dimensional grounds by using $\langle\varepsilon\rangle$ and r as the only quantities for scaling. On the other hand, while eq. (1.31) is certainly in agreement with eq. (1.33), it was derived from the Navier-Stokes equations and did not rely on phenomenological scaling arguments. Indeed, subsequent analysis of inertial range behaviour of structure functions found power-law scaling, but with exponents smaller than $(m+n)/3$ (cf. e.g. figure 3.3 in section 3.1 below) where the difference is increasing with increasing order $m+n$; this observation has been reproduced time and again and is usually called anomalous scaling (i.e. different from K41 scaling eq. (1.33)) in the literature.

Finally, because $\langle\varepsilon\rangle$ is independent of r, it can be thought of as linking the smallest, intermediate and large scales, in spirit of the energy cascade. Thus, one can also scale the mean dissipation $\langle\varepsilon\rangle$ with the large scale quantities $U \sim k^{1/2}$ and the integral length L (cf. Taylor (1935)) *although ε is a small scale quantity*,

$$\langle\varepsilon\rangle \sim \frac{U^3}{L}, \tag{1.34}$$

where the prefactor is a constant of order unity, cf. Sreenivasan (1998) or figure 2 of Ishihara et al. (2009) (but see also Vassilicos (2015) for a discussion regarding influences of the flow geometry).

1.5 Outline

Since the publication of Kolmogorov's seminal papers in 1941, there has been much work done regarding inertial range scaling of structure functions. Most of this work is based on phenomenology, where additional assumptions are introduced. For that reason, most subsequent theories have no connection to the underlying Navier-Stokes equations. Here, the aim is to analyse structure functions in the spirit of K41, i.e. based on equations derived from the Navier-Stokes equations. That is, most of the results given below need no further assumptions than isotropy and homogeneity.

The higher-order structure functions are first discussed in chapter 3, where the derivation of their transport equations for homogeneous isotropic turbulence following Hill (2001) is given. In a first step, the balances of the equations are evaluated for different Reynolds numbers. In these equations, one finds two different source terms, the first ones stemming from correlations between components of the pseudo-dissipation tensor and powers of the velocity differences, the second one from correlations between pressure gradient differences and powers

of the velocity differences. Thus, the structure functions are determined by the source terms in the respective equations. For that reason, the transport equation for the dominant fourth-order source terms are exemplarily derived and the balances discussed. It can be shown that one finds higher powers of the pseudo-dissipation and its components in the system of consecutive equations. Moreover, the balances of structure function equations up to the seventh order are presented to examine the influence of the source terms.

At high enough Reynolds number, the separation into viscous and inertial range is valid. We first look at the viscous range in chapter 4. For that range, it is possible to derive order-dependent cut-off scales which generalise the Kolmogorov scales η and u_η for higher orders. Furthermore, from the equations derived in chapter 3, it is possible to derive the solution for the third-order structure functions $D_{3,0}$ and $D_{1,2}$ in the same spirit Kolmogorov derived the second-order solutions for $D_{2,0}$ and $D_{0,2}$. Indeed, it is further possible to find exact solutions for arbitrary higher even-order structure functions $D_{N,0}$. While phenomenology based on Kolmogorov's first similarity hypothesis predicts that $\langle\varepsilon\rangle^N$ is the correct quantity for the $2N$th order, it is found without further assumptions that rather the moments $\langle\varepsilon^N\rangle$ are the correct quantities. Empirically, it is found that *all* structure functions of arbitrary order N scale with $\langle\varepsilon^{N/2}\rangle$ and ν in the viscous range. Therefore, also the higher-order cut-off scales are valid for mixed and transverse structure functions as well as odd orders.

In chapter 5, the inertial range is examined more closely. Using the results of the previous chapter, one can derive a relation between the Reynolds number scaling of the moments of the dissipation and longitudinal inertial range scaling exponents, when assuming Kolmogorov's refined similarity hypothesis (RSH). Moreover, it is shown that RSH postulates that $D_{N+1,0}$ is determined by $\langle(\Delta u_1)^{N-2}\epsilon_{11}\rangle$. Next, the fourth-order transport equations are examined more closely. The fourth order is of interest, because the second moment of the (pseudo-)dissipation is found in the transport equations of one of its source terms. Generally, it is shown that all higher moments of the (pseudo-)dissipation are found in higher-order equations in the system of structure function equations and equations derived thereof. Different to the second order, the source terms depend on r and are therefore unclosed. While one can derive equations for the source terms, one encounters the peculiar situation that the source terms disappear from these equations when evoking the inertial range assumptions. Thus, closure is inherently needed. Specifically, the scaling exponent of the fifth-order structure function trace is examined more closely.

Under the inertial range assumptions, the unsteady and viscous terms are neglected. Nevertheless, these terms contribute to the structure function equations

balances. These influences and their Reynolds number dependence are examined for the second-order equations, where they modify the 4/5-law eq. (1.31) at finite Reynolds numbers.

Finally, a brief comparison of longitudinal structure functions and moments of the velocity difference of streamline segments conditioned on the segment length is given in chapter 6. While the conditional moments of the velocity difference determined by the segments differ significantly from the longitudinal structure funtions, the streamline segment statistics are found to be very similar for the isotropic and anisotropic flows examined here.

2 Dataset Description

Direct numerical simulation (DNS) aims at solving the Navier-Stokes equations (1.5) for given initial and boundary conditions. Compared to experiments, DNS has the advantage that the full 3D velocity field and all quantities derived thereof such as e.g. its gradients or the pressure are at the disposal of the researcher. On the other hand, the range of Reynolds numbers attainable is limited.

DNS of homogeneous isotropic turbulence was first carried out by Orszag and Patterson Jr (1972) with a Reynolds number $Re_\lambda = 35$ in a periodic box employing a pseudo-spectral method, where the Navier-Stokes equations are solved in wavenumber space. This ensures a high accuracy compared to finite difference methods. Usually, the non-linear transport term is computed in real space to decrease the computational cost, where Fast Fourier Transforms (FFT) are used to transform between physical and wavenumber space and aliasing errors introduced by the FFT need to be removed by filtering. This procedure requires the computational domain to be periodic; oftentimes, it is chosen to be a cubic box with non-dimensional edge length 2π, thus limiting the simulation to cases somewhat removed from geometries encountered in engineering problems.

Using the Kolmogorov scale η as characteristic length for the smallest scales, one can estimate the scaling of the number of grid points required to resolve η as

$$N_{\text{grid}}^3 \sim Re_L^{9/4}. \tag{2.1}$$

Note that there are indeed smaller scales connected to intermittency of the flow which need to be resolved if one is interested in computing higher-order statistics. This is discussed in more detail in section 4.4.2 and yields an upper bound

$$N_{\text{grid}}^3 \sim Re_L^3. \tag{2.2}$$

Moreover, the computational cost is higher, because one has to limit the time step Δt because of numerical stability and accuracy, i.e. the CFL number may not be too large. Estimating $\Delta t = \eta/u^\dagger$, one finds for the number of required

[†]Because η is not the smallest scale for reasons outlined below in section 4.4, one might need to modify this similarly as eq. (2.1), i.e. the time step Δt may need to be smaller.

time steps $N_{\Delta t}$ to compute an integral time $\tau \sim k/\langle\varepsilon\rangle$

$$N_{\Delta t} \sim \frac{\tau}{\Delta t} \sim Re_L^{3/4}. \tag{2.3}$$

The computational cost to resolve an integral time τ then scales as $N_{\text{grid}} N_{\Delta t}$. This is the reason why the Reynolds numbers attainable using DNS has only progressed slowly since 1972* and very likely continues to be limited to smaller Reynolds numbers in the foreseeable future, compared to experiments.

Below, DNS of forced homogeneous isotropic turbulence (section 2.1) is used for most of the analysis. There, energy is introduced into the system by an additional forcing term. Without this forcing term, the turbulence would decay. DNS of decaying homogeneous isotropic turbulence as described in section 2.2 is also employed in chapter 5 and chapter 6. Moreover, data of an anisotropic flow (cf. section 2.3) is used in chapter 6.

2.1 Forced homogeneous isotropic turbulence

For the analyses carried out below, we use data from direct numerical simulations (DNS) of forced homogeneous isotropic turbulence with seven different sets of Taylor based Reynolds numbers ranging from $Re_\lambda = 88$ to $Re_\lambda = 754$. For more details, see Gauding (2014). Here $Re_\lambda = u_{\text{rms}}\lambda/\nu$, λ denotes the Taylor scale $\lambda = \sqrt{10\nu \langle k\rangle / \langle\varepsilon\rangle}$, $u_{\text{rms}} = \sqrt{\langle u_i u_i/3\rangle}$ is the root-mean-square velocity, $\langle k\rangle = \langle u_i u_i\rangle /2$ the mean kinetic energy and $\langle\varepsilon\rangle = 2\nu \langle S_{ij} S_{ij}\rangle$ the mean energy dissipation, where the strain tensor $S_{ij} = (\partial u_i/\partial x_j + \partial u_j/\partial x_i)/2$. Angle brackets $\langle ...\rangle$ denote ensemble averages over the full box and several timesteps (as given by the ratio t_{avg}/τ) spanning more than an integral turnover time after the simulation reached its statistically steady state. M_{avg} denotes the number of times used to compute the averages. The seven datasets have been computed on the JUQUEEN supercomputer at Forschungszentrum Jülich using a pseudo-spectral code with MPI/OpenMP parallelisation. The three-dimensional Navier-Stokes equations were solved in rotational form, where all terms but the non-linear term were evaluated in spectral space. For a faster computation, the non-linear term is evaluated in physical space. The computational domain is a box with periodic boundary conditions and length 2π. For dealiasing, the scheme of Hou and Li (2007) has been used. For the temporal advancement, a second-order Adams-Bashforth scheme is used in case of the non-linear term,

*At the moment of writing, the highest Reynolds number attained was $Re_\lambda = 2300$ with $N_{\text{grid}}^3 = 12288^3$, cf. Ishihara et al. (2016).

Table 2.1: Parameters of the forced isotropic DNS.

	R0	R1	R2	R3	R4	R5	R6
N_{grid}	512^3	1024^3	1024^3	2048^3	2048^3	4096^3	4096^3
Re_λ	88	119	184	215	331	529	754
ν	0.01	0.0055	0.0025	0.0019	0.0010	0.00048	0.00027
$\kappa_{\max}\eta$	3.57	4.54	2.66	4.01	2.30	2.95	1.76
$\langle k \rangle$	11.15	11.38	11.42	12.70	14.35	23.95	24.42
$\langle \varepsilon \rangle$	10.78	11.04	10.30	11.87	12.55	28.51	26.54
λ	0.322	0.238	0.166	0.143	0.107	0.064	0.050
η	0.0175	0.0111	0.0062	0.0049	0.0030	0.0014,	0.00093
L	1.02	0.94	0.97	1.01	0.97	1.02	1.18
τ_η	0.031	0.022	0.016	0.013	0.009	0.004	0.0032
τ	1.03	1.03	1.11	1.07	1.14	0.84	0.92
t_{avg}/τ	100	30	30	10	10	2	3
M_{avg}	112	42	40	10	10	6	6

while the linear terms are updated using a Crank-Nicolson scheme. To keep the simulation statistically steady, the stochastic forcing scheme of Eswaran and Pope (1988) is applied. The 2DECOMP&FFT library (Li and Laizet (2010)) has been used for spatial decomposition and to perform the Fast Fourier Transforms. The only parameter varied to increase the Reynolds number is the viscosity ν; the forcing parameters have been held constant. The properties of the DNS cases can be found in table 2.1. The seven datasets were computed on a computational mesh with 512^3 grid points for case R0 up to 4096^3 grid points for case R6. $\eta = (\nu^3/\langle\varepsilon\rangle)^{1/4}$ is the Kolmogorov length scale with corresponding time scale $\tau_\eta = (\nu/\langle\varepsilon\rangle)^{1/2}$. L is the integral length scale, computed here using the energy spectrum function

$$L = \frac{3\pi}{4} \frac{\int \kappa^{-1} E(\kappa) d\kappa}{\int E(\kappa) d\kappa} \tag{2.4}$$

and $\tau = \langle k \rangle / \langle \varepsilon \rangle$ the integral time scale. The integral length scale L is small compared to the size of the boxes in order to reduce the influence of the periodic boundary condition. The data is well resolved with $\kappa_{\max}\eta \geq 1.7$ for all seven datasets, where $\kappa_{\max}$ is the largest resolved wavenumber. In turn, this also implies that the Reynolds number is not as high as other DNS with comparable mesh size reported in the literature. We discuss this in more detail in section 4.4.2

below.

2.2 Decaying turbulence

For some of the analysis, decaying homogeneous isotropic turbulence is used. The direct numerical simulation has been performed on the supercomputer JUQUEEN at research center Juelich, Germany. The incompressible Navier-Stokes equations are solved in a triply periodic cubic box with size 2π by a pseudo-spectral method. For numerical stability, the non-linear term of the momentum equation is rewritten in rotational form. Using a pseudo-spectral method, the non-linear term is computed in real space and transformed to spectral space for temporal integration. Temporal integration is carried out by a low-storage stability preserving third-order Runge-Kutta method. The viscous term is treated exactly by using an integrating factor technique. A standard isotropic truncation procedure in combination with a random phase-shift technique is used to eliminate aliasing effects allowing us to keep all wave-numbers with $\kappa < \sqrt{2}N/3$. The grid resolution is $N_{\text{grid}} = 2048^3$, which adequately resolves the smallest scales during the simulation. For pseudo-spectral methods, the resolution requirement can be written in terms of the non-dimensional number $\kappa_{\max}\eta$, where again $\kappa_{\max}$ is the largest wave-number appearing in the truncated Fourier series, and η is the Kolmogorov length. The resolution condition $\kappa_{\max}\eta$ for the four time steps under consideration is indicated in table 2.2 and has been shown to be sufficient to compute second-order velocity gradient statistics (Ishihara et al. (2007)). The flow is initialized by a prescribed isotropic energy spectrum of the form

$$E(\kappa) \propto \kappa^4 \exp\left[-2\left(\frac{\kappa}{\kappa_p}\right)^2\right], \tag{2.5}$$

where κ is the wave-number and κ_p is the location at which the initial energy spectrum peaks. Here, we aim at reaching high Reynolds numbers to obtain a well established inertial range. For this reason, κ_p has been set to a comparable small value of 3.5 and small confinement effects due to the finite size of the computational domain (Ishida et al. (2006)) are tolerated. Following Ishida et al., the initial state of freely decaying turbulence can be characterized by a Reynolds number defined as

$$Re = \frac{\langle k(t=0)\rangle^{1/2}}{\kappa_p \nu}, \tag{2.6}$$

Table 2.2: Parameters of the decaying isotropic DNS.

	D_1	D_2	D_3	D_4
Re_λ	121.39	161.11	206.28	254.75
$\kappa_{\max}\eta$	6.83	3.96	1.72	0.89
$\langle k \rangle$	0.0378	0.149	1.00	4.67
$\langle \varepsilon \rangle$	0.00308	0.0271	0.750	10.67
η	0.00741	0.00430	0.00187	0.000965
λ	0.161	0.107	0.0530	0.0303
τ_η	0.261	0.0880	0.0167	0.00444
τ	12.29	5.50	1.34	0.438
ν	0.00021	0.00021	0.00021	0.00021

where $\langle k(t=0) \rangle = \int_0^\infty E(\kappa, t=0) \mathrm{d}\kappa$ denotes the initial turbulent kinetic energy, and ν is the kinematic viscosity. From this definition and with $\langle k(t=0) \rangle = 10$ and $\nu = 0.00021$, an initial Reynolds number of $Re = 4302$ is obtained.

The temporal evolution of $\langle k \rangle \sim t^{-n}$ and $\langle \varepsilon \rangle \sim t^{-n-1}$ is shown in figure 2.1a and figure 2.1b, where the dashed lines correspond to a decay exponent $n = 1.45$. This value is slightly larger than the theoretical value $n = 10/7$ obtained for a κ^4-spectrum as in eq. (2.5), cf. e.g. the discussion in Rotta (1972) or Davidson (2004). The times used for the present analysis are indicated by the dotted vertical black lines in the decaying regime. We use all four times to examine Reynolds number dependencies of the closures presented in section 5.4.2 below and the highest (leftmost dotted black line, $Re_\lambda = 254.75$) and lowest (rightmost dotted black line, $Re_\lambda = 121.39$) Reynolds number for more detailed analysis.

2.3 Fractal flow

In chapter 6, we briefly compare statistics of streamline segments for isotropic and anisotropic flow. The anisotropic data is described below and in more detail in Laizet and Vassilicos (2011).

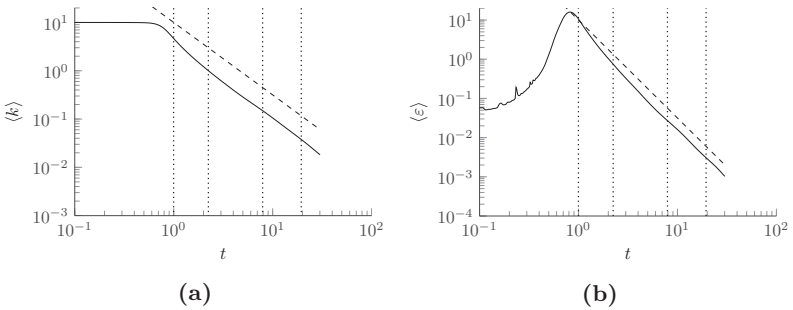

Figure 2.1: Temporal evolution of kinetic energy k and dissipation ε. Times used in the analysis below are indicated with the dotted vertical black lines. Dashed lines corresponds to $\langle k \rangle \sim t^{-n}$ (a) and $\langle \varepsilon \rangle \sim t^{-n-1}$ (b) with $n = 1.45$.

2.3.1 Description of the grid

As shown in figure 2.2, a fractal square grid with a square pattern formed by four bars is considered (see Hurst and Vassilicos (2007) for a detailed description of fractal square grids). It is based on four fractal iterations (with 4^j patterns at iteration j) and the ratio $t_r \equiv t_{\max}/t_{\min}$ between the lateral thickness $t_{\max}$ of the bars making the largest pattern and the lateral thickness $t_{\min}$ of the smallest one is equal to 8.5. L_j with $j = 0, 1, 2, 3$ represents the length of the bars for each fractal iteration. The blockage ratio σ of our turbulence-generating grid is defined as the ratio of its total area in the transverse plane to the area $T^2 = L_y \times L_z$ and is equal to 41%. Unlike regular grids, multiscale/fractal grids do not have a well-defined mesh size. This is why Hurst and Vassilicos (2007) introduced an effective mesh size for multiscale grids, $M_{\text{eff}} = 4T^2\sqrt{1-\sigma}/L_{\text{TG}}$ where L_{TG} is the total perimeter length in the $(y-z)$ plane of the fractal grid. Here, we have $M_{\text{eff}} = 8.7\ t_{\min}$. Note finally that the streamwise thickness of the bars is $3.2\ t_{\min}$.

2.3.2 Numerical Methods

The incompressible Navier-Stokes equations are solved using the high-order flow solver `Incompact3d`, adapted to parallel supercomputers thanks to a highly scalable 2D domain decomposition library and a distributed FFT interface (Laizet and Li (2011)). Sixth-order compact finite-difference schemes are used

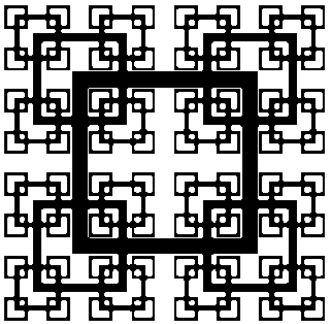

(a)

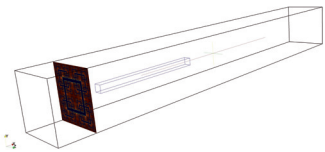

(b)

Figure 2.2: Diagram of the fractal square grid used in this study (a) and illustration of the computational domain where the subdomain used for this study is highlighted in blue (b).

for the spatial differentiation whereas an explicit third-order Adams-Bashforth scheme is used for the time integration. To treat the incompressibility condition, a fractional step method requires solving a Poisson equation. This equation is fully solved in spectral space, via the use of relevant 3D Fast Fourier Transforms combined with the concept of modified wave number (Lele (1992)). Note that the pressure mesh is staggered from that for the velocity by half a grid point, to avoid spurious pressure oscillations. The divergence-free condition is ensured up to machine accuracy. The modeling of the fractal grid is performed using an Immersed Boundary Method (IBM) based on a direct forcing approach that ensures the no-slip boundary condition at the grid walls. The idea is to force the velocity to zero at the wall of the grid, as the particular Cartesian mesh does conform with the geometries of the grid. It mimics the effects of a solid surface on the fluid with an extra forcing in the Navier-Stokes equations. More details about the present code and its validation, especially the original treatment of the pressure in spectral space, can be found in Laizet and Lamballais (2009).

2.3.3 Numerical set-up

The computational domain in the streamwise x and the two lateral y and z directions is $L_x \times L_y \times L_z = 16L_0 \times 2L_0 \times 2L_0$ discretized on a Cartesian mesh

using $n_y \times n_z = 720 \times 720$ mesh nodes in lateral planes and $n_x = 5761$ in the streamwise direction. This high resolution was recommended by Laizet et al. (2015b) especially for the production region. The coordinate system's origin is placed at the centre of the grid which is located at a distance of $1.25L_0$ from the inlet of the computational domain in order to avoid spurious interactions between the grid and the inlet condition. We assume a fluid of uniform density and kinematic viscosity ν. Inflow/outflow boundary conditions are used in the streamwise direction and periodic boundary conditions are used in the two lateral directions. The inflow and initial conditions for the velocity field are $\mathbf{u} \equiv (u_1, u_2, u_3) = (U_\infty, 0, 0)$ where U_∞ is a constant streamwise velocity (u_1 is the streamwise velocity component and (u_2, u_3) are the two lateral velocity components corresponding to (y, z)). The outflow condition is a standard 1D convection equation.

For the particular analysis of chapter 6, data are collected for 5 time-independent snapshots of a 3D subdomain (see figure 2.2) of size $4.25L_0 \times 0.28L_0 \times 0.28L_0$ with $1530 \times 101 \times 101$ mesh nodes. The 3D subdomain is centred around the centreline of the grid starting from a distance $0.15x_*$ downstream of the grid and extending to a distance $0.55x_*$, where x_* is the wake interaction length scale introduced by Mazellier and Vassilicos (2008) and which is equal to L_0^2/t_0. The fractal flow data used in chapter 6 onwards are taken from the production and the decay regions explicitly shown in figure 2.3. For this fractal square grid simulation, the values of the Taylor-based Reynolds number $Re_\lambda = u_{\mathrm{rms}}\lambda/\nu$, the Taylor microscale $\lambda = \sqrt{u_{\mathrm{rms}}/(\partial u/\partial x)^2}$ and the integral scale L are varying with streamwise distance from the grid and their values with respect to x_* can be seen in figure 2.3.

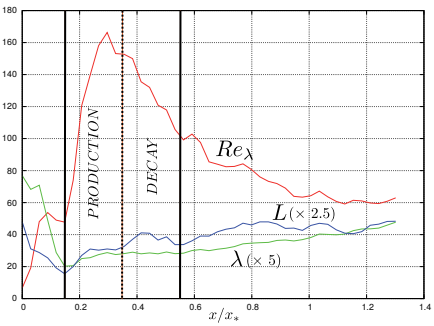

Figure 2.3: Streamwise evolution along the centreline for the fractal square grid of the Taylor-based Reynolds numberRe_λ, the Taylor microscale λ and the integral scale L. The production region (from $x = 0.15x_*$ to $x = 0.35x_*$) and the decay region (from $x = 0.15x_*$ to $x = 0.35x_*$) where the data are collected is highlighted around the Re_λ peak.

3 System of equations

In this chapter, exact equations for structure functions are presented and the balances of the equations are examined, mostly based on Boschung et al. (2017a) and the arxive material Peters et al. (2015); section 3.1.3 is redacted from Peters et al. (2016).

These exact equations for structure functions are derived from the incompressible Navier-Stokes equations (1.5) and simplified for homogeneous, isotropic turbulence. Exact equations for structure functions of arbitrary order were derived by Hill (2001) and Yakhot (2001). In the following, we will use the methodology of Hill, as it allows us to easily derive equations for the source terms in the structure function equations. The underlying notion is that since the structure function equations are exact, they might provide further insight and lead to new results. In section 3.1, the equations for the longitudinal, mixed and transverse structure functions and the resulting system of equations are discussed. Special emphasis is given to the second- and fourth-order equations. For the fourth-order structure function equations, we have also derived the transport equation for its leading-order source terms, since they determine the solution of the fourth-order structure function equations. The balances of the structure function equations up to the seventh order are shown in section 3.2. Furthermore, we have derived the transport equation for the trace of the fourth-order structure function and its leading-order source term in section 3.3, followed by the balances of these equations. As the system of structure function equations is unclosed, we briefly discuss a possible closure in section 3.4. We use the equations derived in this chapter in chapter 4 and chapter 5 below, where we examine the viscous range and the inertial range in more detail.

In the literature, source terms of higher-order structure function equations have been analysed by DNS simulations and, to the extent that this was possible, by hot wire measurements. Hill and Boratav (2001) analysed the third-order structure function equations based on DNS and experiments. From their analysis, it appears that only the pressure source terms determine the solutions at the third order. Kurien and Sreenivasan (2001) discussed the Yakhot (2001) paper and the models presented therein in detail. They then used high Reynolds number experimental data from the atmospheric boundary layer to compute the

pressure terms from Yakhot's model and balance the terms of the transverse and mixed fourth-order structure function equations in the inertial range. Gotoh and Nakano (2003) have examined on the basis of DNS data the balances between the even-order structure functions and the pressure source terms in the odd-order equations up to eighth order and proposed a model for the pressure source terms. Yakhot (2003) has modified this model to obtain the same formula as in Yakhot (2001), but now for longitudinal inertial range scaling exponents. Based on a model for the probability density function for longitudinal velocity increments, Yakhot (2006) discussed the closure of the structure function equations in terms of the dissipation anomaly (cf. Polyakov (1995) and Yakhot and Sreenivasan (2005)). Using DNS data, Nakano et al. (2003) normalised the dissipation source terms in the longitudinal equations up to the eighth order by the next-order structure function. They found that for all even-order equations, the normalised dissipation source terms are of order unity. This suggests that the dissipation source terms rather than the pressure source terms are dominant in the even-order equations.

3.1 Structure function equations

In this section, the system of structure function equations and the resulting coupling between the individual equations is briefly discussed.

3.1.1 General form

Assuming incompressible flow, the momentum equations written at two points denoted by $x_i = (x_1, x_2, x_3)$ and $x'_i = (x'_1, x'_2, x'_3)$ are given by*

$$\frac{\partial u_i}{\partial t} + u_n \frac{\partial u_i}{\partial x_n} = -\frac{\partial p}{\partial x_i} + \nu \frac{\partial^2 u_i}{\partial x_n^2}, \quad i = 1, 2, 3 \tag{3.1}$$

$$\frac{\partial u'_i}{\partial t} + u'_n \frac{\partial u'_i}{\partial x'_n} = -\frac{\partial p'}{\partial x'_i} + \nu \frac{\partial^2 u'_i}{\partial x'^2_n}, \quad i = 1, 2, 3 \tag{3.2}$$

Here u_i and u'_i are the components of the velocity, p is the pressure and ν the kinematic viscosity. Einstein's summation convention for indices appearing twice is used. These equations are completed by the continuity equation which holds

*Note that terms f_i stemming from body forces or large scale forcing are neglected here and in the following.

at both points,

$$\frac{\partial u_i}{\partial x_i} = 0, \quad \frac{\partial u_i'}{\partial x_i'} = 0 \tag{3.3}$$

Following Hill (2001), one obtains an equation for the velocity increment Δu_i defined by $\Delta u_i = u_i(\boldsymbol{x}) - u_i'(\boldsymbol{x'})$ by subtracting eq. (3.2) from eq. (3.1)*,

$$\frac{\partial \Delta u_i}{\partial t} + u_n \frac{\partial \Delta u_i}{\partial x_n} + u_n' \frac{\partial \Delta u_i}{\partial x_n'} = -\underbrace{\left(\frac{\partial p}{\partial x_i} - \frac{\partial p'}{\partial x_i'} \right)}_{\Delta P_i} + \nu \left(\frac{\partial^2 \Delta u_i}{\partial x_n^2} + \frac{\partial^2 \Delta u_i}{\partial x_n'^2} \right) \tag{3.4}$$

Here the difference of the pressure gradient at the two points is defined as ΔP_i. Next, the independent variables x_i and x_i' are changed to the new independent variables

$$X_i = \frac{1}{2}\left(x_i + x_i'\right), \quad r_i = \left(x_i - x_i'\right). \tag{3.5}$$

This coordinate transformation is very helpful in the following, since it incorporates a length scale, the separation vector r_i and its magnitude $r = |r_i|$ into the system of equations. Using the transformation rules

$$\frac{\partial}{\partial x_i} = \frac{\partial}{\partial r_i} + \frac{1}{2}\frac{\partial}{\partial X_i}, \quad \frac{\partial}{\partial x_i'} = -\frac{\partial}{\partial r_i} + \frac{1}{2}\frac{\partial}{\partial X_i} \tag{3.6}$$

one obtains using incompressibility (eq. (3.3)) and the observation that spatial derivatives of quantities at x_i with respect to x_i' and vice versa vanish (i.e. here that $\partial u_i/\partial x_j' = 0$ as well as $\partial u_i'/\partial x_j = 0$),

$$\frac{\partial \Delta u_i}{\partial r_i} = 0, \quad \frac{\partial \Delta u_i}{\partial X_i} = 0, \quad \frac{\partial U_i}{\partial r_i} = 0, \quad \frac{\partial U_i}{\partial X_i} = 0 \tag{3.7}$$

where $U_i = (u_i + u_i')/2$. Inserting this into the transport term in eq. (3.4), one obtains

$$u_n \frac{\partial \Delta u_i}{\partial x_n} + u_n' \frac{\partial \Delta u_i}{\partial x_n'} = \Delta u_n \frac{\partial \Delta u_i}{\partial r_n} + U_n \frac{\partial \Delta u_n}{\partial X_n}. \tag{3.8}$$

*More generally, the two points can also be separated in time by Δt, where the first eq. (3.1) is written at t and the second eq. (3.2) at t'. Consequently, one would have a corresponding coordinate change $\Delta t = t - t'$ and $\mathcal{T} = (t + t')/2$, cf. Hill (2006). Here, we take $t = t'$, i.e. have the two points separated only in space but not in time.

Likewise the Laplacian in eq. (3.4) becomes

$$\frac{\partial^2 \Delta u_i}{\partial x_n^2} + \frac{\partial^2 \Delta u_i}{\partial x_n'^2} = 2\left(\frac{\partial^2 \Delta u_i}{\partial r_n^2} + \frac{\partial^2 \Delta u_i}{\partial X_n^2}\right). \tag{3.9}$$

to finally obtain

$$\frac{\partial \Delta u_i}{\partial t} + \Delta u_n \frac{\partial \Delta u_i}{\partial r_n} + U_n \frac{\partial \Delta u_i}{\partial X_n} = -\Delta P_i + 2\nu\left(\frac{\partial^2 \Delta u_i}{\partial r_n^2} + \frac{\partial^2 \Delta u_i}{\partial X_n^2}\right). \tag{3.10}$$

To derive equations for structure functions of arbitrary order N, $\langle \Delta u_i \Delta u_j \Delta u_k ... \Delta u_l \rangle$, eq. (3.10) is multiplied by $\Delta u_j \Delta u_k ... \Delta u_l$ and similarly equations for $\Delta u_j, \Delta u_k, ..., \Delta u_l$. Summing up the N equations and averaging then yields

$$\begin{aligned}\frac{\partial \boldsymbol{D}_N}{\partial t} + \boldsymbol{\nabla}_{\boldsymbol{X}} \cdot \boldsymbol{F}_{N+1} + \boldsymbol{\nabla}_{\boldsymbol{r}} \cdot \boldsymbol{D}_{N+1} = &- \langle \boldsymbol{T}_N \rangle - \langle \boldsymbol{E}_N \rangle \\ &+ 2\nu\left(\nabla_r^2 \boldsymbol{D}_N + \frac{1}{4}\nabla_X^2 \boldsymbol{D}_N\right),\end{aligned} \tag{3.11}$$

i.e. an equation for the N-rank tensor $\boldsymbol{D}_N$, where

$$\begin{aligned}\boldsymbol{D}_N &= \langle \Delta u_i \Delta u_j \Delta u_k ... \Delta u_l \rangle \\ \boldsymbol{\nabla}_{\boldsymbol{X}} \cdot \boldsymbol{F}_{N+1} &= \frac{\partial}{\partial X_n}\left(\langle U_n \Delta u_i \Delta u_j \Delta u_k ... \Delta u_l \rangle\right) \\ \boldsymbol{\nabla}_{\boldsymbol{r}} \cdot \boldsymbol{D}_{N+1} &= \frac{\partial}{\partial r_n}\left(\langle u_n \Delta u_i \Delta u_j \Delta u_k ... \Delta u_l \rangle\right)\end{aligned} \tag{3.12}$$

and the source terms

$$\langle \boldsymbol{T}_N \rangle = \langle \{\Delta u_j \Delta u_k ... \Delta u_l \Delta P_i\} \rangle \tag{3.13}$$

and

$$\langle \boldsymbol{E}_N \rangle = 2\left\langle \left\{\Delta u_k ... \Delta u_l \left(\epsilon_{ij} + \epsilon'_{ij}\right)\right\}\right\rangle. \tag{3.14}$$

Hereafter, $\langle \boldsymbol{T}_N \rangle$ are called pressure source terms and $\langle \boldsymbol{E}_N \rangle$ dissipation source terms. The curly braces $\{...\}$ denote summation over all combination of indices.

For instance at the fourth order,

$$\begin{aligned}\langle \boldsymbol{E}_4 \rangle &\equiv \langle E_{ijkl} \rangle \\ &= 2 \left\langle \Delta u_k \Delta u_l \left(\epsilon_{ij} + \epsilon'_{ij}\right) + \Delta u_j \Delta u_l \left(\epsilon_{ik} + \epsilon'_{ik}\right) + \Delta u_j \Delta u_k \left(\epsilon_{il} + \epsilon'_{il}\right) \right. \\ &\left. + \Delta u_i \Delta u_l \left(\epsilon_{jk} + \epsilon'_{jk}\right) + \Delta u_i \Delta u_k \left(\epsilon_{jl} + \epsilon'_{jl}\right) + \Delta u_i \Delta u_j \left(\epsilon_{kl} + \epsilon'_{kl}\right) \right\rangle \end{aligned} \tag{3.15}$$

or at the third order

$$\langle \boldsymbol{T}_3 \rangle \equiv \langle T_{ijk} \rangle = \langle \Delta u_i \Delta u_j \Delta P_k + \Delta u_i \Delta u_k \Delta P_j + \Delta u_j \Delta u_k \Delta P_i \rangle \tag{3.16}$$

and thus e.g.

$$\begin{aligned}\langle E_{3,0} \rangle &= 6 \left\langle \Delta u_1 \left(\epsilon_{11} + \epsilon'_{11}\right) \right\rangle \\ \langle E_{2,2} \rangle &= 2 \left\langle \left(\Delta u_2\right)^2 \left(\epsilon_{11} + \epsilon'_{11}\right) + 4 \Delta u_1 \Delta u_2 \left(\epsilon_{12} + \epsilon'_{12}\right) \right. \\ &\qquad \left. + \left(\Delta u_1\right)^2 \left(\epsilon_{22} + \epsilon'_{22}\right) \right\rangle \\ \langle T_{1,2} \rangle &= \left\langle 2 \Delta u_1 \Delta u_2 \Delta P_2 + \left(\Delta u_2\right)^2 \Delta P_1 \right\rangle \\ \langle T_{0,4} \rangle &= 4 \left\langle \left(\Delta u_2\right)^3 \Delta P_2 \right\rangle , \end{aligned} \tag{3.17}$$

where $\langle E_{3,0} \rangle = \langle E_{111} \rangle$, $\langle E_{2,2} \rangle = \langle E_{1122} \rangle$, $\langle T_{1,2} \rangle = T_{122}$ and $\langle T_{0,4} \rangle = \langle T_{2222} \rangle$ and

$$\epsilon_{ij} = \nu \frac{\partial u_i}{\partial x_k} \frac{\partial u_j}{\partial x_k} \tag{3.18}$$

are components of the pseudo-dissipation tensor, where the pseudo-dissipation equals the trace $\epsilon = \epsilon_{ii}$, cf. eq. (1.15).

Clearly, the equations of order N are coupled to the equations of order $N+1$ by the transport term $\boldsymbol{\nabla}_{\boldsymbol{r}} \cdot \boldsymbol{D}_{N+1}$. This set of equations can be further simplified for homogeneous, isotropic turbulence. In case of homogeneity, all derivatives of averaged quantities $\langle ... \rangle$ with respect to X_n vanish, since they do not depend on the position where they are measured. Then, eq. (3.11) reduces to

$$\frac{\partial \boldsymbol{D}_N}{\partial t} + \boldsymbol{\nabla} \cdot \boldsymbol{D}_{N+1} = - \langle \boldsymbol{T}_N \rangle - \langle \boldsymbol{E}_N \rangle + 2\nu \nabla^2 \boldsymbol{D}_N, \tag{3.19}$$

under the assumption of isotropy and homogeneity and where possible additional terms stemming from some large-scale forcing have been neglected. All orders have the same general structure: In the Nth-order structure function equation, there are transport terms containing structure functions of order $N+1$ (i.e.

Table 3.1: Relations between structure functions with 2- and 3-components.

N = 2	$\langle(\Delta u_2)^2\rangle = \langle(\Delta u_3)^2\rangle$
N = 3	$\langle\Delta u_1(\Delta u_2)^2\rangle = \langle\Delta u_1(\Delta u_3)^2\rangle$
N = 4	$\langle(\Delta u_1)^2(\Delta u_2)^2\rangle = \langle(\Delta u_1)^2(\Delta u_3)^2\rangle$ $\langle(\Delta u_2)^4\rangle = 3\langle(\Delta u_2)^2(\Delta u_3)^2\rangle = \langle(\Delta u_4)^4\rangle$
N = 5	$\langle(\Delta u_1)^3(\Delta u_2)^2\rangle = \langle(\Delta u_1)^3(\Delta u_3)^2\rangle$ $\langle\Delta u_1(\Delta u_2)^4\rangle = 3\langle\Delta u_1(\Delta u_2)^2(\Delta u_3)^2\rangle = \langle\Delta u_1(\Delta u_4)^4\rangle$
N = 6	$\langle(\Delta u_1)^4(\Delta u_2)^2\rangle = \langle(\Delta u_1)^4(\Delta u_3)^2\rangle$ $\langle(\Delta u_1)^2(\Delta u_2)^4\rangle = 3\langle(\Delta u_1)^2(\Delta u_2)^2(\Delta u_3)^2\rangle = \langle(\Delta u_1)^2(\Delta u_3)^4\rangle$ $\langle(\Delta u_2)^6\rangle = 5\langle(\Delta u_2)^4(\Delta u_3)^2\rangle = 5\langle(\Delta u_2)^2(\Delta u_3)^4\rangle = \langle(\Delta u_3)^6\rangle$
N = 7	$\langle(\Delta u_1)^5(\Delta u_2)^2\rangle = \langle(\Delta u_1)^5(\Delta u_3)^2\rangle$ $\langle(\Delta u_1)^3(\Delta u_2)^4\rangle = 3\langle(\Delta u_1)^3(\Delta u_2)^2(\Delta u_3)^2\rangle = \langle(\Delta u_1)^3(\Delta u_3)^4\rangle$ $\langle\Delta u_1(\Delta u_2)^6\rangle = 5\langle\Delta u_1(\Delta u_2)^4(\Delta u_3)^2\rangle = 5\langle\Delta u_1(\Delta u_2)^2(\Delta u_3)^4\rangle = \langle\Delta u_1(\Delta u_3)^6\rangle$
N = 8	$\langle(\Delta u_1)^6(\Delta u_2)^2\rangle = \langle(\Delta u_1)^6(\Delta u_3)^2\rangle$ $\langle(\Delta u_1)^4(\Delta u_2)^4\rangle = 3\langle(\Delta u_1)^4(\Delta u_2)^2(\Delta u_3)^2\rangle = \langle(\Delta u_1)^4(\Delta u_3)^4\rangle$ $\langle(\Delta u_1)^2(\Delta u_2)^6\rangle = 30\langle(\Delta u_1)^2(\Delta u_2)^4(\Delta u_3)^2\rangle = 30\langle(\Delta u_1)^2(\Delta u_2)^2(\Delta u_3)^4\rangle = \langle(\Delta u_1)^2(\Delta u_3)^6\rangle$ $\langle(\Delta u_2)^8\rangle = 7\langle(\Delta u_2)^6(\Delta u_3)^2\rangle = \frac{35}{3}\langle(\Delta u_2)^4(\Delta u_3)^4\rangle = 7\langle(\Delta u_2)^2(\Delta u_3)^6\rangle = \langle(\Delta u_3)^8\rangle$

$\nabla \cdot \boldsymbol{D}_{N+1}$) on the l.h.s., on the r.h.s. one has pressure source terms $\langle \boldsymbol{T}_N \rangle$, dissipation source terms $\langle \boldsymbol{E}_N \rangle$ as well as the viscous terms $2\nu\nabla^2 \boldsymbol{D}_N$.

For isotropic turbulence, the statistics do not depend on the orientation of the separation vector r_i, but only its magnitude $r = |r_i|$. This leads to a reduction of components required to completely describe the full tensor. For instance at the fourth order, only three components of the tensor $\langle \Delta u_i \Delta u_j \Delta u_k \Delta u_l \rangle$ are needed, as detailed in appendix A. This greatly simplifies both the analysis as well as the numerical computations involved. Without loss of generality, one may take $r_i = (r, 0, 0)$, i.e. align the separation vector with the x_1-axis. This choice of r_i allows one to express the tensor $\boldsymbol{D}_N$ by Δu_1 and Δu_2 only. For instance, $\langle \Delta u_1 (\Delta u_3)^2 \rangle = \langle \Delta u_1 (\Delta u_2)^2 \rangle$ and $\langle (\Delta u_2)^2 (\Delta u_3)^2 \rangle = \langle (\Delta u_2)^4 \rangle / 3$ and similarly at higher orders, cf. eq. (4.4) of Hill (2001). The resulting relations for $N = 2$ to $N = 8$ are listed in table 3.1. This implies that we do not have to consider transport equations for structure functions with 3-component such as e.g. $\langle (\Delta u_3)^2 \rangle$, since they do not contain additional information. It should be stressed that the relations given in the table are exact under the assumption of isotropy and can therefore be used to check for local isotropy as function of the separation distance r.

In the following, the structure function of order $N = m+n$ is therefore denoted

by

$$D_{m,n} = \langle (\Delta u_1)^m \, (\Delta u_2)^n \rangle \, . \tag{3.20}$$

Note that this choice is somewhat arbitrary but without loss of generality. One could have chosen Δu_3 instead of Δu_2, which would give the same results.

The functional form of the gradient and Laplacian has been calculated by Hill (2001) using a Matrix algorithm* and recently corrected, see `https://arxiv.org/abs/physics/0102063`; they are shown in table 3.2 for $N = 2$ to $N = 8$ for reference. Noticeably, the table suggests that the divergence in the Nth-order structure function equations can be written as

$$\boldsymbol{\nabla} \cdot \boldsymbol{D}_{N+1} = \left(\frac{\partial}{\partial r} + \frac{n+2}{r} \right) D_{m+1,n} - \frac{m}{r} \frac{n+2}{n+1} D_{m-1,n+2} \tag{3.21}$$

and the Laplacian as

$$\begin{aligned} \nabla^2 \boldsymbol{D}_N = & \left(\frac{\partial^2}{\partial r^2} + \frac{2}{r} \frac{\partial}{\partial r} - \frac{n + 2m(n+1)}{r^2} \right) D_{m,n} \\ & + \frac{2}{r^2} \frac{n+2}{n+1} \sum_{\widetilde{N}=1}^{m+n} \left[\widetilde{N} - (n+1) \right] D_{m-2,n+2} + \frac{n^2 - n}{r^2} D_{m+2,n-2}. \end{aligned} \tag{3.22}$$

In eq. (3.21) and eq. (3.22), all structure functions with negative indices are defined to vanish, e.g. $D_{-2,2} \equiv 0$.

Therefore from eq. (3.19), there is a coupling to the next higher-order structure functions via the transport terms $\boldsymbol{\nabla} \cdot \boldsymbol{D}_{N+1}$ and an inter-order coupling by the viscous terms $\nabla^2 \boldsymbol{D}_N$ while the $\langle \boldsymbol{T}_N \rangle$ and $\langle \boldsymbol{E}_N \rangle$ terms act as sources (or sinks, depending on their sign). This tree-like structure is visualised in figure 3.1, where the coupling between different orders is indicated by the red vertical arrows (referring to the transport terms) and the inter-order coupling via the viscous terms by the black horizontal arrows. One therefore finds a system of coupled partial differential equations, where the solutions are obtained by advancing the system in time (or until the system reaches its steady state $\partial \boldsymbol{D}_N / \partial t = 0$ for forced turbulence) with boundary conditions as determined by the viscous range and some initial conditions for the structure functions. However, the resulting system of equations is unclosed due to the coupling to the higher-order

*The computations could be carried out by hand as detailed in appendix A.1 and appendix A.2.1, but doing so is very cumbersome and time-consuming at higher orders.

Table 3.2: Isotropic form of the transport and diffusive terms in the structure function equations for $N = 2$ to $N = 8$ as given by Hill (2001), see `https://arxiv.org/abs/physics/0102063` for the corrected version.

	transport term $\boldsymbol{\nabla} \cdot \boldsymbol{D}_{N+1}$	diffusive term $\nabla^2 \boldsymbol{D}_N$
N = 2	$\left(\partial_r + \frac{2}{r}\right) D_{3,0} - \frac{4}{r} D_{1,2}$ $\left(\partial_r + \frac{4}{r}\right) D_{1,2}$	$\left(\partial_r^2 + \frac{2}{r}\partial_r - \frac{4}{r^2}\right) D_{2,0} + \frac{4}{r^2} D_{0,2}$ $\left(\partial_r^2 + \frac{2}{r}\partial_r - \frac{2}{r^2}\right) D_{0,2} + \frac{2}{r^2} D_{2,0}$
N = 3	$\left(\partial_r + \frac{2}{r}\right) D_{4,0} - \frac{6}{r} D_{2,2}$ $\left(\partial_r + \frac{4}{r}\right) D_{2,2} - \frac{4}{3r} D_{0,4}$	$\left(\partial_r^2 + \frac{2}{r}\partial_r - \frac{6}{r^2}\right) D_{3,0} + \frac{12}{r^2} D_{1,2}$ $\left(\partial_r^2 + \frac{2}{r}\partial_r - \frac{8}{r^2}\right) D_{1,2} + \frac{2}{r^2} D_{3,0}$
N = 4	$\left(\partial_r + \frac{2}{r}\right) D_{5,0} - \frac{8}{r} D_{3,2}$ $\left(\partial_r + \frac{4}{r}\right) D_{3,2} - \frac{8}{3r} D_{1,4}$ $\left(\partial_r + \frac{6}{r}\right) D_{1,4}$	$\left(\partial_r^2 + \frac{2}{r}\partial_r - \frac{8}{r^2}\right) D_{4,0} + \frac{24}{r^2} D_{2,2}$ $\left(\partial_r^2 + \frac{2}{r}\partial_r - \frac{14}{r^2}\right) D_{2,2} + \frac{2}{r^2} D_{4,0} + \frac{8}{3r^2} D_{0,4}$ $\left(\partial_r^2 + \frac{2}{r}\partial_r - \frac{4}{r^2}\right) D_{0,4} + \frac{12}{r^2} D_{2,2}$
N = 5	$\left(\partial_r + \frac{2}{r}\right) D_{6,0} - \frac{10}{r} D_{4,2}$ $\left(\partial_r + \frac{4}{r}\right) D_{4,2} - \frac{12}{3r} D_{2,4}$ $\left(\partial_r + \frac{6}{r}\right) D_{2,4} - \frac{6}{5r} D_{0,6}$	$\left(\partial_r^2 + \frac{2}{r}\partial_r - \frac{10}{r^2}\right) D_{5,0} + \frac{40}{r^2} D_{3,2}$ $\left(\partial_r^2 + \frac{2}{r}\partial_r - \frac{20}{r^2}\right) D_{3,2} + \frac{2}{r^2} D_{5,0} + \frac{8}{r^2} D_{1,4}$ $\left(\partial_r^2 + \frac{2}{r}\partial_r - \frac{14}{r^2}\right) D_{1,4} + \frac{12}{r^2} D_{3,2}$
N = 6	$\left(\partial_r + \frac{2}{r}\right) D_{7,0} - \frac{12}{r} D_{5,2}$ $\left(\partial_r + \frac{4}{r}\right) D_{5,2} - \frac{16}{3r} D_{3,4}$ $\left(\partial_r + \frac{6}{r}\right) D_{3,4} - \frac{12}{5r} D_{1,6}$ $\left(\partial_r + \frac{8}{r}\right) D_{1,6}$	$\left(\partial_r^2 + \frac{2}{r}\partial_r - \frac{12}{r^2}\right) D_{6,0} + \frac{60}{r^2} D_{4,2}$ $\left(\partial_r^2 + \frac{2}{r}\partial_r - \frac{26}{r^2}\right) D_{4,2} + \frac{2}{r^2} D_{6,0} + \frac{16}{r^2} D_{2,4}$ $\left(\partial_r^2 + \frac{2}{r}\partial_r - \frac{24}{r^2}\right) D_{2,4} + \frac{12}{r^2} D_{4,2} + \frac{12}{5r^2} D_{0,6}$ $\left(\partial_r^2 + \frac{2}{r}\partial_r - \frac{6}{r^2}\right) D_{0,6} + \frac{30}{r^2} D_{2,4}$
N = 7	$\left(\partial_r + \frac{2}{r}\right) D_{8,0} - \frac{14}{r} D_{6,2}$ $\left(\partial_r + \frac{4}{r}\right) D_{6,2} - \frac{20}{3r} D_{4,4}$ $\left(\partial_r + \frac{6}{r}\right) D_{4,4} - \frac{18}{5r} D_{2,6}$ $\left(\partial_r + \frac{8}{r}\right) D_{2,6} - \frac{8}{7r} D_{0,8}$	$\left(\partial_r^2 + \frac{2}{r}\partial_r - \frac{14}{r^2}\right) D_{7,0} + \frac{84}{r^2} D_{5,2}$ $\left(\partial_r^2 + \frac{2}{r}\partial_r - \frac{32}{r^2}\right) D_{5,2} + \frac{2}{r^2} D_{7,0} + \frac{80}{3r^2} D_{3,4}$ $\left(\partial_r^2 + \frac{2}{r}\partial_r - \frac{34}{r^2}\right) D_{3,4} + \frac{12}{r^2} D_{5,2} + \frac{36}{5r^2} D_{1,6}$ $\left(\partial_r^2 + \frac{2}{r}\partial_r - \frac{20}{r^2}\right) D_{1,6} + \frac{30}{r^2} D_{3,4}$
N = 8	$\left(\partial_r + \frac{2}{r}\right) D_{9,0} - \frac{16}{r} D_{7,2}$ $\left(\partial_r + \frac{4}{r}\right) D_{7,2} - \frac{8}{r} D_{5,4}$ $\left(\partial_r + \frac{6}{r}\right) D_{5,4} - \frac{24}{5r} D_{3,6}$ $\left(\partial_r + \frac{8}{r}\right) D_{3,6} - \frac{16}{7r} D_{1,8}$ $\left(\partial_r + \frac{10}{r}\right) D_{1,8}$	$\left(\partial_r^2 + \frac{2}{r}\partial_r - \frac{16}{r^2}\right) D_{8,0} + \frac{112}{r^2} D_{6,2}$ $\left(\partial_r^2 + \frac{2}{r}\partial_r - \frac{38}{r^2}\right) D_{6,2} + \frac{2}{r^2} D_{8,0} + \frac{40}{r^2} D_{4,4}$ $\left(\partial_r^2 + \frac{2}{r}\partial_r - \frac{44}{r^2}\right) D_{4,4} + \frac{12}{r^2} D_{6,2} + \frac{72}{5r^2} D_{2,6}$ $\left(\partial_r^2 + \frac{2}{r}\partial_r - \frac{34}{r^2}\right) D_{2,6} + \frac{30}{r^2} D_{4,4} + \frac{16}{7r^2} D_{0,8}$ $\left(\partial_r^2 + \frac{2}{r}\partial_r - \frac{8}{r^2}\right) D_{0,8} + \frac{56}{r^2} D_{2,6}$

structure functions stemming from the transport term, i.e. the closure problem of turbulence. Well-known closures to overcome this issue are the quasi-normal (QN) approximation and its modifications (see Lesieur (1997) and references therein for an overview), where traditionally the fourth-order structure functions are expressed in terms of the square of the second-order structure functions by assuming a vanishing fourth-order cumulant. A similar closure could be conceivable introduced at higher orders. Another approach is to close the system using an eddy viscosity ansatz of the form $\boldsymbol{D}_{N+1} = \nu_{t,(N+1)}(\partial \boldsymbol{D}_N/\partial r)$, see e.g. Oberlack and Peters (1993) or more recently Thiesset et al. (2013). We briefly discuss this possibility in section 3.4 below. The closure of Oberlack and Peters (1993) was used by Schaefer et al. (2011) and is also employed in section 5.3 below to close the second-order equations; it is found to be in very good agreement with DNS data. In any case, the source terms $\langle \boldsymbol{T}_N \rangle$ (eq. (3.13)) and $\langle \boldsymbol{E}_N \rangle$ (eq. (3.14)) need to be closed and the resulting closure may introduce additional coupling between orders and structure functions. Source term closures have been developed e.g. by Gotoh and Nakano (2003) and Yakhot (2001, 2003), but are not discussed here in the following*. Note that it is possible to derive equations for the source terms, cf. section 3.1.3 for the fourth-order dissipation source terms. One could similarly proceed at higher orders. However, these equations contain additional unclosed terms.

The system of structure function equations is complemented by two equations relating the second- and third-order structure functions,

$$\frac{\partial D_{2,0}}{\partial r} + \frac{2}{r} D_{2,0} - \frac{2}{r} D_{0,2} = 0 \tag{3.23}$$

and

$$\frac{\partial D_{3,0}}{\partial r} + \frac{1}{r} D_{3,0} - \frac{6}{r} D_{1,2} = 0 \tag{3.24}$$

derived from the continuity equation, cf. e.g. Monin and Yaglom (1975). However, there are no analogous higher-order relations.

If the flow is statistically steady, the derivatives with respect to time may be neglected. For that reason, the unsteady terms $\partial \boldsymbol{D}_N/\partial t$ are not discussed in the numerical analysis of the structure functions below in section 3.2 and section 3.3.

*Possible attempts at closing the source terms are briefly sketched in appendix B but not further pursued here.

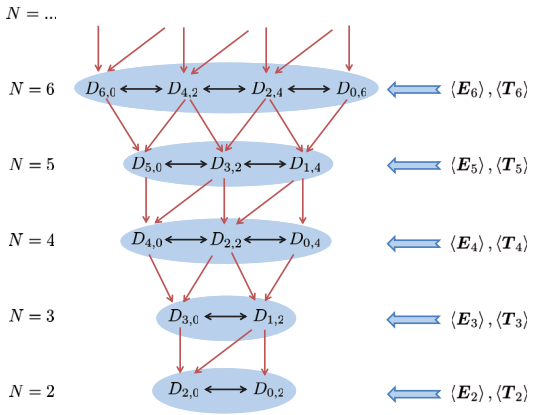

Figure 3.1: System of structure function equations and coupling between different orders.

Viscous range $r \to 0$

For $r \to 0$, $\boldsymbol{D}_N \sim r^N$ to leading order as can be seen by expanding the structure functions in Taylor series,

$$D_{m,n} = \left\langle \left(\frac{\partial u_1}{\partial x_1} \right)^m \left(\frac{\partial u_2}{\partial x_1} \right)^n \right\rangle r^N, \tag{3.25}$$

since the separation vector r_i and the x_1-axis are aligned. Similarly, the pressure source terms $\langle \boldsymbol{T}_N \rangle \sim r^N$, while the dissipation source terms are to leading order $\langle \boldsymbol{E}_N \rangle \sim r^{N-2}$, because $\epsilon_{ij} + \epsilon'_{ij} \to 2\epsilon_{ij}$ for $r \to 0$. Moreover, the transport terms $\boldsymbol{\nabla} \cdot \boldsymbol{D}_{N+1} \sim r^N$ as well as the viscous terms $\nabla^2 \boldsymbol{D}_N \sim r^{N-2}$. Therefore, the viscous terms are balanced by the dissipation source terms in the viscous range. Consequently, one may neglect the convective terms of order $N+1$ as well as the pressure source terms for small $r \to 0$. This implies that the equations of order N are decoupled from the equations of order $N+1$ (however there might be coupling induced by closing the source terms). In other words, the viscous range is completely determined by the dissipation source terms. At first glance, it would seem that there are as many equations as unknown structure functions for all orders in the viscous range if the dissipation source terms $\langle \boldsymbol{E}_N \rangle$ are known, cf.

figure 3.1 and the right column of table 3.2. However, this is not the case, as not all equations are linearly independent. For instance, at the second order, there are two equations for $D_{2,0}$ and $D_{0,2}$, which are linearly dependent, while at the fourth order, there are three equations for the three unknowns $D_{4,0}$, $D_{2,2}$ and $D_{0,4}$, again one of which can be written as sum of the other two (cf. section 4.3.2 below). Note that there is an additional equation stemming from continuity at $N = 2$ and $N = 3$, i.e. eq. (3.23) and eq. (3.24), which can be used to close the second and third-order equations in the viscous range. The exact results for $N = 2$ were first derived by Kolmogorov (1941a,b) and are briefly discussed in section 3.1.2, while third- and fourth-order results can be found in section 4.3. The viscous range is discussed in more detail in chapter 4 below.

Inertial range

Kolmogorov (1941b) introduced the concept of an inertial range situated between the very small scales and the large integral scales L, $\eta \ll r \ll L$. In the inertial range, viscosity has a negligible influence and therefore the viscous terms $2\nu\nabla^2 \boldsymbol{D}_N$ can be neglected. In this limit, the structure functions of order $N+1$ are determined by integrating the equations of order N and are completely determined by the source terms $\langle \boldsymbol{E}_N \rangle$ and $\langle \boldsymbol{T}_N \rangle$. Particularly, there are only enough equations to determine the structure functions for *even* orders, e.g. there are four equations for four structure functions $D_{7,0}$, $D_{5,2}$, $D_{3,4}$ and $D_{1,6}$ at the sixth order. If the source terms are known, one can then proceed to successively integrate the equations starting with the equation with the most transversal components (i.e. here $D_{1,6}$). On the other hand, at the fifth order, there are only three equations for four structure functions $D_{6,0}$, $D_{4,2}$, $D_{2,4}$ and $D_{0,6}$ and the same holds for all odd orders. That is, there is the peculiar situation that while it is possible to derive equations for all structure functions at arbitrary order, only odd-order structure functions can be determined using inertial range assumptions without resorting to additional closures, even if the source terms are known. Again, the second order is special inasmuch as the pressure source terms vanish due to isotropy (cf. e.g. Hill (1997)) and the dissipation source terms are proportional to the pseudo-dissipation $\langle \epsilon \rangle$, cf. eq. (3.14)*. This is not the case for all other orders, were the pressure source terms contribute and both source terms depend on r. Kolmogorov (1941b) suggested in combination with dimensional analysis a second similarity hypothesis, namely that structure functions in the

*Noticeably, Kolmogorov's equation eq. (1.31) contains rather the dissipation $\langle \varepsilon \rangle$ instead of the pseudo-dissipation $\langle \epsilon \rangle$. This apparent discrepancy is resolved due to $\langle \epsilon \rangle = \langle \varepsilon \rangle$ under the constraints of homogeneity and isotropy, cf. e.g. section 4.2.1 below.

inertial range should be determined by $\langle\varepsilon\rangle$ and r only; consequently, they would follow a power-law in the inertial range,

$$D_{m,n} \sim \left(\langle\varepsilon\rangle\, r\right)^{(m+n)/3}, \tag{3.26}$$

i.e. have power-law scaling with order-dependent exponents $\zeta_{m,n} = (m+n)/3$. This implicitly assumes that there are no correlations between velocity increments and the pseudo-dissipation, i.e. assumes that

$$\langle \boldsymbol{E}_N \rangle \sim \left\{ \langle (\Delta u_i \Delta u_j ...) \rangle \, \langle (\epsilon_{kl} + \epsilon'_{kl}) \rangle \right\}, \tag{3.27}$$

noting that due to homogeneity $\langle\epsilon_{kl}\rangle = \langle\epsilon'_{kl}\rangle$ and due to isotropy $\langle\epsilon_{kl}\rangle = \langle\epsilon\rangle\delta_{kl}$, $\langle\epsilon\rangle = \langle\varepsilon\rangle$. However, this assumption does not hold for the dissipation source terms except trivially for the second-order equations.

Indeed, the exponents $\zeta_{m,n}$ are found to be smaller than $(m+n)/3$ for $m+n > 3$, with the deviations increasing with increasing order. This observation, which implies a negative correlation between $\Delta u_i \Delta u_j ...$ and $(\epsilon_{kl} + \epsilon'_{kl})$, is known as anomalous scaling; measurements and simulations of many different flow types and Reynolds numbers confirm that $\zeta_{m,n} < (m+n)/3$, cf. e.g. Anselmet et al. (1984), Attili and Bisetti (2012), Benzi et al. (1995), and Gotoh et al. (2002) as well as the scaling exponents computed from datasets R5 and R6 below.

Simultaneously, a lot of theoretical work has been done to determine the longitudinal scaling exponents $\zeta_{N,0}$*, the most important one probably being the refined similarity hypothesis as presented by Kolmogorov (1962) which shaped most consecutive work.

The K41 theory of Kolmogorov (1941b) had postulated that ν and $\langle\varepsilon\rangle$ are the only scaling parameters for the entire distribution function of two-point velocity differences, cf. section 1.4. Because only two quantities with different physical units are needed to non-dimensionalise the structure function equations, this was viewed as a claim for universality. However, Landau has argued that universality would be violated by variations of the dissipation at the large scales (cf. Landau and Lifshitz (1959), Frisch (1995)). To address Landau's criticism, Kolmogorov† suggested to replace $\langle\epsilon\rangle^{(m+n)/3}$ in eq. (3.26) by $\langle\varepsilon_r^{(m+n)/3}\rangle$, where ε_r is the dissipation locally averaged over a sphere of radius r. Thus, he effectively

*Mixed and transverse scaling exponents have received much less attention, at least regarding theoretical work. See e.g. Chen et al. (1997) for a modification based on phenomenology explicitly taylored for transverse structure functions, where rather sphere-averaged moments of the enstrophy ω_r^2 instead of ε_r are used.

†Kolmogorov (1962) attributes this ansatz to Obukhov, see e.g. Obukhov (1962).

incorporated the r-dependence of the source terms into $\langle \varepsilon_r^{(m+n)/3} \rangle$, i.e. assumed that

$$D_{N,0} \sim \left\langle \varepsilon_r^{N/3} \right\rangle r^{N/3}. \tag{3.28}$$

This ansatz is also known in the literature as refined similarity hypothesis (RSH). Kolmogorov then assumed a log-normal distribution for ε_r, which yields

$$D_{N,0} \sim \langle \varepsilon \rangle^{N/3} r^{N/3} \left(\frac{r}{L} \right)^{\mu N(3-N)/18}, \tag{3.29}$$

i.e. used this to predict the inertial range scaling exponents $\zeta_{N,0}$ as

$$\zeta_{N,0} = \frac{N}{3} + \frac{\mu N}{18}(3 - N), \tag{3.30}$$

where μ is a model parameter, sometimes called intermittency constant. General consensus is that $\mu = 0.25 \pm 0.05$ is the "best estimate", cf. Sreenivasan and Kailasnath (1993). However, the log-normal model is not without its drawbacks. It is readily seen that for any $\mu > 0$, $\zeta_{N,0}$ decreases after exceeding some value of N due to the quadratic term, which is at odds with measurements and DNS data in the literature and which violates the Hölder inequality, see p. 133f of Frisch (1995). From another point of view, it is well-known that the pdf of the dissipation is not log-normal. While its core (and consequently the lower moments) can be approximated by a log-normal distribution reasonably well, the tails differ significantly. Consequently, the log-normal assumption does not capture the higher-order scaling exponents*. It should be noted though that the shortcomings of the log-normal model do not necessarily imply that eq. (3.28) is invalid.

While this modification of Kolmogorov's previous theory is based on phenomenology, it paved the way for the multi-fractal theory, which is in excellent agreement with experimental and numerical data, see e.g. Nelkin (1994) or Sreenivasan and Antonia (1997) and references therein as well as Paladin and Vulpiani (1987a) for an extensive overview. Meneveau and Sreenivasan (1989, 1991) examined multi-fractal behaviour of ε_r in detail, for which they found very good agreement with their experimental data. Assuming multi-fractality of ε_r, Meneveau and Sreenivasan (1987) proposed a model based on the idea that the energy contained in one eddy is transported towards two smaller eddies, each of which receiving a fraction p and $1 - p$ of the larger eddy's energy. With

*The connection between moments of the dissipation and scaling exponents is more closely examined in section 5.2 below.

eq. (3.28), the p-model then yields

$$\zeta_{N,0} = \frac{N}{3} - \log_2\left(p^{N/3} + (1-p)^{N/3}\right) - \left(\frac{N}{3} - 1\right), \tag{3.31}$$

where $p = 0.7$ gives good agreement with experimental data.

Different to the multi-fractal framework, She and Leveque (1994) proposed a hierarchy of powers of the dissipation moments defined by successive moments $\langle \varepsilon_r^{M+1} \rangle / \langle \varepsilon_r^M \rangle$. The She-Leveque model yields

$$\zeta_{N,0} = \frac{N}{9} + 2\left[1 - \left(\frac{2}{3}\right)^{N/3}\right], \tag{3.32}$$

which is in excellent agreement with data from the literature and does not contain a model parameter. She and Waymire (1995) as well as Dubrulle (1994) found that the She-Leveque model amounts to assuming a log-poisson distribution of the dissipation.

There are many more models presented and described in the literature, e.g. the β-model cf. Frisch et al. (1978), models based on a mean-field theory proposed by Yakhot (Kurien and Sreenivasan (2001) and Yakhot (2001)) other models based on multi-fractality (e.g. Schumacher et al. (2007) and Yakhot (2006)), fusion rules which generalise from two-point differences to multi-point differences (L'vov and Procaccia (1995, 1996a,b)) and many more not listed here.

Noticeably, most models assume eq. (3.28). While the 4/5-law eq. (1.31) is based on the Navier-Stokes equations, RSH remains a phenomenological model. However, since dissipation fluctuations must be contained in the Navier-Stokes equations, the parameters describing them should be hidden somewhere in the equations for the higher-order structure functions or in additional equations related to them. More specifically, the moments of the dissipation distribution function should appear in averaged two-point equations derived from the Navier-Stokes equations. For that reason, one would expect to find the moments $\langle \varepsilon_r^{(m+n)/3} \rangle$ in the system of equations. For $N = 2$, the K62 assumption has been proved by Hill (2002) by spherical integration of the second-order trace equations, resulting in

$$D_{[3]} = 2\nu \frac{\partial D_{[2]}}{\partial r} - \frac{4r}{3} \langle \varepsilon_r \rangle \tag{3.33}$$

(eq. (3.22) in Hill (2002)) where $D_{[3]} = D_{3,0} + 2D_{1,2}$ and $D_{[2]} = D_{2,0} + 2D_{0,2}$ are the traces of the third and second-order structure functions. Using incompressibility then yields the 4/5-law (eq. (1.31) and eq. (3.41)). However, similar

results cannot be obtained at higher orders, as $\langle \varepsilon_r^{m+n} \rangle$ does not equal the spherical averages of the trace of the dissipation source terms $\langle \boldsymbol{E}_N \rangle$. Noticeably, the second moment $\langle \varepsilon_r^2 \rangle$ is implicitly found in the transport equation for the fourth-order dissipation source terms (cf. section 3.1.3 and section 5.3), since ε_r^2 is related to the correlation $\langle \varepsilon\varepsilon' \rangle$ which in turn is included in the two-point sum proportional to $\langle (\epsilon + \epsilon')^2 \rangle$ (called here the ε^2-term). However, the ε^2-term is far from being the dominant term in the fourth-order dissipation source term transport equations and indeed is nearly cancelled out from the balance by a different term. Moreover, $\langle \varepsilon_r^2 \rangle$ is found in the fourth-order equations (thus contributing to the *fifth*-order structure functions) and not in the fifth-order equations which would determine the inertial range solutions of the sixth-order structure functions $m + n = 6$, as discussed in section 5.3 in more detail. It should be noted though that RSH assumes that $(\partial D_{N+1,0}/\partial r)/\langle E_{N,0} \rangle = const.$ (cf. section 5.1), which is found to be in good agreement with the DNS data of section 2.1.

If one assumes that the structure functions follow a power-law in the inertial range of the form

$$D_{m,n} = C_{m,n} r^{\zeta_{m,n}}, \tag{3.34}$$

the scaling exponents $\zeta_{m,n}$ (as well as the prefactors $C_{m,n}$) have to be contained in the system of equations. Obviously, this is only the case if also the source terms follow a power-law in the inertial range. Noticeably, the sum of two pure power-laws $P_1 = A_1 r^{\alpha_1}$ and $P_2 = A_2 r^{\alpha_2}$ (with A_1, A_2 and α_1 and α_2 being constants) only results exactly in a *pure* power-law $P_3 = P_1 + P_2$ if $\alpha_1 = \alpha_2 = \alpha_3$. In other words, a scaling as eq. (3.34) with r-independent $C_{m,n}$ and $\zeta_{m,n}$ would require all pressure source terms and dissipation source terms at a given order to have pure power-law scaling with the same exponent $\zeta_{m,n} - 1$ as well as r-independent prefactors or cancellation of some of the terms in the balance equations. Similarly, one can derive equations for the terms in the source term equations, and so on ad infinitum, implying that all terms stemming from the dissipation and pressure source terms of a certain order have to scale the same or cancel out to have a pure power-law for the respective structure function as defined by eq. (3.34). Then, the longitudinal, mixed and transverse structure function exponents $\zeta_{m,n}$ will also be the same at every order by definition, since the transverse feed into the mixed and the mixed into the longitudinal structure functions, cf. the red vertical arrows in figure 3.1 and the left column of table 3.2. On the other hand, if $P_1 \gg P_2$ or if $\alpha_1 \approx \alpha_2$, the result is an *approximate* power-law. By this, we mean that $P_3 = P_1 + P_2$ is not a power-law, but can be approximated by one reasonably well. This would require terms with inertial

range scaling different from the transport terms to be negligible.

Naturally, the third-order structure functions have the same r-dependence, since the pressure source terms vanish and the dissipation source terms are proportional to the pseudo-dissipation $\langle\epsilon\rangle$ and do not depend on r. The same holds for the second-order structure functions if power-laws are assumed, since they are related by the continuity equation (3.23). However, the situation is different at higher orders, as their source terms are not constant but depend on r and there are no relations between higher-order structure functions stemming from continuity as mentioned above. Rather, there are terms in the source term equations which are (nearly) constant. For instance the ε^2-term is nearly independent of r in the inertial range, cf. section 3.1.3, while other terms in the fourth-order dissipation source term equations show a clear r-dependence. Consequently, the source terms $\langle E_{4,0}\rangle$ etc. are also mixtures of different power-laws at best (if one approximates their source terms by power-laws in the inertial range), i.e. cannot be pure power-laws themselves. Similar characteristics are encountered at higher orders.

There are several approaches to determine the scaling exponents $\zeta_{m,n}$. For instance, one could fit eq. (3.34) to data of $D_{m,n}$. However, the range for which such a power-law can be observed is very limited for the Reynolds numbers obtainable from DNS as of writing, such as the DNS of chapter 2. For that reason, it is somewhat difficult to choose the range of the fit. This issue is somewhat mitigated by using extended self similarity (ESS), as introduced by Benzi et al. (1993) and Benzi et al. (1995) (but see also the more critical discussion in Grossmann et al. (1997)). Using ESS, one plots the structure functions not over r, but rather over other structure functions, in the hope that this leads to cancellation of errors and fluctuations. Since odd-order structure functions can be negative or undergo a change of sign, one usually considers rather the moments of the absolute value of the velocity difference,

$$\widehat{D}_{m,n} = \langle |\Delta u_1|^m \, |\Delta u_2|^m \rangle \,. \tag{3.35}$$

Employing ESS, one then has to assume that the scaling exponents $\xi_{m,n}$ of

$$\widehat{D}_{m,n} = \widehat{C}_{m,n} r^{\xi_{m,n}} \tag{3.36}$$

equal those of $D_{m,n}$, i.e. $\xi_{m,n} = \zeta_{m,n}$. To determine $\zeta_{2,0}$, one would plot e.g. $\widehat{D}_{2,0}$ over $\widehat{D}_{3,0}$ in a log-log graph and then fit a straight line. Since by assumption $\xi_{3,0} = \zeta_{3,0} = 1$, the slope of the fit equals $\xi_{2,0} = \zeta_{2,0}$. However, there is still the issue which part to fit, which could lead to different vales of $\xi_{2,0} = \zeta_{2,0}$.

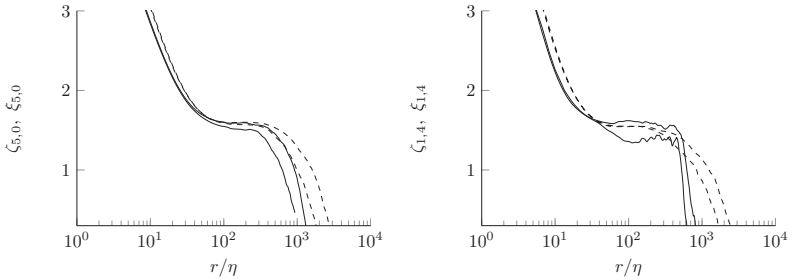

Figure 3.2: Scaling exponents $\zeta_{5,0}$ (solid lines) and $\xi_{5,0}$ (dashed lines) (a) and $\zeta_{1,4}$ (solid lines) and $\xi_{1,4}$ (dashed lines) (b) as computed by eq. (3.37) for datasets R5 and R6.

Another approach is to compute the local slope

$$\zeta_{m,n} = \frac{r}{D_{m,n}} \frac{\partial D_{m,n}}{\partial r}, \quad \xi_{m,n} = \frac{r}{\widehat{D}_{m,n}} \frac{\partial \widehat{D}_{m,n}}{\partial r}, \tag{3.37}$$

where r-independent prefactors and scaling exponents are assumed. This gives reasonable results for even orders*. For odd orders, however, the scaling exponents converge much slower. This can be ameliorated by again using $\widehat{D}_{m,n}$ and thus computing rather $\xi_{m,n}$ instead of $\zeta_{m,n}$, which converge much quicker. However, it should be kept in mind that this assumes the same scaling behaviour of $D_{m,n}$ and $\widehat{D}_{m,n}$. In figure 3.2a, both $\zeta_{5,0}$ (solid lines) and $\xi_{5,0}$ (dashed lines) as well as $\zeta_{1,4}$ (solid lines) and $\xi_{1,4}$ (dashed lines) (figure 3.2b) as computed by eq. (3.37) are shown for the two datasets R5 ($Re_\lambda = 529$) and R6 ($Re_\lambda = 754$). Clearly, $\xi_{5,0}$ and $\xi_{1,4}$ are better converged than $\zeta_{5,0}$ and $\zeta_{1,4}$ and the higher the order and the larger n at fixed $N = m + n$, the larger the difference in statistical convergence. However, it is unclear whether indeed $\zeta_{5,0} = \xi_{5,0}$ and $\zeta_{1,4} = \xi_{1,4}$.

Nevertheless, following tentatively the literature, $\zeta_{m,n} = \xi_{m,n}$ is assumed for the rest of this section, although the different symbols are kept. The numerical values of $\xi_{m,n}$ up to the 10th order are listed in table 3.3 for the two cases R5 and R6. It should be emphasised that the higher the order, the larger

*Of course, for even orders $\xi_{m,n} = \zeta_{m,n}$ by definition.

Table 3.3: Scaling exponents $\xi_{m,n}$ up to the 10th order as computed by eq. (3.37) for datasets R5/R6.

	$n=0$	$n=2$	$n=4$	$n=6$	$n=8$	$n=10$
$\zeta_{2-n,n}$	0.719/0.724	0.718/0.720				
$\xi_{3-n,n}$	1.033/1.044	1.027/1.032				
$\zeta_{4-n,n}$	1.317/1.335	1.308/1.315	1.292/1.299			
$\xi_{5-n,n}$	1.571/1.600	1.557/1.567	1.544/1.548			
$\zeta_{6-n,n}$	1.792/1.838	1.774/1.793	1.759/1.764	1.710/1.730		
$\xi_{7-n,n}$	1.975/2.051	1.952/1.988	1.934/1.962	1.900/1.931		
$\zeta_{8-n,n}$	2.125/2.236	2.095/2.169	2.080/2.143	2.065/2.102	1.961/1.987	
$\xi_{9-n,n}$	2.342/2.434	2.247/2.326	2.174/2.262	2.163/2.246	2.092/2.181	
$\zeta_{10-n,n}$	2.494/2.615	2.356/2.486	2.275/2.417	2.230/2.394	2.207/2.309	2.151/2.222

the uncertainty and the less exact the values. Nevertheless, we find very good agreement with $\xi_{m,n}$ reported in the literature as detailed below. Noticeably, there is still a small influence of the Reynolds number, while the differences of longitudinal, mixed and transverse scaling exponents is more pronounced. Particularly, $\zeta_{N,0} > \zeta_{N-2,2} > \zeta_{N-4,4} > \zeta_{N-6,6} > \zeta_{N-8,8} > \zeta_{N-10,10}$ for all $N = 2 \ldots 10$ computed from both datasets R5 and R6, in agreement with the findings of Gotoh et al. (2002) at lower Reynolds numbers. The scaling exponents computed from the datasets R5 and R6 are plotted together with $\xi_{m,n}$ from the literature in figure 3.3a: forced homogeneous isotropic turbulence (Gotoh et al. (2002)) where $\xi_{m,n}$ were computed via the local slope (eq. (3.37)), measurements of duct flow and two jets (Anselmet et al. (1984)), windtunnel measurements using jets, cylinders and grids (Benzi et al. (1995)) where the scaling exponents were computed using ESS, wind measurements using ESS (Kurien and Sreenivasan (2001)) as well as hot wire measurements in a wind tunnel for two different Reynolds numbers, both with shear and without (Shen and Warhaft (2002)). In figure 3.3a, the symbols indicate the averages of the respective scaling exponents; the bars are not error-bars, but denote the maximal and minimal values of $\xi_{m,n}$ found in the listed literature. Because there are less measurements of higher-order $\xi_{m,n}$, the bars are narrower for higher N. This does not mean that the higher-order $\xi_{m,n}$ are more accurate. The exponents are sorted by their number of 2-components: Longitudinal scaling exponents $\xi_{N,0}$ are denoted by a blue $\circ$ symbol, mixed and transverse with red $\square$ ($\xi_{N-2,2}$), black $\diamond$ ($\xi_{N-4,4}$), green $\triangledown$ ($\xi_{N-6,6}$), orange $\triangle$ ($\xi_{N-8,8}$) and purple $\star$ ($\xi_{N-10,10}$). As can be seen in figure 3.3a, longitudinal, mixed and transverse scaling exponents

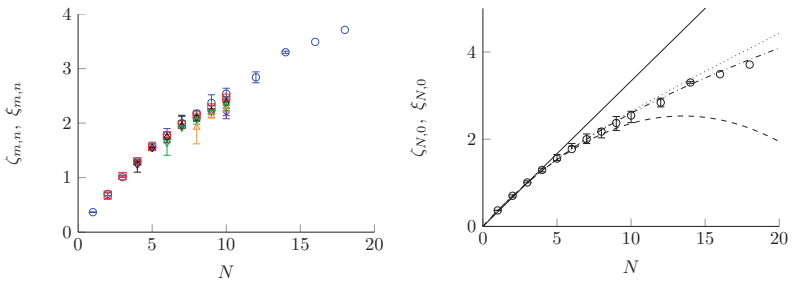

Figure 3.3: Averaged scaling exponents from the literature and DNS cases $R5$ and $R6$ as described in the text, where the bars indicate maximum and minimum values of $\xi_{m,n}$ (a). Averaged longitudinal scaling exponents $\zeta_{N,0}$ and $\xi_{N,0}$ as described in the text; solid line: K41 prediction, dashed line: Log-normal model with $\mu = 0.25$, dotted line: p-model with $p = 0.7$, dash-dotted line: She-Leveque model (b).

clearly differ and the difference increases with increasing order N.

Finally, the longitudinal exponents $\xi_{N,0}$ are shown in figure 3.3b together with the model predictions eq. (3.26), eq. (3.29), eq. (3.31) and eq. (3.32) described above. The longitudinal scaling exponents seem to collapse onto a single curve, if one attributes the small differences to measurement uncertainties. Clearly, K41 theory $\zeta_{N,0} = N/3$ (solid line) does not accurately predict higher-order scaling exponents, and similarly the K62 model (dashed line) for $N > 8$. While both the She-Leveque model (dash-dotted line) and the p-model (dotted line) give reasonable results, only the She-Leveque model seems to capture the behaviour at large N^*. The large N limit will be briefly discussed in section 5.2 below.

3.1.2 Second- and fourth-order structure function equations

In chapter 4 and chapter 5, we will look at the second and fourth order in more detail. For that reason, we list here the required equations specifically. We begin with the second-order structure function equations.

*This should be taken *cum grano salis*, since there is not much data available for high N and measurement uncertainties increase with increasing order.

Second-order structure function equations

A second-order two-point tensor with interchangeable indices such as $\langle \Delta u_i \Delta u_j \rangle$ is completely determined by two of its components under the assumption of isotropy. Therefore, we have the two equations

$$\frac{\partial D_{2,0}}{\partial t} + \frac{1}{r^2}\frac{\partial r^2 D_{3,0}}{\partial r} - \frac{4}{r} D_{1,2} = 2\nu \left[\frac{\partial^2 D_{2,0}}{\partial r^2} + \frac{2}{r}\frac{\partial D_{2,0}}{\partial r} + \frac{4}{r^2}\left(D_{0,2} - D_{2,0}\right) \right] - \frac{4}{3}\langle \epsilon \rangle \quad (3.38)$$

and

$$\frac{\partial D_{0,2}}{\partial t} + \frac{1}{r^4}\frac{\partial r^4 D_{1,2}}{\partial r} = 2\nu \left[\frac{\partial^2 D_{0,2}}{\partial r^2} + \frac{2}{r}\frac{\partial D_{0,2}}{\partial r} - \frac{2}{r^2}\left(D_{0,2} - D_{2,0}\right) \right] - \frac{4}{3}\langle \epsilon \rangle , \quad (3.39)$$

under the additional assumption of homogeneity, where $\langle E_{2,0} \rangle = 4\langle \epsilon_{11} \rangle = 4\langle \epsilon \rangle / 3$ and $\langle E_{0,2} \rangle = 4\langle \epsilon_{22} \rangle = 4\langle \epsilon \rangle / 3$, where $\langle \epsilon \rangle$ is the mean of the pseudo-dissipation defined by eq. (1.15) and ν the kinematic viscosity. Under the assumption of homogeneity and continuity, $\langle \epsilon \rangle = \langle \varepsilon \rangle$, where ε is the mean dissipation of kinetic energy, defined by eq. (1.13).

The two equations (3.38) and (3.39) are analogous to eq. (1.27) derived by Kolmogorov (1941a) from the Kármán-Howarth equation (cf. Kármán and Howarth (1938)). Due to isotropy, the pressure source terms $\langle T_{2,0} \rangle = 0$ and $\langle T_{0,2} \rangle = 0$, cf. Hill (1997) and the second-order dissipation source terms $\langle E_{2,0} \rangle$ and $\langle E_{0,2} \rangle$ are independent of r. Therefore, one can consider $\langle \epsilon \rangle$ as external parameter and *all source terms are known at the second order*. This is not the case at higher orders, as will be seen below; there, also the pressure source terms contribute and both $\langle \boldsymbol{T}_N \rangle$ and $\langle \boldsymbol{E}_N \rangle$ depend on r.

Noticeably, there are two equations for four unknowns ($D_{2,0}$, $D_{0,2}$, $D_{3,0}$ and $D_{1,2}$). However for very large Reynolds numbers, the ratio of the largest to the smallest scales increases, i.e. a scale separation occurs. Therefore, the viscous terms may be neglected in the inertial range (cf. section 1.4) and there are two equations for the two unknown third-order structure functions $D_{3,0}$ and $D_{1,2}$ as discussed in section 3.1.1 if the flow is steady, i.e. when the unsteady terms are

neglected. Then, one can integrate eq. (3.39) in r*, which yields

$$D_{1,2} = -\frac{4}{15}\,\langle\epsilon\rangle\, r \tag{3.40}$$

since $\langle\epsilon\rangle$ is constant. Inserting this in eq. (3.38), one obtains Kolmogorov (1941a)'s famous result eq. (1.31) the so-called 4/5-law

$$D_{3,0} = -\frac{4}{5}\,\langle\epsilon\rangle\, r, \tag{3.41}$$

if the equality $\langle\epsilon\rangle = \langle\varepsilon\rangle$ is used. Both eqs. (3.40) and (3.41) are exact results under the assumption of isotropy and very large (infinite) Reynolds numbers.

Similarly for $r \to 0$, one may neglect the transport terms and there are two equations for the two unknowns $D_{2,0}$ and $D_{0,2}$ in the viscous range†. This then yields the exact results for the second-order structure functions

$$D_{2,0} = \frac{1}{15}\frac{\langle\epsilon\rangle}{\nu}r^2, \quad D_{0,2} = \frac{2}{15}\frac{\langle\epsilon\rangle}{\nu}r^2. \tag{3.42}$$

Note that again the pseudo-dissipation $\langle\epsilon\rangle$ instead of the dissipation $\langle\varepsilon\rangle$ is found from solving the second-order equations in the viscous range. Since $\langle\epsilon\rangle = \langle\varepsilon\rangle$, this is consistent with the result Kolmogorov (1941a) obtained from the Kármán-Howarth equations as well as the relation

$$15\nu\left\langle\left(\frac{\partial u_1}{\partial x_1}\right)^2\right\rangle = \langle\varepsilon\rangle\,, \quad \frac{15}{2}\nu\left\langle\left(\frac{\partial u_2}{\partial x_1}\right)^2\right\rangle = \langle\varepsilon\rangle\,, \tag{3.43}$$

derived from the general isotropic velocity gradient tensor $\langle(\partial u_i/\partial x_j)(\partial u_k/\partial x_l)\rangle$ under the constraints of homogeneity and continuity, cf. e.g. Hinze (1975) or section 4.2 below.

*Again, one implicitly assumes that $D_{1,2}(r_{\text{start}}) = 0$, where r_{start} indicates the beginning of the inertial range.

†From a Taylor series for $r \to 0$, $D_{2,0} = F_1 r^2$ and $D_{0,2} = F_2 r^2$ where $F_1 = \langle(\partial u_1/\partial x_1)^2\rangle$ and $F_2 = \langle(\partial u_2/\partial x_1)^2\rangle$, cf. eq. (3.25). One then obtains $2\nu(2F_1 + 4F_2) = \frac{4}{3}\langle\epsilon\rangle$ from both eq. (3.38) and eq. (3.39) as first equation and $2F_1 = F_2$ from the continuity equation (3.23) as second equation to solve for the two unknowns F_1 and F_2, resulting in eq. (3.42). One can proceed similarly for the third-order equations, cf. section 4.3.1 below.

Fourth-order structure function equations

For $N = 4$, there are three independent equations under the assumption of isotropy. Specifically, for the longitudinal structure function $D_{4,0}$ one obtains

$$\frac{\partial D_{4,0}}{\partial t} + \frac{\partial D_{5,0}}{\partial r} + \frac{2}{r} D_{5,0} - \frac{8}{r} D_{3,2} = -\langle T_{4,0} \rangle - \langle E_{4,0} \rangle + 2\nu \left[\frac{\partial^2 D_{4,0}}{\partial r^2} + \frac{2}{r} \frac{\partial D_{4,0}}{\partial r} - \frac{8}{r^2} D_{4,0} + \frac{24}{r^2} D_{2,2} \right], \quad (3.44)$$

for the mixed structure function $D_{2,2}$

$$\frac{\partial D_{2,2}}{\partial t} + \frac{\partial D_{3,2}}{\partial r} + \frac{4}{r} D_{3,2} - \frac{8}{3r} D_{1,4} = -\langle T_{2,2} \rangle - \langle E_{2,2} \rangle + 2\nu \left[\frac{2}{r^2} D_{4,0} + \frac{\partial^2 D_{2,2}}{\partial r^2} + \frac{2}{r} \frac{\partial D_{2,2}}{\partial r} - \frac{14}{r^2} D_{2,2} + \frac{8}{3r^2} D_{0,4} \right] \quad (3.45)$$

and for the transverse structure function $D_{0,4}$

$$\frac{\partial D_{0,4}}{\partial t} + \frac{\partial D_{1,4}}{\partial r} + \frac{6}{r} D_{1,4} = -\langle T_{0,4} \rangle - \langle E_{0,4} \rangle + 2\nu \left[\frac{12}{r^2} D_{2,2} + \frac{\partial^2 D_{0,4}}{\partial r^2} + \frac{2}{r} \frac{\partial D_{0,4}}{\partial r} - \frac{4}{r^2} D_{0,4} \right]. \quad (3.46)$$

The explicit derivation of the divergence and Laplacian is given in appendix A.1 and appendix A.2.1. The pressure source terms $\langle T_{4,0} \rangle$, $\langle T_{2,2} \rangle$ and $\langle T_{0,4} \rangle$ are defined as

$$\langle T_{4,0} \rangle = \left\langle 4 \left(\Delta u_1 \right)^3 \Delta P_1 \right\rangle \quad (3.47)$$

$$\langle T_{2,2} \rangle = \left\langle 2 \left(\Delta u_2 \right)^2 \Delta u_1 \Delta P_1 + 2 \left(\Delta u_1 \right)^2 \Delta u_2 \Delta P_2 \right\rangle \quad (3.48)$$

$$\langle T_{0,4} \rangle = \left\langle 4 \left(\Delta u_2 \right)^3 \Delta P_2 \right\rangle, \quad (3.49)$$

where $\Delta P_i = (\partial p / \partial x_i - \partial p' / \partial x_i')$ is the difference of pressure gradients at the two points. The dissipation source terms $\langle E_{4,0} \rangle$, $\langle E_{2,2} \rangle$, and $\langle E_{0,4} \rangle$ are defined

as

$$\langle E_{4,0}\rangle = \left\langle 12\left(\Delta u_1\right)^2\left(\epsilon_{11}+\epsilon'_{11}\right)\right\rangle, \tag{3.50}$$

$$\langle E_{2,2}\rangle = \Big\langle 2\left(\Delta u_2\right)^2\left(\epsilon_{11}+\epsilon'_{11}\right)+8\Delta u_1\Delta u_2\left(\epsilon_{12}+\epsilon'_{12}\right) +2\left(\Delta u_1\right)^2\left(\epsilon_{22}+\epsilon'_{22}\right)\Big\rangle \tag{3.51}$$

$$\langle E_{0,4}\rangle = \left\langle 12\left(\Delta u_2\right)^2\left(\epsilon_{22}+\epsilon'_{22}\right)\right\rangle, \tag{3.52}$$

respectively, with $\epsilon_{ij} = \nu(\partial u_i/\partial x_k)(\partial u_j/\partial x_k)$. Both the pressure source terms $\langle T_{4,0}\rangle$, $\langle T_{2,2}\rangle$ and $\langle T_{0,4}\rangle$ as well as the dissipation source terms $\langle E_{4,0}\rangle$, $\langle E_{2,2}\rangle$ and $\langle E_{0,4}\rangle$ depend on r, i.e. are not constant.

Noticeably, we have three equations for three unknown structure functions under the inertial range assumptions. This implies that we can then integrate the equations starting with eq. (3.46), inserting the solution into eq. (3.45), integrating this equation and then finally solve eq. (3.44), if the source terms are known. This characteristic is found for all even orders, but not for odd orders (cf. also the right column of table 3.2 as well as figure 3.1). In the viscous range, the three equations are linearly dependent, which leads to compatibility constraints as discussed in more detail in section 4.3.2.

3.1.3 Fourth-order dissipation source term equations

The longitudinal, mixed and transverse fourth-order dissipation source term equations are needed for the discussion in section 4.3.2, section 5.3 and to derive an equation for the trace of the fourth-order dissipation source term $\langle E_{[4]}\rangle$ in section 3.3.1. For that reason, they are briefly listed here. A detailed derivation of the individual equations for the fourth-order dissipation source terms can be found in the Archive material Peters et al. (2015) at `https://arxiv.org/abs/1504.07490` and is not reprinted here.

For better readability, the definitions

$$A_{ij} = \frac{\partial u_i}{\partial x_k}\frac{\partial u_j}{\partial x_l}\frac{\partial u_k}{\partial x_l}, \tag{3.53}$$

$$\chi_{ij} = 2\nu\left[\frac{\partial}{\partial x_k}\left(\frac{\partial u_i}{\partial x_l}\right)\frac{\partial}{\partial x_k}\left(\frac{\partial u_j}{\partial x_l}\right)\right], \tag{3.54}$$

$$P_{ij} = \frac{\partial u_i}{\partial x_k} \frac{\partial^2 p}{\partial x_k \partial x_j} \tag{3.55}$$

are used in the following. Since

$$A_{ij} + A_{ji} = 2 \frac{\partial u_i}{\partial x_k} S_{kl} \frac{\partial u_j}{\partial x_l}, \tag{3.56}$$

where $S_{ij} = (\partial u_i/\partial x_j + \partial u_j/\partial x_i)/2$ is the symmetric part of the velocity gradient tensor $\partial u_i/\partial x_j$, it plays a similar role as the vortex stretching term $\omega_i S_{ij} \omega_j$, i.e. is a production term by stretching of the velocity gradient. Furthermore, χ_{ii} can be interpreted as the dissipation of the pseudo-dissipation ϵ.

The transport equation for $\langle E_{4,0} \rangle$ reads

$$\begin{aligned} &\frac{\partial \langle E_{4,0} \rangle}{\partial t} + \frac{\partial \langle \Delta u_1 E_{4,0} \rangle}{\partial r} + \frac{2}{r} \langle \Delta u_1 E_{4,0} \rangle - \frac{8}{r} \langle \Delta u_2 E_{3,1} \rangle = \\ &\qquad 2\nu \left[\frac{\partial^2 \langle E_{4,0} \rangle}{\partial r^2} + \frac{2}{r} \frac{\partial \langle E_{4,0} \rangle}{\partial r} - \frac{8}{r^2} \langle E_{4,0} \rangle + \frac{24}{r^2} \langle E_{2,2} \rangle \right] - \Sigma P^E_{4,0}, \end{aligned} \tag{3.57}$$

where the isotropic form of the transport term $\partial \langle \Delta u_i E_{4,0} \rangle / \partial r_i$ is derived in appendix A.2.2. The sum of source terms is

$$\begin{aligned} \Sigma P^E_{4,0} = {} & 24\nu \left\langle (\Delta u_1)^2 (A_{11} + A'_{11}) \right\rangle + 12\nu \left\langle (\Delta u_1)^2 (\chi_{11} + \chi'_{11}) \right\rangle \\ & + 24 \langle \Delta u_1 \Delta P_1 (\varepsilon_{11} + \varepsilon'_{11}) \rangle + 24\nu \langle \Delta u_1 \Delta u_1 (P_{11} + P'_{11}) \rangle \\ & + 24\nu \left\langle \left(\frac{\partial (\Delta u_1)^2}{\partial x_n} \frac{\partial \varepsilon_{11}}{\partial x_n} + \frac{\partial (\Delta u_1)^2}{\partial x'_n} \frac{\varepsilon'_{11}}{\partial x'_n} \right) \right\rangle + 24 \left\langle (\epsilon_{11} + \epsilon'_{11})^2 \right\rangle. \end{aligned} \tag{3.58}$$

Analogously, for the mixed dissipation source term $\langle E_{2,2} \rangle$ one obtains the transport equation

$$\begin{aligned} &\frac{\partial \langle E_{2,2} \rangle}{\partial t} + \frac{\partial \langle \Delta u_1 E_{2,2} \rangle}{\partial r} + \frac{2}{r} \langle \Delta u_1 E_{2,2} \rangle + \frac{2}{r} \langle \Delta u_2 E_{3,1} \rangle - \frac{8}{3r} \langle \Delta u_2 E_{1,3} \rangle \\ &\quad = 2\nu \left[\frac{\partial^2 \langle E_{2,2} \rangle}{\partial r^2} + \frac{2}{r} \frac{\partial \langle E_{2,2} \rangle}{\partial r} - \frac{14}{r^2} \langle E_{2,2} \rangle + \frac{2}{r^2} \langle E_{4,0} \rangle + \frac{8}{3r^2} \langle E_{0,4} \rangle \right] \\ &\qquad\qquad - \Sigma P^E_{2,2}, \end{aligned} \tag{3.59}$$

where the sum of source terms is

$$\begin{aligned}
\Sigma P^E_{2,2} = {} & 2\nu \left\langle 2\left(\Delta u_1\right)^2 A_{22} + 4\Delta u_1 \Delta u_2 \left(A_{12} + A_{21}\right) + 2\left(\Delta u_2\right)^2 A_{11} \right\rangle \\
& + 2\nu \left\langle 2\left(\Delta u_1\right)^2 A'_{22} + 4\Delta u_1 \Delta u_2 \left(A'_{12} + A'_{21}\right) + 2\left(\Delta u_2\right)^2 A'_{11} \right\rangle \\
& + 2\nu \left\langle \left(\Delta u_1\right)^2 \left(\chi_{22} + \chi'_{22}\right) + 2\Delta u_1 \Delta u_2 \left(\chi_{12} + \chi'_{12}\right) + \left(\Delta u_2\right)^2 \left(\chi_{11} + \chi'_{11}\right) \right\rangle \\
& + 4 \left\langle \Delta u_1 \Delta P_1 \epsilon_{22} + 2\left(\Delta u_1 \Delta P_2 + \Delta u_2 \Delta P_1\right) \epsilon_{12} + \Delta u_2 \Delta P_2 \epsilon_{11} \right\rangle \\
& + 4 \left\langle \Delta u_1 \Delta P_1 \epsilon'_{22} + 2\left(\Delta u_1 \Delta P_2 + \Delta u_2 \Delta P_1\right) \epsilon'_{12} + \Delta u_2 \Delta P_2 \epsilon'_{11} \right\rangle \\
& + 2\nu \left\langle 2\left(\Delta u_1\right)^2 P_{22} + 4\Delta u_1 \Delta u_2 \left(P_{12} + P_{21}\right) + 2\left(\Delta u_2\right)^2 P_{11} \right\rangle \\
& + 2\nu \left\langle 2\left(\Delta u_1\right)^2 P'_{22} + 4\Delta u_1 \Delta u_2 \left(P'_{12} + P'_{21}\right) + 2\left(\Delta u_2\right)^2 P'_{11} \right\rangle \\
& + 4\nu \left\langle \left(\frac{\partial \left(\Delta u_1\right)^2}{\partial x_n} \frac{\partial \epsilon_{22}}{\partial x_n} + 4 \frac{\partial \Delta u_1 \Delta u_2}{\partial x_n} \frac{\partial \epsilon_{12}}{\partial x_n} + \frac{\partial \left(\Delta u_2\right)^2}{\partial x_n} \frac{\partial \epsilon_{11}}{\partial x_n} \right) \right\rangle \\
& + 4\nu \left\langle \left(\frac{\partial \left(\Delta u_1\right)^2}{\partial x'_n} \frac{\epsilon'_{22}}{\partial x'_n} + 4 \frac{\partial \Delta u_1 \Delta u_2}{\partial x'_n} \frac{\epsilon'_{12}}{\partial x'_n} + \frac{\partial \left(\Delta u_2\right)^2}{\partial x'_n} \frac{\epsilon'_{11}}{\partial x'_n} \right) \right\rangle \\
& + 8 \left\langle \left(\epsilon_{11} + \epsilon'_{11}\right)\left(\epsilon_{22} + \epsilon'_{22}\right) + 2\left(\epsilon_{12} + \epsilon'_{12}\right)\left(\epsilon_{12} + \epsilon'_{12}\right) \right\rangle . \quad (3.60)
\end{aligned}$$

The transport equation for the transverse dissipation source term $\langle E_{0,4} \rangle$ is

$$\begin{aligned}
& \frac{\partial \langle E_{0,4} \rangle}{\partial t} + \frac{\partial \langle \Delta u_1 E_{0,4} \rangle}{\partial r} + \frac{2}{r} \langle \Delta u_1 E_{0,4} \rangle + \frac{4}{r} \langle \Delta u_2 E_{1,3} \rangle = \\
& \qquad 2\nu \left[\frac{\partial^2 \langle E_{0,4} \rangle}{\partial r^2} + \frac{2}{r} \frac{\partial \langle E_{0,4} \rangle}{\partial r} - \frac{4}{r} \langle E_{0,4} \rangle + \frac{12}{r^2} \langle E_{2,2} \rangle \right] - \sum P^E_{0.4}, \quad (3.61)
\end{aligned}$$

where the sum of the source term is

$$\begin{aligned}
\sum P^E_{0,4} = {} & 24\nu \left\langle \left(\Delta u_2\right)^2 \left(A_{2,2} + A'_{2,2}\right) \right\rangle + 12\nu \left\langle \left(\Delta u_2\right)^2 \left(\chi_{22} + \chi'_{22}\right) \right\rangle \\
& + 24 \left\langle \Delta u_2 \Delta P_2 (\epsilon_{22} + \epsilon'_{22}) \right\rangle + 24\nu \left\langle \Delta u_2^2 (P_{22} + P'_{22}) \right\rangle \\
& + 24\nu \left\langle \frac{\partial \Delta u_2^2}{\partial x_n} \frac{\partial \epsilon_{22}}{\partial x_n} + \frac{\partial \Delta u_2^2}{\partial x'_n} \frac{\partial \epsilon'_{22}}{\partial x'_n} \right\rangle + 24 \left\langle \left(\epsilon_{22} + \epsilon'_{22}\right)^2 \right\rangle . \quad (3.62)
\end{aligned}$$

Again, the isotropic form of the transport terms is derived in appendix A.2.2. Noticeably, they differ from the transport terms in the fourth-order structure function equations, since the tensors $\langle \Delta u_i E_{jklm} \rangle$ and $\langle \Delta u_i \Delta u_j \Delta u_k \Delta u_l \Delta u_m \rangle$

have different symmetries. Consequently, more scalar functions are needed to fully describe the isotropic form of the transport terms $\langle \Delta u_i E_{jklm} \rangle$. However, the Laplacian $\partial \langle E_{ijkl} \rangle / \partial r_n^2$ has the same isotropic form as $\partial \langle \Delta u_i \Delta u_j \Delta u_k \Delta u_l \rangle / \partial r_n^2$, since E_{ijkl} is also symmetric under interchange of all indices.

Noticeably, we find the second-order dissipation parameters $\langle (\epsilon_{ij} + \epsilon'_{ij})(\epsilon_{kl} + \epsilon'_{kl}) \rangle$ in the fourth-order dissipation source term equations. This is discussed in more detail in section 5.3 below.

3.2 Balances of structure function equations

In the following, we look at the balance of longitudinal, mixed and transverse structure functions for $N = 2$ to $N = 7$ for the two datasets R0 ($Re_\lambda = 88$) and R6 ($Re_\lambda = 754$). The balances for the other Reynolds numbers R1 to R5 are not shown here, but can be found in the supporting material Boschung et al. (2017c). Since one would obtain the $(N+1)$th structure functions by integration in the inertial range beginning with the transverse equations and feeding the solutions into the mixed and longitudinal equations, we have indicated the mixed or transverse part of the transport term with dotted lines where applicable. For instance, in subfigure 3.4a, the dotted line corresponds to $(\partial_r + 2/r) D_{3,0}$, while the solid line with the $\circ$ marker is the full transport term $(\partial_r + 2/r) D_{3,0} - (4/r) D_{1,2}$, i.e. $D_{1,2}$ contributes to the second-order longitudinal balance. This allows to estimate the relative influence of the source terms to the contribution by the coupled structure function (here $D_{1,2}$). It needs to be stressed that while the divergence (i.e. the transport term) is covariant, its decomposition (here into $D_{3,0}$ and $D_{1,2}$) depends on the chosen coordinate-system* and similarly for the Laplacian. Dashed lines indicate that we plotted the respective terms with a negative sign. This is necessary, since some of the terms undergo a change of sign over the plotted range r. We normalise the structure functions of order N with the respective power of $\langle \varepsilon^{N/2} \rangle$ and ν and the separation distance r with respective order-dependent cut-off length scales $\eta_{C,N}$ (cf. eq. (4.81) in section 4.4 below). We have chosen to plot the balances for the two different Reynolds numbers in separate figures, which facilitates readability but unfortunately makes it harder to quantify the influence of the Reynolds number. However, normalising the ordinate with $\langle \varepsilon^{N/2} \rangle$ and ν and the abscissa with $\eta_{C,N}$ leads to a collapse of the dissipation source term and the viscous terms in the viscous range for both Reynolds numbers. In the inertial range, this normalisation brings all terms closer together (but does not lead to a collapse) compared to normalising with

*I.e. would differ if one would write the equations e.g. in cylindrical coordinates.

Table 3.4: Legends of even-order structure function balance figures.

Figure 3.4a, 3.4b	$\circ$: $-\boldsymbol{\nabla\cdot D}_{3,0}$		$\diamond$: $\langle E_{2,0}\rangle$	$\triangledown$: $\nabla^2\boldsymbol{D}_{2,0}$	$\cdots$: $-(\partial_r D_{3,0}+\frac{2}{r}D_{3,0})$
Figure 3.4c, 3.4d	$\circ$: $-\boldsymbol{\nabla\cdot D}_{1,2}$		$\diamond$: $\langle E_{0,2}\rangle$	$\triangledown$: $\nabla^2\boldsymbol{D}_{0,2}$	
Figure 3.5a, 3.5b	$\circ$: $-\boldsymbol{\nabla\cdot D}_{5,0}$	$\square$: $\langle T_{4,0}\rangle$	$\diamond$: $\langle E_{4,0}\rangle$	$\triangledown$: $\nabla^2\boldsymbol{D}_{4,0}$	$\cdots$: $-(\partial_r D_{5,0}+\frac{2}{r}D_{5,0})$
Figure 3.5c, 3.5d	$\circ$: $-\boldsymbol{\nabla\cdot D}_{3,2}$	$\square$: $\langle T_{2,2}\rangle$	$\diamond$: $\langle E_{2,2}\rangle$	$\triangledown$: $\nabla^2\boldsymbol{D}_{2,2}$	$\cdots$: $-(\partial_r D_{3,2}+\frac{4}{r}D_{3,2})$
Figure 3.5e, 3.5f	$\circ$: $-\boldsymbol{\nabla\cdot D}_{1,4}$	$\square$: $\langle T_{0,4}\rangle$	$\diamond$: $\langle E_{0,4}\rangle$	$\triangledown$: $\nabla^2\boldsymbol{D}_{0,4}$	
Figure 3.6a, 3.6b	$\circ$: $-\boldsymbol{\nabla\cdot D}_{7,0}$	$\square$: $\langle T_{6,0}\rangle$	$\diamond$: $\langle E_{6,0}\rangle$	$\triangledown$: $\nabla^2\boldsymbol{D}_{6,0}$	$\cdots$: $-(\partial_r D_{7,0}+\frac{2}{r}D_{7,0})$
Figure 3.6c, 3.6d	$\circ$: $-\boldsymbol{\nabla\cdot D}_{5,2}$	$\square$: $\langle T_{4,2}\rangle$	$\diamond$: $\langle E_{4,2}\rangle$	$\triangledown$: $\nabla^2\boldsymbol{D}_{4,2}$	$\cdots$: $-(\partial_r D_{5,2}+\frac{4}{r}D_{5,2})$
Figure 3.6e, 3.6f	$\circ$: $-\boldsymbol{\nabla\cdot D}_{3,4}$	$\square$: $\langle T_{2,4}\rangle$	$\diamond$: $\langle E_{2,4}\rangle$	$\triangledown$: $\nabla^2\boldsymbol{D}_{2,4}$	$\cdots$: $-(\partial_r D_{3,4}+\frac{6}{r}D_{3,4})$
Figure 3.7a, 3.7b	$\circ$: $-\boldsymbol{\nabla\cdot D}_{1,6}$	$\square$: $\langle T_{0,6}\rangle$	$\diamond$: $\langle E_{0,6}\rangle$	$\triangledown$: $\nabla^2\boldsymbol{D}_{0,6}$	

Table 3.5: Legends of odd-order structure function balance figures.

Figure 3.8a, 3.8b	$\circ$: $\boldsymbol{\nabla\cdot D}_{4,0}$	$\square$: $-\langle T_{3,0}\rangle$	$\diamond$: $-\langle E_{3,0}\rangle$	$\triangledown$: $-\nabla^2\boldsymbol{D}_{3,0}$	$\cdots$: $\partial_r D_{4,0}+\frac{2}{r}D_{4,0}$
Figure 3.8c, 3.8d	$\circ$: $-\boldsymbol{\nabla\cdot D}_{2,2}$	$\square$: $\langle T_{1,2}\rangle$	$\diamond$: $-\langle E_{1,2}\rangle$	$\triangledown$: $-\nabla^2\boldsymbol{D}_{1,2}$	$\cdots$: $\partial_r D_{2,2}+\frac{4}{r}D_{2,2}$
Figure 3.9a, 3.9b	$\circ$: $\boldsymbol{\nabla\cdot D}_{6,0}$	$\square$: $-\langle T_{5,0}\rangle$	$\diamond$: $-\langle E_{5,0}\rangle$	$\triangledown$: $-\nabla^2\boldsymbol{D}_{5,0}$	$\cdots$: $\partial_r D_{6,0}+\frac{2}{r}D_{6,0}$
Figure 3.9c, 3.9d	$\circ$: $\boldsymbol{\nabla\cdot D}_{4,2}$	$\square$: $-\langle T_{3,2}\rangle$	$\diamond$: $-\langle E_{3,2}\rangle$	$\triangledown$: $-\nabla^2\boldsymbol{D}_{3,2}$	$\cdots$: $\partial_r D_{4,2}+\frac{4}{r}D_{4,2}$
Figure 3.9e, 3.9f	$\circ$: $-\boldsymbol{\nabla\cdot D}_{2,4}$	$\square$: $\langle T_{1,4}\rangle$	$\diamond$: $-\langle E_{1,4}\rangle$	$\triangledown$: $-\nabla^2\boldsymbol{D}_{1,4}$	$\cdots$: $\partial_r D_{2,4}+\frac{6}{r}D_{2,4}$
Figure 3.10a, 3.10b	$\circ$: $\boldsymbol{\nabla\cdot D}_{8,0}$	$\square$: $-\langle T_{7,0}\rangle$	$\diamond$: $-\langle E_{7,0}\rangle$	$\triangledown$: $-\nabla^2\boldsymbol{D}_{7,0}$	$\cdots$: $\partial_r D_{8,0}+\frac{2}{r}D_{8,0}$
Figure 3.10c, 3.10d	$\circ$: $\boldsymbol{\nabla\cdot D}_{6,2}$	$\square$: $-\langle T_{5,2}\rangle$	$\diamond$: $-\langle E_{5,2}\rangle$	$\triangledown$: $-\nabla^2\boldsymbol{D}_{5,2}$	$\cdots$: $\partial_r D_{6,2}+\frac{4}{r}D_{6,2}$
Figure 3.10e, 3.10f	$\circ$: $-\boldsymbol{\nabla\cdot D}_{4,4}$	$\square$: $\langle T_{3,4}\rangle$	$\diamond$: $-\langle E_{3,4}\rangle$	$\triangledown$: $-\nabla^2\boldsymbol{D}_{3,4}$	$\cdots$: $\partial_r D_{4,4}+\frac{6}{r}D_{2,6}$
Figure 3.11a, 3.11b	$\circ$: $-\boldsymbol{\nabla\cdot D}_{2,6}$	$\square$: $\langle T_{1,6}\rangle$	$\diamond$: $-\langle E_{1,6}\rangle$	$\triangledown$: $-\nabla^2\boldsymbol{D}_{1,6}$	$\cdots$: $\partial_r D_{2,6}+\frac{8}{r}D_{2,6}$

the K41 quantities $\langle\varepsilon\rangle$ and η. Note that we have not computed terms stemming from the large-scale forcing; consequently, the terms found in the balances as shown in the figures do not sum exactly to zero; we implicitly assume that the additional terms due to the forcing are negligible for our analysis. The legends for the even-order figures may be found in table 3.4, the corresponding odd-order figure legends in table 3.5. Furthermore, the Taylor scale λ is indicated by vertical dash-dotted lines in the figures.

3.2.1 Even orders ($N = 2, 4, 6$)

The balances of the second-order structure function equations are shown in figure 3.4, where the longitudinal balance for $D_{2,0}$ is shown in figure 3.4a and 3.4b and the transverse in figure 3.4c and 3.4d. The smaller Reynolds number case R0 corresponds to the left column, while the balances for R6 are depicted in the right column. Since we have normalised the terms with $\langle\varepsilon\rangle$, both dissipation

source terms $\langle E_{2,0}\rangle = \langle E_{0,2}\rangle = 4\langle\varepsilon\rangle/3$ are constants over all r/η. As expected, the dissipation source terms balance the viscous terms in the dissipative range, while they (nearly) balance the transport terms in the inertial range. Noticeably, the inertial range becomes broader with increasing Reynolds number in agreement with the notion of an increasing scale separation L/η. Consequently, the 4/5-law is more distinctive for the case R6, for which the viscous terms can be neglected in the inertial range. For R0 ($Re_\lambda = 88$), the viscous terms contribute to some extent to the balance in the inertial range. Noticeably, For $N = 2$, the pressure source terms vanish under the assumption of (local) isotropy and have therefore not been plotted. Considering the longitudinal equation, it is clearly seen that there is significant cancellation between the term $\partial D_{3,0}/\partial r + 2D_{3,0}/r$ and the term $-4D_{1,2}/r$ feeding into the equation as indicated by the dotted line. Indeed, from a straightforward calculation (which is only possible for the second-order equations, since the dissipation source term $\langle E_{2,0}\rangle = \langle E_{0,2}\rangle = 4\langle\epsilon\rangle/3$) one finds that $-4D_{1,2}/r$ contributes exactly 4/9 to the 4/5-law when one neglects the viscous terms.

We find qualitatively similar behaviour at the fourth order $N = 4$, as seen in figure 3.5. The balances for $D_{4,0}$ are shown in figure 3.5a and figure 3.5b, for $D_{2,2}$ in figure 3.5c and figure 3.5d and for $D_{0,4}$ in figure 3.5e and figure 3.5f. Since $\langle\varepsilon^2\rangle$ and ν are the correct quantities to normalise the fourth-order structure functions in the viscous range, see eq. (4.86), we have normalised the terms with $\langle\varepsilon^2\rangle^{6/8}\nu^{1/2}$ plotted over $r/\eta_{C,4}$. Again, this normalisation leads to a collapse of the viscous and dissipation source terms of the respective orders in the viscous range, where these two terms are dominant. The mixed pressure source term $\langle T_{2,2}\rangle$ has a different sign in the viscous range compared to the inertial range. However, this observation does not seem significant, as the pressure source terms are negligible in the viscous range anyway. Noticeably, there are no r-independent terms in the inertial range. In the transverse equation for $D_{0,4}$, the transport term is nearly balanced by the dissipation source term, while the pressure source terms are negligible, both for the smaller and the larger Reynolds number. Consequently, in the inertial range

$$\frac{\partial D_{1,4}}{\partial r} + \frac{6}{r} D_{1,4} \approx -\langle E_{0,4}\rangle. \tag{3.63}$$

For the mixed and longitudinal equation, the pressure source term contributes to the balance for the higher Reynolds number $Re_\lambda = 754$, which is not the case at the lower Reynolds number $Re_\lambda = 88$. However, this is somewhat deceiving, since there is again significant cancellation in the transport term, as indicated

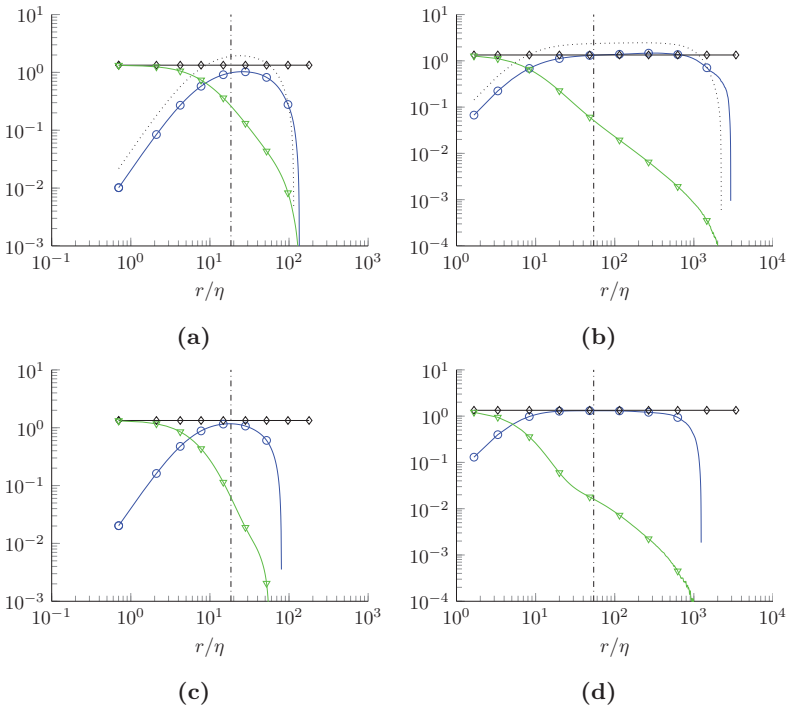

Figure 3.4: Balances of normalised second-order structure function equations $N = 2$. Left column: $Re_\lambda = 88$. Right column: $Re_\lambda = 754$. Ratio λ/η is indicated by the vertical dash-dotted lines. Legend in table 3.4. All terms are divided by $\langle\varepsilon\rangle$.

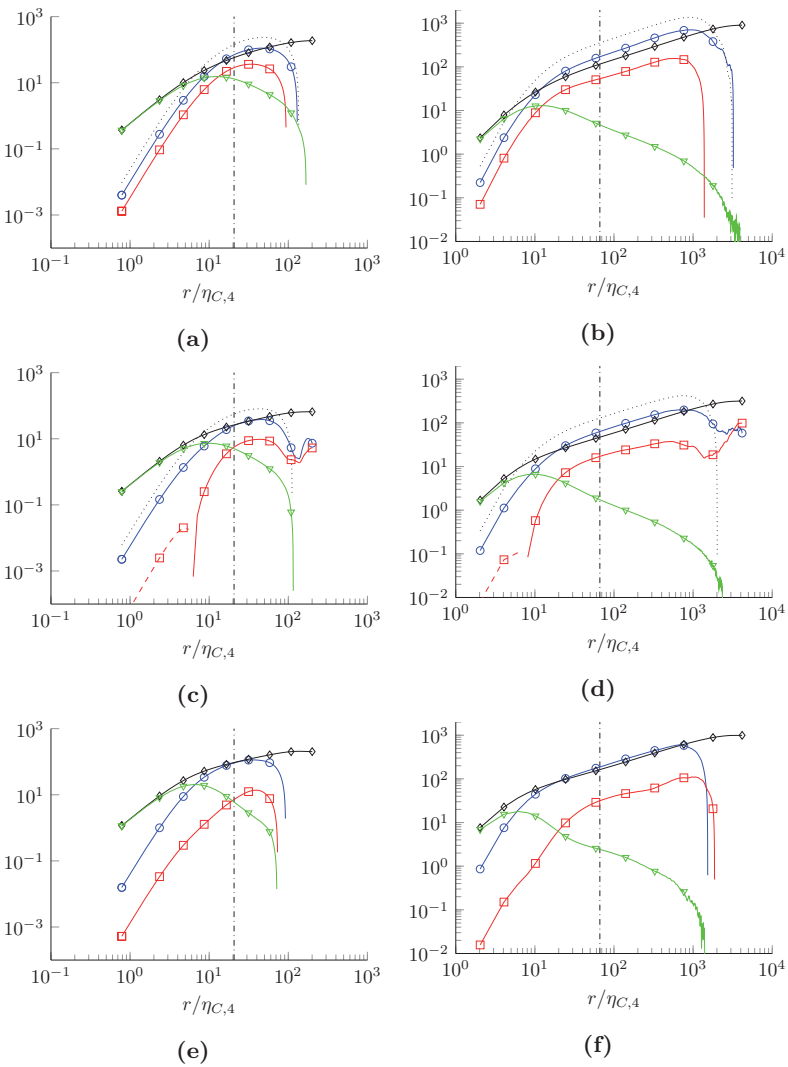

Figure 3.5: Balances of normalised fourth-order structure function equations $N = 4$. Left column: $Re_\lambda = 88$. Right column: $Re_\lambda = 754$. Ratio $\lambda/\eta_{C,4}$ is indicated by the vertical dash-dotted lines. Legend in table 3.4. Changes of signs are indicated by the dashed lines. All terms are divided by $\langle\varepsilon^2\rangle^{6/8}\nu^{1/2}$.

by the dotted lines.

Finally, we show the sixth-order equations $N = 6$ in figure 3.6 and figure 3.7, where the balance for $D_{6,0}$ can be found in figure 3.6a and 3.6b, $D_{4,2}$ in figure 3.6c and 3.6d, $D_{2,4}$ in figure 3.6e and 3.6f and $D_{0,6}$ in figure 3.7a and 3.7b, where we have normalised the terms with $\langle\varepsilon^3\rangle^{8/12}\nu$ and the abscissa with $\eta_{C,6}$ from eq. (4.81). Again, we observe mostly similar characteristics as for $N = 4$. In the viscous range, the dissipation source term and the viscous terms dominate and balance to leading order for all sixth-order equations. In the inertial range, the transport term of the transverse equation for $D_{0,6}$ is mostly balanced by the dissipation source term $\langle E_{0,6}\rangle$, i.e.

$$\frac{\partial D_{1,6}}{\partial r} + \frac{8}{r} D_{1,6} \approx -\langle E_{0,6}\rangle, \tag{3.64}$$

similarly to the fourth order where the transverse transport term was balanced by $\langle E_{0,4}\rangle$ (cf. eq. (3.63) and figures 3.5e and 3.5f). While the dissipation source terms are larger than the pressure source terms in the inertial range for all sixth-order balances, the ratio of dissipation to pressure source terms decreases the more longitudinal the underlying structure function is: In the equation for $D_{6,0}$, the pressure source terms are of the same order as the dissipation source terms, while $\langle T_{0,6}\rangle$ is negligible compared to $\langle E_{0,6}\rangle$ in the transverse equation. Also noteworthy is that again the mixed pressure source terms $\langle T_{4,2}\rangle$ and $\langle T_{2,4}\rangle$ exhibit a change of sign as indicated by the dotted lines from the viscous to the inertial range, as did the mixed pressure source term $\langle T_{2,2}\rangle$ in the fourth-order equations. Finally, there is again cancellation in the transport terms of all but the transverse equation due to the contribution by the coupling to the other equations. As for $N = 4$, this is indicated by the dashed lines which are larger than the full transport terms in the inertial range.

We may conclude with general observations regarding the even-order balances: In the viscous range for all orders analysed here, the dissipation source terms and the viscous terms are dominant and balance each other. As discussed above, this is to be expected for all higher orders as well. In the inertial range, the transverse dissipation source terms $\langle E_{0,N}\rangle$ balances the transport term for $N = 2, 4, 6$ and probably for higher even N as well. The solution of this approximate balance then feeds into the transverse and longitudinal equations, where these terms lead to significant cancellation in the longitudinal and mixed transport term. While this observation is certainly valid for all orders as well as the range of Reynolds numbers examined here, it is not clear whether these findings generalise

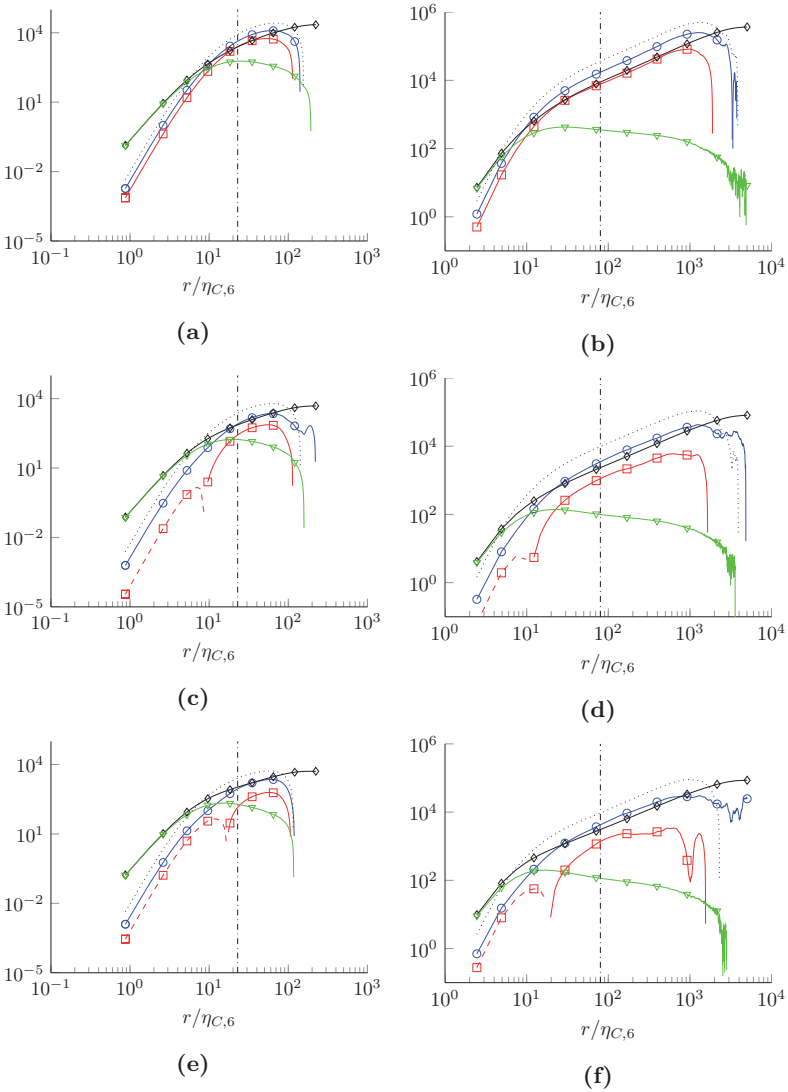

Figure 3.6: Balances of normalised sixth-order structure function equations $N = 6$. Left column: $Re_\lambda = 88$. Right column: $Re_\lambda = 754$. Ratio $\lambda/\eta_{C,6}$ is indicated by the vertical dash-dotted lines. Legend in table 3.4. Changes of signs are indicated by the dashed lines. All terms are divided by $\langle\varepsilon^3\rangle^{8/12}\nu$.

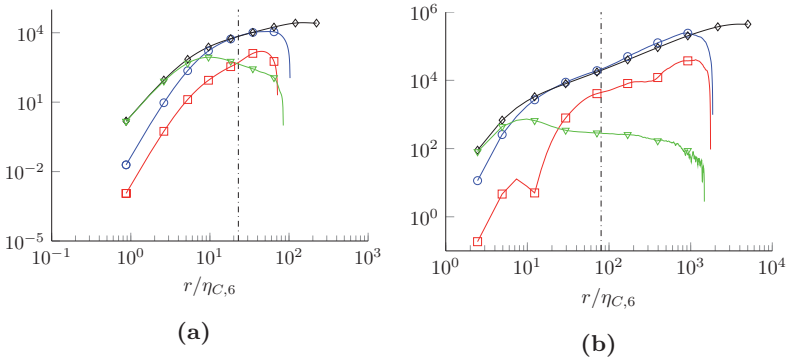

Figure 3.7: Balances of normalised sixth-order structure function equations $N = 6$. Left: $Re_\lambda = 88$. Right: $Re_\lambda = 754$. Ratio $\lambda/\eta_{C,6}$ is indicated by the vertical dash-dotted lines. Legend in table 3.4. Changes of signs are indicated by the dashed lines. All terms are divided by $\langle\varepsilon^3\rangle^{8/12}\nu$.

as well. Caution may be warranted because the pressure source terms become more important the higher the order and the more longitudinal the respective equation. Since all even-order dissipation source terms $\langle E_{m,n}\rangle$ are positive and consequently the transport terms $\boldsymbol{\nabla}\cdot\boldsymbol{D}_N < 0$, the odd-order structure functions in the inertial range are negative.

3.2.2 Odd orders ($N = 3, 5, 7$)

After having looked at the even orders, the balance of odd-order equations is presented in the following. The third-order longitudinal equations are shown in figure 3.8a and 3.8b and the transverse in figure 3.8c and 3.8d. We have normalised the terms with $\langle\varepsilon^{3/2}\rangle^{5/6}\nu^{1/4}$ and plotted them over $\eta_{C,3}$ as defined by eq. (4.81). In the viscous range, there is again the balance between dissipation source terms and viscous terms, which are dominant for the lower Reynolds number data R0, $Re_\lambda = 88$. However, for the higher $Re_\lambda = 754$ (R6), both the transport and the pressure source term are of the same order of magnitude for our data. This seems at odds with eq. (4.86), which was found to hold for odd orders as well, but could be resolved by plotting to smaller r, since the scaling of the terms for $r \to 0$ as discussed in section 3.1.1 is exact. Noticeably, the pressure and transport term also balance each other nearly perfectly. Indeed, the pressure source term balances the transport term not only in the viscous

range, but also in the inertial range, where

$$\frac{\partial D_{4,0}}{\partial r}+\frac{2}{r}D_{4,0}-\frac{6}{r}D_{2,2}\approx-\langle T_{3,0}\rangle,\quad \frac{\partial D_{2,2}}{\partial r}+\frac{4}{r}D_{2,2}-\frac{4}{3r}D_{0,4}\approx-\langle T_{1,2}\rangle, \tag{3.65}$$

i.e. the dissipation source terms may be neglected in the inertial range. As seen from the dotted lines, there is a large cancellation in the transport terms. We note in passing that the findings of Grauer et al. (2012) correspond to neglecting the pressure source terms $\langle T_{3,0}\rangle$ and $\langle T_{1,2}\rangle$ in eq. (3.65). The third-order structure function balances were previously examined by Hill and Boratav (2001) using wind-tunnel data with $Re_\lambda = 208$ as well as DNS of isotropic turbulence with $Re_\lambda = 82$. Their results are in good agreement with our figures 3.8. Noticeably, the two third-order pressure source terms have different signs, $\langle T_{3,0}\rangle < 0$ and $\langle T_{1,2}\rangle > 0$ differently to the even orders. Consequently, also the transport terms $\boldsymbol{\nabla}\cdot\boldsymbol{D}_{4,0} > 0$ and $\boldsymbol{\nabla}\cdot\boldsymbol{D}_{2,2} < 0$, which implies $4D_{0,4}/(3r) > \partial_r D_{2,2}+(4/r)D_{2,2} > 0$ and $\partial_r D_{4,0}+(2/r)D_{4,0} > (6/r)D_{2,2} > 0$ and the fourth-order structure functions are positive as required by definition.

The $N = 5$ structure function equations are shown in figure 3.9, where the terms are normalised with $\langle\varepsilon^{5/2}\rangle^{7/10}\nu^{3/4}$ and the abscissa with $\eta_{C,5}$. The longitudinal equation for $D_{5,0}$ is depicted in figure 3.9a and 3.9b, the mixed equation for $D_{3,2}$ in figure 3.9c and 3.9d and the transverse $D_{1,4}$ in figure 3.9e and 3.9f. Similar to the $N = 3$ equations, the viscous terms and the dissipation source terms balance but would need to be plotted towards smaller r to be dominant at the higher Reynolds number $Re_\lambda = 754$. Both terms are negligible in the inertial range. The pressure source terms balance the transport terms over the full range for the longitudinal and transverse equations, cf. figures 3.9a, 3.9b, 3.9e and 3.9f. In the mixed equation, they also balance but have a zero-crossing at different $r/\eta_{C,5}$. Thus, the balance between the pressure source term $\langle T_{3,2}\rangle$ and the mixed transport term breaks down close to the respective zero-crossings. Besides the viscous range, there is again a large cancellation of terms in the transport terms as indicated by the dotted lines. Again, we find different signs for the pressure source terms: The transversal $\langle T_{1,4}\rangle > 0$ and mixed $\langle T_{3,2}\rangle > 0$, while the longitudinal and $\langle T_{5,0}\rangle < 0$. With the respective signs of the transport terms, $6D_{0,6}/(5r) > \partial_r D_{2,4} + (6/r)D_{2,4} > 0$, $\partial_r D_{4,2} + (4/r)D_{4,2} > 12D_{2,4}/(3r) > 0$ and $\partial_r D_{6,0} + (2/r)D_{6,0} > (12/r)D_{4,2} > 0$.

Lastly, we look at the balances for $N = 7$ as seen in figure 3.10 and figure 3.11.

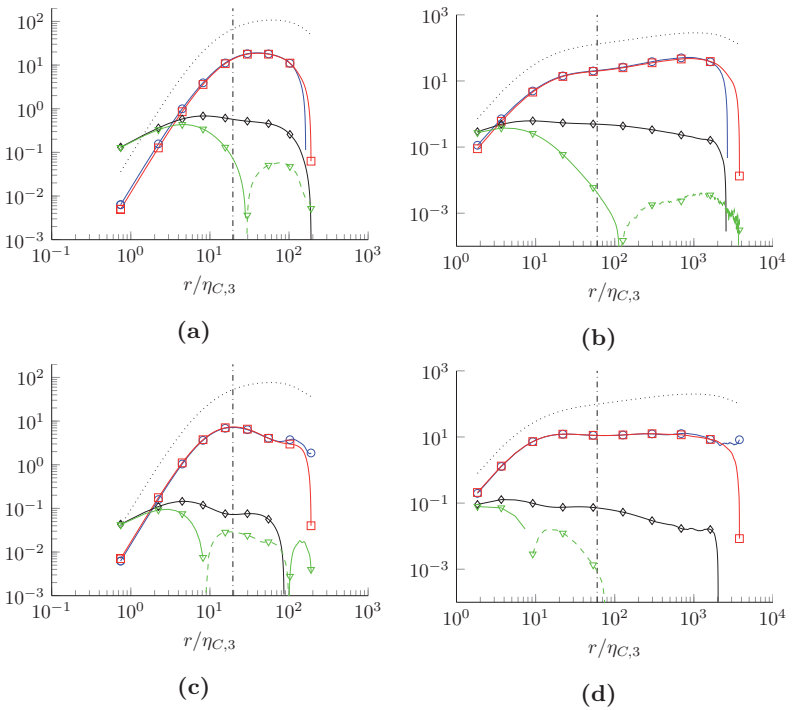

Figure 3.8: Balances of normalised third-order structure function equations $N = 3$. Left column: $Re_\lambda = 88$. Right column: $Re_\lambda = 754$. Ratio $\lambda/\eta_{C,3}$ is indicated by the vertical dash-dotted lines. Legend in table 3.5. Changes of signs are indicated by the dashed lines. All terms are divided by $\langle\varepsilon^{3/2}\rangle^{5/6}\nu^{1/4}$.

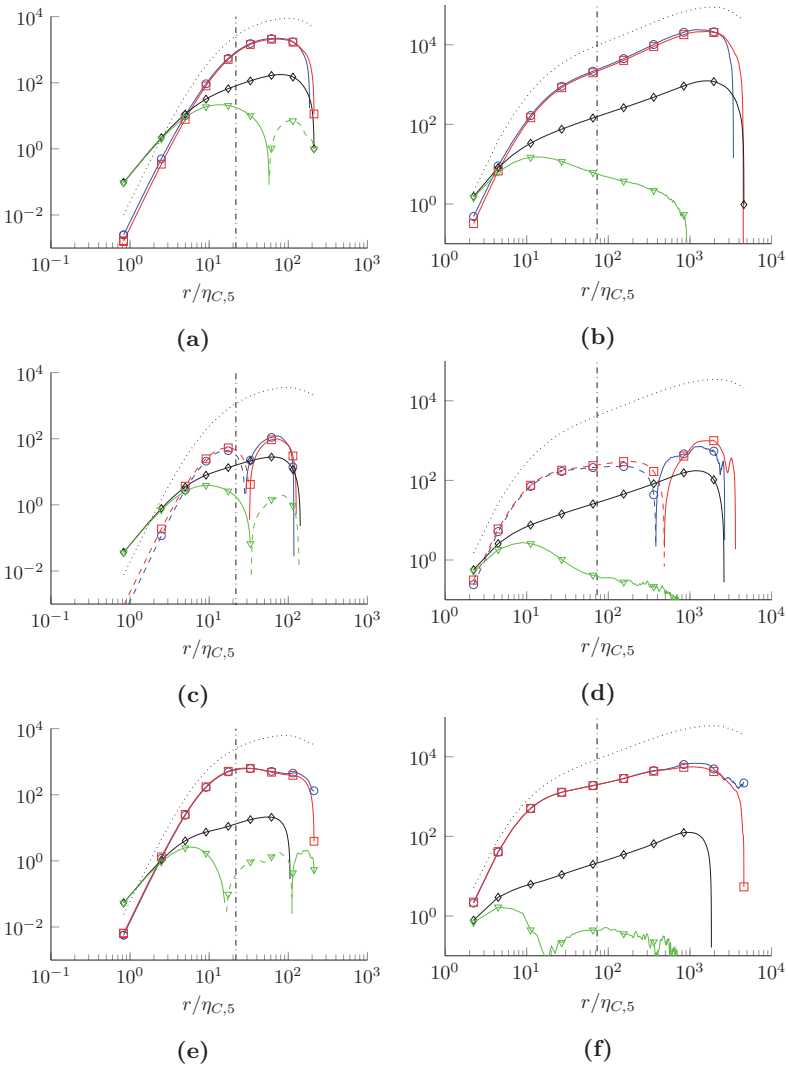

Figure 3.9: Balances of normalised fifth-order structure function equations $N = 5$. Left column: $Re_\lambda = 88$. Right column: $Re_\lambda = 754$. Ratio $\lambda/\eta_{C,5}$ is indicated by the vertical dash-dotted lines. Legend in table 3.5. Changes of signs are indicated by the dashed lines. All terms are divided by $\langle\varepsilon^{5/2}\rangle^{7/10}\nu^{3/4}$.

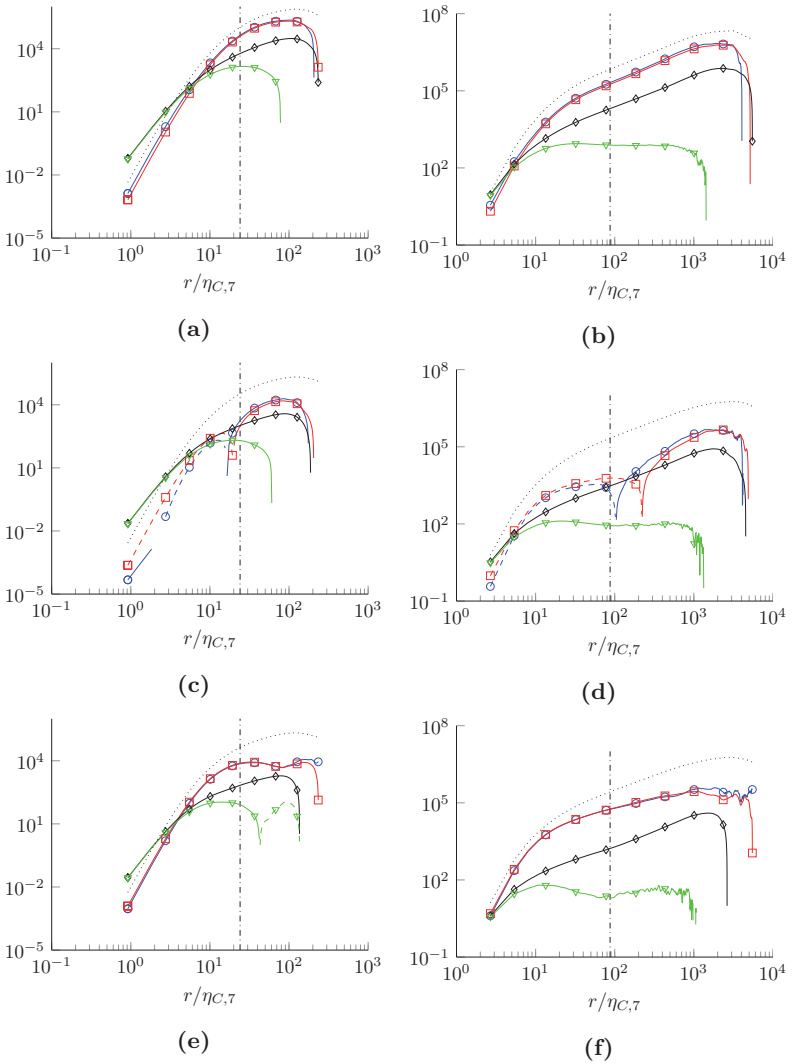

Figure 3.10: Balances of normalised seventh-order structure function equations $N = 7$. Left column: $Re_\lambda = 88$. Right column: $Re_\lambda = 754$. Ratio $\lambda/\eta_{C,7}$ is indicated by the vertical dash-dotted lines. Legend in table 3.5. Changes of signs are indicated by the dashed lines. All terms are divided by $\langle\varepsilon^{7/2}\rangle^{9/14}\nu^{5/4}$.

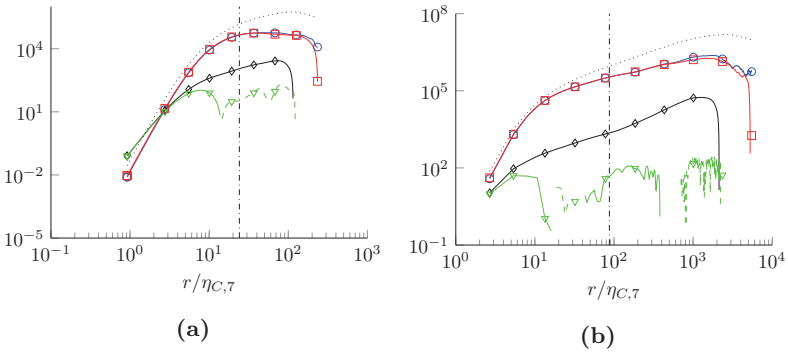

Figure 3.11: Balances of normalised seventh-order structure function equations $N = 7$. Left: $Re_\lambda = 88$. Right: $Re_\lambda = 754$. Ratio $\lambda/\eta_{C,7}$ is indicated by the vertical dash-dotted lines. Legend in table 3.5. Changes of signs are indicated by the dashed lines. All terms are divided by $\langle\varepsilon^{7/2}\rangle^{9/14}\nu^{5/4}$.

Specifically, the longitudinal balance for $D_{7,0}$ normalised with $\langle\varepsilon^{7/2}\rangle^{9/14}\nu^{5/4}$ is plotted over $r/\eta_{C,7}$ in figure 3.10a and figure 3.10b, the equally normalised balances for $D_{5,2}$ in figure 3.10c and figure 3.10d, for $D_{3,4}$ in figure 3.10e and figure 3.10f and for $D_{1,6}$ in figure 3.11a and figure 3.11b. In the viscous range, there is the same balance of dissipation source terms and viscous terms as observed for the lower orders; while they dominate at the lower Reynolds number, the pressure source terms and the transport terms are of the same order of magnitude for the higher Reynolds number dataset R6. As was found for the lower odd orders, the pressure source terms and the transport terms balance for the full range of $r/\eta_{C,7}$ we have evaluated. Both the pressure source term and the transport term dominate the inertial range, where the dissipation source terms and the viscous terms can be neglected. Interestingly enough, only $\langle T_{5,2}\rangle$ and the corresponding transport term in the equation for $D_{5,2}$ change their sign, while the other mixed pressure source term $\langle T_{3,4}\rangle$ and the transport term balanced by it remains positive for all $r/\eta_{C,7}$. Moreover comparing to $N = 5$, the change of sign of $\langle T_{5,2}\rangle$ is at smaller $r/\eta_{C,7}$ compared to the zero-crossover of $\langle T_{3,2}\rangle$ plotted over $r/\eta_{C,5}$. For the seventh-order balance, we have $\langle T_{7,0}\rangle < 0$, a change of sign of $\langle T_{5,2}\rangle$, $\langle T_{3,4}\rangle > 0$ and $\langle T_{1,6}\rangle > 0$. Therefore, not only the transverse pressure source terms are negative in general (as one might have conjectured from the $N = 5$ balances), but also some of the mixed. We expect similar characteristics at higher orders as well. With the signs of the transport terms in mind, one has

$8D_{0,8}/(7r) > \partial_r D_{2,6} + (8/r)D_{2,6} > 0$, $18D_{2,6}/(5r) > \partial_r D_{4,4} + (6/r)D_{4,4} > 0$, $\partial_r D_{6,2} + (4/r)D_{6,2} > 20D_{4,4}/(3r) > 0$ and $\partial_r D_{8,0} + (2/r)D_{8,0} > (14/r)D_{6,2} > 0$.

Let us briefly summarise the odd orders: For $r \to 0$, again the dissipation source terms and viscous terms are dominant, if plotted towards small enough r. Consequently, the order-dependent viscous scales, eq. (4.81), are also valid for the odd orders, since the viscous terms and dissipation source terms balance. Indeed, the normalisation with $\eta_{C,N}$ and $u_{C,N}$ collapses the viscous and dissipation source terms in the viscous range for different Reynolds numbers (not easily seen from the figures). Noticeably, all odd-order dissipation source terms are negative while the corresponding even-order dissipation source terms are positive. Both contribute to the respective signs of the structure functions: The positive even-order dissipation source terms lead to negative odd-order structure functions, while the negative odd-order dissipation source terms add to the positive even-order structure functions, albeit not much. In the inertial range, both the viscous and dissipation source terms can be neglected, so that to leading order the transport terms and the pressure source terms balance, as was also found by Gotoh and Nakano (2003). This is also in agreement with Yakhot's mean-field theory (Yakhot (2001)) applied to longitudinal and mixed equations with odd N. This leading order balance in the inertial range is much better satisfied than the analogous balance of transport terms and dissipation source terms for the even orders, cf. the figures above. However, under the inertial range assumptions it is not possible to determine the solution of the even-order structure functions from these balances, since there are more unknown structure functions than equations. Finally, it needs to be mentioned that the dissipation source terms have a different scaling in the inertial range than the pressure source terms and the full transport terms, at least for balances other than the longitudinal in the fifth- and seventh-order equations. Nevertheless, since they are much smaller and can be neglected, power-law behaviour of the even-order structure functions in the inertial range with equal scaling exponents does not seem out of hand. There is one conflicting observation, though: If one approximates the dissipation source terms with a power-law, *parts* of the transport term (the dotted lines) can be approximated by a power-law with same scaling exponent (except for $N = 3$)*. This result immediately clashes with the finding that the *full* transport terms collapse with the pressure source terms which would have a different scaling exponent compared to the dissipation source terms save for the longitudinal balances at $N = 5$ and $N = 7$. That is, even-order structure

*This observation is relevant for the discussion in section 5.1, where the implications of RSH regarding the dissipation source terms are discussed in more detail.

functions have the same inertial range scaling exponents only if one neglects the pressure source terms or assumes that they have the same inertial range scaling as the dissipation source terms. Indeed, going back to table 3.3, the differences of even-order $\zeta_{m,n}$ seem to be larger percentwise than those of odd-order $\xi_{m,n}$ (but see the caveats regarding statistical convergence and interchangeability of $\zeta_{m,n}$ and $\xi_{m,n}$.)

3.3 Trace of structure function equations

In this section, we look at the balances of the traces of the structure function equations for $N = 2$ to $N = 7$. For the even-order equations, there is an even number of indices which are pairwise contracted leaving no free index resulting in scalar equations. For even N, we have

$$\begin{aligned} D_{[2]} &= \left\langle (\Delta u_i)^2 \right\rangle , \\ D_{[4]} &= \left\langle (\Delta u_i)^2 (\Delta u_j)^2 \right\rangle , \\ D_{[6]} &= \left\langle (\Delta u_i)^2 (\Delta u_j)^2 (\Delta u_k)^2 \right\rangle . \end{aligned} \tag{3.66}$$

However for the odd-order equations, there remains a single index after contracting, resulting in a vector equation for the trace. As the separation vector r_i has been chosen to be aligned with the x_1-axis, only the 1-component of the vector equation does not vanish. Consequently, we define

$$\begin{aligned} D_{[3]} &= \left\langle \Delta u_1 (\Delta u_i)^2 \right\rangle , \\ D_{[5]} &= \left\langle \Delta u_1 (\Delta u_i)^2 (\Delta u_j)^2 \right\rangle , \\ D_{[7]} &= \left\langle \Delta u_1 (\Delta u_i)^2 (\Delta u_j)^2 (\Delta u_k)^2 \right\rangle . \end{aligned} \tag{3.67}$$

Note that $\langle \Delta u_2 [(\Delta u_i)^2]^{(N-1)/2} \rangle = 0$ (N odd) due to isotropy, since we have aligned the separation vector r_i with the x_1-axis, i.e. $r_2 = 0$ and equally for the 3-component.

Together with the relations given in table 3.1 due to isotropy, one can then express the trace of the general structure function tensor $\langle \Delta u_i \Delta u_j ... \rangle$ in terms of the longitudinal, mixed and transverse structure functions $D_{m,n} = \langle (\Delta u_1)^m (\Delta u_2)^n \rangle$. The resulting sums are listed in table 3.6. The tabulated trace relations apply to any isotropic tensor that is symmetric under interchange of all indices, i.e. also to $\langle \boldsymbol{E}_N \rangle$ and $\langle \boldsymbol{T}_N \rangle$, e.g. $\langle E_{[4]} \rangle = \langle E_{4,0} \rangle + 4\langle E_{2,2} \rangle + 8\langle E_{0,4} \rangle / 3$.

Table 3.6: Second- to eighth-order structure function traces as defined by eq. (3.66) and eq. (3.67) in combination with the isotropic relations from table 3.1.

$N = 2$	$D_{[2]} = D_{2,0} + 2D_{0,2}$
$N = 3$	$D_{[3]} = D_{3,0} + 2D_{1,2}$
$N = 4$	$D_{[4]} = D_{4,0} + 4D_{2,2} + \frac{8}{3}D_{0,4}$
$N = 5$	$D_{[5]} = D_{5,0} + 4D_{3,2} + \frac{8}{3}D_{1,4}$
$N = 6$	$D_{[6]} = D_{6,0} + 6D_{4,2} + 8D_{2,4} + \frac{16}{5}D_{0,6}$
$N = 7$	$D_{[7]} = D_{7,0} + 6D_{5,2} + 8D_{3,4} + \frac{16}{5}D_{1,6}$
$N = 8$	$D_{[8]} = D_{8,0} + 8D_{6,2} + 16D_{4,4} + \frac{64}{5}D_{2,6} + \frac{128}{5}D_{0,8}$

We examine the trace equations for two reasons: First, the trace is invariant (i.e. independent of the coordinate system) for the even-order equations. Therefore, one finds for instance for $N = 2$ the mean of the pseudo-dissipation $\langle\epsilon\rangle$ instead of the components $\langle\epsilon_{11}\rangle$ and $\langle\epsilon_{22}\rangle$, cf. section 3.1.2. Similarly, at $N = 4$ one finds in the trace of the dissipation source term equation a term proportional to $\langle\epsilon^2\rangle + \langle\epsilon_{ij}\epsilon_{ji}\rangle$ instead of sums of the components $\langle\epsilon_{11}^2\rangle$, $\langle\epsilon_{22}^2\rangle$ and $\langle\epsilon_{12}^2\rangle$ (cf. section 3.3.1). Second, since the even-order trace is a scalar, one always has only a single equation for a single quantity at even N both in the viscous and inertial range, differently to the components equations. For the odd orders, one can project the trace equations in r-direction, but the resulting 1-components and the additional term $D_{22ii\ldots}$ depend on the coordinate system, cf. appendix A.3.

Noticeably, the structure and relations between the different orders as highlighted in figure 3.1 and discussed in section 3.1 above do not hold for the traces defined in eq. (3.66) and eq. (3.67). Consider the second order, $N = 2$. There, the trace of the transport term is

$$\frac{\partial\langle\Delta u_i(\Delta u_j)^2\rangle}{\partial r_i} = \frac{\partial D_{3,0}}{\partial r} + 2\frac{\partial D_{1,2}}{\partial r} + \frac{2}{r}\left(D_{3,0} + 2D_{1,2}\right) = \frac{\partial D_{[3]}}{\partial r} + \frac{2}{r}D_{[3]}, \quad (3.68)$$

i.e. a similar coupling between the third- and second-order traces is found and similar relations are easily derived for the trace of transport terms in the higher

even-order equations. However, for the *third*-order trace,

$$\frac{\partial\langle \Delta u_i \Delta u_1 (\Delta u_j)^2\rangle}{\partial r_i} = \frac{\partial D_{[4]}}{\partial r} + \frac{2}{r} D_{[4]} - 2\left(\frac{\partial D_{2,2}}{\partial r} + \frac{3}{r} D_{2,2}\right) - \frac{8}{3}\left(\frac{\partial D_{0,4}}{\partial r} + \frac{3}{r} D_{0,4}\right) \quad (3.69)$$

and therefore there are additional terms in the odd-order trace of the transport terms which need to be closed. Again, similar additional terms are found for the trace of transport terms in all odd-order equations.

This implies that it is possible to directly integrate the transport term in the even-order trace equations,

$$D_{[N+1]} = -\frac{1}{r^2}\int_0^r y^2 \left(\langle E_{[N]}\rangle + \langle T_{[N]}\rangle\right) \mathrm{d}y + 2\nu \frac{\partial D_{[N]}}{\partial r}. \quad (3.70)$$

In the inertial range, the last term on the r.h.s. can be neglected and the solution for the odd-order structure function trace then depends on the integrated sum of the traces of the dissipation and pressure source terms. Again, a power-law for $D_{[N+1]}$, N even, can only be obtained if both $\langle E_{[N]}\rangle$ and $\langle T_{[N]}\rangle$ follow the same power-law as well. All even N can be integrated in the viscous range by solving for the viscous term to determine the respective solutions if the dissipation source term is known, since both terms balance each other. One then obtains for $r \to 0$

$$D_{[N]} = \frac{1}{2\nu r}\iint_0^r y \langle E_{[N]}\rangle \mathrm{d}y^2 \quad (3.71)$$

or equivalently from an integration by parts

$$D_{[N]} = \frac{1}{2\nu}\int_0^r \left(y - \frac{y^2}{r}\right)\langle E_{[N]}\rangle \mathrm{d}y. \quad (3.72)$$

For $r \to 0$, $\langle E_{[N]}\rangle = B_N r^{N-2}$ where B_N is a scalar, which then gives from both eq. (3.71) and eq. (3.72)

$$D_{[N]} = \frac{1}{2\nu}\frac{\langle E_{[N]}\rangle}{N(N+1)} r^2 \quad (3.73)$$

for the trace of even-order structure functions in the viscous range.

The integration of the trace of the fourth-order structure function equations

is carried out below both in the inertial (section 5.3) and the viscous range (section 4.3.3). One can similarly proceed for higher even orders.

For odd orders in the inertial range, one has additional terms as seen from eq. (3.68) for $N = 3$ and similarly for higher odd orders. Thus, one needs to close these additional terms and then integrate in r resulting in a solution for $D_{[N+1]}$ or compute the gradient and then project in r-direction. Then, one obtains

$$D_{11ii...} - \frac{2}{r^2}\int_0^r rD_{22ii...}\mathrm{d}y = -\frac{1}{r^2}\int_0^r y^2\left(\langle E_{[N]}\rangle + \langle T_{[N]}\rangle\right)\mathrm{d}y + 2\nu\frac{\partial D_{[N]}}{\partial r} - \frac{4\nu}{r^2}\int_0^r D_{[N]}\mathrm{d}y \quad (3.74)$$

where $D_{11ii...} = \langle(\Delta u_1)^2[(\Delta u_i)^2]^{(N-1)/2}\rangle$ and $D_{22ii...} = \langle(\Delta u_2)^2[(\Delta u_i)^2]^{(N-1)/2}\rangle$. Note that because of N odd, $\langle E_{[N]}\rangle = \langle E_{1ii...}\rangle$ and $\langle T_{[N]}\rangle = \langle T_{1ii...}\rangle$, differently to N even. One could then write due to isotropy

$$\begin{aligned} D_{[N+1]} &= \left\langle(\Delta u_i)^{N+1}\right\rangle = D_{11ii...} + 2D_{22ii...} \\ &= \left\langle(\Delta u_1)^2\left[(\Delta u_i)^2\right]^{(N-1)/2}\right\rangle + 2\left\langle(\Delta u_2)^2\left[(\Delta u_i)^2\right]^{(N-1)/2}\right\rangle \end{aligned} \quad (3.75)$$

but would need to close $\langle(\Delta u_2)^2[(\Delta u_i)^2]^{(N-1)/2}\rangle$. In the viscous range, the balance reduces to

$$2\nu\frac{\partial D_{[N]}}{\partial r} - \frac{4\nu}{r^2}\int_0^r D_{[N]}\mathrm{d}y = \frac{1}{r^2}\int_0^r y^2\left\langle E_{[N]}\right\rangle\mathrm{d}y \quad (3.76)$$

for odd N. In the viscous range, $D_{[N]} \sim r^N$ (cf. eq. (3.25)) and consequently

$$D_{[N]} = \frac{1}{2\nu}\frac{E_{[N]}}{N(N+1)-2}r^2 \quad (3.77)$$

which is consistent with the third-order solutions given in section 4.3.1.

3.3.1 Equation for the fourth-order trace of structure functions and its dissipation source term

In this section, the fourth-order trace equations are given explicitly, both for the structure functions as well as the dissipation source terms. These equations are used in section 5.3 below, where they are analysed in more detail. Higher-order

equations can be derived analogously.

Trace of fourth-order structure function equations

From eq. (3.66), the fourth-order trace amounts to the sum

$$D_{[4]} = D_{4,0} + 4D_{2,2} + \frac{8}{3}D_{0,4}. \tag{3.78}$$

Consequently, the transport equation for $D_{[4]}$ is derived by adding the individual structure function equations eq. (3.44), (3.45) and (3.46) as given in section 3.1.2. This results in

$$\frac{\partial D_{[4]}}{\partial t} + \frac{\partial}{\partial r_n}\left\langle \Delta u_n \left(\Delta u_i\right)^2 \left(\Delta u_j\right)^2 \right\rangle = 2\nu \frac{\partial^2 D_{[4]}}{\partial r_n^2} - \left\langle T_{[4]} \right\rangle - \left\langle E_{[4]} \right\rangle. \tag{3.79}$$

Here, the second term on the left-hand side is the transport term containing the fifth-order longitudinal, mixed, and transverse structure functions $D_{5,0}$, $D_{3,2}$ and $D_{1,4}$, respectively. The first term on the right-hand side of eq. (3.79) is the viscous term containing the fourth-order structure functions $D_{4,0}$, $D_{2,2}$ and $D_{0,4}$. The remaining two terms in the equation are the pressure source term and the dissipation source term in that order. Eq. (3.79) is closely related to eq. (4.3) of Falkovich et al. (2010) (also a fourth-order equation), which they derived from the kinetic energy equation. From this, they found a new relation for the pressure-velocity correlation in the inertial range, similar to Kolmogorov's 4/5-law stemming from the second order.

In explicit notation, the transport term is written as

$$\begin{aligned}\frac{\partial}{\partial r_n}\left\langle \Delta u_n \left(\Delta u_i\right)^2 \left(\Delta u_j\right)^2 \right\rangle &= \frac{\partial D_{5,0}}{\partial r} + 4\frac{\partial D_{3,2}}{\partial r} + \frac{8}{3}\frac{\partial D_{1,4}}{\partial r} \\ &\quad + \frac{2}{r}D_{5,0} + \frac{8}{r}D_{3,2} - \frac{16}{3r}D_{1,4} = \frac{\partial D_{[5]}}{\partial r} + \frac{2}{r}D_{[5]},\end{aligned} \tag{3.80}$$

where $D_{[5]}$ is the trace of the general fifth-order structure function tensor,

$$D_{[5]} = \left\langle \Delta u_1 \left(\Delta u_i\right)^2 \left(\Delta u_j\right)^2 \right\rangle = D_{5,0} + 4D_{3,2} + \frac{8}{3}D_{1,4}. \tag{3.81}$$

The pressure source term is given by

$$\langle T_{[4]} \rangle = 4 \left\langle (\Delta u_i)^2 \, \Delta u_j \Delta P_j \right\rangle = 4 \left\langle (\Delta u_1)^3 \, \Delta P_1 \right\rangle + 8 \left\langle (\Delta u_2)^2 \, \Delta u_1 \Delta P_1 + (\Delta u_1)^2 \, \Delta u_2 \Delta P_2 \right\rangle + \frac{32}{3} \left\langle (\Delta u_2)^3 \, \Delta P_2 \right\rangle, \quad (3.82)$$

the dissipation source term by

$$\begin{aligned} \langle E_{[4]} \rangle &= \left\langle 4 (\Delta u_i)^2 \left(\epsilon_{jj} + \epsilon'_{jj} \right) + 8 \Delta u_i \Delta u_j \left(\epsilon_{ij} + \epsilon'_{ij} \right) \right\rangle \\ &= 12 \left\langle (\Delta u_1)^2 \left(\epsilon_{11} + \epsilon'_{11} \right) \right\rangle + 32 \left\langle \Delta u_1 \Delta u_2 \left(\epsilon_{12} + \epsilon'_{12} \right) \right\rangle \\ &\quad + 8 \left\langle (\Delta u_2)^2 \left(\epsilon_{11} + \epsilon'_{11} \right) + (\Delta u_1)^2 \left(\epsilon_{22} + \epsilon'_{22} \right) \right\rangle \\ &\quad + \frac{32}{3} \left\langle (\Delta u_2)^2 \left(\epsilon_{22} + \epsilon'_{22} \right) \right\rangle, \end{aligned} \quad (3.83)$$

and the viscous term by

$$\begin{aligned} 2\nu \frac{\partial^2 D_{[4]}}{\partial r_n^2} &= 2\nu \left[\frac{\partial^2 D_{4,0}}{\partial r^2} + \frac{2}{r} \frac{\partial D_{4,0}}{\partial r} + 4 \frac{\partial^2 D_{2,2}}{\partial r^2} + \frac{8}{r} \frac{\partial D_{2,2}}{\partial r} \right. \\ &\quad \left. + \frac{8}{3} \frac{\partial^2 D_{0,4}}{\partial r^2} + \frac{16}{3r} \frac{\partial D_{0,4}}{\partial r} \right] = 2\nu \left[\frac{\partial^2 D_{[4]}}{\partial r^2} + \frac{2}{r} \frac{\partial D_{[4]}}{\partial r} \right]. \end{aligned} \quad (3.84)$$

In eqs. (3.79) to (3.84), the definitions

$$\Delta P_i = \frac{\partial p}{\partial x_i} - \frac{\partial p'}{\partial x'_i}, \quad \epsilon_{ij} = \nu \frac{\partial u_i}{\partial x_k} \frac{\partial u_j}{\partial x_k}, \quad (3.85)$$

have been used.

The balance of the different terms in eq. (3.79) is shown in figure 3.12a for the case R0 ($Re_\lambda = 88$) and in figure 3.12b for the case R5 ($Re_\lambda = 529$) of our DNS simulation. We will need this balance to estimate which terms we may neglect when we integrate eq. (3.79) in the viscous range in section 4.3.3 and in the inertial range in section 5.3 below. The terms have been normalised with $(\nu^2 \langle \varepsilon^2 \rangle^3)^{1/4}$ and the separation distance r with the Kolmogorov scale η. It is seen that in the viscous range for values of r/η up to about 5, the transport term and the pressure source term are an order of magnitude smaller than the viscous terms and the dissipation source term for the six datasets R0 to

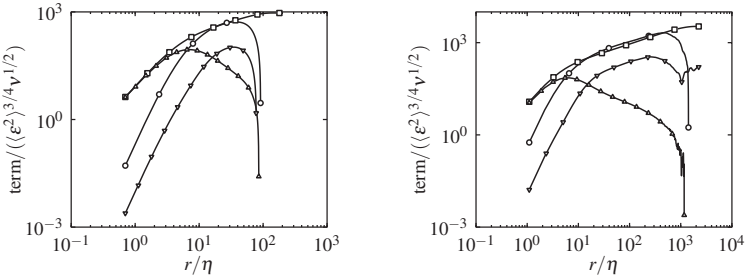

Figure 3.12: Balance of the different terms in eq. (3.79) for the case R0 ($Re_\lambda = 88$) (a) and R5 ($Re_\lambda = 529$) (b). ○: -transport term, □: dissipation source term, ▽: pressure source term, △: viscous term.

R5 (R1 to R4 are not shown here). These terms therefore balance to leading order, which will lead to exact relations in the viscous range, as will be shown in section 4.3.3. As expected, the inertial range increases with increasing Reynolds number: beginning at $r/\eta = 30$, for the case R0 ($Re_\lambda = 88$) there is only a very small inertial range identifiable, whereas for R5 ($Re_\lambda = 529$) it extends to $r/\eta \approx 300$. In the inertial range and for all data sets, the pressure source term is smaller by a factor of four on average and the viscous term is much smaller. This order of magnitude estimate will be used in section 5.3.

The dissipation term $\langle E_{[4]} \rangle$ defined in eq. (3.83) is a correlation between squared velocity increments Δu_1 and Δu_2 and the instantaneous dissipations defined by eq. (3.85) at x_i and likewise at x_i'. Since it balances the transport term in the inertial range and the viscous term in the viscous range, $\langle E_{[4]} \rangle$ is of particular interest and will be further examined in the following. Furthermore, one might expect the dissipation source term to contain dissipative fluctuations.

For very large $r \to \infty$, $D_{[4]} \to 8\langle k^2 \rangle$ i.e. eq. (3.79) then equals the transport equation for $\langle k^2 \rangle$ derived from eq. (1.14), analogously to the second-order equation where $D_{[2]} \to 4\langle k \rangle$ for $r \to \infty$.

Trace of fourth-order dissipation source term equation

Next, the transport equation for the trace of the fourth-order dissipation source terms $\langle E_{[4]} \rangle$ is derived. Similarly to the derivation of the trace of structure

function, one can sum up the longitudinal, mixed and transverse transport equations given above.

The equation for the dissipation source term

$$\left\langle E_{[4]} \right\rangle = \langle E_{4,0} \rangle + 4 \langle E_{2,2} \rangle + \frac{8}{3} \langle E_{0,4} \rangle \tag{3.86}$$

reads with the equations for $\langle E_{4,0} \rangle$, $\langle E_{2,2} \rangle$ and $\langle E_{0,4} \rangle$, cf. eq. (3.57), (3.59) and (3.61) given in section 3.1.3,

$$\begin{aligned} \frac{\left\langle \partial E_{[4]} \right\rangle}{\partial t} + \frac{\partial \left\langle \Delta u_n E_{[4]} \right\rangle}{\partial r_n} &= \nu \frac{\partial^2}{\partial r_n^2} \left\langle E_{[4]} \right\rangle \\ &\quad - \underbrace{\left(F_{[4]} + Q_{[4]} + P_{[4]} + T_{[4]} + \mathcal{D}_{[4]} + \varepsilon_{[4]}^2 \right)}_{\Sigma P_{[4]}^E}, \end{aligned} \tag{3.87}$$

where $\Sigma P_{[4]}^E$ is the trace of the sum of source terms in the dissipation source term equation, where the transport term is defined as

$$\begin{aligned} \frac{\partial \left\langle \Delta u_n E_{[4]} \right\rangle}{\partial r_n} &= \frac{\partial \langle \Delta u_1 E_{4,0} \rangle}{\partial r} + 4 \frac{\partial \langle \Delta u_1 E_{2,2} \rangle}{\partial r} + \frac{8}{3} \frac{\partial \langle \Delta u_1 E_{0,4} \rangle}{\partial r} \\ &\quad + \frac{2}{r} \langle \Delta u_1 E_{4,0} \rangle + \frac{8}{r} \langle \Delta u_1 E_{2,2} \rangle + \frac{16}{3r} \langle \Delta u_1 E_{0,4} \rangle \\ &= \frac{\partial \left\langle \Delta u_1 E_{[4]} \right\rangle}{\partial r} + \frac{2}{r} \left\langle \Delta u_1 E_{[4]} \right\rangle \end{aligned} \tag{3.88}$$

with

$$\Delta u_1 E_{[4]} = \Delta u_1 E_{4,0} + 4 \Delta u_1 E_{2,2} + \frac{8}{3} \Delta u_1 E_{0,4}, \tag{3.89}$$

the viscous term

$$2\nu \frac{\partial^2 \left\langle E_{[4]} \right\rangle}{\partial r_n^2} = 2\nu \left[\frac{\partial^2 \left\langle E_{[4]} \right\rangle}{\partial r^2} + \frac{2}{r} \frac{\partial \left\langle E_{[4]} \right\rangle}{\partial r} \right], \tag{3.90}$$

the F-term

$$F_{[4]} = 8\nu \left\langle (\Delta u_i)^2 \left(A_{jj} + A'_{jj} \right) + \Delta u_i \Delta u_j \left(A_{ij} + A'_{ij} + A_{ji} + A'_{ji} \right) \right\rangle, \tag{3.91}$$

the Q-term

$$Q_{[4]} = 4\nu \left\langle (\Delta u_i)^2 \left(\chi_{jj} + \chi'_{jj}\right) + 2\Delta u_i \Delta u_j \left(\chi_{ij} + \chi'_{ij}\right) \right\rangle, \tag{3.92}$$

the P-term

$$P_{[4]} = 8 \left\langle \Delta u_i \Delta P_i \left(\varepsilon_{jj} + \varepsilon'_{jj}\right) + \left(\Delta u_i \Delta P_j + \Delta u_j \Delta P_i\right) \left(\varepsilon_{ij} + \varepsilon'_{ij}\right) \right\rangle, \tag{3.93}$$

the T-term

$$T_{[4]} = 8\nu \left\langle (\Delta u_i)^2 \left(P_{jj} + P'_{jj}\right) + \Delta u_i \Delta u_j \left(P_{ij} + P'_{ij} + P_{ji} + P'_{ji}\right) \right\rangle, \tag{3.94}$$

the $\mathcal{D}$-term

$$\begin{aligned} \mathcal{D}_{[4]} = 8\nu & \left\langle \left(\frac{\partial (\Delta u_i)^2}{\partial x_n} \frac{\partial \varepsilon_{jj} + \varepsilon'_{jj}}{\partial x_n} + \frac{\partial (\Delta u_i)^2}{\partial x'_n} \frac{\partial \varepsilon'_{jj} + \varepsilon'_{jj}}{\partial x'_n} \right) \right\rangle \\ & + 8\nu \left\langle 2 \left(\frac{\partial \Delta u_i \Delta u_j}{\partial x_n} \frac{\partial \varepsilon_{ij} + \varepsilon'_{ij}}{\partial x_n} + \frac{\partial \Delta u_i \Delta u_j}{\partial x'_n} \frac{\partial \varepsilon'_{ij} + \varepsilon'_{ij}}{\partial x'_n} \right) \right\rangle, \end{aligned} \tag{3.95}$$

and the ε^2-term

$$\begin{aligned} \varepsilon^2_{[4]} &= \left\langle 8 \left(\epsilon_{ii} + \epsilon'_{ii}\right) \left(\epsilon_{jj} + \epsilon'_{jj}\right) + 16 \left(\epsilon_{ij} + \epsilon'_{ij}\right)^2 \right\rangle \\ &= 8 \left\langle \left(\epsilon + \epsilon'\right)^2 \right\rangle + 16 \left\langle \left(\epsilon_{ij} + \epsilon'_{ij}\right)^2 \right\rangle. \end{aligned} \tag{3.96}$$

For better readability, the definitions

$$A_{ij} = \frac{\partial u_n}{\partial x_m} \frac{\partial u_i}{\partial x_n} \frac{\partial u_j}{\partial x_m}, \quad P_{ij} = \frac{\partial u_i}{\partial x_m} \frac{\partial^2 p}{\partial x_j \partial x_m} \tag{3.97}$$

and

$$\chi_{ij} = 2\nu \left[\frac{\partial^2 u_i}{\partial x_n \partial x_m} \frac{\partial^2 u_j}{\partial x_n \partial x_m} \right] \tag{3.98}$$

have been used in eqs. (3.91) to (3.94).

For the stationary case, the transport term on the left-hand side in eq. (3.87) balances the viscous term and the sum of source terms $\Sigma P^E_{[4]}$. The source terms are defined in eq. (3.91) to (3.96) and are shown in figure 3.13 for the cases R1 ($Re_\lambda = 119$) and R4 ($Re_\lambda = 331$), together with the transport term and the viscous term. Negative terms are denoted with a minus sign, meaning that we

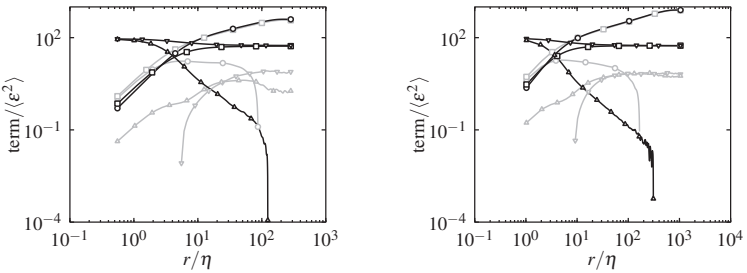

Figure 3.13: Balance of the different terms in eq. (3.87) for the case R1 ($Re_\lambda = 119$) (a) and case R4 ($Re_\lambda = 331$) (b). ○: -transport term, □: -F-term, ▽: -P-term, △: T-term, ○: Q-term, □: -D-term, ▽: ε^2-term, △: viscous term.

have changed their sign in order to be able to show them in a log-log plot. As seen in figure 3.13, the largest ones are the F-term and the Q-term, which nearly balance each other. The F-term is a correlation between the velocity increments squared and the triple product of velocity gradients ($A_{ij} + A'_{ij}$). The Q-term is a correlation between the velocity increments, and ($\chi_{ij} + \chi'_{ij}$). χ_{ij} describes the dissipation of velocity gradients squared, while A_{ij} describes their production by stretching. The next two source terms, called the T-term and the P-term containing pressure derivatives, are relatively small and will not be discussed here in detail. Finally, there are the D-term and the ε^2-term, which balance each other in the inertial range, but strongly diverge from each other in the viscous range. In the following, the focus will be on the ε^2-term, which is the sum of the second-order dissipation parameters.

The ε^2-term is defined as $8\left\langle(\varepsilon_{ii} + \varepsilon'_{ii})^2\right\rangle + 16\left\langle(\varepsilon_{ij} + \varepsilon'_{ij})^2\right\rangle$ and is a two-point quantity depending on r. Noticeably, Hill (2002) showed that the sum of the two-point dissipation $\langle\epsilon + \epsilon'\rangle$ also appears in the trace of the second-order structure function equations, which then reduces to $4\langle\epsilon\rangle$ independent of r for homogeneous flows, cf. the $N = 2$ equations in section 3.1.2.

Since ϵ_{ij} becomes equal to ϵ'_{ij} for $r \to 0$, $\epsilon^2_{[4]}$ approaches the value $32\langle\epsilon^2_{ii}\rangle + 64\langle\epsilon^2_{ij}\rangle$ and balances the viscous term there as seen in figure. 3.13. The quantity $\langle\epsilon^2_{ii}\rangle = \langle\epsilon^2\rangle$ is the second-order moment of the pseudo-dissipation distribution of ϵ. It is a sum of dissipation parameters which appear in the set of successive equations. It is worth noting that the ε^2-term in figure 3.13 starts as a constant

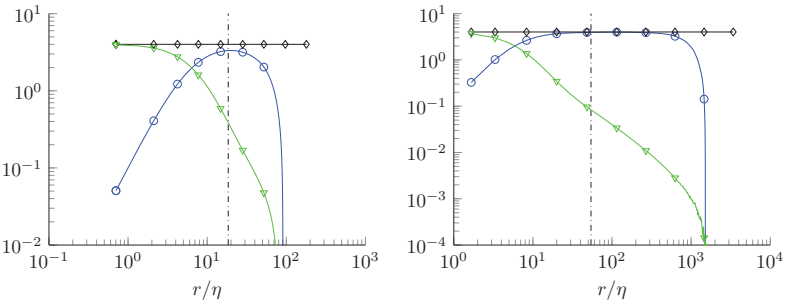

Figure 3.14: Balances of the normalised second-order structure function trace equation $N = 2$. Left: $Re_\lambda = 88$. Right: $Re_\lambda = 754$. Ratio λ/η is indicated by the vertical dash-dotted lines. ○: $-\partial_{r_i}\langle \Delta u_i (\Delta u_j)^2 \rangle$, ◇: $E_{[2]}$, ▽: $2\nu\partial^2_{r_n} D_{[2]}$. All terms are divided by $\langle\varepsilon\rangle$.

for small values of r, then decreases slightly and becomes constant again at the large scales. In the latter range, $8\langle(\epsilon_{ii} + \epsilon'_{ii})^2\rangle + 16\langle(\epsilon_{ij} + \epsilon'_{ij})^2\rangle$ becomes a constant; i.e., it differs from the value for $r \to 0$ only by a constant factor. That is, the ε^2-term links the remaining terms of eq. (3.87) at the very large and very small scales, similar to $\langle\epsilon\rangle$ at the second order. We are mostly interested in the influence of the ε^2-term, since this term is closest to the classical picture of dissipative fluctuations in turbulent flows in the spirit of Kolmogorov. This is discussed im more detail in section 5.3.

3.3.2 Balance of traces of even-order structure function equations

The balances for the traces of the structure functions for even orders as defined by eq. (3.66) were computed by summing up the individual even-order balances according to table 3.6. The balance for the second-order trace equations normalised with $\langle\varepsilon\rangle$ is plotted over r/η and shown in figure 3.14a and 3.14b, while the balance of the $N = 4$ trace* $D_{[4]}$ normalised with $\langle\varepsilon^2\rangle^{6/8}\nu^{1/2}$ over $r/\eta_{C,4}$ and

*This balance was already shown and discussed in section 3.3.1 above.

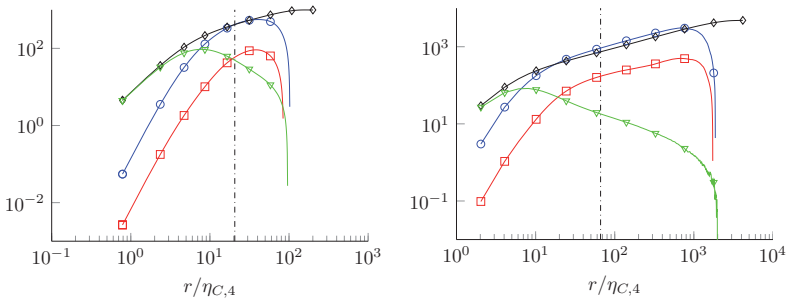

Figure 3.15: Balances of the normalised fourth-order structure function trace equation $N = 4$. Left: $Re_\lambda = 88$. Right: $Re_\lambda = 754$. Ratio $\lambda/\eta_{C,4}$ is indicated by the vertical dash-dotted lines. ○: $-\partial_{r_i}\langle \Delta u_i[(\Delta u_j)^2]^2\rangle$, □: $T_{[4]}$, ◇: $E_{[4]}$, ▽: $2\nu\partial^2_{r_n} D_{[4]}$. All terms are divided by $\langle\varepsilon^2\rangle^{6/8}\nu^{1/2}$.

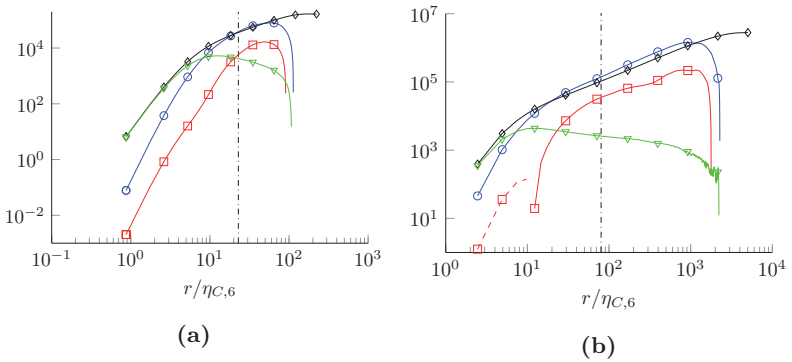

Figure 3.16: Balances of the normalised sixth-order structure function trace equation $N = 6$. Left: $Re_\lambda = 88$. Right: $Re_\lambda = 754$. Ratio $\lambda/\eta_{C,6}$ is indicated by the vertical dash-dotted lines. ○: $-\partial_{r_i}\langle \Delta u_i[(\Delta u_j)^2]^3\rangle$, □: $T_{[6]}$, ◇: $E_{[6]}$, ▽: $2\nu\partial^2_{r_n} D_{[6]}$. Changes of signs are indicated by the dashed lines. All terms are divided by $\langle\varepsilon^{7/2}\rangle^{8/12}\nu$.

the $N = 6$ balance for $D_{[6]}$ normalised with $\langle\varepsilon^3\rangle^{8/12}\nu$ over $r/\eta_{C,6}$ are depicted in figure 3.15a and 3.15b and figure 3.16a and 3.16b, respectively. Since the trace balances are the sum of the individual balances of section 3.2.1, similar conclusions can be drawn. For all three even orders examined here, the trace of the dissipation source terms $\langle E_{[N]}\rangle$ balance the trace of the viscous source terms in the viscous range, where the traces of the pressure source terms $\langle T_{[N]}\rangle$ and transport terms can be neglected. If one then derives consecutive transport equations for $\langle E_{[N]}\rangle$, one finds that $\langle E_{[N]}\rangle \sim \langle\epsilon^N\rangle r^{N-2}$ in the viscous range as discussed in section 3.1.1. In the inertial range, the trace of the viscous terms and the trace of the pressure source terms can be neglected to yield to leading order

$$\frac{\partial D_{[N+1]}}{\partial r} + \frac{2}{r} D_{[N+1]} \approx -\left\langle E_{[N]}\right\rangle . \tag{3.99}$$

Noticeably, this balance is better satisfied at the lower Reynolds number $Re_\lambda = 88$. For that reason, one should be somewhat cautious when neglecting the trace of the pressure source terms at high Reynolds numbers and orders, although neglecting $\langle T_{[N]}\rangle$ at the higher Reynolds number for $N = 6$ seems justified. Approximating the traces in the inertial range with a power-law would result in the same scaling exponent for $\langle E_{[N]}\rangle$, $\langle T_{[N]}\rangle$ and the transport term (cf. figures 3.15 and 3.16) as was also found for the individual equations discussed above in section 3.2.1.

3.3.3 Balance of traces of odd-order structure function equations

We show the balances for the odd-order trace equations for the third order in figure 3.17, the fifth order in figure 3.18 and the seventh order in figure 3.19, where we have normalised the traces as the individual equations discussed in section 3.2.2. We find similar characteristics for the odd-order trace equations as for the respective longitudinal, mixed and transverse equations. While the trace of the dissipation source terms and the viscous terms dominate the trace of transport terms and pressure source terms in the viscous range for the lower Reynolds number case R0, all terms are of the same order of magnitude in the viscous range for the higher Reynolds number for all odd orders we have examined. Nevertheless, the balance of the trace of the viscous and dissipative terms holds also for the odd orders. In the inertial range, the trace of dissipation

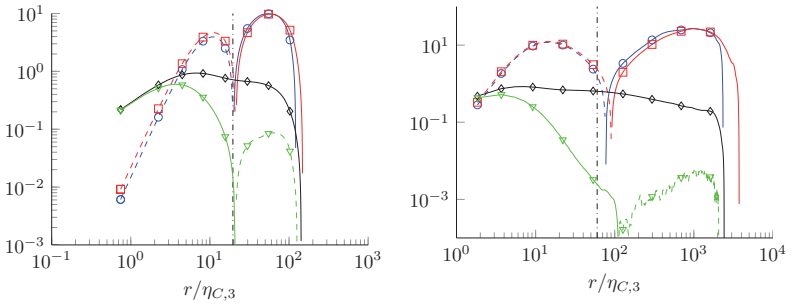

Figure 3.17: Balances of the normalised third-order structure function trace equation $N = 3$. Left: $Re_\lambda = 88$. Right: $Re_\lambda = 754$. Ratio $\lambda/\eta_{C,3}$ is indicated by the vertical dash-dotted lines. ○: $\partial_{r_i}\langle \Delta u_i \Delta u_1 (\Delta u_j)^2 \rangle$, □: $-T_{[3]}$, ◇: $-E_{[3]}$, ▽: $-2\nu\partial^2_{r_n} D_{[3]}$. Changes of signs are indicated by the dashed lines. All terms are divided by $\langle \varepsilon^{3/2} \rangle^{5/6} \nu^{1/4}$.

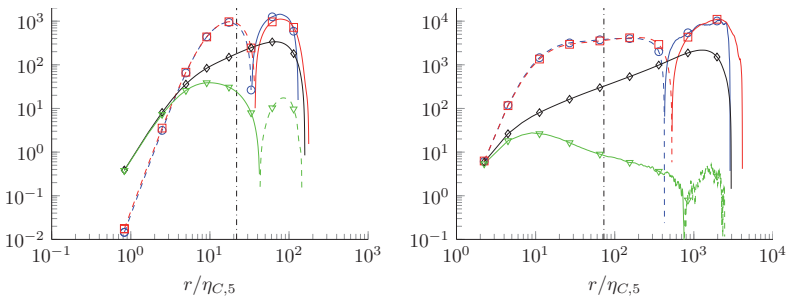

Figure 3.18: Balances of the normalised fifth-order structure function trace equation $N = 5$. Left: $Re_\lambda = 88$. Right: $Re_\lambda = 754$. Ratio $\lambda/\eta_{C,5}$ is indicated by the vertical dash-dotted lines. ○: $\partial_{r_i}\langle \Delta u_i \Delta u_1 [(\Delta u_j)^2]^2 \rangle$, □: $-T_{[5]}$, ◇: $-E_{[5]}$, ▽: $-2\nu\partial^2_{r_n} D_{[5]}$. Changes of signs are indicated by the dashed lines. All terms are divided by $\langle \varepsilon^{5/2} \rangle^{7/10} \nu^{3/4}$.

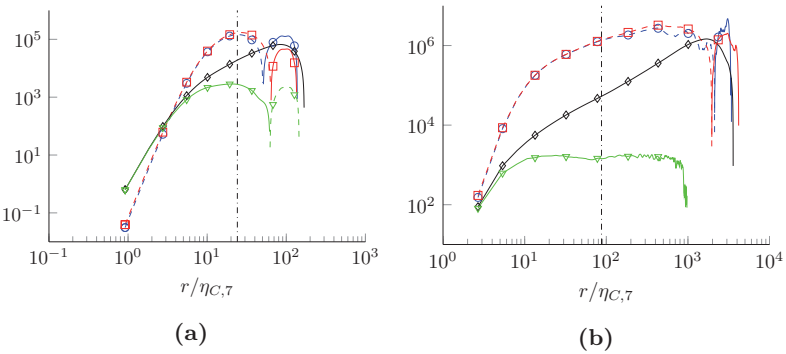

Figure 3.19: Balances of the normalised seventh-order structure function trace equation $N = 7$. Left: $Re_\lambda = 88$. Right: $Re_\lambda = 754$. Ratio $\lambda/\eta_{C,7}$ is indicated by the vertical dash-dotted lines. ○: $\partial_{r_i}\langle \Delta u_i \Delta u_1 [(\Delta u_j)^2]^3 \rangle$, □: $-T_{[7]}$, ◇: $-E_{[7]}$, ▽: $-2\nu\partial^2_{r_n} D_{[7]}$. Changes of signs are indicated by the dashed lines. All terms are divided by $\langle \varepsilon^{7/2} \rangle^{9/14} \nu^{5/4}$.

source terms can be neglected and the trace of pressure source terms and the transport terms collapse. That is, $\langle E_{[N]} \rangle$ in eq. (3.74) can be dropped,

$$D_{[N+1]} = 2 \left\langle (\Delta u_2)^2 \left[(\Delta u_i)^2 \right]^{(N-1)/2} \right\rangle + \frac{2}{r^2} \int r \left\langle (\Delta u_2)^2 \left[(\Delta u_i)^2 \right]^{(N-1)/2} \right\rangle \mathrm{d}r - \frac{1}{r^2} \int r^2 \left\langle T_{[N]} \right\rangle \mathrm{d}r \quad (3.100)$$

for all odd-order traces examined here. Noticeably, eq. (3.100) also holds in the viscous range as does eq. (3.71), cf. the figures 3.17, 3.18, and 3.19. Furthermore, the zero-crossing of the trace of transport and pressure source terms where their collapse is diminished and moves to larger normalised r with increasing order and Reynolds number. Consequently, the approximation eq. (3.100) holds over a larger range of r with increasing order and Re_λ. Assuming power-laws in the inertial range, the trace of dissipation source terms scales differently than both the trace of pressure source terms and transport terms, as seen from the figures.

3.4 Eddy viscosity closure for the transport terms

The system of equations is unclosed, as has been discussed in section 3.1 above. Here, we briefly discuss a conceivable approach to close the system. This closure introduces additional assumptions and it should be stressed that there are other possible ansatzes. Furthermore, the focus of the present work is not on closing the system. For that reason, no numerical solutions of the fully closed system up to some order N were carried out. However, we will look at the closed second-order equations in section 5.4.

From figure 3.1, it is clearly seen that the structure functions of order $N+1$ feed into the equations for structure functions at order N via the transport term. This coupling stems from the non-linearity of the Navier-Stokes equations and is similar to the unclosed transport terms in RANS. Therefore, one has to truncate the system at some order, if one is interested in solving the system of equations numerically. Consequently, the structure functions of the next higher order appear after truncation as unknown, unclosed quantities in the remaining system of equations.

A straightforward approach to close the system at order N is to employ an eddy viscosity ansatz, by writing

$$D_{m+1,n} = -\nu_{t,(m+1,n)} \frac{\partial D_{m,n}}{\partial r} \tag{3.101}$$

for all but the transverse structure functions $D_{0,m+n}$. These can be closed by assuming

$$D_{0,(m+n)} = -\nu_{t,(0,m+n)} \frac{\partial D_{1,(m+n-2)}}{\partial r}. \tag{3.102}$$

Thus, the $(N+1)$th-order structure functions are expressed by the Nth-order structure functions, in agreement with the red arrows in figure 3.1. Therefore, the transport terms are closed when the ν_t are specified. In general, one would expect

$$\nu_t = f(r, Re_\lambda, m, n), \tag{3.103}$$

i.e. that the eddy viscosities depend on r, the Reynolds number and the order. For this ansatz to be meaningful, one would hope that one can relax the dependence on these parameters. For that reason, the influence of the Reynolds number and the order are briefly examined in the following.

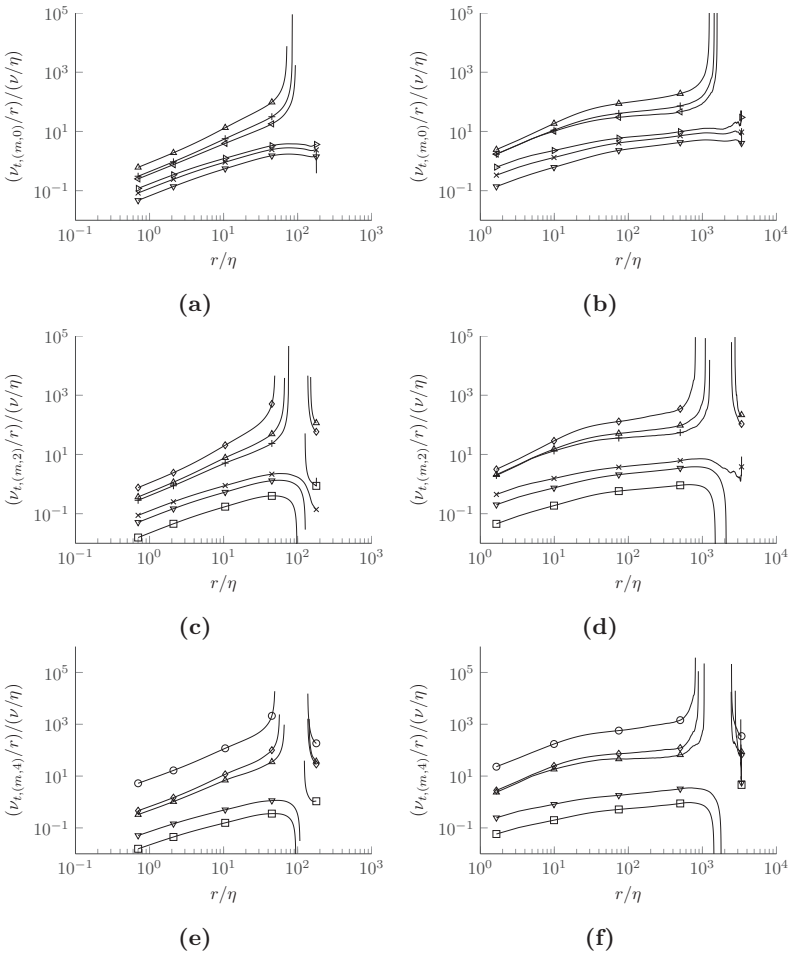

Figure 3.20: Normalised eddy viscosities $\nu_{t,(m,n)}$ for $Re_\lambda = 88$ (left column) and $Re_\lambda = 754$ (right column). $\circ$: $m = 0$, $\square$: $m = 1$, $\diamond$: $m = 2$, $\triangledown$: $m = 3$, $\triangle$: $m = 4$, x: $m = 5$, $+$: $m = 6$, $\triangleright$: $m = 7$, $\triangleleft$: $m = 8$.

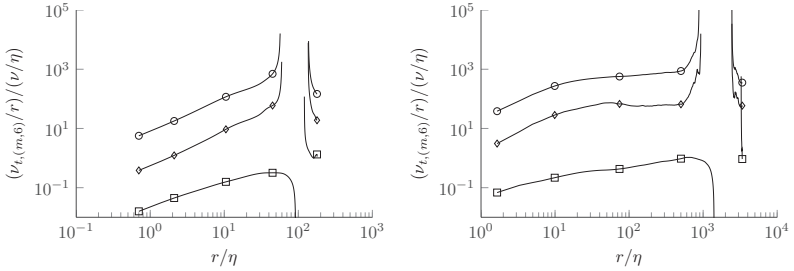

Figure 3.21: Normalised eddy viscosities $\nu_{t,(m,n)}$ for $Re_\lambda = 88$ (left column) and $Re_\lambda = 754$ (right column). ○: $m = 0$, □: $m = 1$, ◇: $m = 2$, ▽: $m = 3$, △: $m = 4$, x: $m = 5$, +: $m = 6$, ▷: $m = 7$, ◁: $m = 8$.

First, the influence of the order is shown in figure 3.20 and figure 3.21. The eddy viscosities up to the eighth order were sorted by the second index n. In figure 3.20a and 3.20b, $\nu_{t,(3,0)}$, $\nu_{t,(4,0)}$, $\nu_{t,(5,0)}$, $\nu_{t,(6,0)}$, $\nu_{t,(7,0)}$ and $\nu_{t,(8,0)}$ are plotted for the two cases R0 (left column, $Re_\lambda = 88$) and R6 (right column, $Re_\lambda = 754$). Similarly, $\nu_{t,(1,2)}$, $\nu_{t,(2,2)}$, $\nu_{t,(3,2)}$, $\nu_{t,(4,2)}$, $\nu_{t,(5,2)}$ and $\nu_{t,(6,2)}$ are shown in figure 3.20c and 3.20d and $\nu_{t,(0,4)}$, $\nu_{t,(1,4)}$, $\nu_{t,(2,4)}$, $\nu_{t,(3,4)}$ and $\nu_{t,(4,4)}$ in figure 3.20e and 3.20f. Finally, $\nu_{t,(0,6)}$, $\nu_{t,(1,6)}$ and $\nu_{t,(2,6)}$ are plotted in figure 3.21a and 3.21b. All eddy viscosities were normalised with the viscosity ν, divided by r/η and plotted over r/η. $\nu_{t,(0,8)}$ is not shown, since it is the only eddy viscosity with $n = 8$ up to the eighth order and therefore it is not possible to examine the general behaviour of $\nu_{t,(m,8)}$ here. However, one might expect that also $\nu_{t,(m,8)}$ and eddy viscosities with higher n are qualitatively similar to those shown in figure 3.20.

In figure 3.20 and figure 3.21, an interesting characteristic can be observed: For fixed n and increasing order $N = m + n$ (i.e. increasing m), $\nu_{t,(m,n)}$ seems to approach a single curve: Those with even m approach from above, while eddy viscosities with odd m approach from below. This implies that the eddy viscosity (with fixed n) could be modeled by a prescribed $\nu_{t,(m,n)}$ if the system of equations is cut off at a high enough order N.

In order to analyse the influence of the Reynolds number, the eddy viscosities at the eighth order are plotted for all datasets R0 to R6. The eighth order has been chosen because the order-dependency discussed above suggests to close the

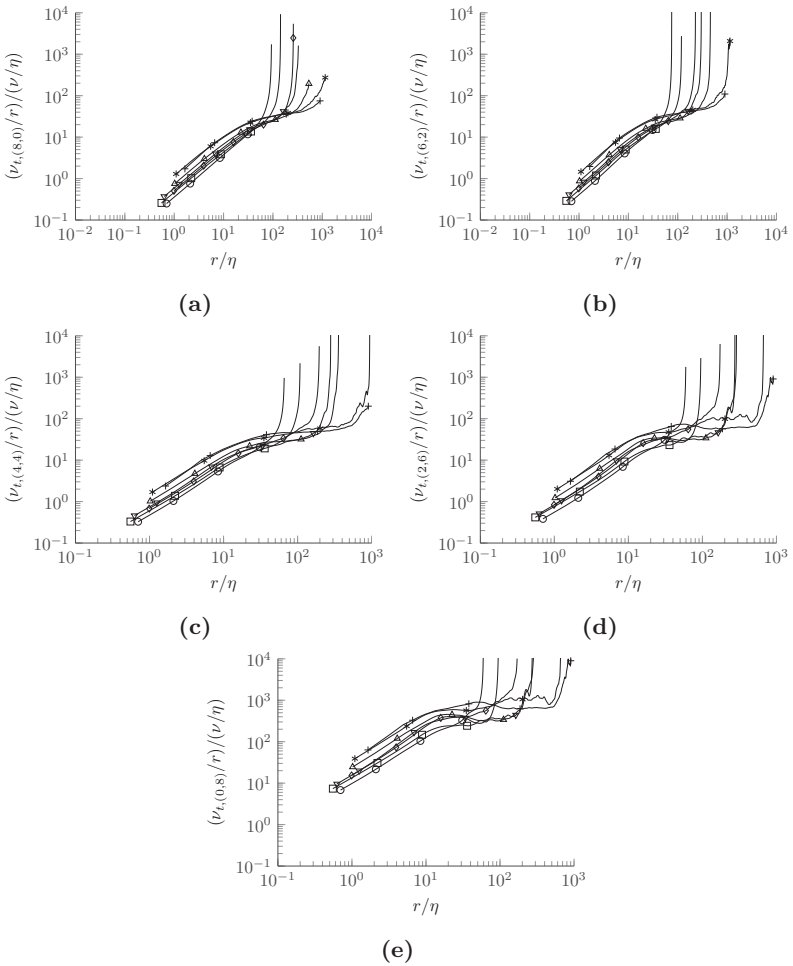

Figure 3.22: Normalised eddy viscosities $\nu_{t,(m,n)}$ with $m + n = 8$ for different Reynolds numbers. ○: $Re_\lambda = 88$, □: $Re_\lambda = 119$, ◇: $Re_\lambda = 184$, ▽: $Re_\lambda = 254$, △: $Re_\lambda = 331$, x: $Re_\lambda = 529$, +: $Re_\lambda = 754$.

system at higher orders; the eighth order is the highest that we have computed numerically in the present work. $\nu_{t,(8,0)}$ is shown in figure 3.22a, $\nu_{t,(6,2)}$ in figure 3.22b, $\nu_{t,(4,4)}$ in figure 3.22c, $\nu_{t,(2,6)}$ in figure 3.22d and $\nu_{t,(0,8)}$ is shown in figure 3.22e. Interestingly, the eddy viscosities collapse on a single curve for the two cases R5 and R6 ($Re_\lambda = 529$ and $Re_\lambda = 754$, respectively), while the smaller datasets show a Reynolds number influence. As expected, the inertial range for which a power-law scaling of the eddy viscosities at intermediate r/η is observed, increases with increasing Reynolds number. Assuming tentatively a power-law for the eddy viscosities in the inertial range,

$$\nu_{t,(m,n)} \sim r^{1+\beta_{m,n}}, \tag{3.104}$$

it is evident that $0 < \beta_{m,n} \ll 1$ for the larger Reynolds numbers. Indeed, $\beta_{m,n}$ becomes smaller with increasing order, cf. figure 3.20 and figure 3.22. If one assumes a power-law scaling for the structure functions such as eq. (3.34) together with eq. (3.101) and eq. (3.104), this is in agreement with the observation that $\zeta_{m+1,n} - \zeta_{m,n} \to 0$ with increasing N, i.e. that the difference between the scaling exponents becomes smaller the higher the order, cf. e.g. Anselmet et al. (1984). This is also in agreement with the Hölder inequality of the scaling exponents, cf. the discsussion in Frisch (1995).

We may conclude that the eddy viscosity ansatz is promising inasmuch that it may be independent of the order and Reynolds number, provided both are large enough. Nevertheless, one needs to specify ν_t or make additional assumptions relating it to other quantities appearing in the truncated system of equations. We will use the eddy viscosity ansatz in section 5.4 below, where we truncate at the second order, i.e. use $\nu_{t,(3,0)}$ and $\nu_{t,(1,2)}$. There, we employ an ansatz by Oberlack and Peters (1993), which relates the eddy viscosities to the second-order structure function equations, thereby closing the system. This is discussed in more detail in section 5.4 below. However, one should keep in mind that this is but one of many conceivable possibilities to close the system.

4 Viscous range

In this chapter, we look at the viscous range in more detail. With the exception of section 4.4.3, the chapter is based on Boschung (2015) (section 4.1), Boschung et al. (2017b) (section 4.2), Boschung et al. (2017a,c) and Peters et al. (2016) (section 4.3) as well as Boschung et al. (2016c) (section 4.4).

As a result, we find exact relations in the viscous range. In section 4.1, we use a methodology introduced by Siggia (1981) to exactly relate the moments of the dissipation to the even-order moments of the longitudinal velocity gradient. In section 4.2, we proceed to examine the ratios of moments of the pseudo-dissipation, its components and dissipation surrogates (proportional to moments of longitudinal and mixed velocity gradients) to same-order moments of the dissipation. In section 4.3, analytical results for third- and fourth-order structure functions in the viscous range $r \to 0$ are presented. Based on the results of section 4.1 and section 4.2, exact order-dependent dissipative scales in the spirit of Kolmogorov (1941b) are introduced in section 4.4. Since these scales are smaller than the Kolmogorov scale, they have implications for the grid resolution of DNS as discussed in section 4.4.2.

4.1 Exact relations between even moments of the longitudinal velocity gradient and moments of the dissipation ε

The dissipation ε of kinetic energy is thought to be one of the key quantities characterizing turbulent flows. In 1941, Kolmogorov (1941b) postulated that small-scale statistics depend on the viscosity ν and the dissipation ε only. This notion received significant support by Kolmogorov (1941a)'s result that the second-order structure function $D_{2,0}$ has an analytic solution

$$D_{2,0} = \frac{1}{15} \frac{\langle \varepsilon \rangle}{\nu} r^2 \tag{4.1}$$

for $r \to 0$ which was derived from the Navier-Stokes equations under the assumption of homogeneity and isotropy, see eq. (1.32) and section 1.4. It is

noteworthy that the second-order structure function equation is unique in the sense that it is the only order for which the mean dissipation $\langle\varepsilon\rangle$ directly acts as source term, while higher orders are determined by correlations between velocity increments and the dissipation (i.e. the dissipation source terms $\langle \boldsymbol{E}_N \rangle$, cf. eq. (3.14)) as well as pressure terms (the pressure source terms $\langle \boldsymbol{T}_N \rangle$ defined by eq. (3.13)), see the discussion in section 3.1. It is well-known that the higher moments of the dissipation ε and the moments of the longitudinal velocity gradient $\partial u_1/\partial x_1$ increase with increasing Reynolds number, a phenomenon called (internal) intermittency in the literature. Indeed, we will show that the moments of ε and $\partial u_1/\partial x_1$ are closely related.

4.1.1 Derivation of the connectors

Specifically, we need to relate the moments of the dissipation $\varepsilon/(2\nu) = S_{ij}S_{ij}$, where $S_{ij} = (\partial u_i/\partial x_j + \partial u_j/\partial x_i)/2$, to the moments of the longitudinal velocity gradient $\partial u_1/\partial x_1$. That is, we need to compute the coefficients C_M of

$$I_1^{(M)} = \left\langle (S_{ij}S_{ij})^M \right\rangle = C_M \left\langle \left(\frac{\partial u_1}{\partial x_1} \right)^{2M} \right\rangle , \tag{4.2}$$

where $M = 1, 2, 3, ...$ and $M = N/2$. For $M = 1$ and assuming isotropy, eq. (4.1) shows that $C_1 = 15/2$ (cf. Kolmogorov (1941b)) as $\langle(\Delta u_1)^2\rangle = \langle(\partial u_1/\partial x_1)^2\rangle r^2$ for $r \to 0$, cf. eq. (3.25). The same result can be obtained by writing the general velocity gradient tensor $\langle(\partial u_i/\partial x_j)(\partial u_k/\partial x_l)\rangle$ as the sum of scalar functions multiplied by all possible combinations of $\delta_{ij}\delta_{kl}$ and using homogeneity and continuity as additional constraints, cf. eq. (4.29) below or Hinze (1975). However, this procedure is not feasible for higher orders of M, because the number of scalar functions quickly increases (cf. Hierro and Dopazo (2003) for illustrative purposes, where $M = 2$). Siggia (1981) derived $C_2 = 105/4$ in a different way. Specifically, he used a generating function (the second characteristic function,

cf. Papoulis (1991))

$$F = \ln\left[\int \delta(\mathrm{tr}(S)) \exp\left(-\sum_a \lambda_a S_{aa}^2 - 2\left(\mu_1 S_{12} + \mu_2 S_{13} + \mu_3 S_{23}\right)\right) \times \left(\prod_{a\geq b} \mathrm{d}S_{ab}\right)\right] = -\frac{1}{2}\ln\left(\lambda_1\lambda_2 + \lambda_2\lambda_3 + \lambda_1\lambda_3\right) - \frac{1}{2}\ln\left(\mu_1\mu_2\mu_3\right), \quad (4.3)$$

where $\mathrm{tr}(S) = S_{ii} = 0$ due to continuity and the symmetry $S_{ij} = S_{ji}$ has been used. We will use the procedure as outlined by Siggia (1981) in the following. However, we rather use the characteristic function

$$\Phi = \exp(F) = \left[\left(\lambda_1\lambda_2 + \lambda_1\lambda_3 + \lambda_2\lambda_3\right)\mu_1\mu_2\mu_3\right]^{-1/2}, \quad (4.4)$$

since we are only interested in the moments and not the cumulants. Here, we only need the connection between $\langle (S_{11}^2)^M \rangle$ and $I_1^{(M)}$, where due to isotropy $\langle (S_{11}^2)^M \rangle = \langle (S_{22}^2)^M \rangle = \langle (S_{33}^2)^M \rangle$. $I_1^{(M)}$ is an invariant of the general velocity gradient tensor $\langle (\partial u_i/\partial x_j)(\partial x_k/\partial x_l)... \rangle$ of order $2M$, though it is not sufficient to completely determine it for $M > 1$ (cf. Siggia (1981) for details). Using eq. (4.4), it is possible to give the relations for all (even) combinations of $\langle S_{ij}S_{kl}... \rangle$ as well, e.g. $\langle S_{11}^2 S_{12}^4 \rangle = 9/80 \langle S_{11}^6 \rangle$ and $\langle S_{23}^6 \rangle = 27/64 \langle S_{11}^6 \rangle$. For instance, adding the first derivative of Φ with respect to λ_i and μ_j for all λ_i and μ_j and then setting $\lambda_i = \mu_j = \lambda$ due to isotropy, we find $I_1^{(1)} = f(\lambda)$ and similarly $\langle S_{11}^2 \rangle = f(\lambda)$, resulting in $I_1^{(1)} = 15/2 \langle S_{11}^2 \rangle$. As $\langle \varepsilon \rangle = 2\nu I_1^{(1)}$ and $\langle S_{11}^2 \rangle = \langle (\partial u_1/\partial x_1)^2 \rangle$, we recover the well-known relation between the mean of the dissipation and the square of the velocity gradient. We proceed similarly for higher M. Note that it is not possible to use eq. (4.4) to derive connectors between moments of mixed velocity gradients or components of the pseudo-dissipation and the longitudinal velocity gradient, because they cannot be written in terms of $S_{ij}S_{kl}...$ only*.

We list in table 4.1 the resulting C_M for M up to $M = 6$ which have been calculated using a simple computer script based on eq. (4.4) (higher orders could easily be derived, although this is somewhat time-consuming) and compare them with direct numerical simulations (DNS) of homogeneous isotropic turbulence

*E.g. $\partial u_2/\partial x_1 \neq S_{12} = S_{21} = (\partial u_2/\partial x_1 + \partial u_1/\partial x_2)/2$.

Table 4.1: Comparison of the theoretical and numerical values of the coefficients C_M of eq. (4.6) for $Re_\lambda = 88$ $\kappa_{\max}\eta = 3.57$, $Re_\lambda = 215$ ($\kappa_{\max}\eta = 4.01$) and $Re_\lambda = 529$ ($\kappa_{\max}\eta = 2.7$).

C_M	Theory	$Re_\lambda = 88$	$Re_\lambda = 215$	$Re_\lambda = 529$
M = 1	15/2 = 7.5	7.5009	7.4947	7.4998
M = 2	105/4 = 26.25	26.3471	26.1881	26.2499
M = 3	567/8 ≈ 70.88	69.5970	68.3641	69.3524
M = 4	2673/16 ≈ 167.1	157.8169	154.6424	160.9237
M = 5	11583/32 ≈ 362.0	336.5539	341.4591	353.9049
M = 6	47385/64 ≈ 740.4	769.1128	775.5550	734.6193

with Reynolds numbers $Re_\lambda = 88$, $Re_\lambda = 215$ and $Re_\lambda = 529$ (i.e. datasets R0, R3 and R5). We find satisfactory agreement with the theoretical values, as the deviations do not exceed ±5%. The deviations from the theoretical values of C_M tend to be larger for higher M. This is to be expected and most probably due to (numerical) resolution effects (see Donzis et al. (2008) for a study of the influence of the resolution $\kappa_{\max}\eta$ on the statistics of ε), although the three DNS cases are fairly well resolved. Particularly, we have $\kappa_{\max}\eta = 3.57$, $\kappa_{\max}\eta = 4.01$ and $\kappa_{\max}\eta = 2.7$, respectively, where $\kappa_{\max}$ is the maximal wavenumber and $\eta = (\nu^3/\langle\varepsilon\rangle)^{1/4}$ the Kolmogorov scale, cf. section 2.1. It follows that one could also use the ratio of the numerical values of C_M to the theoretical ones as measure of the degree of (local, small-scale) isotropy of the flow. Furthermore, table 4.1 could be used to determine the last completely resolved order M in DNS studies. Factorizing the theoretical values of C_M suggests that they are given by the series

$$C_M = \frac{3^{M-1}(2M+1)(2M+3)}{2^M}, \tag{4.5}$$

i.e. C_M does not exhibit power-law behavior and strongly increases with increasing M. This is to be expected as the number of bilinear combinations $\delta_{ij}\delta_{kl}...$, $\delta_{ik}\delta_{jl}...$, $\delta_{il}\delta_{jk}...$ and so on determining the general tensor $\langle(\partial u_i/\partial x_j)(\partial u_k/\partial x_l)...\rangle$ of order $2M$ also strongly increases with M, cf. Kearsley and Fong (1975).

Thus we find that there is an exact relation between the moments of the dissipation ε and the longitudinal velocity derivative $\partial u_1/\partial x_1$,

$$\left\langle \varepsilon^M \right\rangle = (2\nu)^M C_M \left\langle \left(\frac{\partial u_1}{\partial x_1} \right)^{2M} \right\rangle, \tag{4.6}$$

where the C_M are independent of the Reynolds number and given by table 4.1 and eq. (4.5).

4.1.2 Relation between moments of the longitudinal velocity gradient and the dissipation

As $\langle \partial u_1/\partial x_1 \rangle = 0$ due to homogeneity, this also implies that for the even standardised moments $\mathcal{M}_{2M}$ of $\partial u_1/\partial x_1$ like the flatness ($M = 2$), hyperflatness ($M = 3$) and so on,

$$\mathcal{M}_{2M} = \frac{\left\langle (\partial u_1/\partial x_1)^{2M} \right\rangle}{\left\langle (\partial u_1/\partial x_1)^{2} \right\rangle^{M}} = \frac{C_1^M}{C_M} \frac{\langle \varepsilon^M \rangle}{\langle \varepsilon \rangle^M}. \tag{4.7}$$

Therefore, the even standardised moments of the longitudinal velocity gradient distribution function have the same Reynolds number dependence as the ratio of the moments of dissipation to $\langle \varepsilon \rangle^M$. We note that the ratio C_1^M/C_M increases with M and $\mathcal{M}_{2M}$ increases with M at constant Reynolds number also. Schumacher et al. (2014) recently found that the ratio $\langle \varepsilon^M \rangle / \langle \varepsilon \rangle^M$ seems to be universal in the sense that the same Reynolds number scaling was found for different kinds of flows, namely homogeneous isotropic turbulence, turbulent channel flows and Rayleigh-Bénard convection. Thus also the normalised even moments $\mathcal{M}_{2M}$ of $\partial u_1/\partial x_1$ seem to be universal and the same holds for the moments of $\partial u_2/\partial x_2$ and $\partial u_3/\partial x_3$ due to isotropy. This is the case at least for the flatness of $\partial u_1/\partial x_1$, cf. Ishihara et al. (2007) and Sreenivasan and Antonia (1997) for a compilation of several different data sets. We note that even if we assume that all moments of ε were known such that its probability density function (pdf) could be constructed from its characteristic function, this does not imply that the pdf of $\partial u_1/\partial x_1$ could be determined, because there is no obvious connection between the odd moments of $\partial u_1/\partial x_1$ and the moments of ε. For instance, it is well-known that the skewness of the velocity gradient is related to the vortex stretching term $\langle \omega_i S_{ij} \omega_j \rangle$, cf. Betchov (1956), and there is no apparent connection to $\langle \varepsilon^{3/2} \rangle$. As seen from eq. (4.7), one can only achieve a partial collapse of the pdf $P(\partial u_1/\partial x_1)$ if $\langle \varepsilon^M \rangle / \langle \varepsilon \rangle^M$ scales differently with the Reynolds number for different M.

Furthermore, it is clearly seen from eq. (4.7) that the ratio $\langle \varepsilon^M \rangle / \langle \varepsilon \rangle^M$ would be independent of the Reynolds number if $\partial u_1/\partial x_1$ was Gaussian, $\partial u_1/\partial x_1 \sim \mathcal{N}(0, \sigma^2)$. Then, all moments of $\partial u_1/\partial x_1$ would be determined by the variance σ^2 only. Of course, σ^2 might be Reynolds number dependent, but this dependency

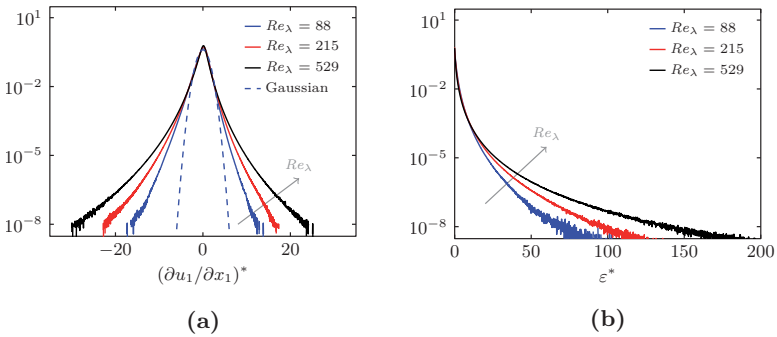

Figure 4.1: Pdfs of (a) the standardised longitudinal velocity gradient $(\partial u_1/\partial x_1)^*$ and (b) the standardised dissipation ε^* for $Re_\lambda = 88$, $Re_\lambda = 215$ and $Re_\lambda = 529$.

would cancel out in eq. (4.7).

The pdfs of $(\partial u_1/\partial x_1)^*$ and ε^* are plotted in figure 4.1a and figure 4.1b, respectively. We normalised both variables to better compare the different Reynolds numbers, i.e. $(\partial u_1/\partial x_1)^* = [(\partial u_1/\partial x_1) - \langle(\partial u_1/\partial x_1)\rangle]/\sqrt{\mathrm{Var}(\partial u_1/\partial x_1)}$ and $\varepsilon^* = [\varepsilon - \langle\varepsilon\rangle]/\sqrt{\mathrm{Var}(\varepsilon)}$, where $\mathrm{Var}(\partial u_1/\partial x_1) = \langle(\partial u_1/\partial x_1)^2\rangle$ and $\mathrm{Var}(\varepsilon) = \langle[\varepsilon - \langle\varepsilon\rangle]^2\rangle$. It is well-known that the longitudinal velocity gradient is non-gaussian (Gylfason et al. (2004) and Ishihara et al. (2007)) and that the deviations increase with increasing Reynolds number, as is also highlighted by our data. As discussed above, the pdfs do not collapse. More specifically, they overlap at the core only, because we used the variance when we normalised the pdfs. This behavior has been frequently observed numerically and experimentally; specifically, the tails of both the (normalised) velocity gradient and dissipation pdf increase with increasing Reynolds number, i.e. the moments also show a Reynolds number dependence. We simply remark that the Reynolds number dependence of the (even) moments of the longitudinal velocity gradient translates to the Reynolds number dependent moments of the dissipation. Without specifying the former, the latter remains unknown and vice versa. Specifically, any theory which determines one of these quantities makes a statement about the other. In that sense, K41 (Kolmogorov (1941a,b)) and K62 theory (Kolmogorov (1962)) as well as the multi-fractal theories (see Nelkin (1994) and Frisch (1995) for an overview) specify the (even) moments of the longitudinal velocity gradient.

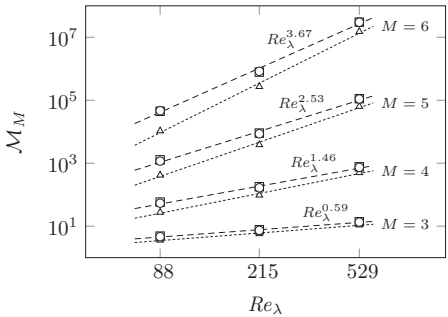

Figure 4.2: Standardised moments of the dissipation $\widetilde{\mathcal{M}}_M$ for $Re_\lambda = 88$, $Re_\lambda = 215$ and $Re_\lambda = 529$. Symbols $\circ$ denote the moments as evaluated from eq. (4.8), $\diamond$ using eq. 4.6 with the theoretical C_M from table 4.1 and $\square$ from eq. (4.13) again with the theoretical C_M. The exponents have been determined using least-square fits.

We can also use eq. (4.7) to relate the standardised moments

$$\widetilde{\mathcal{M}}_M = \frac{\left\langle \left[\varepsilon - \langle\varepsilon\rangle\right]^M \right\rangle}{\left[\mathrm{Var}\,(\varepsilon)\right]^{M/2}} \tag{4.8}$$

of the dissipation ε and the longitudinal velocity gradient $\mathcal{M}_{2M}$. In particular, we have for $M = 3$ (skewness of ε) and $M = 4$ (flatness)

$$\widetilde{\mathcal{M}}_3 = \frac{C_3\mathcal{M}_6 - 3C_2C_1\mathcal{M}_4 + 2C_1^3}{\left[C_2\mathcal{M}_4 - C_1^2\right]^{3/2}} \tag{4.9}$$

$$\widetilde{\mathcal{M}}_4 = \frac{C_4\mathcal{M}_8 - 4C_3C_1\mathcal{M}_6 + 6C_2C_1^2\mathcal{M}_4 - 3C_1^4}{\left[C_2\mathcal{M}_4 - C_1^2\right]^2}. \tag{4.10}$$

Therefore, the standardised moments of the dissipation turn out to be a mixture of all the standardised moments of the longitudinal structure functions at the same and lower order weighted by the C_M. At intermediate to high Re_λ, $\mathcal{M}_6 > \mathcal{M}_4$ so that $P(\varepsilon)$ is positively skewed, cf. figure 4.1b. The flatness $\widetilde{\mathcal{M}}_4 \geq 0$ always, independent of the Reynolds number. Therefore, $C_4\mathcal{M}_8 \geq 4C_3C_1\mathcal{M}_6 - 6C_2^2\mathcal{M}_4 + 3C_1^4$ always and similar relations between the moments of the longitudinal velocity gradient $\partial u_1/\partial x_1$ can be derived from the higher

even moments $\widetilde{\mathcal{M}}_M$.

We show the standardised moments $\widetilde{\mathcal{M}}_M$ of the dissipation in figure 4.2 for $M = 2$ to $M = 6$. Noticeably, $\mathcal{M}_{2M}$ increases with increasing Reynolds number and order M and exhibits power-law behaviour, where the exponent of $\mathcal{M}_4$ agrees with the compiled data of Ishihara et al. (2007). We find that $\widetilde{\mathcal{M}}_M$ consequently also increases with the Reynolds number and order M and also follows a power-law. The differences between using eq. (4.9) and eq. (4.10) (where we used the theoretical C_M given in table 4.1) and eq. (4.8) are small as expected. We note that for large Reynolds numbers $Re_\lambda \gg 1$, $\mathcal{M}_{2M} \gg \mathcal{M}_{2M-2}$ and therefore

$$\widetilde{\mathcal{M}}_3 \to \frac{C_3}{C_2^{3/2}} \frac{\mathcal{M}_6}{\mathcal{M}_4^{3/2}} \tag{4.11}$$

$$\widetilde{\mathcal{M}}_4 \to \frac{C_4}{C_2^2} \frac{\mathcal{M}_8}{\mathcal{M}_4^2}, \tag{4.12}$$

i.e. a single power-law behaviour is approximated. We may generalise this result to

$$\widetilde{\mathcal{M}}_M \to \frac{C_M}{C_2^{M/2}} \frac{\mathcal{M}_{2M}}{\mathcal{M}_4^{M/2}}. \tag{4.13}$$

This can be seen in figure 4.2, where we also plotted eq. (4.13) using the theoretical C_M from table 4.1. We find that eq. (4.13) converges quicker for higher orders M, as may have been expected. Therefore, the standardised moments of $P(\varepsilon)$ are related to the higher even standardised moments M_{2M} and the flatness $\mathcal{M}_4$ of $\partial u_1/\partial x_1$ for large Reynolds numbers. As the ratio of $\mathcal{M}_{2M}/\mathcal{M}_4$ increases with increasing Reynolds number, the standardised moments of ε increase as well. We note that the ratio $C_M/C_2^{M/2}$ decreases with increasing M (cf. eq. (4.5)), so that $\mathcal{M}_{2M}/\mathcal{M}_4^{M/2}$ has to increase (for fixed Re_λ) for $\widetilde{\mathcal{M}}_M > \widetilde{\mathcal{M}}_{M-1}$ in agreement with figure 4.1b. In other words, the ratio $C_M/C_2^{M/2}$ provides a lower bound for the order-dependency of the ratio of even standardised moments of the pdf $P(\partial u_1/\partial x_1)$ to the respective power of its flatness. Furthermore, if we use a power-law

$$\mathcal{M}_{2M} \sim Re_\lambda^{\tilde{\alpha}_{2M}} \tag{4.14}$$

and

$$\widetilde{\mathcal{M}}_M \sim Re_\lambda^{\tilde{\beta}_M} \tag{4.15}$$

with $\tilde{\beta}_{M+1} \geq \tilde{\beta}_M$ as seen from figure 4.1b and figure 4.2, we find from eq. (4.13)

a lower limit

$$\tilde{\alpha}_{2M+2} \geq \tilde{\alpha}_{2M} + \frac{1}{2}\tilde{\alpha}_4 \tag{4.16}$$

for $M \geq 2$, i.e. a lower bound for the Reynolds number dependence of both the even standardised moments of the velocity gradient pdf $\mathcal{M}_{2M}$ and the ratio $\langle\varepsilon^M\rangle/\langle\varepsilon\rangle^M$, that is $\tilde{\alpha}_{2M}$ is increasing with M (note that by using eq. (4.13) we already implicitly assumed that $\tilde{\alpha}_{2M+2} > \tilde{\alpha}_{2M}$ but could modify this result).

Lastly, we would like to point out that it is possible to measure all moments $\langle\varepsilon^M\rangle$ and not only the mean value $\langle\varepsilon\rangle$ using eq. (4.6) with the coefficients given in table 4.1 by employing Taylor's hypothesis, if local isotropy and homogeneity holds. In other words, it is not necessary to resort to one-dimensional surrogates of ε.

4.2 Relation between moments of dissipation, pseudo-dissipation and dissipation surrogates

The kinetic energy dissipation is defined as

$$\varepsilon = 2\nu S_{ij}S_{ij} = \nu\left(\frac{\partial u_i}{\partial x_j}\frac{\partial u_i}{\partial x_j} + \frac{\partial u_i}{\partial x_j}\frac{\partial u_j}{\partial x_i}\right) \tag{4.17}$$

where the strain tensor $S_{ij} = (\partial u_i/\partial x_j + \partial u_j/\partial x_i)/2$ is the symmetric part of the velocity gradient tensor $\partial u_i/\partial x_j$. However, in the system of structure function equations as discussed in section 3.1, the dissipation source terms and transport equations derived thereof contain products of components of the pseudo-dissipation tensor

$$\epsilon_{ij} = \nu\frac{\partial u_i}{\partial x_k}\frac{\partial u_j}{\partial x_k}, \tag{4.18}$$

rather than the dissipation ε, where the pseudo-dissipation ϵ is defined as the trace ϵ_{ii}, i.e,

$$\epsilon = \epsilon_{ii} = \nu\frac{\partial u_i}{\partial x_k}\frac{\partial u_i}{\partial x_k}. \tag{4.19}$$

In this section, we look at the scaling of the ratio of the moments of the pseudo-dissipation to the dissipation, $\langle\epsilon^M\rangle/\langle\varepsilon^M\rangle$ for $M = 1, ..., 4$ using DNS data of forced homogeneous isotropic turbulence with Reynolds numbers from $Re_\lambda = 88$ to $Re_\lambda = 754$ as described in chapter 2. If these ratios are constant,

the moments of ε and ϵ can be used interchangeably.

Similarly, we also examine the ratio of the components of the pseudo-dissipation tensor $\epsilon_{ij}\epsilon_{kl}...$ to the respective moments of the dissipation. In this context, it should be emphasised that the parameters determining the viscous range should be invariants and not depend on the choice of coordinate system. Since $\langle \epsilon^M \rangle$ is invariant but not the components $\langle \epsilon_{ij}\epsilon_{kl}... \rangle$, their ratios to the dissipation $\langle \varepsilon^M \rangle$ as well as to $\langle \epsilon^M \rangle$ and the corresponding Reynolds number scaling are of particular interest. We do not explicitly show the ratios of $\langle \epsilon_{ij}\epsilon_{kl}... \rangle$ to $\langle \epsilon^M \rangle$, though they can be inferred from the reported data by multiplying with $(\langle \epsilon^M \rangle / \langle \varepsilon^M \rangle)^{-1}$.

Lastly, we consider the ratio of

$$G_{p,q} = \nu^{p+q} \left\langle \left(\frac{\partial u_1}{\partial x_1} \right)^{2p} \left(\frac{\partial u_2}{\partial x_1} \right)^{2q} \right\rangle, \tag{4.20}$$

where $p+q=M$ to the moments of the dissipation $\langle \varepsilon^M \rangle$. $G_{M,0}$ is sometimes used as 1D surrogate for the moments of the dissipation $\langle \varepsilon^M \rangle$, since it is easily measurable under the assumption of Taylor's hypothesis. Furthermore, the ratio $G_{p,q}/\langle \varepsilon^M \rangle$ is of some interest, since one may expand structure functions $D_{m,n} = \langle (\Delta u_1)^m (\Delta u_2)^n \rangle$ of arbitrary order N for $r \to 0$ using Taylor series, cf. eq. (3.25). Exact relations between $G_{M,0}$ and $\langle \varepsilon^M \rangle$ were already derived and discussed in section 4.1 above.

As before in section 4.1, M denotes the Mth moment of the dissipation. This is not to be confused with the order of the underlying structure function equation (which is $N = 2M$) or with the order of a tensor. For instance in case of $M = 2$, $\langle \epsilon_{ij}\epsilon_{kl} \rangle$ is a fourth-order tensor found in the fourth-order structure function equations corresponding to the sum of components of the eighth-order velocity gradient tensor $\langle (\partial u_i/\partial x_j)(\partial u_k/\partial x_l)(\partial u_m/\partial x_n)(\partial u_o/\partial x_p) \rangle$. Since we are interested in relations between tensor components in homogeneous isotropic flows, we make extensive use of linear decompositions into the independent fundamental isotropic components, cf. appendix A and e.g. Kearsley and Fong (1975) for more details.

4.2.1 Pseudo-dissipation

We begin by examining the Reynolds number dependence of ratios of moments of the pseudo-dissipation ϵ as defined by eq. (4.19) and the dissipation ε defined by eq. (4.17). The ratio $\langle \epsilon^M \rangle / \langle \varepsilon^M \rangle$ for all seven datasets described in section 2.1 with $Re_\lambda = 88$ to $Re_\lambda = 754$ for $M = 1, ..., 4$ is shown in figure 4.3(a). We find that the ratio increases for all $M > 1$ with increasing Reynolds number for

Table 4.2: Ratio of moments of pseudo-dissipation and dissipation. Exact value indicated by †-symbol.

$\langle\epsilon\rangle/\langle\varepsilon\rangle$	$\langle\epsilon^2\rangle/\langle\varepsilon^2\rangle$	$\langle\epsilon^3\rangle/\langle\varepsilon^3\rangle$	$\langle\epsilon^4\rangle/\langle\varepsilon^4\rangle$
$1^\dagger$	1.1865	1.7565	2.9695

datasets R0-R4 ($Re_\lambda = 88$ to $Re_\lambda = 331$) and becomes a constant for the larger Reynolds number cases R5 and R6 ($Re_\lambda = 529$ and $Re_\lambda = 754$).

Under the assumption of (local) homogeneity and continuity, the mean of the pseudo-dissipation equals the mean of the dissipation, i.e.

$$\langle\epsilon\rangle = \langle\varepsilon\rangle\,, \tag{4.21}$$

since $\langle(\partial u_i/\partial x_j)(\partial u_j/\partial x_i)\rangle = \nabla^2\langle p\rangle = 0$, see e.g. Hill (1997). However, similar equalities do not hold for the higher moments. This can clearly be seen from our data (cf. figure 4.3); we have indicated $\langle\epsilon\rangle\,/\,\langle\varepsilon\rangle = 1$ with a dashed line in figure 4.3 and find very good agreement.

We provide the large Reynolds number asymptotic values of the ratio as obtained from our DNS in table 4.2. As described above, these ratios become independent of the Reynolds number, when Re_λ is large enough. However, the large Reynolds number asymptotic values increase with increasing order M. This observation is not obvious and indicates significant cancellation due to the additional terms like $(\partial u_i/\partial x_j)(\partial u_j/\partial x_i)$ and the respective products (cf. the definitions eq. (4.17) and eq. (4.19)). Consequently, one would expect heavier tails for the pseudo-dissipation probability density function $P(\epsilon)$ than the respective distribution of the dissipation $P(\varepsilon)$; this implies that the pseudo-dissipation ϵ is *more* intermittent than the dissipation ε, in the sense that very large values of ϵ are found more frequently than equally large values of ε. This is in agreement with the observation that $\nabla^2 p = (\epsilon - \varepsilon)/\nu$ is positively skewed, cf. Yeung et al. (2012).

4.2.2 Components of the pseudo-dissipation tensor

Next, the ratio of the components of the pseudo-dissipation tensor $\langle\epsilon_{ij}\epsilon_{kl}...\rangle$ to the dissipation are examined. These ratios are of importance, since the moments of the components rather than the dissipation are found in the viscous range

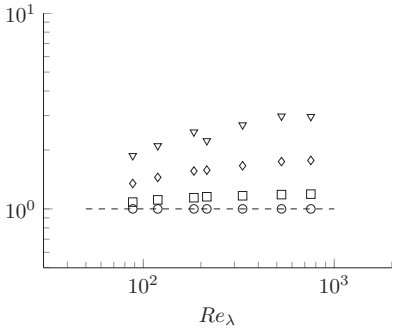

Figure 4.3: Ratio of moments of $\langle \epsilon^M \rangle / \langle \varepsilon^M \rangle$ as function of the Reynolds number Re_λ. $\circ : M = 1$, $\square : M = 2$, $\diamond : M = 3$, $\triangledown : M = 4$, $-- = 1$.

$(r \to 0)$ in the system of structure function equations, cf. chapter 3. On the other hand, phenomenology in the spirit of Kolmogorov (1941a,b) assumes that the structure functions depend on the moments of the dissipation ε, see the discussion above in section 3.1.1 as well as section 4.4. This implies that these ratios should be Reynolds number independent, provided the Reynolds number is large enough. Furthermore, from another point of view, dissipation parameters should be invariant with respect to the coordinate system and consequently the trace $\langle \epsilon^M \rangle$ or the moments of the dissipation $\langle \varepsilon^M \rangle$ should be chosen. This implies that the ratios of the moments of components to the dissipation (or the pseudo-dissipation) should be constant and independent of the Reynolds number.

Since $\langle \epsilon_{ij} \rangle$ is a second-order tensor, one can write

$$\langle \epsilon_{ij} \rangle = A_1 \delta_{ij} \tag{4.22}$$

under the assumption of isotropy, where A_1 is a scalar and δ_{ij} the Kronecker delta (i.e. $\delta_{ij} = 1$ for $i = j$ and $\delta_{ij} = 0$ for $i \neq j$). This implies that $\langle \epsilon_{11} \rangle = \langle \epsilon_{22} \rangle = \langle \epsilon_{33} \rangle = \langle \epsilon \rangle / 3 = \langle \varepsilon \rangle / 3$, where $\epsilon = \epsilon_{ii}$ is the trace of the second-order pseudo-dissipation tensor.

For $M = 2$ and assuming isotropy, one can write

$$\langle \epsilon_{ij} \epsilon_{kl} \rangle = A_1 \delta_{ij} \delta_{kl} + A_2 \left(\delta_{ik} \delta_{jl} + \delta_{il} \delta_{jk} \right), \tag{4.23}$$

since $\epsilon_{ij} = \epsilon_{ji}$ (and $\epsilon_{kl} = \epsilon_{lk}$), i.e. one can reduce the number of scalars A_i

required to describe the full tensor by one due to symmetry (a general fourth-order one-point isotropic tensor is determined by three scalar functions, cf. Kearsley and Fong (1975)). Consequently, $\langle \epsilon_{ij}\epsilon_{kl}\rangle$ is completely determined by e.g. $\langle \epsilon_{11}^2\rangle$ and $\langle \epsilon_{12}^2\rangle$ (or any other two independent combinations of indices in eq. (4.23)). Using eq. (4.23) then results in $\langle \epsilon_{11}^2\rangle = \langle \epsilon_{11}\epsilon_{22}\rangle + 2\langle \epsilon_{12}^2\rangle$, which is derived differently in section 4.3.2 below. Note that since all powers of $\langle \epsilon^M\rangle$ are determined by an even number of indices, components with only a single unique index (i.e. $i = 1, j = k = ... = 2$) necessarily vanish for all orders (cf. eq. (4.23) for the fourth-order tensor, e.g. $\langle \epsilon_{11}\epsilon_{12}\rangle = 0$).

Similarly, one obtains for $M = 3$

$$\begin{aligned}\langle \epsilon_{ij}\epsilon_{kl}\epsilon_{mn}\rangle = {} & A_1\delta_{ij}\delta_{kl}\delta_{mn} \\ & + A_2\left(\delta_{ij}\delta_{km}\delta_{ln} + \delta_{ij}\delta_{kn}\delta_{lm}\right) \\ & + A_3\left(\delta_{ik}\delta_{jl}\delta_{mn} + \delta_{il}\delta_{jk}\delta_{mn}\right) \\ & + A_4\left(\delta_{ik}\delta_{jm}\delta_{ln} + \delta_{im}\delta_{jk}\delta_{ln} + \delta_{ik}\delta_{jn}\delta_{lm} + \delta_{in}\delta_{jk}\delta_{lm}\right. \\ & \quad \left. + \delta_{il}\delta_{jm}\delta_{kn} + \delta_{im}\delta_{jl}\delta_{kn} + \delta_{il}\delta_{jn}\delta_{km} + \delta_{in}\delta_{jl}\delta_{km}\right) \\ & + A_5\left(\delta_{im}\delta_{jn}\delta_{kl} + \delta_{in}\delta_{jm}\delta_{kl}\right)\end{aligned} \tag{4.24}$$

again using symmetry. Thus, the full tensor is determined by five scalars, e.g. $\langle \epsilon_{11}^3\rangle$, $\langle \epsilon_{11}\epsilon_{22}^2\rangle$, $\langle \epsilon_{11}\varepsilon_{12}^2\rangle$, $\langle \epsilon_{11}\epsilon_{23}^2\rangle$ and $\langle \epsilon_{12}\epsilon_{13}\epsilon_{23}\rangle$ (other choices are possible, though) and one finds e.g. $\langle \epsilon_{11}^3\rangle = \langle \epsilon_{22}^3\rangle$, $\langle \epsilon_{11}\epsilon_{22}^2\rangle = \langle \epsilon_{22}\epsilon_{11}^2\rangle$ and $\langle \epsilon_{11}\epsilon_{12}^2\rangle = \langle \epsilon_{22}\epsilon_{12}^2\rangle$. Again, components such as $\langle \epsilon_{11}^2\epsilon_{12}\rangle$ vanish. One can continue for $M = 4$ starting from the general tensor (cf. Kearsley and Fong (1975)), but since this results in a sum of 105 terms, we do not want to write down the resulting expression here.

In the system of structure function equations as detailed in chapter 3, the higher moments of the pseudo-dissipation are found by deriving consecutive transport equations for the source terms

$$\langle E_{ij...kl}\rangle = \left\langle \Delta u_i \Delta u_j ...(\varepsilon_{kl} + \varepsilon'_{kl}) + \Delta u_i \Delta u_k ...(\varepsilon_{jl} + \varepsilon'_{jl}) + ...\right\rangle \tag{4.25}$$

appearing in these equations as sketched in section 3.1. This has been done in section 3.1.3 for the fourth-order equations (cf. also the Archive material `www.arxiv.org/abs/1504.07490` for the sixth-order equations), and could be carried out similarly for all higher orders. In the notation used here, $\langle E_{ij...kl}\rangle$ are the dissipation source terms defined in section 3.1. These terms dominate the other source terms in the structure function equations in the viscous range for $r \to 0$, where they balance the Laplacian of the structure functions, cf. the

figures in section 3.2.

In the following, we briefly discuss only the fourth order for simplicity, but the findings are also valid for all higher even orders. In the fourth-order structure function equations, one finds the dissipation source terms

$$\begin{aligned}\langle E_{ijkl}\rangle = \big\langle &\Delta u_i \Delta u_j \left(\epsilon_{kl} + \epsilon'_{kl}\right) + \Delta u_i \Delta u_k \left(\epsilon_{jl} + \epsilon'_{jl}\right) \\ &+ \Delta u_i \Delta u_l \left(\epsilon_{jk} + \epsilon'_{jk}\right) + \Delta u_j \Delta u_k \left(\epsilon_{il} + \epsilon'_{il}\right) \\ &+ \Delta u_j \Delta u_l \left(\epsilon_{ik} + \epsilon'_{ik}\right) + \Delta u_k \Delta u_l \left(\epsilon_{ij} + \epsilon'_{ij}\right)\big\rangle ,\end{aligned} \tag{4.26}$$

where $\langle E_{4,0}\rangle = \langle E_{1111}\rangle$ is found in the longitudinal, $\langle E_{2,2}\rangle = \langle E_{1122}\rangle$ in the mixed and $\langle E_{0,4}\rangle = \langle E_{2222}\rangle$ in the transverse fourth-order structure function equation, cf. eq. (3.15) and eqs. (3.50)-(3.52). Noticeably, all indices of $\langle E_{ijkl}\rangle$ are interchangeable (e.g. $\langle E_{ijkl}\rangle = \langle E_{iklj}\rangle$). As carried out in section 3.1.3 above, one can derive a transport equation for the dissipation source term $\langle E_{ijkl}\rangle$. In this transport equation, the term

$$\begin{aligned}\langle \Sigma_{ijkl}\rangle = 2\big[&\big\langle \left(\epsilon_{ij} + \epsilon'_{ij}\right)\left(\epsilon_{kl} + \epsilon'_{kl}\right)\big\rangle + \big\langle \left(\epsilon_{ik} + \epsilon'_{ik}\right)\left(\epsilon_{jl} + \epsilon'_{jl}\right)\big\rangle \\ &+ \big\langle \left(\epsilon_{il} + \epsilon'_{il}\right)\left(\epsilon_{jk} + \epsilon'_{jk}\right)\big\rangle\big]\end{aligned} \tag{4.27}$$

is found, which is a two-point sum of squares of the pseudo-dissipation separated by the distance r. $\langle \Sigma_{iijj}\rangle$ is the ε^2-term of eq (3.96). In the viscous range, $\langle \Sigma_{ijkl}\rangle$ then balances the Laplacian of $\langle E_{ijkl}\rangle$, cf. section 4.3.3 below. Since $\langle E_{ijkl}\rangle$ is symmetric under interchange of all indices, so is $\langle \Sigma_{ijkl}\rangle$. For $r \to 0$, $\langle \Sigma_{ijkl}\rangle$ is a one-point tensor*. One then finds

$$\langle \Sigma_{ijkl}\rangle = 8\left[\langle \epsilon_{ij}\epsilon_{kl}\rangle + \langle \epsilon_{ik}\epsilon_{jl}\rangle + \langle \epsilon_{il}\epsilon_{jk}\rangle\right] = A\left(\delta_{ij}\delta_{kl} + \delta_{ik}\delta_{jl} + \delta_{il}\delta_{jk}\right), \tag{4.28}$$

which may be expressed by a *single* scalar function under the assumption of isotropy. One may choose $A = 8\langle \epsilon_{11}^2\rangle$ and consequently relate the $\langle \Sigma_{1111}\rangle$, $\langle \Sigma_{1122}\rangle$ and $\langle \Sigma_{2222}\rangle$ found in the fourth-order equations to the second moment of the pseudo-dissipation $\langle \epsilon_{11}^2\rangle$. For that reason, we abstain from plotting ratios such as $\langle \Sigma_{1111}\rangle/\langle \varepsilon^2\rangle$. One can proceed similarly for higher even orders; e.g. at the sixth order one would find $\langle \epsilon_{11}^3\rangle$ which can be exactly related to $\langle \Sigma_{111122}\rangle$, say (and also to $\langle \varepsilon^3\rangle$, via figure 4.5a).

The relations between the components can be used to check for isotropy: We have computed some of the superfluous quantities such as $\langle \epsilon_{22}^2\rangle$ to check our datasets and find good agreement, as detailed below. We also focus mostly

*However, $\langle E_{ijkl}\rangle \sim \mathcal{O}(r^2)$ for $r \to 0$.

on those components which can be found in the system of structure function equations in chapter 3, e.g. we have not computed $\langle\epsilon_{12}\epsilon_{13}\epsilon_{23}\rangle/\langle\varepsilon^3\rangle$. The large Reynolds number asymptotic values of the quantities we have examined are listed in table 4.3.

For $M = 1$, we show the ratios $\langle\epsilon_{11}\rangle/\langle\varepsilon\rangle$ and $\langle\epsilon_{22}\rangle/\langle\varepsilon\rangle$ for our datasets in figure 4.4a, where the dashed line indicates a ratio of 1/3. We find very good agreement with the isotropic results $\langle\epsilon_{11}\rangle = \langle\epsilon_{22}\rangle = \langle\varepsilon\rangle/3$ as expected. For $M = 2$ (cf. eq. (4.23)), we have computed the ratios of $\langle\epsilon_{11}^2\rangle/\langle\varepsilon^2\rangle$, $\langle\epsilon_{22}^2\rangle/\langle\varepsilon^2\rangle$, $\langle\epsilon_{11}\epsilon_{22}\rangle/\langle\varepsilon^2\rangle$ and $\langle\epsilon_{12}^2\rangle/\langle\varepsilon^2\rangle$ as shown in figure 4.4b. We find that $\langle\epsilon_{11}^2\rangle = \langle\epsilon_{22}^2\rangle$ as required by isotropy. Moreover, the numerical values in table 4.3 agree very well with the result $\langle\epsilon_{11}^2\rangle = \langle\epsilon_{11}\epsilon_{22}\rangle + 2\langle\epsilon_{12}^2\rangle$. Noticeably, $\langle\epsilon_{11}^2\rangle > \langle\epsilon_{11}\epsilon_{22}\rangle > \langle\epsilon_{12}^2\rangle$.

For $M = 3$, we have computed the ratios $\langle\epsilon_{11}^3\rangle/\langle\varepsilon^3\rangle$, $\langle\epsilon_{11}^2\epsilon_{22}\rangle/\langle\varepsilon^3\rangle$, $\langle\epsilon_{11}\epsilon_{22}^2\rangle/\langle\varepsilon^3\rangle$ and $\langle\epsilon_{22}^3\rangle/\langle\varepsilon^3\rangle$ as shown in figure 4.5a as well as the ratios $\langle\epsilon_{11}\epsilon_{12}^2\rangle/\langle\varepsilon^3\rangle$ and $\langle\epsilon_{22}\epsilon_{12}^2\rangle/\langle\varepsilon^3\rangle$, cf. figure 4.5b for all seven datasets. We find that $\langle\epsilon_{11}^3\rangle = \langle\epsilon_{22}^3\rangle$, $\langle\epsilon_{11}^2\epsilon_{22}\rangle = \langle\epsilon_{11}\epsilon_{22}^2\rangle$ and $\langle\epsilon_{11}\epsilon_{12}^2\rangle = \langle\epsilon_{22}\epsilon_{12}^2\rangle$ in agreement with eq. (4.24). Moreover, we find that $\langle\epsilon_{11}^3\rangle > \langle\epsilon_{11}\epsilon_{12}^2\rangle > \langle\epsilon_{11}\epsilon_{22}^2\rangle$. Nevertheless, since we have not computed a fourth and fifth independent ratio (such as $\langle\epsilon_{11}\epsilon_{23}^2\rangle/\langle\varepsilon^3\rangle$ and $\langle\epsilon_{12}\epsilon_{13}\epsilon_{23}\rangle/\langle\varepsilon^3\rangle$ for instance), we cannot say that all components of the tensor $\langle\epsilon_{ij}\epsilon_{kl}\epsilon_{mn}\rangle$ have the same Reynolds number scaling, although one would expect that to be the case.

For $M = 4$, the computed ratios are shown in figure 4.6a and figure 4.6b respectively. Similarly to $N = 3$, we have not computed all independent ratios needed to completely determine the eighth-order tensor $\langle\epsilon_{ij}\epsilon_{kl}\epsilon_{mn}\epsilon_{op}\rangle$, but again only those found in the system of structure function equations. Specifically, the ratios $\langle\epsilon_{11}^4\rangle/\langle\varepsilon^4\rangle$, $\langle\epsilon_{11}^3\epsilon_{22}\rangle/\langle\varepsilon^4\rangle$, $\langle\epsilon_{11}^2\epsilon_{22}^2\rangle/\langle\varepsilon^4\rangle$, $\langle\epsilon_{11}\epsilon_{22}^3\rangle/\langle\varepsilon^4\rangle$ and $\langle\epsilon_{22}^4\rangle/\langle\varepsilon^4\rangle$ in figure 4.6a and $\langle\epsilon_{12}^4\rangle/\langle\varepsilon^4\rangle$, $\langle\epsilon_{11}^2\epsilon_{12}^2\rangle/\langle\varepsilon^4\rangle$ and $\langle\epsilon_{22}^2\epsilon_{12}^2\rangle/\langle\varepsilon^4\rangle$ in figure 4.6b are shown. Isotropy requires $\langle\epsilon_{11}^4\rangle = \langle\epsilon_{22}^4\rangle$, $\langle\epsilon_{11}^3\epsilon_{22}\rangle = \langle\epsilon_{11}\epsilon_{22}^3\rangle$ and $\langle\epsilon_{11}^2\epsilon_{12}^2\rangle = \langle\epsilon_{22}\epsilon_{12}^2\rangle$ which is in good agreement with our DNS data and we find $\langle\epsilon_{11}^4\rangle > \langle\epsilon_{11}^2\epsilon_{12}^2\rangle > \langle\epsilon_{11}^3\epsilon_{22}\rangle > \langle\epsilon_{11}^2\epsilon_{22}^2\rangle > \langle\epsilon_{11}^2\epsilon_{12}^2\rangle$. Noticeably, the collapse of these quantities which are equal under the assumption of isotropy is not as good as for $M = 1$ to $M = 3$, but still satisfactory. This is most likely due to the resolution of our DNS data, which is sufficient for $M = 4$ but might not be good enough to compute higher moments. For that reason, we have not computed higher-order statistics $M > 4$. However, we have still averaged all of those ratios which are required to be equal to compute the large Reynolds number asymptotic values given in table 4.3. Again, we cannot say that all components of the tensor $\langle\epsilon_{ij}\epsilon_{kl}\epsilon_{mn}\epsilon_{op}\rangle$ have the same Reynolds number scaling for the reasons outlined above.

Comparing the ratio of components of the pseudo-dissipation and dissipation to the ratio of the pseudo-dissipation and dissipation, the former approach

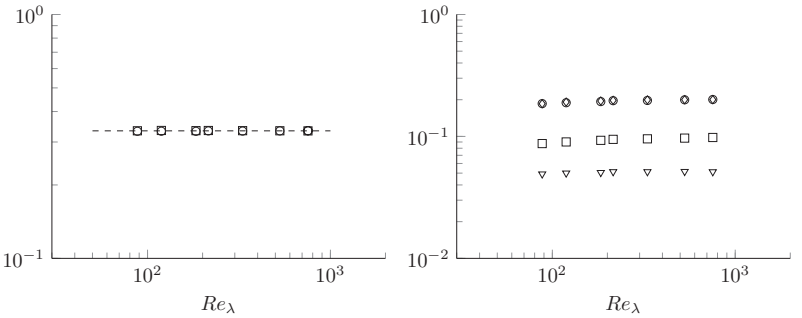

Figure 4.4: (a) Ratio of moments $\langle \epsilon_{11}^p \epsilon_{22}^q \rangle / \langle \varepsilon \rangle$ as function of the Reynolds number Re_λ. $\circ : p = 1, q = 0$, $\square : p = 0, q = 1$, $-- = 1/3$. (b) Ratio of moments $\langle \epsilon_{11}^p \epsilon_{22}^q \rangle / \langle \varepsilon^2 \rangle$ as function of the Reynolds number Re_λ where $\circ : p = 2, q = 0$, $\square : p = 1, q = 1$, $\diamond : p = 0, q = 2$ and $\triangledown : \langle \epsilon_{12}^2 \rangle / \langle \varepsilon^2 \rangle$.

Reynolds number independent values quicker than the latter. This is somewhat puzzling since the ratio of individual components at some order seem to approach the asymptotic values equally fast and one would therefore expect the same for their sum (e.g. the trace). However, we have not evaluated all required quantities to fully describe the pseudo-dissipation tensor for $M = 3$ and $M = 4$. Therefore, the ratio of quantities we have not looked at like $\langle \epsilon_{12} \epsilon_{13} \epsilon_{23} \rangle / \langle \varepsilon^3 \rangle$ might become constant at larger Reynolds numbers compared to e.g. $\langle \epsilon_{11}^3 \rangle / \langle \varepsilon^3 \rangle$.

4.2.3 Velocity gradients

Finally, we examine the ratio of the even moments of the velocity gradient tensor and the dissipation. Particularly, we compare the ratio of $G_{p,q}$ defined by eq. (4.20) and the moments of the dissipation $\langle \varepsilon^M \rangle$ defined by eq. (4.17). It should be mentioned though that the $G_{p,q}$ alone are not sufficient to uniquely determine the general isotropic velocity gradient tensor of order $4M$.

As seen from the Taylor series of $D_{m,n}$ in the viscous range for $r \to 0$, eq. (3.25), the ratios of $G_{p,q}$ and the moments of the dissipation are of interest, since $G_{p,q}$

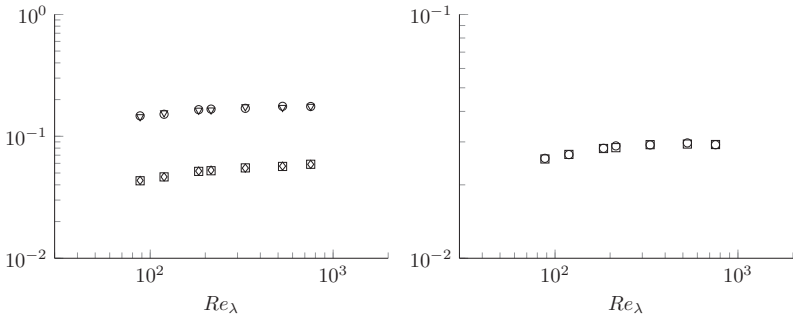

(a) **(b)**

Figure 4.5: (a) Ratio of moments $\langle \epsilon_{11}^p \epsilon_{22}^q \rangle / \langle \varepsilon^3 \rangle$ as function of the Reynolds number Re_λ. $\circ : p = 3, q = 0$, $\square : p = 1, q = 2$, $\diamond : p = 2, q = 1$, $\triangledown : p = 0, q = 3$. (b) Ratio of moments $\langle \epsilon_{11} \epsilon_{12}^2 \rangle / \langle \varepsilon^3 \rangle$ ($\circ$) and $\langle \epsilon_{22} \epsilon_{12}^2 \rangle / \langle \varepsilon^3 \rangle$ ($\square$) as function of the Reynolds number Re_λ.

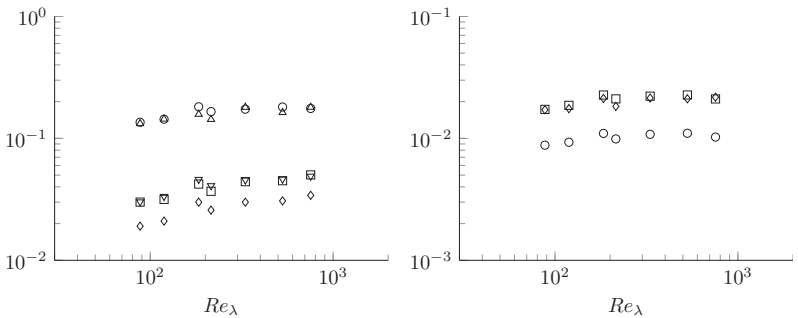

(a) **(b)**

Figure 4.6: (a) Ratio of moments $\langle \varepsilon_{11}^p \varepsilon_{22}^q \rangle / \langle \varepsilon^4 \rangle$ as function of the Reynolds number Re_λ. $\circ : p = 4, q = 0$, $\square : p = 1, q = 3$, $\diamond : p = 2, q = 2$, $\triangledown : p = 3, q = 1$, $\triangle$: $p = 0, q = 4$. (b) Ratio of moments $\langle \epsilon_{12}^4 \rangle / \langle \varepsilon^4 \rangle$ ($\circ$), $\langle \epsilon_{11}^2 \epsilon_{12}^2 \rangle / \langle \varepsilon^4 \rangle$ ($\square$) and $\langle \epsilon_{22}^2 \epsilon_{12}^2 \rangle / \langle \varepsilon^4 \rangle$ ($\diamond$) as function of the Reynolds number Re_λ.

Table 4.3: Ratio of moments of components of the pseudo-dissipation tensor and dissipation. Exact value indicated by †-symbol.

	$q=0$	$q=1$	$q=2$	$q=3$	$q=4$
$\langle \epsilon_{11}^{1-q}\epsilon_{22}^{q}\rangle/\langle\varepsilon\rangle$	$1/3^{\dagger}$	$1/3^{\dagger}$			
$\langle \epsilon_{11}^{2-q}\epsilon_{22}^{q}\rangle/\langle\varepsilon^2\rangle$	$1.999\cdot10^{-1}$	$9.678\cdot10^{-2}$	$1.999\cdot10^{-1}$		
$\langle \epsilon_{11}^{3-q}\epsilon_{22}^{q}\rangle/\langle\varepsilon^3\rangle$	$1.7503\cdot10^{-1}$	$5.785\cdot10^{-2}$	$5.785\cdot10^{-2}$	$1.7503\cdot10^{-1}$	
$\langle \epsilon_{11}^{4-q}\epsilon_{22}^{q}\rangle/\langle\varepsilon^4\rangle$	$1.7552\cdot10^{-1}$	$4.666\cdot10^{-2}$	$3.242\cdot10^{-2}$	$4.666\cdot10^{-2}$	$1.7552\cdot10^{-1}$
$\langle \epsilon_{12}^{q}\rangle/\langle\varepsilon\rangle$			$5.138\cdot10^{-2}$		$1.068\cdot10^{-2}$
$\langle \epsilon_{11}^{q}\epsilon_{12}^{2}\rangle/\langle\varepsilon^{m+2}\rangle$		$5.865\cdot10^{-2}$	$2.171\cdot10^{-2}$		

determines the solution of structure functions $D_{m,n}=\langle(\Delta u_1)^m(\Delta u_2)^n\rangle$ in the viscous range. Consequently, $G_{p,q}$ and the kinematic viscosity ν are the correct quantities to define viscous scales, the most famous one being the Kolmogorov length scale $\eta=(\nu^3/\langle\varepsilon\rangle)^{1/4}$ and the corresponding velocity $u_\eta=(\nu\langle\varepsilon\rangle)^{1/4}$ for the second-order structure functions $D_{2,0}$ and $D_{0,2}$ for $M=1$. For higher-order structure functions, the corresponding $G_{p,q}$ result in general scales $\eta_{C,N}$ and $u_{C,N}$, cf. section 4.4.1 below. This ties into a modified similarity hypothesis in the spirit of Kolmogorov (1941b), which states that structure function of order $2M$ should be determined in the viscous range by $\langle\varepsilon^M\rangle$ (instead of $\langle\varepsilon\rangle^M$) and ν only, which requires a connection between $G_{p,q}$ and $\langle\varepsilon^M\rangle$, where again $M=p+q$. We briefly discuss this in the following.

The best-known relation is probably given by eq. (3.43), which exactly relates the mean dissipation $\langle\varepsilon\rangle$ to the second moment of the longitudinal velocity gradient $\langle(\partial u_1/\partial x_1)^2\rangle$ as shown by Kolmogorov (1941b) for homogeneous isotropic turbulence in incompressible flows. Eq. (3.43) can be easily derived by writing the general fourth-order isotropic tensor

$$\begin{aligned}\left\langle \frac{\partial u_i}{\partial x_j}\frac{\partial u_k}{\partial x_l}\right\rangle &= B_1\delta_{ij}\delta_{kl}+B_2\delta_{ik}\delta_{jl}+B_3\delta_{il}\delta_{jk}\\ &= B_1\left(\delta_{ij}\delta_{kl}-4\delta_{ik}\delta_{jl}+\delta_{il}\delta_{jk}\right),\end{aligned} \tag{4.29}$$

where in the second line homogeneity (which implies $\langle(\partial u_i/\partial x_j)(\partial u_j/\partial x_i)\rangle=0$) and incompressibility ($\langle(\partial u_i/\partial x_i)(\partial u_j/\partial x_k)\rangle=0$) have been used to further constrain the three scalars B_1, B_2 and B_3; see Hinze (1975) for a detailed derivation. With eq. (4.17), one then finds that $B_1=-\langle\varepsilon\rangle/(30\nu)$. Eq. (3.25) and eq. (4.29) allowed Kolmogorov (1941a) to exactly determine the second-order structure function $D_{2,0}$ in the viscous range (cf. the discussion in section 3.1.1

and section 3.1.2). It follows that the mean dissipation $\langle\varepsilon\rangle$ and the kinematic viscosity ν are the two quantities to determine the characteristic second-order dissipative scales, the Kolmogorov length $\eta = (\nu^3/\langle\varepsilon\rangle)^{1/4}$ and the corresponding velocity $u_\eta = (\nu\langle\varepsilon\rangle)^{1/4}$.

It is possible to continue in the spirit of eq. (4.29) for higher orders, but the number of scalar functions (the B_i) increases very quickly. For instance, Hierro and Dopazo (2003) examined the general isotropic eighth-order velocity gradient tensor ($M = 2$ in our notation) under the constraints of homogeneity and continuity. Instead of a single independent scalar as in eq. (4.29), there are four independent scalars at the eighth order. If all four scalars are known, one can then derive for instance the relation between $\langle\varepsilon^2\rangle$ and any component of the eighth-order velocity gradient tensor in terms of the B_i.

In fact, the four independent scalars were determined by Siggia (1981) before, who derived four invariants and related them to the eighth-order longitudinal, mixed and transverse velocity gradient components. Furthermore, as detailed in section 4.1 above, he derived a generating function eq. (4.3) which allows the computation of any of the connectors of different combinations of the strain tensor $\langle S_{ij}S_{kl}...\rangle$ where $S_{ij} = (\partial u_i/\partial x_j + \partial u_j/\partial x_i)/2$. Since $\varepsilon = 2\nu S_{ij}S_{ij}$, Siggia effectively derived

$$105\nu^2 \left\langle \left(\frac{\partial u_1}{\partial x_1}\right)^4 \right\rangle = \langle\varepsilon^2\rangle\,. \tag{4.30}$$

Theoretically, one could carry out the steps given in Hierro and Dopazo (2003) for higher-order velocity gradient tensors. However, for $M = 3$ one would have a 12th-order isotropic tensor (with 10395 components) and for $M = 4$ a 16th-order isotropic tensor (with 2027025 components) and applying the constraints of homogeneity, continuity and symmetry becomes very cumbersome. Nevertheless, it is possible to use Siggia's generating function to derive relations between even-order moments of the longitudinal velocity gradient and the moments of the dissipation for arbitrary orders in a much more feasible manner. This was carried out in section 4.1 and results in eq. (4.6) with the exact C_M given by eq. (4.5). Consequently, $C_3 = 567$ and $C_4 = 2673$, for instance. Eq. (4.5) can be used to determine exactly the longitudinal even-order structure functions in the viscous range as function of the moments of the dissipation and the kinematic viscosity as will be done in section 4.4 below. As discussed in section 4.1, it is not possible to analytically relate the moments of mixed and transverse velocity gradients in general because $S_{12} = S_{21} \neq \partial u_2/\partial x_1$, with the exception of $\langle(\partial u_2/\partial x_1)^2\rangle = 2\langle(\partial u_1/\partial x_1)^2\rangle$ (as seen from eq. (4.29), cf. also eq. (3.43)). Only if the ratio of $G_{p,q}$ and the moments of the dissipation at fixed M have

the same Reynolds number scaling, the characteristic scales in the viscous range are the same for all structure functions at the same order M. Consequently also the ratio of different $G_{p,q}$ at order M would then be constant, e.g. the ratio $G_{2,0}/G_{0,2}$ for $M = 2$.

While one cannot derive the exact connectors between the moments of longitudinal, mixed and transverse velocity gradients, it is possible to at least determine whether they exhibit the same Reynolds number scaling and therefore to conclude that all structure functions at the same order have the same characteristic scales in the viscous range. As discussed in section 3.2, the fourth-order structure functions in the viscous range $r \to 0$ are determined by $\langle \Sigma_{1111} \rangle$, $\langle \Sigma_{1122} \rangle$ and $\langle \Sigma_{2222} \rangle$, which are all related via eq. (4.28) and consequently may be expressed in terms of $\langle \epsilon_{11}^2 \rangle$. Since the ratio of $\langle \epsilon_{11}^2 \rangle / \langle \varepsilon^2 \rangle$ is constant (cf. section 3.2), this implies that all fourth-order structure functions $D_{4,0}$, $D_{2,2}$ and $D_{0,4}$ in the viscous range depend on either $\langle \epsilon_{11}^2 \rangle$ or equivalently $\langle \varepsilon^2 \rangle$. Similar results are obtained for higher even orders.

We have computed the ratio of $G_{p,q}/\langle \varepsilon^M \rangle$ for $M = 1$ to $M = 4$ for our datasets, where $M = p + q$. The large Reynolds number asymptotic values can be found in table 4.4. Again, the $G_{p,q}$ are not sufficient to completely determine the general velocity gradient tensor of order $4M$. For that reason, we cannot say that all components of the velocity gradient tensor of order $M > 1$ have the same Reynolds number scaling, although one would expect that to be the case.

The ratios $G_{1,0}/\langle \varepsilon \rangle$ and $G_{0,1}/\langle \varepsilon \rangle$ for $M = 1$ are shown in figure 4.7a. The exact values of 1/15 and 2/15 are indicated by the dashed and the dash-dotted horizontal lines, respectively. We find very good agreement with these theoretical results (cf. eq. (3.43)) obtained under the assumption of isotropy.

For $M = 2$, the ratios $G_{2,0}/\langle \varepsilon^2 \rangle$, $G_{1,1}/\langle \varepsilon^2 \rangle$ and $G_{0,2}/\langle \varepsilon^2 \rangle$ are shown in figure 4.7b. The exact result $G_{2,0}/\langle \varepsilon^2 \rangle = 1/105$, cf. eq. (4.5), is indicated by a dashed horizontal line, for which we have very good agreement with our DNS data. We find that $G_{0,2} > G_{2,0} > G_{1,1}$. All three ratios become Reynolds number independent for the datasets $R3$ to $R6$.

Figure 4.8 shows the ratios $G_{3,0}/\langle \varepsilon^3 \rangle$, $G_{2,1}/\langle \varepsilon^3 \rangle$, $G_{1,2}/\langle \varepsilon^3 \rangle$ and $G_{0,3}/\langle \varepsilon^3 \rangle$. Again, we have very good agreement of the ratio $G_{3,0}/\langle \varepsilon^3 \rangle$ as evaluated from our DNS and the theoretical value 1/567 of eq. (4.5) (the dashed horizontal line). We find $G_{0,3} > G_{1,2} > G_{3,0} > G_{1,2}$.

Finally, the ratios $G_{4,0}/\langle \varepsilon^4 \rangle$, $G_{3,1}/\langle \varepsilon^4 \rangle$, $G_{2,2}/\langle \varepsilon^4 \rangle$, $G_{1,3}/\langle \varepsilon^4 \rangle$ and $G_{0,4}/\langle \varepsilon^4 \rangle$ are exhibited in figure 4.8b for $M = 4$. We find satisfactory agreement of $G_{4,0}/\langle \varepsilon^4 \rangle$ as computed from our DNS and the theoretical value 1/2673 of eq. (4.5) as indicated by the dashed horizontal line. Moreover, $G_{0,4} > G_{1,3} > G_{4,0} \approx G_{2,2} > G_{1,3}$. Interestingly enough, our data indicates that $G_{2,2} \approx G_{4,0} = \langle \varepsilon^4 \rangle / 2673$. This

Table 4.4: Ratio of moments of components of the velocity gradient tensor and dissipation. Exact values indicated by †-symbol.

	$q=0$	$q=1$	$q=2$	$q=3$	$q=4$
$G_{1-q,q}/\langle\varepsilon\rangle$	$1/15^\dagger$	$2/15^\dagger$			
$G_{2-q,q}/\langle\varepsilon^2\rangle$	$1/105^\dagger$	$8.1213\cdot10^{-3}$	$5.9267\cdot10^{-2}$		
$G_{3-q,q}/\langle\varepsilon^3\rangle$	$1/567^\dagger$	$1.1163\cdot10^{-3}$	$1.2604\cdot10^{-2}$	$4.4023\cdot10^{-2}$	
$G_{4-q,q}/\langle\varepsilon^4\rangle$	$1/2673^\dagger$	$1.9597\cdot10^{-4}$	$3.7173\cdot10^{-4}$	$1.8901\cdot10^{-3}$	$4.0167\cdot10^{-2}$

immediately implies that the mixed structure function $D_{4,4}$ and the longitudinal structure function $D_{8,0}$ are equal in the viscous range. We have checked this with our DNS data (not shown here), which indeed confirms this. At first glance, the result $G_{2,2}=G_{4,0}$ seems puzzling considering that they would seem to correspond to different independent components of the general 16th-order velocity gradient tensor. However, Kearsley and Fong (1975) found that 14 out of the 105 components of the general eighth-order isotropic tensor (corresponding here to $M=2$) are linearly dependent. One might also expect similar reductions at higher orders $M>2$, so that some of the higher-order structure functions might be equal in the viscous range; one might therefore think that these additional constraints could lead to $G_{2,2}=G_{4,0}$. In principle, it should be possible to show this rigorously by writing down the general 16th-order velocity gradient tensor, applying the constraints of homogeneity and continuity as outlined by Hierro and Dopazo (2003) and then following the steps of Kearsley and Fong (1975). However since this procedure is very cumbersome, we have not verified this.

Noticeably, the $G_{p,q}/\langle\varepsilon^M\rangle$ approach their large Reynolds number values much faster than $\langle\epsilon^M\rangle/\langle\varepsilon^M\rangle$. Of course, the $\langle\epsilon^M\rangle$ are a sum of many terms, some of which are the $G_{p,q}$. Thus, one would expect that some other components of the general velocity gradient tensor of order $4M$ approach their large Reynolds number asymptotic values slower than $G_{p,q}$.

As for the ratios of section 4.2.1 and section 4.2.2, we have not computed higher orders $M>4$*.

*Note that table 4.1 suggest that we could have computed $G_{p,q}/\langle\varepsilon^M\rangle$ up to $M=6$.

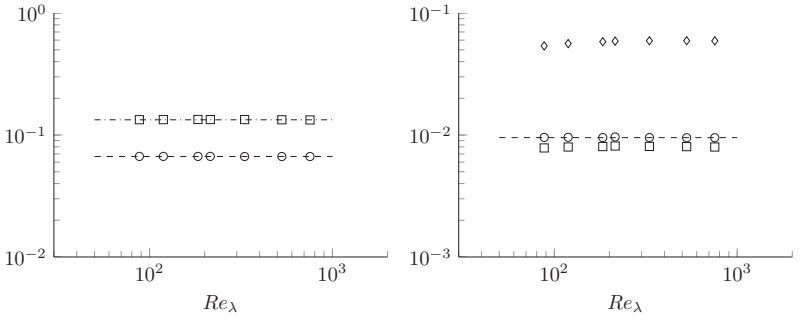

Figure 4.7: Ratio of moments $\langle G_{p,q} \rangle / \langle \varepsilon^M \rangle$ as function of the Reynolds number Re_λ. (a) $M = p + q = 1$, $\circ : p = 1, q = 0$, $\square : p = 0, q = 1$, $-- = 1/15$, $-. = 2/15$. (b) $M = p + q = 2$, $\circ : p = 2, q = 0$, $\square : p = 1, q = 1$, $\diamond : p = 0, q = 2$, $-- = 1/105$.

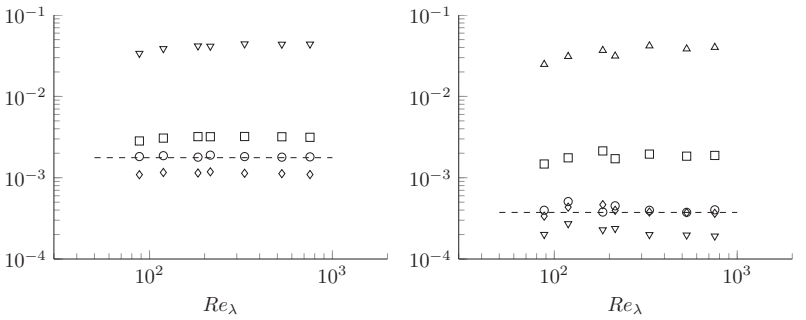

Figure 4.8: Ratio of moments $\langle G_{p,q} \rangle / \langle \varepsilon^M \rangle$ as function of the Reynolds number Re_λ. (a) $M = p + q = 3$, $\circ : p = 3, q = 0$, $\square : p = 1, q = 2$, $\diamond : p = 2, q = 1$, $\triangledown : p = 0, q = 3$, $-- = 1/567$. (b) $M = p + q = 4$, $\circ := 4, q = 0$, $\square : p = 1, q = 3$, $\diamond : p = 2, q = 2$, $\triangledown : p = 3, q = 1$, $\triangle : p = 0, n = q$, $-- = 1/2673$.

4.3 Third- and fourth-order solutions in the viscous range

In this section, we derive exact results for the third- and fourth-order structure functions in the viscous range in section 4.3.1 and section 4.3.2, similar to the second-order results derived by Kolmogorov. For the third order, the trace $D_{[3]}$ can easily be found by summing up the results for $D_{3,0}$ and $D_{1,2}$. However, as discussed above in section 3.1, we do not have enough equations to solve for the longitudinal, mixed and transverse structure functions $D_{4,0}$, $D_{2,2}$ and $D_{0,4}$. For that reason, we also look specifically at the trace of the fourth-order structure function equations in section 4.3.3.

4.3.1 Third order structure functions in the viscous range

In the viscous range $r \to 0$, the viscous terms and the dissipation source terms balance. Then, from table 3.2,

$$\begin{aligned} 2\nu\left[\frac{\partial^2 D_{3,0}}{\partial r^2}+\frac{2}{r}\frac{\partial D_{3,0}}{\partial r}-\frac{6}{r^2}D_{3,0}+\frac{12}{r^2}D_{1,2}\right] &= \langle E_{3,0}\rangle \\ 2\nu\left[\frac{\partial^2 D_{1,2}}{\partial r^2}+\frac{2}{r}\frac{\partial D_{1,2}}{\partial r}-\frac{8}{r^2}D_{1,2}+\frac{2}{r^2}D_{3,0}\right] &= \langle E_{1,2}\rangle\,. \end{aligned} \tag{4.31}$$

For $r \to 0$, the structure functions can be expanded as

$$D_{3,0} = F_1 r^3 + \mathcal{O}(r^4), \quad D_{1,2} = F_2 r^3 + \mathcal{O}(r^4), \tag{4.32}$$

cf. eq. (3.25), i.e. $F_1 = \langle(\partial u_1/\partial x_1)^3\rangle$ and $F_2 = \langle(\partial u_1/\partial x_1)(\partial u_2/\partial x_1)^2\rangle$. Inserting eq. (4.32) into eq. (4.31) then yields

$$F_1 + 2F_2 = \frac{\langle E_{3,0}\rangle}{12\nu r} \tag{4.33}$$

as well as the relation $\langle E_{3,0}\rangle = 3\,\langle E_{1,2}\rangle$. From incompressibility, one has

$$r\frac{\partial D_{3,0}}{\partial r} + D_{3,0} - 6D_{1,2} = 0, \tag{4.34}$$

i.e. eq. (3.24), which yields the additional constraint $2F_1 = 3F_2$. The third-order dissipation source terms are defined as

$$\langle E_{ijk} \rangle = 2 \left\langle \Delta u_i \left(\epsilon_{jk} + \epsilon'_{jk} \right) + \Delta u_j \left(\epsilon_{ik} + \epsilon'_{ik} \right) + \Delta u_k \left(\epsilon_{ij} + \epsilon'_{ij} \right) \right\rangle , \tag{4.35}$$

where $\langle E_{3,0} \rangle = \langle E_{111} \rangle$ and $\langle E_{1,2} \rangle = \langle E_{122} \rangle$. Consider $\langle \Delta u_i (\epsilon_{jk} + \epsilon'_{jk}) \rangle$. For $r \to 0$, $\langle \Delta u_i (\epsilon_{jk} + \epsilon'_{jk}) \rangle = 2 \langle \Delta u_i \epsilon_{jk} \rangle$ and the Taylor expansion yields

$$\langle \Delta u_i \epsilon_{jk} \rangle = \left\langle \frac{\partial u_i}{\partial x_1} \epsilon_{jk} \right\rangle r + \mathcal{O}(r^2) \tag{4.36}$$

Therefore, inserting this into eq. (4.35) yields

$$E_{ijk} = 4 \left\langle \frac{\partial u_i}{\partial x_1} \epsilon_{jk} + \frac{\partial u_j}{\partial x_1} \epsilon_{ik} + \frac{\partial u_k}{\partial x_1} \epsilon_{ij} \right\rangle r + \mathcal{O}(r^2) \tag{4.37}$$

for $r \to 0$. Then,

$$D_{3,0} = \frac{3}{7\nu} \left\langle \frac{\partial u_1}{\partial x_1} \epsilon_{11} \right\rangle r^3, \quad D_{1,2} = \frac{2}{7\nu} \left\langle \frac{\partial u_1}{\partial x_1} \epsilon_{11} \right\rangle r^3 \tag{4.38}$$

in the viscous range and $\langle (\partial u_1 / \partial x_1) \epsilon_{11} \rangle = \langle (\partial u_1 / \partial x_1) \epsilon_{22} + 2 (\partial u_2 / \partial x_1) \epsilon_{12} \rangle$ as well as $D_{3,0} = 3 D_{1,2} / 2$ satisfying the continuity equation. Moreover,

$$\left\langle \left(\frac{\partial u_1}{\partial x_1} \right)^3 \right\rangle = \frac{3}{7} \left\langle \frac{\partial u_1}{\partial x_1} \left(\frac{\partial u_1}{\partial x_i} \right)^2 \right\rangle , \tag{4.39}$$

$$\left\langle \frac{\partial u_1}{\partial x_1} \left(\frac{\partial u_2}{\partial x_1} \right)^2 \right\rangle = \frac{2}{7} \left\langle \frac{\partial u_1}{\partial x_1} \left(\frac{\partial u_1}{\partial x_i} \right)^2 \right\rangle \tag{4.40}$$

in agreement with the isotropic expression of the general third-order velocity gradient tensor as given on p. 206 of Pope (2000).

4.3.2 Relations between fourth-order structure functions and second-order dissipation parameters in the viscous range

Next, we will show how the second-order dissipation parameters $\langle \epsilon_{11}^2 \rangle$, $\langle \epsilon_{22}^2 \rangle$ and $\langle \epsilon_{11} \epsilon_{22} \rangle + 2 \langle \epsilon_{12}^2 \rangle$ are related to $\langle \epsilon^2 \rangle$. We will also show how they are related to the fourth-order moments of the velocity gradient distribution and to the

solutions of the fourth-order structure function equations in the viscous range.

Again, in the viscous range we need to consider only the balance between the viscous terms and the dissipation source terms in the fourth-order longitudinal, mixed and transverse structure functions, cf. figure 3.5 and therefore with table 3.2,

$$2\nu\left[\frac{\partial^2 D_{4,0}}{\partial r^2}+\frac{2}{r}\frac{\partial D_{4,0}}{\partial r}-\frac{8}{r^2}D_{4,0}+\frac{24}{r^2}D_{2,2}\right]=\langle E_{4,0}\rangle \tag{4.41}$$

$$2\nu\left[\frac{2}{r^2}D_{4,0}+\frac{\partial^2 D_{2,2}}{\partial r^2}+\frac{2}{r}\frac{\partial D_{2,2}}{\partial r}-\frac{14}{r^2}D_{2,2}+\frac{8}{3r^2}D_{0,4}\right]=\langle E_{2,2}\rangle \tag{4.42}$$

$$2\nu\left[\frac{12}{r^2}D_{2,2}+\frac{\partial^2 D_{0,4}}{\partial r^2}+\frac{2}{r}\frac{\partial D_{0,4}}{\partial r}-\frac{4}{r^2}D_{0,4}\right]=\langle E_{0,4}\rangle\,. \tag{4.43}$$

Similarly to the balance of the trace $\langle E_{[4]}\rangle$ shown in figure 3.13, the viscous terms in the equations for $\langle E_{4,0}\rangle$, $\langle E_{2,2}\rangle$ and $\langle E_{0,4}\rangle$ also balance the respective ε^2-terms, cf. figure 3.5. Therefore in the equations for the $\langle E_{4,0}\rangle$, $\langle E_{2,2}\rangle$ and $\langle E_{0,4}\rangle$ given in section 3.1.3, the balance between these terms is given by

$$2\nu\left[\frac{\partial^2\langle E_{4,0}\rangle}{\partial r^2}+\frac{2}{r}\frac{\partial\langle E_{4,0}\rangle}{\partial r}-\frac{8}{r^2}\langle E_{4,0}\rangle+\frac{24}{r^2}\langle E_{2,2}\rangle\right]=24\left\langle(\epsilon_{11}+\epsilon'_{11})^2\right\rangle \tag{4.44}$$

$$\begin{aligned}2\nu\left[\frac{2}{r^2}\langle E_{4,0}\rangle+\frac{\partial^2\langle E_{2,2}\rangle}{\partial r^2}+\frac{2}{r}\frac{\partial\langle E_{2,2}\rangle}{\partial r}-\frac{14}{r^2}\langle E_{2,2}\rangle+\frac{8}{3r^2}\langle E_{0,4}\rangle\right]\\ =8\left\langle(\epsilon_{11}+\epsilon'_{11})(\epsilon_{22}+\epsilon'_{22})\right\rangle+16\left\langle(\epsilon_{12}+\epsilon'_{12})^2\right\rangle\end{aligned} \tag{4.45}$$

$$\begin{aligned}2\nu\left[\frac{12}{r^2}\langle E_{2,2}\rangle+\frac{\partial^2\langle E_{0,4}\rangle}{\partial r^2}+\frac{2}{r}\frac{\partial\langle E_{0,4}\rangle}{\partial r}-\frac{4}{r^2}\langle E_{0,4}\rangle\right]\\ =24\left\langle(\epsilon_{22}+\epsilon'_{22})^2\right\rangle.\end{aligned} \tag{4.46}$$

Expanding the structure functions as

$$D_{4,0} = F_1 r^4 + \ldots = \left\langle \left(\frac{\partial u_1}{\partial x_1} \right)^4 \right\rangle r^4 + \ldots \tag{4.47}$$

$$D_{2,2} = F_2 r^4 + \ldots = \left\langle \left(\frac{\partial u_1}{\partial x_1} \right)^2 \left(\frac{\partial u_2}{\partial x_1} \right)^2 \right\rangle r^4 + \ldots \tag{4.48}$$

$$D_{0,4} = F_3 r^4 + \ldots = \left\langle \left(\frac{\partial u_2}{\partial x_1} \right)^4 \right\rangle r^4 + \ldots \tag{4.49}$$

as in eq. (4.32) and similarly for the dissipation source terms as

$$\langle E_{4,0} \rangle = \beta^0_{4,0} r^2 + \ldots = 24 \left\langle \left(\frac{\partial u_1}{\partial x_1} \right)^2 \epsilon_{11} \right\rangle r^2 + \ldots \tag{4.50}$$

$$\begin{aligned} \langle E_{2,2} \rangle = \beta^0_{2,2} r^2 + \ldots = \Bigg(& 4 \left\langle \left(\frac{\partial u_2}{\partial x_1} \right)^2 \epsilon_{11} \right\rangle \\ & + 16 \left\langle \left(\frac{\partial u_1}{\partial x_1} \right) \left(\frac{\partial u_2}{\partial x_1} \right) \epsilon_{12} \right\rangle + 4 \left\langle \left(\frac{\partial u_1}{\partial x_1} \right)^2 \epsilon_{22} \right\rangle \Bigg) r^2 + \ldots \end{aligned} \tag{4.51}$$

$$\langle E_{0,4} \rangle = \beta^0_{0,4} r^2 + \ldots = 24 \left\langle \left(\frac{\partial u_2}{\partial x_1} \right)^2 \epsilon_{22} \right\rangle r^2 + \ldots, \tag{4.52}$$

we obtain to leading order the relations for F_1, F_2 and F_3 after inserting eq. (4.47) to eq. (4.49) into eq. (4.41) to eq. (4.43),

$$12F_1 + 24F_2 = \frac{\beta^0_{4,0}}{2\nu} \tag{4.53}$$

$$2F_1 + 6F_2 + \frac{8}{3} F_3 = \frac{\beta^0_{2,2}}{2\nu} \tag{4.54}$$

$$12F_2 + 16F_3 = \frac{\beta^0_{0,4}}{2\nu}. \tag{4.55}$$

Gauss elimination leads to a singular system and thereby to the compatibility condition

$$\beta^0_{4,0} + \beta^0_{0,4} = 6\beta^0_{2,2} \tag{4.56}$$

By inserting eq. (4.50)and eq. (4.51) into the equations for the fourth-order

dissipation source terms we obtain to leading order the relations

$$-2\beta^0_{4,0} + 24\beta^0_{2,2} = 24\frac{\left\langle \epsilon^2_{11}\right\rangle}{2\nu} \tag{4.57}$$

$$2\beta^0_{4,0} - 8\beta^0_{2,2} + \frac{8}{3}\beta^0_{0,4} = \frac{8\left\langle \epsilon_{11}\epsilon_{22}\right\rangle + 16\left\langle \epsilon^2_{12}\right\rangle}{2\nu} \tag{4.58}$$

$$12\beta^0_{2,2} + 2\beta^0_{0,4} = 24\frac{\left\langle \epsilon^2_{22}\right\rangle}{2\nu} \tag{4.59}$$

Gauss elimination leads again to a singular system and a compatibility condition relating the dissipation parameters

$$3\left\langle \epsilon^2_{11}\right\rangle + \left\langle \epsilon_{11}\epsilon_{22}\right\rangle + 2\left\langle \epsilon^2_{12}\right\rangle = 4\left\langle \epsilon^2_{22}\right\rangle \tag{4.60}$$

Note that there is no incompressibility equation analogous to eq. (3.23) for the second and eq. (3.24) for the third order. Therefore, it is *not* possible to solve the system at hand, which is only possible for the second and third order. Since due to isotropy $\left\langle \epsilon^2_{11}\right\rangle = \left\langle \epsilon^2_{22}\right\rangle$, eq. (4.60) may be written as

$$\left\langle \epsilon^2_{11}\right\rangle - \left\langle \epsilon_{11}\epsilon_{22}\right\rangle - 2\left\langle \epsilon^2_{12}\right\rangle = 0, \tag{4.61}$$

cf. eq (4.23) and eq. (4.28). By using eqs. (4.53) and (4.54) in eq. (4.57) one obtains a relation between F_1, F_2, F_3 and $\left\langle \varepsilon^2_{11}\right\rangle$ as

$$4F_1 + 16F_2 + \frac{32}{3}F_3 = \frac{\left\langle \epsilon^2_{11}\right\rangle}{\nu^2}. \tag{4.62}$$

Siggia (1981) has identified the four invariants of the fourth order velocity gradient tensor as

$$I_1 \equiv \left\langle s^4\right\rangle, \quad I_2 \equiv \left\langle s^2\omega^2\right\rangle, \quad I_3 \equiv \left\langle \omega_i S_{ij}\omega_k S_{kj}\right\rangle, \quad I_4 \equiv \left\langle \omega^4\right\rangle \tag{4.63}$$

where $s = S_{ii}$ is the trace of the rate of strain tensor and $\omega^2 = \omega_i^2$ the enstrophy with vorticity $\omega_i = \epsilon_{ijk}(\partial u_k/\partial x_j)$ where ϵ_{ijk} is the Levi-Civita symbol. Then, we have

$$F_1 = 4I_1/105 \tag{4.64}$$

$$F_2 = I_1/105 + I_2/70 - I_3/105 \tag{4.65}$$

$$F_3 = 3I_1/140 + 11I_2/140 - 3I_3/35 + I_4/80 \tag{4.66}$$

Table 4.5: Ratios of invariants of the fourth-order velocity derivative tensor.

Re_λ	88	119	184	215	331	529	680 (Ishihara et al. (2007))
I_2/I_1	1.6726	1.6951	1.40015	1.7247	1.7347	1.7443	1.75
I_3/I_1	0.2132	0.2181	0.2236	0.2267	0.2294	0.2341	0.24
I_4/I_1	6.6402	7.0349	7.3893	7.5573	7.7334	7.9494	8.0

and all second-order dissipation parameters may be expressed in terms of Siggia's invariants

$$\frac{\left\langle \epsilon_{11}^2 \right\rangle}{\nu^2} = \frac{\left\langle \epsilon_{22}^2 \right\rangle}{\nu^2} = \frac{\langle \epsilon_{11}\epsilon_{22} \rangle + 2\left\langle \epsilon_{12}^2 \right\rangle}{\nu^2} = \frac{8}{15} I_1 + \frac{16}{15} I_2 - \frac{16}{15} I_3 + \frac{2}{15} I_4 \tag{4.67}$$

As noted by Siggia (1981), the ratios I_2/I_1, I_3/I_1 and I_4/I_1 should be Reynolds number independent for large Reynolds numbers. This is shown to be approximately true for the Reynolds numbers of our DNS calculations as shown in table 4.5, where the ratios are also compared to the values obtained by Ishihara et al. (2007) calculated at $Re_\lambda = 680$, see also section 4.2. Taking the numbers of Ishihara et al. for these ratios we obtain with $I_1 = \langle \varepsilon^2 \rangle / (4\nu^2)$

$$\left\langle \epsilon_{11}^2 \right\rangle = \left\langle \epsilon_{22}^2 \right\rangle = \langle \epsilon_{11}\epsilon_{22} \rangle + 2\left\langle \epsilon_{12}^2 \right\rangle \approx 0.8 \left\langle \varepsilon^2 \right\rangle . \tag{4.68}$$

All second-order dissipation parameters should therefore scale with the Reynolds number in the same way as $\langle \varepsilon^2 \rangle$, in agreement with section 4.2.2 and section 4.2.3.

4.3.3 Relations between the trace of fourth-order structure functions $D_{[4]}$ and $\langle \varepsilon_{[4]}^2 \rangle$ in the viscous range

Here, we look at the trace $D_{[4]}$ in the viscous range. Different to the individual equations in section 4.3.2, we have one equation for one unknown trace which allows us to solve for it. We find that for $r \to 0$, $D_{[4]}$ is exactly determined by $\epsilon_{[4]}^2$, ν and r.

As discussed in section 3.1.1, the transport term of the fourth-order structure function eq. (3.79) as well as the pressure source terms are proportional to r^4 for $r \to 0$, while the viscous term and the dissipation source term are proportional

to r^2 in the viscous range. Therefore, to leading order the transport and pressure source terms may be neglected in the viscous range and eq. (3.79) simplifies to

$$2\nu\left(\frac{\partial^2 D_{[4]}}{\partial r^2}+\frac{2}{r}\frac{\partial D_{[4]}}{\partial r}\right)=\left\langle E_{[4]}\right\rangle. \tag{4.69}$$

Similarly, from the equation for $\left\langle E_{[4]}\right\rangle$ in section 3.3.1, the viscous term and ε^2-term balance,

$$2\nu\left(\frac{\partial^2\left\langle E_{[4]}\right\rangle}{\partial r^2}+\frac{2}{r}\frac{\partial\left\langle E_{[4]}\right\rangle}{\partial r}\right)=\varepsilon^2_{[4]}. \tag{4.70}$$

where $\varepsilon^2_{[4]}$ is constant in the viscous range. Solving eq. (4.70) and inserting the result into eq. (4.69) then gives

$$D_{[4]}=\frac{\varepsilon^2_{[4]}}{480\nu^2}r^4,\quad \left\langle E_{[4]}\right\rangle=\frac{\varepsilon^2_{[4]}}{12\nu}r^2. \tag{4.71}$$

Since $D_{[4]}$ is the sum of $D_{4,0}$, $D_{2,2}$ and $D_{0,4}$, all of which are also proportional to r^4 for $r\to 0$, the individual structure functions are also determined by $\varepsilon^2_{[4]}$ in the viscous range. Since $D_{[4]}=D_{4,0}+4D_{2,2}+8D_{1,3}/3$, one can use the expansions given in eq. (4.47) to eq. (4.49) to relate $\varepsilon^2_{[4]}/\nu^2$ to the sum of F_1, F_2 and F_3 as well as Siggia's invariants defined in eq. (4.63) resulting in

$$\frac{\varepsilon^2_{[4]}}{480\nu^2}=F_1+4F_2+\frac{8}{3}F_3=\frac{2}{15}I_1+\frac{4}{15}I_2-\frac{4}{15}I_3+\frac{1}{30}I_4. \tag{4.72}$$

With eq. (4.67) above, the trace $\varepsilon^2_{[4]}$ is related in the viscous range to the dissipation parameters

$$\varepsilon^2_{[4]}=120\left\langle\varepsilon^2_{11}\right\rangle=120\left\langle\varepsilon^2_{22}\right\rangle=120\left\langle\varepsilon_{11}\varepsilon_{22}\right\rangle+240\left\langle\varepsilon^2_{12}\right\rangle. \tag{4.73}$$

A similar analysis can be carried out for higher even orders in the viscous range. However, there are more intermediate equations linking the higher-order moments of the dissipation to the higher-order dissipation source term and ultimately to the structure function, cf. the Archive material (`http://arxiv.org/abs/1504.07490`) for the sixth-order equations. For instance, one then finds for the sixth order $D_{[6]}\sim r^6\varepsilon^3_{[6]}/\nu^3$ in the viscous range, with two intermediate equations.

4.4 Order-dependent cut-off length and velocity scales η_C and u_C

We have seen in section 4.1 that there are exact relations between even moments of the longitudinal velocity gradient $\langle(\partial u_1/\partial x_1)^{2M}\rangle$ and the moments of the dissipation $\langle\varepsilon^M\rangle$. Furthermore, it was shown in section 4.2 that also the moments of the mixed velocity gradients $G_{p,q}$ as well as the components of the pseudo-dissipation tensor $\langle\epsilon_{ij}\epsilon_{kl}...\rangle$ have the same Reynolds number scaling as the respective moments of the dissipation $\langle\varepsilon^M\rangle$. Additionally, it has been shown in section 4.3 that higher-order structure functions in the viscous range are determined by higher moments of the dissipation. This implies that the mean $\langle\varepsilon\rangle$ is not the correct quantity to define higher-order dissipative scales, i.e. that basic K41 scaling does not hold at higher orders. In this section, exact order-dependent dissipative scales are introduced.

The notion of order-dependent cut-off length scales is also related to the multi-fractal framework, cf. e.g. Paladin and Vulpiani (1987a,b), who used the multi-fractal model to estimate grid resolution scaling. Frisch and Vergassola (1991) used the notion of scales smaller than the Kolmogorov scale to modify the second-order structure function as well as the energy spectrum in the so-called intermediate dissipation range (situated in between the Kolmogorov scale and the smallest scale determined by the lowest fractal exponent). They then proposed a renormalisation of the energy spectrum to collapse it to an universal curve.

Meneveau (1996) examined the viscous range by employing an order-dependent interpolation formula accompanied by using a multi-fractal model to examine order- and Reynolds number dependent collapse of structure functions in the viscous range. He showed that order-dependent cut-off length scales as given by a multi-fractal model are consistent with extended self-similarity (ESS, cf. Benzi et al. (1993)) for small Reynolds numbers, but that the collapse of ESS worsens for high Reynolds numbers and orders.

Yakhot (2003) derived order-dependent cut-off length scales by matching the viscous range and the inertial range and related these cut-off scales to the inertial range exponents $\zeta_{N,0}$. Yakhot and Sreenivasan (2005) then used Yakhot's result and derived additional constraints on the inertial range scaling exponents. Furthermore, they considered the implications regarding the grid resolution of numerical studies in the context of Yakhot's theory. More recently, Schumacher et al. (2007) examined structure functions using highly resolved DNS and found that they collapse in the dissipation range when normalised with the cut-off lengths defined by the inertial range exponents given by Yakhot (2003).

The approach presented here differs from those described above inasmuch as we derive cut-off scales by using information gained from the (isotropic) tensorial properties of the velocity gradient tensor, for which we do not need any specific assumptions other than isotropy, homogeneity and incompressibility. This allows to define the cut-off scales with dissipative quantities only (namely the moments of the dissipation), and we find exact relations for the longitudinal structure functions of arbitrary even order, using only the same assumptions as in Kolmogorov's seminal 1941 work.

4.4.1 Dissipative cut-off scales

Kolmogorov's first similarity hypothesis states that *'For the locally isotropic turbulence the distributions F_n are uniquely determined by the quantities ν and $\langle\varepsilon\rangle$'*, where F_n are the distributions of the velocity increments, cf. Kolmogorov (1941b)*. In other words, all structure functions $D_{m,n} = \langle(\Delta u_1)^m(\Delta u_2)^n\rangle$ (where $\Delta u_j = u_j(x_i + r_i) - u_j(x_i)$ and the separation vector r_i with magnitude r is aligned without loss of generality with the x_1-axis) are supposed to be uniquely determined by the viscosity ν and the mean dissipation $\langle\varepsilon\rangle$ for $r \to 0$. Kolmogorov backed this claim by determining the solution for the second-order structure functions in the viscous range, eq. (3.42). Figure 4.9 shows the second-order structure function $D_{2,0}$ normalised with the second-order dissipative scales u_η and η (i.e. the Kolmogorov scales defined in eq. (1.30)) for the different Reynolds numbers given in section 2.1, which we show here to allow a visual comparison with higher-order structure functions normalised with the Kolmogorov scales η and u_η as presented below. In that spirit, the 'goodness of collapse' of the different curves onto a single curve as seen in fig. 4.9 can be used as reference for the collapse or non-collapse of higher orders. We find that $D_{2,0}$ collapses indeed as expected and scales as r^2 for $r \to 0$. The viscous range extends to $r/\eta \sim 10$ and is followed by a transitional region. For larger r/η, there is the inertial range which increases with increasing Reynolds number, in agreement with the classical picture of turbulent flows.

Generalising Kolmogorov's first similarity hypothesis implies

$$D_{N,0} = K_{N,0} \frac{\langle\varepsilon\rangle^{N/2}}{\nu^{N/2}} r^N, \tag{4.74}$$

where the constant $K_{N,0}$ should depend on the order N only and is supposed to be

*Note that Frisch (1995) interprets F_n more generally as 'small-scale properties'.

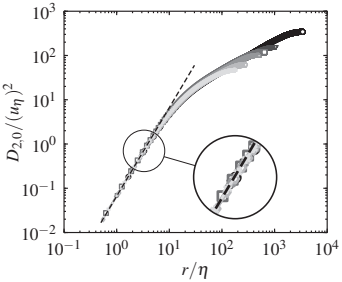

Figure 4.9: Longitudinal structure function $D_{2,0}$ normalised with η and u_η. $\star$ $Re_\lambda = 88$, $\diamond$ $Re_\lambda = 119$, $\triangle$ $Re_\lambda = 184$, $\square$ $Re_\lambda = 215$, $\triangledown$ $Re_\lambda = 331$, $\circ$ $Re_\lambda = 754$. Dashed line corresponds to eq. (4.83) with $\widetilde{K}_{2,0} = 1/15$.

independent of the Reynolds number. Non-dimensionalising this relation with the Kolmogorov velocity $u_\eta = (\nu \langle\varepsilon\rangle)^{1/4}$ and the Kolmogorov length $\eta = (\nu^3/\langle\varepsilon\rangle)^{1/4}$ gives

$$\frac{D_{N,0}}{(u_\eta)^N} = K_{N,0} \left(\frac{r}{\eta}\right)^N. \tag{4.75}$$

This implies that the structure functions should collapse for small $r \to 0$ according to eq. (4.75) if normalised with u_η and η. In the following, we focus on longitudinal structure functions, for which there are exact results as presented below. We then have for $r \to 0$ from eq. (3.25)

$$D_{N,0} = \left\langle \left(\frac{\partial u_1}{\partial x_1}\right)^N \right\rangle r^N. \tag{4.76}$$

Similarly to Kolmogorov's approach for the second order, we proceed to relate the moments of the longitudinal velocity gradient to the moments of the dissipation. One would immediately estimate that

$$\left\langle \left(\frac{\partial u_1}{\partial x_1}\right)^N \right\rangle \sim \frac{\left\langle \varepsilon^{N/2} \right\rangle}{\nu^{N/2}}, \tag{4.77}$$

i.e.

$$\left\langle \left(\frac{\partial u_1}{\partial x_1}\right)^N \right\rangle = \frac{\left\langle (S_{ij}S_{ij})^{N/2} \right\rangle}{\widetilde{C}_{N,0}}, \tag{4.78}$$

in disagreement with Kolmogorov's first similarity hypothesis and eq. (4.74), as the exponent and the averaging operator do not commute. The question then becomes whether $\widetilde{C}_{N,0}$ is Reynolds number independent. For even N, it is possible to find the exact values of $\widetilde{C}_{N,0}$ following Siggia (1981), as described in section 4.1 above. From this, we have $\widetilde{C}_{2,0} = 15/2$ (cf. eq. (3.42)), $\widetilde{C}_{4,0} = 105/4$ (cf. Siggia (1981), $\widetilde{C}_{6,0} = 567/8$, $\widetilde{C}_{8,0} = 2673/16$ and so on, cf. eq. (4.2) and eq. (4.5) for N even. Consequently, for even N we have

$$D_{N,0} = \widetilde{K}_{N,0} \frac{\left\langle \varepsilon^{N/2} \right\rangle}{\nu^{N/2}} r^N, \tag{4.79}$$

with $\widetilde{K}_{N,0} = (2^{N/2}\ \widetilde{C}_{N,0})^{-1}$ and where the $\widetilde{C}_{N,0}$ are exact, Reynolds number independent values as given by eq. (4.5). Therefore, the even longitudinal structure function of order N is determined by the moment $\left\langle \varepsilon^{N/2} \right\rangle$ of the dissipation and the viscosity ν for $r \to 0$. In other words, we have found the exact solution for arbitrary even-order longitudinal structure functions in the viscous range analogously to Kolmogorov's result at the second order. Note that it is not possible to arrive at these conclusions simply on dimensional grounds, because $\langle \varepsilon^N \rangle$ and $\langle \varepsilon \rangle^N$ have the same dimensions.

What about the mixed and transversal structure functions at even orders? We note that these structure functions are not uniquely determined this way except for the second order $N = 2$, because the mixed derivatives $\langle (\partial u_1/\partial x_1)^m (\partial u_2/\partial x_1)^n \rangle$ are not completely determined by $\langle \varepsilon^{N/2} \rangle$. In other words, the higher-order tensors are not determined by only a single scalar function under the constraints of homogeneity and incompressibility. For instance, the general eighth-order velocity gradient tensor is determined by the four invariants I_1, I_2, I_3 and I_4 given by Siggia (1981) (cf. also Hierro and Dopazo (2003)), see eq. (4.64) to eq. (4.66). The invariants I_1, I_2, I_3 and I_4 are independent and therefore there are no relations between $I_1, ..., I_4$ and similarly at higher orders; consequently, the fourth-order mixed and transversal structure functions depend also on I_2, I_3 and I_4 and not solely on $I_1 \sim \langle \varepsilon^2 \rangle / \nu^2$. However, Ishihara et al. (2007) found that the ratios I_2/I_1, I_3/I_1 and I_4/I_1 are constant if the Reynolds number is large enough, cf. also table 4.5. This implies that all fourth-order structure functions scale with $\langle \varepsilon^2 \rangle$ for $r \to 0$ with universal prefactors including the mixed and transversal structure functions, although their prefactors cannot be determined analytically as multiples of the longitudinal prefactor and the same holds at higher orders, see the discussion as well as the tables and figures in section 4.3.2. Furthermore, the present approach cannot relate odd moments of the velocity

gradients to moments of the dissipation. For the third order, we have the exact result eq. (4.38) given in section 4.3.1 as well as $\langle(\partial u_1/\partial x_1)^3\rangle = -2\langle\omega_i S_{ij}\omega_j\rangle/35$, which can be derived from the general sixth-order velocity gradient tensor, see Pope (2000) and which leads to the well-known relation between vortex-stretching and the negative skewness of the velocity gradient (cf. e.g. Betchov (1956), Rotta (1972), and Townsend (1951)). As we have seen that the even longitudinal orders are determined by the moments of the dissipation, we will try to use $\langle\varepsilon^{3/2}\rangle$ and its generalisation, i.e. we will assume eq. (4.79) to hold also for odd orders (albeit with unknown, but Reynolds number independent $\widetilde{K}_{N,0}$). The only justification for odd orders up to this point is that this equation has the correct dimensions. Rather, we would expect the odd orders to scale with $\langle\omega_i S_{ij} S_{jk} ... \omega_l\rangle$ (or a generalisation of the above result for $D_{3,0}$), as these terms can be given in terms of the general velocity gradient tensor while terms like $\langle\varepsilon^{3/2}\rangle$ cannot.

We show higher even orders $D_{4,0}$, $D_{6,0}$ and $D_{8,0}$ normalised by u_η and η in the left column of figure 4.10 for different Reynolds numbers. Noticeably, these higher orders do not collapse and the disparity increases with Reynolds number and order N. This was anticipated by Landau and Lifshitz (1959) (cf. also Frisch (1995)), who argued that $\langle\varepsilon\rangle$ could not be the relevant quantity for all orders N, which implies that the proportionality factor K_N of eq. (4.75) should be flow dependent. Normalising eq. (4.79), K41 scaling then implies

$$\frac{D_{N,0}}{(u_\eta)^N} = \widetilde{K}_{N,0} \frac{\left\langle\varepsilon^{N/2}\right\rangle}{\langle\varepsilon\rangle^{N/2}} \left(\frac{r}{\eta}\right)^N . \tag{4.80}$$

where the Reynolds number dependence of $\left\langle\varepsilon^{N/2}\right\rangle / \langle\varepsilon\rangle^{N/2}$ increases with increasing order N^*. Consequently, Kolmogorov scaling cannot collapse structure functions different than those at the second-order ($N = 2$) in the viscous range, as is clearly seen in the left column of figure 4.10. By introducing a modified order-dependent cut-off length scale

$$\eta_{C,N} = \left(\frac{\nu^3}{\left\langle\varepsilon^{N/2}\right\rangle^{2/N}}\right)^{1/4} \tag{4.81}$$

and a cut-off velocity

$$u_{C,N} = \left(\nu \left\langle\varepsilon^{N/2}\right\rangle^{2/N}\right)^{1/4} \tag{4.82}$$

*K41 theory would imply that $\langle\varepsilon^{N/2}\rangle/\langle\varepsilon\rangle^{N/2} \neq f(Re_\lambda)$ so that u_η and η would collapse all orders.

we find a normalised eq. (4.79)

$$\frac{D_{N,0}}{(u_{C,N})^N} = \widetilde{K}_{N,0} \left(\frac{r}{\eta_{C,N}} \right)^N , \tag{4.83}$$

in the spirit of Kolmogorov's 1941 work on the viscous range for the second order, where the prefactor is constant. This scaling is shown in the right column of figure 4.10 again for $D_{4,0}$, $D_{6,0}$ and $D_{8,0}$ for different Reynolds numbers. Thus, eq. (4.83) indeed collapses the structure functions for $r \to 0$ and $\widetilde{K}_{N,0}$ is universal in the sense that it does not depend on the Reynolds number but is an order-dependent constant with the exact values $\widetilde{K}_{2,0} = 1/15$, $\widetilde{K}_{4,0} = 1/105$ and so on. This collapse also serves as a numerical confirmation of the relation between the moments of the dissipation and the even moments of the longitudinal velocity gradient derived in section 4.1 and as seen in figure 4.7 and figure 4.8. We find eq. (4.83) to hold for $r = 0$ to $r/\eta_{C,N} \approx 10$ independent of the order. That is, the order-dependent dissipation range scales with $\eta_{C,N}$ as expected. As seen in figure 4.10, this clearly holds for even orders in general, due to eq. (4.79). We note in passing that

$$Re_{C,N} = \frac{u_{C,N}\eta_{C,N}}{\nu} = 1 \tag{4.84}$$

as we might have expected, i.e. that inertial and viscous forces balance. Consequently, $\eta_{C,N}$ and $u_{C,N}$ are indeed viscous scales; for order $N = 2$, K41 scaling (i.e. the classical Kolmogorov scaling) is recovered, as $\eta_{C,2} = \eta$ and $u_{C,2} = u_\eta$.

Let us look at the cut-off length from a slightly different point of view. Considering only the longitudinal even-order structure functions, which are determined by the velocity gradients $\langle(\partial u_1/\partial x_1)^N\rangle$ with dimensional units $[s^{-m}]$, one needs a second quantity with dimensions $[m^\alpha s^\beta]$ (with $\alpha \neq 0$ and $\beta \neq 0$) to find a characteristic length scale l_N with dimensional units $[m]$. As we are concerned with the viscous range, the viscosity ν with dimensions $[m^2 s^{-1}]$ is a

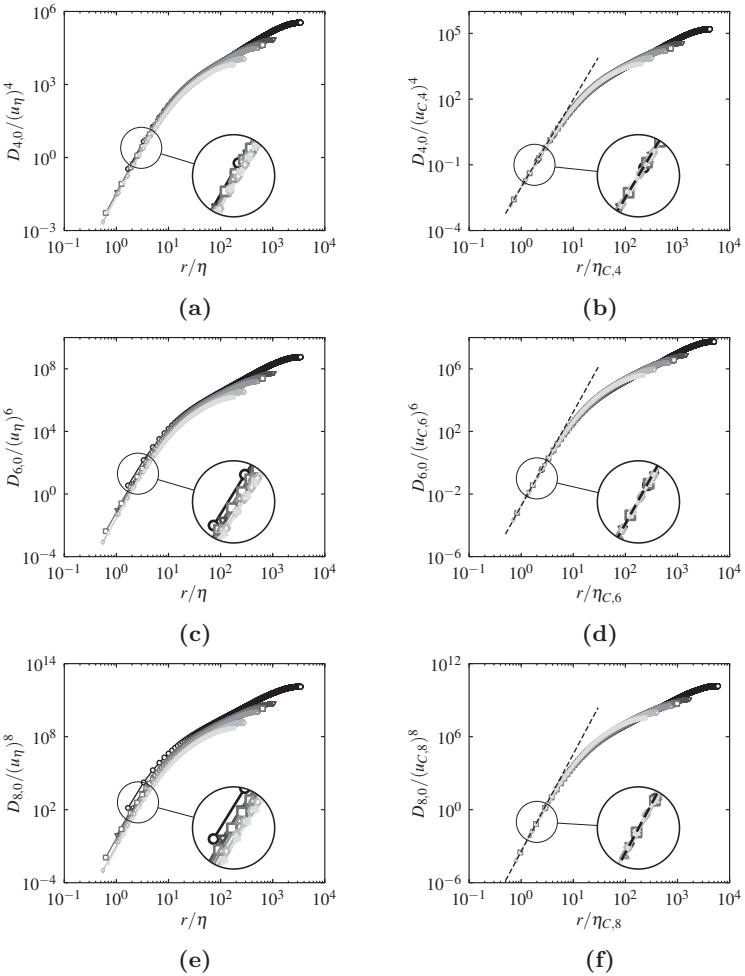

Figure 4.10: Longitudinal structure functions $D_{N,0}$. Left column: Kolmogorov scaling with η and u_η. Right column: Scaling with η_C (eq. (4.81)) and u_C (eq. (4.82)). (a) and (b) $D_{4,0}$, (c) and (d) $D_{6,0}$, (e) and (f) $D_{8,0}$. $\star$ $Re_\lambda = 88$, $\diamond$ $Re_\lambda = 119$, $\triangle$ $Re_\lambda = 184$, $\square$ $Re_\lambda = 215$, $\triangledown$ $Re_\lambda = 331$, $\circ$ $Re_\lambda = 754$. Dashed lines correspond to eq. (4.83) with $\widetilde{K}_{4,0} = 1/105$ (b), $\widetilde{K}_{6,0} = 1/567$ (d) and $\widetilde{K}_{8,0} = 1/2673$ (f).

natural choice. We then have

$$l_N = \left[\frac{\nu^N}{\left\langle (\partial u_1/\partial x_1)^N \right\rangle}\right]^{\frac{1}{2N}} = \left[\frac{\nu^{(3/2)N}}{\nu^{N/2}\left\langle (\partial u_1/\partial x_1)^N \right\rangle}\right]^{\frac{1}{2N}} \sim \left[\frac{\nu^3}{\left\langle \varepsilon^{N/2}\right\rangle^{2/N}}\right]^{1/4} = \eta_{C,N} \quad (4.85)$$

and similarly for $u_{C,N}$. That is, when choosing the viscosity as second quantity to build the length scale, $\eta_{C,N}$ and $u_{C,N}$ naturally follow. Different scales can only be obtained by choosing a different quantity than ν.

Different to the viscous range it is not possible to determine a priori how to normalise $D_{N,0} = C_{N,0} r^{\zeta_{N,0}}$ in the inertial range so that $C_{N,0}$ does not depend on the Reynolds number. This is due to the fact that we do not know the exact value of $\zeta_{N,0}$ and thus cannot choose a suitable velocity and length scale so that $C_{N,0}$ is non-dimensional; therefore we cannot expect the structure functions to collapse in the inertial range. The only exception is of course the third-order structure function $D_{3,0} = -4/5\,\langle\varepsilon\rangle\, r$, which collapses using the K41 scales u_η and η. Deviations from K41 for the second-order structure functions in the inertial range are usually attributed to intermittency effects. For higher orders, it is therefore necessary to consider deviations of the higher-order structure functions normalised in a way that they collapse for $r \to 0$ (as do the second-order structure functions when normalised with the K41 quantities), i.e. not with η and u_η but with $\eta_{C,N}$ (eq. (4.81)) and $u_{C,N}$ (eq. (4.82)). If one examines deviations of higher-order structure functions normalised with the second-order quantities η and u_η, one includes the well known increase of higher-order derivative moments scaled by the second moment. These effects are not present when using $\eta_{C,N}$ and $u_{C,N}$, as with these scales the Reynolds number dependence cancels out.

Next, we also look at the odd orders, which should be determined by $\langle\omega_i S_{ij}\omega_j\rangle$ (third order), $\langle\omega_i S_{ij}S_{jk}S_{kl}\omega_l\rangle$ (fifth order) and so on*. We find that their behaviour resembles that of the even orders, inasmuch as Kolmogorov scaling eq. (4.75) does not collapse the structure functions for $r \to 0$, cf. the left column of figure 4.11. Again, we find that deviations increase with increasing order and Reynolds number, as was the case for the even orders. Using $\eta_{C,N}$ (eq. (4.81)) and $u_{C,N}$ (eq. (4.82)) collapses the data and again we have an order-dependent dissipation range up to $r/\eta_{C,N} \sim 10$. Thus, the general relation eq. (4.83)

*Or by $\nu^{2/(N-1)}\langle\epsilon_{11}^{(N-1)/2}(\partial u_1/\partial x_1)\rangle$ in the spirit of section 4.3.1.

also holds for odd orders, although we cannot determine the prefactors $\widetilde{K}_{N,0}$ analytically. Furthermore, we would expect the odd moments of the (longitudinal) velocity gradient pdf to scale with $\langle\varepsilon^{N/2}\rangle/\langle\varepsilon\rangle^{N/2}$, if $\langle(\partial u_1/\partial x_1)^N\rangle \sim \nu^{N/2}\langle\varepsilon^{N/2}\rangle$ for odd orders as well, as our data suggests. Ishihara et al. (2007) found a scaling exponent of 0.11 ± 0.1 for Reynolds number dependence of the skewness of $\partial u_1/\partial x_1$, which agrees with the scaling $\langle\varepsilon^{3/2}\rangle/\langle\varepsilon\rangle^{3/2} \sim Re_\lambda^{0.12}$ from our DNS. This implies that $\langle\varepsilon^{3/2}\rangle \sim \nu^{3/2}\langle\omega_i S_{ij}\omega_j\rangle$ and so on, with constant proportionality factors. However, these factors cannot be determined by the isotropic form of the general velocity gradient tensor, as $\langle\varepsilon^{3/2}\rangle$ etc. cannot be expressed in terms of it.

In view of section 4.3.1, this implies that the ratio $\langle(\partial u_1/\partial x_1)\epsilon_{11}\rangle/\langle\varepsilon^{3/2}\rangle$ is constant as well and similarly at higher odd orders. Moreover, all ratios $\langle(\partial u_1/\partial x_1)^m(\partial u_2/\partial x_1)^n\rangle/\langle\varepsilon^{N/2}\rangle$ should be constant at sufficiently large Reynold numbers, cf. section 4.2.3, even though only those of the even order longitudinal velocity gradient can be derived analytically. This implies that *all* structure functions in the viscous range can be written as

$$D_{m,n} = \widetilde{K}_{m,n}\frac{\langle\varepsilon^{N/2}\rangle}{\nu^{N/2}}r^N, \tag{4.86}$$

where $\widetilde{K}_{N,0} = (2^{N/2}C_N)^{-1}$ with C_N from eq. (4.5) for even N. Consequently, the dissipative scales defined by eq. (4.81) and eq. (4.82) hold for *all* structure functions of order N and not only the longitudinal $D_{N,0}$. Furthermore, Kolmogorov (1941b)'s first similarity hypothesis needs to be modified by replacing $\langle\varepsilon\rangle$ by the respective moments $\langle\varepsilon^{N/2}\rangle$.

To summarise, $\eta_{C,N}$ and $u_{C,N}$ are the right quantities to normalise structure functions of order N in the viscous range, as shown in figure 4.10 and figure 4.11. Using the new scales $\eta_{C,N}$ and $u_{C,N}$ collapses the higher orders as well as η and u_η in case of the second order, cf. figure 4.9. Moreover, the probability density function (pdf) of the dissipation ε in combination with the viscosity ν can therefore be thought of as boundary conditions $r \to 0$ for the structure functions in the system of partial differential equations equations shown in figure 3.1.

Naturally, the question arises how $\eta_{C,N}$ scales with η. From eq. (4.81) we find

$$\frac{\eta_{C,N}}{\eta} = \left(\frac{\langle\varepsilon\rangle^{N/2}}{\langle\varepsilon^{N/2}\rangle}\right)^{\frac{1}{2N}} \sim Re_\lambda^{-(\alpha_{N/2})/(2N)}. \tag{4.87}$$

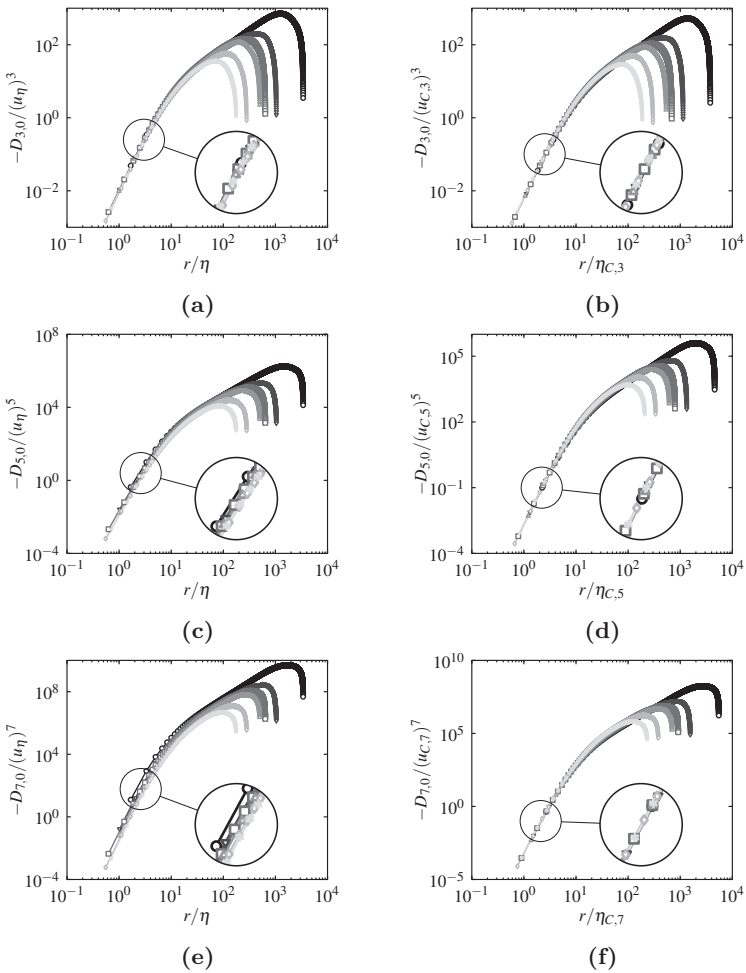

Figure 4.11: Longitudinal structure functions $D_{N,0}$. Left column: Kolmogorov scaling with η and u_η. Right column: Scaling with η_C (eq. (4.81)) and u_C (eq. (4.82)). (a) and (b) $D_{3,0}$, (c) and (d) $D_{5,0}$, (e) and (f) $D_{7,0}$. $\star$ $Re_\lambda = 88$, $\diamond$ $Re_\lambda = 119$, $\triangle$ $Re_\lambda = 184$, $\square$ $Re_\lambda = 215$, $\triangledown$ $Re_\lambda = 331$, $\circ$ $Re_\lambda = 754$.

Figure 4.12a shows the scaling of $\left\langle \varepsilon^{N/2} \right\rangle / \left\langle \varepsilon \right\rangle^{N/2}$ as function of the Reynolds number Re_λ as evaluated from our DNS,

$$\frac{\left\langle \varepsilon^{N/2} \right\rangle}{\left\langle \varepsilon \right\rangle^{N/2}} \sim Re_\lambda^{\alpha_{N/2}}, \tag{4.88}$$

where the dashed lines correspond to a least-squares fit and we use the values of $\alpha_{N/2}$ from our DNS in the following. Noticeably, the scaling exponent $\alpha_{N/2}$ of eq. (4.88) increases with N, in agreement with the notion of intermittency of ε. Donzis et al. (2008) compared $\langle \varepsilon^{N/2} \rangle$, $\langle \varepsilon \rangle^{N/2}$ as well as the ratio for different orders $N/2 = 2, 3, 4$ as function of the Reynolds number and grid resolution. They found that a grid resolution $\kappa_{\max}\eta$ somewhere between $\kappa_{\max}\eta = 1$ and $\kappa_{\max}\eta = 3$ is sufficient to resolve the second to fourth moments of ε. Interestingly enough, the sensitivity of the normalised moments with respect to the resolution $\kappa_{\max}\eta$ seems to decrease with increasing Reynolds number, at least for the two cases $Re_\lambda = 140$ and $Re_\lambda = 240$ they considered (their figure 4 and table 2). For that matter, we feel rather confident that the data shown in our figures 4.12a and 4.12b is adequate for the issues addressed here (cf. also the discussion and figures of section 4.3), although we cannot claim that there might be no (small) errors in the values of $\alpha_{N/2}$ used below. In a recent paper, Schumacher et al. (2014) compared different flows for $N/2 = 2, 3, 4$ and found that the Reynolds number dependence of $\langle \varepsilon^{N/2} \rangle / \langle \varepsilon \rangle^{N/2}$ is the same for the different flows they examined (homogeneous isotropic turbulence, a turbulent channel flow and turbulent Rayleigh-Bénard convection). This implies that the moments of the (longitudinal) velocity gradient should also have the same Reynolds number dependence for the different flow types. This seems to be case; Sreenivasan and Antonia (1997) and Ishihara et al. (2007) compiled data of different flows and found a good collapse of the skewness and flatness of the longitudinal velocity gradient. Moreover, from eq. (4.7) with $M = 2$, the Reynolds number dependence of $\langle \varepsilon^2 \rangle / \langle \varepsilon \rangle^2$ must be the same as the Reynolds number dependence of $\langle (\partial u_1/\partial x_1)^4 \rangle / \langle (\partial u_1/\partial x_1)^2 \rangle^2$, i.e. the normalised second moment of the dissipation must scale the same as the flatness of the longitudinal velocity gradient. From our data, we find a scaling $\langle \varepsilon^2 \rangle / \langle \varepsilon \rangle^2 \sim Re_\lambda^{0.33}$, while Ishihara et al. (2007) reported $\langle (\partial u_1/\partial x_1)^4 \rangle / \langle (\partial u_1/\partial x_1)^2 \rangle^2 \sim Re_\lambda^{0.34 \pm 0.03}$, i.e. we find excellent agreement.

Thus, the cut-off length $\eta_{C,N}$ decreases with increasing Reynolds number Re_λ, while the order-dependency needs to be examined more closely. Figure 4.12b shows the ratio $\alpha_{N/2}/(2N)$ for $N = 1, ..., 8$ where $\alpha_{N/2}$ has been obtained by

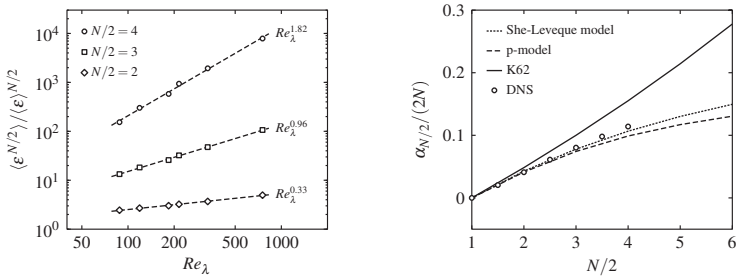

Figure 4.12: (a) Scaling of $\langle \varepsilon^{N/2} \rangle / \langle \varepsilon \rangle^{N/2}$ as function of the Reynolds number. (b) $\alpha_{N/2}/2N$ as function of $N/2$. Symbols: DNS data, solid line: Log-normal model with $\mu = 0.25$, dashed line: p-model with $p_1 = 0.7$, dotted line: She-Leveque model. Model predictions are described in section 5.2 below.

fitting the data of figure 4.12a. We find that $\alpha_{N/2}/(2N)$ plotted over $N/2$ is concave and non-decreasing, at least for the orders observed. This can also be seen in figure 4.10, where the transitional range is shifted towards smaller scales with increasing order. This immediately raises the question of the asymptotic behaviour of $\alpha_{N/2}$ at high orders, as it would imply that there is a myriad of smaller and smaller scales ($N/2$ is unbounded in principle). If there is no upper limit of $\alpha_{N/2}/(2N)$ for $N \to \infty$, then the smallest scale $\eta_{N\to\infty} \to 0$ independent of the Reynolds number, as seen from eq. (4.87). Indeed, there is an upper limit $\alpha_{N/2}/(2N) \leq 1/2$, as discussed in section 5.1.

4.4.2 Implications for the resolution of DNS

From the existence of scales smaller than the Kolmogorov scale, it follows that this might influence the resolution requirements of direct numerical simulations, as characterised by the product $\kappa_{\max}\eta$, where $\kappa_{\max}$ is the maximum wavenumber resolved by the simulation. Different to earlier work e.g. by Yakhot and Sreenivasan (2005), where the multi-fractal model was used to determine the cut-off scales, we use here the exact length scales eq. (4.81). It is therefore worthwhile to examine the required grid resolution in some detail, although it has been studied in the literature by employing different approaches before. Naturally, there is a trade-off for a given number of grid points corresponding to a given $\kappa_{\max}$ between a highly resolved simulation (i.e. a large $\kappa_{\max}\eta$) and a

high Reynolds number implying a low $\kappa_{\max}\eta$. Common wisdom is to resolve at least $\kappa_{\max}\eta = 1$ and usually, $\kappa_{\max}\eta = 1.3$ is considered high enough. Note that some studies require a higher resolution, especially if the examined quantities depend on higher-order derivatives of the velocity field. An example is the study of Jiménez et al. (1993), which required $\kappa_{\max}\eta = 2$.

It is evident that $\kappa_{\max}\eta > 1$ is needed to resolve the higher moments of the velocity gradient pdf, as these are linked to the higher moments of the dissipation. The higher the order of the moment, the higher the required resolution. This can also be seen from the data of Ishihara et al. (2007) as well as Donzis et al. (2008), where the velocity gradient pdf did not collapse at similar Reynolds number with $\kappa_{\max}\eta = 1$ and $\kappa_{\max}\eta = 2$; the dissimilarity is less in the core of the pdf and stronger in the tails, which are determined by the higher moments.

From eq. (4.87), we see that the cut-off lengths $\eta_{C,N}$ are less resolved for a given $\kappa_{\max}\eta$ with increasing order N. In order to compare these influences, the normalised resolution

$$\left[\kappa_{\max}\eta_{C,N}\right]^* = \frac{\kappa_{\max}\eta_{C,N}}{\kappa_{\max}\eta} \tag{4.89}$$

is provided in table 4.6, where we have used the values of $\langle\varepsilon^{N/2}\rangle/\langle\varepsilon\rangle^{N/2}$ from our data. We also give extrapolated resolutions for $Re_\lambda = 10^3$ and $Re_\lambda = 10^4$, which were computed using the fits shown in figure 4.12a. These resolutions are not meant to give exactly the required resolution to resolve the eighth order at $Re_\lambda = 10^3$, say, but rather to provide an estimate and to show the influence of the Reynolds number and order. For instance, $\kappa_{\max}\eta = 1.3$ would suggest that the fourth-order structure function (and with it the flatness of the velocity gradient pdf) is completely resolved at $Re_\lambda = 10^4$, while higher orders are only partially resolved. Equivalently, we would expect $\kappa_{\max}\eta = 1.3$ at $Re_\lambda = 215$ to fully resolve the sixth-order structure function, i.e. this rule of thumb ensures a well-enough resolved DNS, if one is interested in lower-order moments at (from the present point of view) low to intermediate Reynolds numbers.

To summarise, if $\kappa_{\max}\eta = \kappa_{\max}\eta_{C,2} = 1$ completely resolves the second-order structure function, the variance of the velocity gradient pdf, the mean dissipation $\langle\varepsilon\rangle$ and low-order statistics like the mean kinetic energy $\langle k\rangle$ (cf. Yeung and Pope (1989)), then $\kappa_{\max}\eta_{C,3} = 1$ additionally completely resolves the third-order structure function, skewness of the velocity gradient pdf and the vortex stretching $\langle\omega_i S_{ij}\omega_j\rangle$, while $\kappa_{\max}\eta_{C,4} = 1$ also resolves the flatness of the velocity gradient pdf, the variance of the pdf $P(\varepsilon)$ and the fourth-order structure function and so on.

Thus, we need more grid points to resolve a certain order when increasing the

Table 4.6: Normalised resolution $[\kappa_{\max}\eta_{C,m}]^* = \kappa_{\max}\eta_{C,m}/\kappa_{\max}\eta$ as function of Reynolds number Re_λ and order m.

	R0	R1	R2	R3	R4	R6	$Re_\lambda = 10^3$	$Re_\lambda = 10^4$
$[\kappa_{\max}\eta]^*$	1.000	1.000	1.000	1.000	1.000	1.000	1.000	1.000
$[\kappa_{\max}\eta_{C,4}]^*$	0.894	0.883	0.871	0.864	0.849	0.819	0.805	0.738
$[\kappa_{\max}\eta_{C,6}]^*$	0.806	0.785	0.763	0.749	0.725	0.678	0.663	0.551
$[\kappa_{\max}\eta_{C,8}]^*$	0.730	0.700	0.672	0.652	0.623	0.571	0.551	0.424

Reynolds number than the classical estimate using K41 would suggest. There are several estimates of the scaling of numbers of grid points with the Reynolds number, see for instance Davidson (2004), Paladin and Vulpiani (1987b), and Yakhot and Sreenivasan (2005). In the following, we will use eq. (4.87). If we assume that $\alpha_{N/2}/(2N)$ converges to a finite number for $N \to \infty$, we can use eq. (4.87) to estimate the number of grid points to completely resolve all scales, sometimes also called the number of degrees of freedom of the flow. That is, we can estimate the scaling of grid points with the Reynolds number via

$$\begin{aligned} N_{\text{grid}} \sim \left(\frac{L_{\text{Box}}}{\Delta x}\right)^3 &\sim \left(\frac{L_{\text{Box}}}{L}\right)^3 \left(\frac{L}{\eta_{C,N\to\infty}}\right)^3 \\ &\sim \left(\frac{L_{\text{Box}}}{L}\right)^3 \left(\frac{L}{\eta}\right)^3 \left(\frac{\eta}{\eta_{C,N\to\infty}}\right)^3 \\ &\sim \left(\frac{L_{\text{Box}}}{L}\right)^3 Re_L^{9/4[1+\alpha_{N/2}/(3N)]}, \end{aligned} \tag{4.90}$$

where Δx is the grid spacing, L_{Box} the length of the DNS box (cube) and L the integral length. Consequently, N_{grid} is larger than the K41 estimate $N_{\text{grid}} \sim Re_L^{9/4}$ since $\alpha_{N/2} \geq 0$ and the scaling of N_{grid} depends on the asymptotic behaviour of $\alpha_{N/2}/(2N)$ for $N/2 \to \infty$. From eq. (5.22), $\alpha_{N/2}/(2N) \leq 1/2$ (i.e. $\alpha_{N/2}/(3N) \leq 1/3$) and therefore

$$N_{\text{grid}} \sim \left(\frac{L_{\text{Box}}}{L}\right)^3 Re_L^3, \tag{4.91}$$

as upper bound. Paladin and Vulpiani (1987b) used the multi-fractal framework to also obtain $N \sim Re_L^3$ as the largest Reynolds number scaling possible (see also Yakhot and Sreenivasan (2005), where also a Re_L^3 scaling has been found).

For the She-Leveque model, $\alpha_{N/2}/(2N) \to 3/10$ (cf. eq. (5.25)) and one obtains $N \sim Re_L^{27/10}$. Paladin and Vulpiani (1987b) reported $N \sim Re_L^{2.3}$ using data from Anselmet et al. (1984).

4.4.3 A short remark on passive scalar cut-off scales

Let us briefly digress and discuss the passive scalar ϕ. One might have expected that similar results as eq. (4.81) and eq. (4.82) existed for the passive scalar. Furthermore, one might have also hoped that the scalar analogon is easier to derive, since the passive scalar is by definition a *scalar* quantity and not a *vectorial* quantity like the velocity field, which simplifies the necessary computations regarding isotropic tensor calculus.

From a Taylor series, one obtains for even N for $r \to 0$

$$\left\langle (\Delta\phi)^N \right\rangle = \left\langle \left(\frac{\partial \phi}{\partial x_1} \right)^N \right\rangle r^N + \ldots, \tag{4.92}$$

similarly to eq. (3.25) for the structure functions, where $\Delta\phi = \phi - \phi'$ is the passive scalar increment separated by the vector r_i, analogous to the velocity increment $\Delta u_i = u_i - u_i'$. Consequently, $\langle (\Delta\phi)^N \rangle$ are passive scalar structure functions of order N.

Assuming tentatively that the passive scalar is isotropic for $r \to 0$, there are exact relations of the form

$$\left\langle \chi^{N/2} \right\rangle = \frac{1}{\mathcal{C}_N} D^{N/2} \left\langle \left(\frac{\partial \phi}{\partial x_1} \right)^N \right\rangle \tag{4.93}$$

for even N in analogy to eq. (4.86), where

$$\chi = 2D \frac{\partial \phi}{\partial x_i} \frac{\partial \phi}{\partial x_i} \tag{4.94}$$

is the scalar dissipation with D as scalar diffusion coefficient. Therefore for $r \to 0$,

$$\left\langle (\Delta\phi)^N \right\rangle = \mathcal{C}_N \frac{\left\langle \chi^{N/2} \right\rangle}{D^{N/2}} r^N, \tag{4.95}$$

for even N. Indeed, one can compute the $\mathcal{C}_N$ rather easily. In the following, we briefly sketch the derivation of $\mathcal{C}_2$ and $\mathcal{C}_4$. For $N = 2$, one can write assuming

isotropy

$$\left\langle \frac{\partial\phi}{\partial x_i}\frac{\partial\phi}{\partial x_j}\right\rangle = A_1\delta_{ij}, \quad \langle\chi\rangle = 2DA_1\delta_{ii} = 6DA_1. \tag{4.96}$$

Consequently,

$$\left\langle \left(\frac{\partial\phi}{\partial x_1}\right)^2\right\rangle = \frac{\langle\chi\rangle}{6D} \tag{4.97}$$

and $\mathcal{C}_2 = 1/6$. For $N = 4$, one can write assuming isotropy

$$\begin{aligned}\left\langle \frac{\partial\phi}{\partial x_i}\frac{\partial\phi}{\partial x_j}\frac{\partial\phi}{\partial x_k}\frac{\partial\phi}{\partial x_l}\right\rangle &= A_1\delta_{ij}\delta_{kl} + A_2\delta_{ik}\delta_{jl} + A_3\delta_{il}\delta_{jk} \\ &= A\left(\delta_{ij}\delta_{kl} + \delta_{ik}\delta_{jl} + \delta_{il}\delta_{jk}\right)\end{aligned} \tag{4.98}$$

since all indices are interchangeable and therefore $A_1 = A_2 = A_3 = A$. This is also true at higher N, which is one of the main differences compared to the general velocity gradient tensor; all $\mathcal{C}_N$ can be uniquely determined by isotropy alone, since they depend on a single scalar function which can be related to the higher moments of χ. One then finds

$$\left\langle\chi^2\right\rangle = 4D^2A\left(\delta_{ii}\delta_{jj} + 2\delta_{ij}\delta_{ij}\right) = 60D^2A \tag{4.99}$$

which yields

$$\left\langle \left(\frac{\partial\phi}{\partial x_1}\right)^4\right\rangle = \frac{\left\langle\chi^2\right\rangle}{20D^2} \tag{4.100}$$

and $\mathcal{C}_4 = 1/20$. Similarly, higher order $\mathcal{C}_N$ can be easily computed. We now continue as for the velocity field. Normalising eq. (4.95) then gives

$$\frac{\left\langle(\Delta\phi)^N\right\rangle}{\left(\phi_{C,N}\right)^N} = \mathcal{C}_N\left(\frac{r}{\eta_{\phi,N}}\right)^N \tag{4.101}$$

with the Nth-order cut-off scale

$$\eta_{\phi,N} = \frac{\phi_{C,N}D^{1/2}}{\left\langle\chi^{N/2}\right\rangle^{1/N}} \tag{4.102}$$

where $\phi_{C,N}$ is the Nth-order cut-off scalar. Here, an apparent difference to eq. (4.86) is observable: $\phi_{C,N}$ is a-priori undetermined. From dimensional analysis, this is due to the fact that there are *three* dimensional units, $[m]$, $[s]$

and $[K]$ (the unit of the passive scalar) but only *two* scaling quantities D and $\langle\chi^{N/2}\rangle$ with dimensions $[m^2/s]$ and $[K^2/s]$, while in eq. (4.86) there are only two dimensional units $[m]$ and $[s]$ and two scaling quantities ν and $\langle\varepsilon^{N/2}\rangle$ with dimensions $[m^2/s]$ and $[m^2/s^3]$. Consequently, $\eta_{\phi,N}$ cannot be expressed solely in terms of D and $\langle\chi^{N/2}\rangle$, while $\eta_{C,N}$ can be expressed by ν and $\langle\varepsilon^{N/2}\rangle$. From a physical point of view, $\eta_{\phi,N}$ cannot be determined by D and $\langle\chi^{N/2}\rangle$ alone, because they do not describe the influence of the velocity field on the passive scalar (since the passive scalar is *passive* and not active, it does not influence the velocity field and therefore eq. (4.86) remains unchanged, i.e. there is no influence of the passive scalar on the velocity field cut-off scales $\eta_{C,N}$ and $u_{C,N}$).

That is, in order to proceed, one has to further specify $\phi_{C,N}$*. It is well known that the Schmidt-number

$$Sc = \frac{\nu}{D} \tag{4.103}$$

plays a crucial role, i.e. the cases $Sc \gg 1$ and $Sc \ll 1$ differ physically. For $Sc > 1$, $\nu > D$ and the passive scalar diffusion is less effective than the kinematic diffusion. Therefore, one would expect a fine-scale structure of ϕ with $\eta_{\phi,N} < \eta_{C,N}$. On the other hand, if $Sc < 1$ and $D > \nu$, the passive scalar diffusion is more effective and $\eta_{\phi,N} > \eta_{C,N}$. The differences between the small and large Schmidt-number cases are easily seen when examining the spectra for $Sc \ll 1$ (figure 4.13a) and $Sc \gg 1$ (figure 4.13b), where Γ is the scalar spectrum and E the energy spectrum. In case of $Sc < 1$, Γ falls rapidly off at wavenumbers $\kappa \sim \eta_{\phi,2}^{-1}$ while the energy spectrum still exhibits inertial range scaling. The slope of $\Gamma \sim \kappa^{-17/3}$ in the range $\eta_{\phi,2}^{-1} < \kappa < \eta^{-1}$ was derived by Batchelor et al. (1959). For $Sc > 1$, passive scalar fluctuations are rather dissipated at a wavenumber $\kappa \sim \eta_{\phi,2}^{-1} > \eta^{-1}$ and Batchelor (1959) found that $\Gamma \sim \kappa^{-1}$ in the range $\eta^{-1} < \kappa < \eta_{\phi,2}^{-1}$.

In general, one would expect that

$$\phi_{C,N} = f(\chi, D, \varepsilon, \nu). \tag{4.104}$$

One issue immediately arises: from dimensional analysis alone, it is not possible to distinguish between $\langle\varepsilon^2\rangle$ and $\langle\varepsilon\rangle^2$, say. Therefore, additional analysis needs to be carried out.

Indeed for $N = 2$, the exact results for $\eta_{\phi,2}$ are known as detailed below. For $Sc < 1$, the corresponding $\eta_{\phi,2}$ was independently derived by Obukhov and Corrsin (see the discussion in Batchelor (1959)), while the high Schmidt-number

*Or, equivalently, the cut-off scale $\eta_{\phi,N}$.

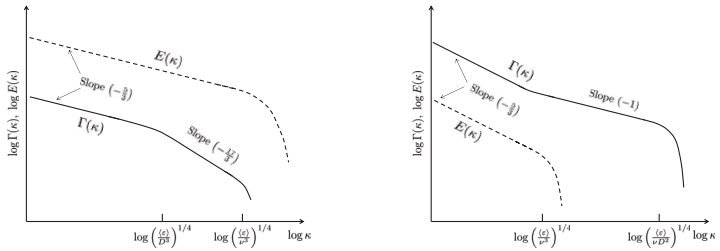

Figure 4.13: Scalar and energy spectra for $Sc \ll 1$ (a) and $Sc \gg 1$ (b). Figures adapted from Batchelor (1959) and Batchelor et al. (1959).

result was derived by Batchelor (1959).

- For $Sc \ll 1$, one would expect that the viscosity ν plays no role, because the cut-off of the scalar spectrum occurs at a much lower wavenumber than the cut-off of the velocity spectrum, i.e. $\phi_{C,N} = f(\chi, D, \varepsilon)$. Furthermore since $N = 2$, one would assume $\langle\varepsilon\rangle$ and $\langle\chi\rangle$ to be the relevant quantities and not higher moments such as $\langle\varepsilon^2\rangle$ or $\langle\chi^2\rangle$. Dimensional analysis then yields

$$\phi_{C,2} = \frac{\langle\chi\rangle^{1/2} D^{1/4}}{\langle\varepsilon\rangle^{1/4}}, \quad \eta_{\phi,2} = \left(\frac{D^3}{\langle\varepsilon\rangle}\right)^{1/4} = Sc^{-3/4}\eta \tag{4.105}$$

  where $\eta = \eta_{C,2}$ is the second-order velocity cut-off scale, i.e. the Kolmogorov scale. This result is consistent with the scaling reported in the literature by Obukhov and Corrsin for $Sc \ll 1$.

- For $Sc = 1$, one would expect the cut-off of both the scalar spectrum and the velocity spectrum at the same wavenumber, and consequently $\eta_{\phi,2} = \eta$. Thus from eq. (4.102),

$$\phi_{C,2} = \frac{\langle\chi\rangle^{1/2}\eta}{D^{1/2}}, \tag{4.106}$$

  i.e. the viscosity also plays a role as expected and $\phi_{C,N} = f(\chi, \varepsilon)$ and either ν or D, since $\nu = D$.

- Lastly, for $Sc \gg 1$, the energy spectrum falls off rapidly and viscosity plays an important role in teasing out very thin sheets or ribbons of ϕ upon which the scalar viscosity acts as detailed by Batchelor. Thus, $\phi_{C,2} = f(\nu, \varepsilon, \chi)$, i.e.

$$\phi_{C,2} = \frac{\langle\chi\rangle^{1/2}\,\nu^{1/4}}{\left\langle\varepsilon^{1/4}\right\rangle}, \quad \eta_{\phi,2} = \left(\frac{\nu D^2}{\langle\varepsilon\rangle}\right)^{1/4} = Sc^{-1/2}\eta. \tag{4.107}$$

  For $Sc \gg 1$, the scale $\eta_{\phi,2} = Sc^{-1/2}\eta$ is known as Batchelor scale.

These results can be used to collapse second-order passive scalar structure functions for $r \to 0$. However, there are no known results at higher orders. For instance in case of $\eta_{\phi,4}$, it is not clear whether to scale $\phi_{C,4}$ with $\langle\varepsilon^2\rangle$, $\langle\varepsilon\rangle^2$ or both, i.e. whether $\eta_{\phi,4} = \eta$, $\eta_{\phi,4} = \eta_{C,4}$ or a combination of the two. For that matter, any assumption $\phi_{C,N} = f(\chi, D, \varepsilon, \nu)$ would need to be checked against DNS data or experiments with different Reynolds and Schmidt number*. Such an endeavour is out of the scope of the present analysis. We may conclude that the correct cut-off scales of the passive scalar cannot be determined by the same procedure as for the velocity field, although deriving the $\mathcal{C}_N$ is much easier than the analogous connectors $C_{m,n}$ of eq. (4.86).

Finally, it should be mentioned that the assumption of isotropy might not be correct regarding the passive scalar, even in the range $r \to 0$, cf. the discussion in Sreenivasan (1991) as well as Warhaft (2000). Isotropy requires that the gradient pdf $P(\partial\phi/\partial x_1) = P(\partial\phi/\partial x_2) = P(\partial\phi/\partial x_3)$, i.e. all gradients have the same statistics. Furthermore, all odd moments of the scalar gradient must vanish because they are determined by odd-order tensors†. Hence, the scalar gradient pdf would be symmetric. Specifically, isotropy thus implies that $P(\partial\phi/\partial x_1)$ as well as $P(\partial\phi/\partial x_2)$ and $P(\partial\phi/\partial x_3)$ are unskewed. However, the implications of isotropy are at odds with experiments, cf. e.g. Mydlarski and Warhaft (1998) or Tong and Warhaft (1994).

Moreover, for *odd* orders N, $\left\langle(\Delta\phi)^N\right\rangle$ would scale as r^{N+1} for $r \to 0$, which is why we have limited the discussion to even orders in this section. For instance

*Note that this would require a more refined computational grid, since the ratio $\eta_{\phi,N}/\eta_{C,N} < 1$ for $Sc \gg 1$, which would modify eq. (4.90).

†Assuming isotropy, odd-order tensors such as $\langle(\partial\phi/\partial x_i)(\partial\phi/\partial x_j)(\partial\phi/\partial x_k)\rangle$ or similar higher-order tensors vanish, because the only odd-order isotropic tensor is the ϵ-tensor ϵ_{ijk} (third order) or combinations thereof such as $\delta_{ij}\epsilon_{klm}$, see appendix A. Since ϵ_{ijk} changes sign under interchange of two of its indices, e.g. $\epsilon_{ijk} = -\epsilon_{ikj}$, odd-order tensors vanish since statistics are supposed to be invariant not only with respect to rotations of the coordinate system, but also with respect to reflections when assuming isotropic flows.

for $N = 3$, one finds

$$\left\langle (\Delta\phi)^3 \right\rangle = \frac{3}{2} \left\langle \left(\frac{\partial \phi}{\partial x_1} \right)^2 \left(\frac{\partial^2 \phi}{\partial x_1^2} \right) \right\rangle r^4 + \mathcal{O}(r^5) \tag{4.108}$$

and similarly for higher order, i.e. is dependent on combinations of higher derivatives of ϕ and not only $(\partial\phi/\partial x_1)^N$. We note in closing that this is different for the velocity gradient pdf, because there the odd moments such as $\langle(\partial u_1/\partial x_1)^3\rangle$ are determined by *even*-order tensors, i.e. do not vanish. Therefore, the odd-order moments of the velocity gradient pdf do not vanish under the assumption of isotropy and consequently $\langle(\Delta u_1)^m(\Delta u_2)^n\rangle \sim \langle(\partial u_1/\partial x_1)^m(\partial u_2/\partial x_1)^n\rangle r^N$ for $r \to 0$ for both even and odd N.

5 Inertial range

After having discussed the viscous range in chapter 4, let us now turn to the inertial range in the present chapter, mostly based on Boschung et al. (2016c) (section 5.2), Peters et al. (2016) (section 5.3) and Boschung et al. (2016a) (section 5.4).

In section 5.1, it is shown that assuming RSH implicitly implies that the ratio $(\partial D_{N+1}/\partial r)/\langle E_{N,0}\rangle = const.$, i.e. that the longitudinal structure functions of order $N+1$ are determined by the longitudinal dissipation source terms of order N. This assumption is found to be in good agreement with the DNS data of section 2.1.

In section 5.2, we look at the connection between normalised moments of the dissipation $\langle\varepsilon^M\rangle/\langle\varepsilon\rangle^M$ as discussed in chapter 4 and longitudinal inertial range scaling exponents $\zeta_{N,0}$. We find very good agreement with the scaling exponents reported in section 3.1.1 as well as those found in the literature.

In section 5.3, we will investigate the effect of dissipation parameters such as $\langle(\epsilon_{11}+\epsilon'_{11})^{N/2}\rangle$ on the inertial range scaling exponents by integrating the structure function equations in the inertial range. Since there are exact results stemming from the second-order structure function equations (Kolmogorov's 4/5-law, cf. section 1.4), it seems promising to examine the higher-order equations. Here, we focus specifically on the fourth order. Using order-of-magnitude estimates for the different source terms, we determine the fifth-order scaling exponents. We will also look at the connection between dissipation fluctuations traditionally represented by the volume-averaged dissipation ε_r and its connection to the dissipation parameters identified in the dissipation source term equations given in section 3.1.3. We focus on the trace of the fourth-order structure function equations rather than the component's equations, because it simplifies the treatment of the equations. Additionally, there is an analogy to the trace of the second-order structure function equations, which contain the mean dissipation $\langle\varepsilon\rangle$. We may therefore expect to find the second moment $\langle\varepsilon^2\rangle$ in the fourth-order equations. In this context, it is also worth mentioning that the trace is of particular interest because it is invariant, i.e., independent of the coordinate system, as are $\langle\varepsilon\rangle$ and Siggia's invariants (Siggia (1981)). This is especially important if one is interested in scaling parameters such as $\langle\varepsilon^M\rangle$. For instance,

Hill (2002) showed that the mean dissipation $\langle\varepsilon\rangle$ is found in the trace of the second-order structure function equations (those quantities being invariants), while the equations for the components of the second-order structure function contain the pseudo-dissipation tensor $\langle\epsilon_{ij}\rangle$. Kolmogorov's K41 eq. (1.28) relating a component of the third-order structure function to the invariant $\langle\varepsilon\rangle$ is obtained because of the incompressibility relation eq. (3.24). Analogous incompressibility relations do not exist at higher order such that one should not expect equations relating individual components of higher-order structure functions to an invariant quantity analogous to $\langle\varepsilon\rangle$. We further find that the approach of using ε_r is consistent with the two-point theory of small-scale turbulence in the sense that ε_r appears in the system of the newly derived equations.

In section 5.4 we examine the influence of the unsteady/forcing terms and the viscous terms in the inertial range, exemplified for the second-order equations. Both the unsteady/forcing terms and viscous terms have been neglected in the inertial range thus far. Here, we use rather DNS of decaying homogeneous isotropic turbulence as described in section 2.2 as compared to the forced turbulence (described in section 2.1) employed up to this point, for two reasons: First, using decaying turbulence means that there is no contribution by the large-scale forcing to the balance equations, but rather the unsteady term which can be rewritten after normalising the equations to make it amenable for closer examination. Second, while the unsteady term vanishes after averaging for the forced turbulence, it plays a very similar role for decaying turbulence as the forcing term for forced turbulence, i.e. is acting on the large-scales in a similar way.

5.1 Kolmogorov's refined similarity hypothesis and the dissipation source terms

In this section, we briefly show that Kolmogorov's refined similarity hypothesis implicitly assumes that longitudinal structure functions of order $N+1$ are determined by the longitudinal dissipation source terms of order N found in the structure function equations.

As discussed in section 3.1, the K41 postulate eq. (1.33),

$$D_{N,0} = A_N \langle\varepsilon\rangle^{N/3} r^{N/3}, \tag{5.1}$$

where A_N are order-dependent prefactors which may depend on the Reynolds number, was found to be in disagreement with measurements and simulations of

higher-order structure functions, cf. e.g. figure 3.3b. For that reason, Kolmogorov (1962) introduced the refined similarity hypothesis (RSH) eq. (3.28),

$$D_{N,0} = \widetilde{A}_N \left\langle \varepsilon_r^{N/3} \right\rangle r^{N/3}, \tag{5.2}$$

where $\widetilde{A}_N$ is another order-dependent constant and ε_r given by

$$\varepsilon_r = \frac{1}{r} \int \varepsilon \mathrm{d}r. \tag{5.3}$$

In this framework, deviations from K41 scaling are then due to the r-dependence of $\langle \varepsilon_r^{N/3} \rangle$. More specifically, RSH states that

$$\Delta u_1 = V \varepsilon_r^{1/3} r^{1/3}, \tag{5.4}$$

where V is a stochastic variable which is postulated to be independent of ε_r and r, but depends only on a local Reynolds number $Re_r = (\varepsilon_r r)^{1/3} r/\nu$. For $Re_r \gg 1$, V is furthermore supposed to be independent of Re_r (second refined similarity hypothesis). Therefore, $\widetilde{A}_N = \langle V^N \rangle$. One then has a power-law eq. (3.34), $D_{N,0} \sim r^{\zeta_{N,0}}$ with $\zeta_{N,0} = N/3 + \gamma_{N/3}$, if one assumes a power-law $\langle \varepsilon_r^{N/3} \rangle \sim r^{\gamma_{N/3}}$. The validity of eq. (5.2) has been checked by Chen et al. (1993, 1995), Stolovitzky et al. (1992), Thoroddsen (1995), and Thoroddsen and Van Atta (1992) mostly by examining statistics of V, in support of RSH. Note that eq. (5.2) has been questioned by Hosokawa (2007), who discussed an apparent paradox of RSH. However under closer inspection of his argument, the ansatz eq. (5.2) and eq. (5.4) is *not* self-contradictory, since Hosokawa's eq. (5) is equal to the 4/5-law and therefore combined with eq. (5.4) (which results in his eq. (8)) then yields $\langle V^3 \rangle = -4/5$. Only if $\langle V^3 \rangle \neq -4/5$, there would be an inconsistency.

For some time, there has been an expectation that the connection between the Navier-Stokes equations and RSH would be discovered one day or, as Kaneda and Morishita (2013) proffered: *The link between these models and the NS dynamics governing the fluid motion appears still to be missing.* This would require that a correlation exists between ε_r and the terms representing dissipation fluctuations in the Navier-Stokes equations. If one wanted to reconcile RSH with the two-point equations, one would have to develop a closure between the moments of ε_r and the dominating source terms in the structure function equations.

The exact transport equations for the structure functions $D_{N,0}$ of arbitrary order N under the assumptions of (local) homogeneity and (local) isotropy are

given by eq. (3.19). For the longitudinal component, they read

$$\frac{\partial D_{N,0}}{\partial t} + \nabla_r D_{(N+1),0} = -\left\langle E_{N,0}\right\rangle - \left\langle T_{N,0}\right\rangle + \nu\nabla_r^2 D_{N,0}, \tag{5.5}$$

where $\langle E_{N,0}\rangle$ are the longitudinal dissipation source terms and $\langle T_{N,0}\rangle$ the longitudinal pressure source terms defined by eq. (3.14) and eq. (3.13), respectively. As detailed in section 3.1.1, the longitudinal transport terms are defined as

$$\nabla_r D_{(N+1),0} = \frac{\partial D_{N+1,0}}{\partial r} + \frac{2}{r} D_{N+1,0} - \frac{2N}{r} D_{N-1,2} \tag{5.6}$$

and the longitudinal dissipation source terms as

$$\begin{aligned} \left\langle E_{N,0}\right\rangle &= C_N \left\langle \left(\Delta u_1\right)^{N-2} \left(\epsilon_{11} + \epsilon'_{11}\right) \right\rangle \\ &= 2C_N \left\langle \left(\Delta u_1\right)^{N-2} \epsilon_{11} \right\rangle, \end{aligned} \tag{5.7}$$

where $C_N = C_{N-1} + (N-1)$ with $C_2 = 1$ are order-dependent prefactors independent of the Reynolds number and where $\langle(\Delta u_1)^{N-2}\epsilon_{11}\rangle = \langle(\Delta u_1)^{N-2}\epsilon'_{11}\rangle$ due to symmetry (this has been checked with the DNS data of section 2.1). Assuming an inertial range $\eta \ll r \ll L$, where η is the Kolmogorov scale and L a large scale, the diffusive term $\nu\nabla_r^2 D_{N,0}$ as well as possible contributions by large-scale forcing may be neglected. For statistically stationary flows, one then obtains

$$\nabla_r D_{N+1,0} = -\left\langle E_{N,0}\right\rangle - \left\langle T_{N,0}\right\rangle. \tag{5.8}$$

Since eq. (3.19) is derived from the Navier-Stokes equations, its solution determines the structure functions of order N. In other words, eq. (5.2) should be compatible with eq. (5.8).

It was shown in section 3.1.3, as well as section 5.3 below, that the higher moments $\langle(\epsilon_{11} + \epsilon'_{11})^{N/2}\rangle$ are contained in the structure function equations of order N with N even, where they are found in consecutive transport equations for the longitudinal dissipation source terms $\langle E_{N,0}\rangle$. Thus, one would expect that RSH is connected to the dissipation source terms or equations derived therefrom.

Taking the derivative of $\langle \varepsilon_r^{(N+1)/3} \rangle r^{(N+1)/3}$ with respect to r yields

$$\begin{aligned}\frac{\partial}{\partial r}\left(\left\langle \varepsilon_r^{(N+1)/3}\right\rangle r^{(N+1)/3}\right) &= \frac{\partial}{\partial r}\left\langle \left[\int_0^r \varepsilon(x)\mathrm{d}x\right]^{(N+1)/3}\right\rangle \\ &= \left\langle \frac{N+1}{3}\left[\int_0^r \varepsilon(x)\mathrm{d}x\right]^{(N-2)/3}\frac{\partial}{\partial r}\left[\int_0^r \varepsilon(x)\mathrm{d}x\right]\right\rangle \\ &= \frac{N+1}{3}\left\langle (\varepsilon_r r)^{(N-2)/3}\,\varepsilon\right\rangle \quad (5.9)\end{aligned}$$

and after inserting the RSH assumption eq. (5.4) into eq. (5.9), we find

$$\frac{\partial D_{N+1,0}}{\partial r} = \frac{N+1}{3}\frac{\langle V^{N+1}\rangle}{\langle V^{N-2}\rangle}\left\langle (\Delta u_1)^{N-2}\,\varepsilon\right\rangle. \quad (5.10)$$

As expected, $N = 2$ recovers after integration the 4/5-law eq. (1.31). Note that RSH states that $\langle V\rangle = 0$ due to homogeneity, because then also $\langle \Delta u_1\rangle = 0$. That is, eq. (5.10) breaks down for $N = 3$, i.e. the fourth-order longitudinal structure function $D_{4,0}$ cannot be determined by eq. (5.10).

Eq. (5.10) should be compared to the dissipation source term eq. (5.7). If one rather defines

$$\varepsilon_r = \frac{1}{r}\int \epsilon_{11}\mathrm{d}r, \quad (5.11)$$

then there would be ϵ_{11} instead of ε in eq. (5.10)*. Sometimes, also the surrogate $\nu(\partial u_1/\partial x_1)^2$ is used instead of ϵ_{11} in eq. (5.11), because it can be measured more easily using Taylor's hypothesis. The choice at hand may impact the scaling of $\langle \varepsilon_r^{N/3}\rangle$, though one would surmise that the ratios of $\langle(\Delta u)^{N-2}\varepsilon\rangle/\langle(\Delta u)^{N-2}\epsilon_{11}\rangle$ and $\langle(\Delta u)^{N-2}\varepsilon\rangle/\langle(\Delta u)^{N-2}\nu(\partial u_1/\partial x_1)^2\rangle$ do not depend on r in the inertial range. In any way, there is no ambiguity if one uses eq. (5.11) instead of eq. (5.3). Similarly, eq. (5.10) and eq. (3.14) suggest that if one would try to extend eq. (5.2) for mixed and transverse structure functions, one should choose ϵ_{22} for the transverse and combinations of ϵ_{11}, ϵ_{22} and ϵ_{12} for the mixed structure functions.

Thus, we find that RSH implicitly assumes that

$$\frac{\partial D_{N+1,0}/\partial r}{\langle E_{N,0}\rangle} = const. \quad (5.12)$$

*This would then require that $\langle V^3\rangle = -12/5$ to recover the 4/5-law, because $\langle\epsilon_{11}\rangle = \langle\varepsilon\rangle/3$.

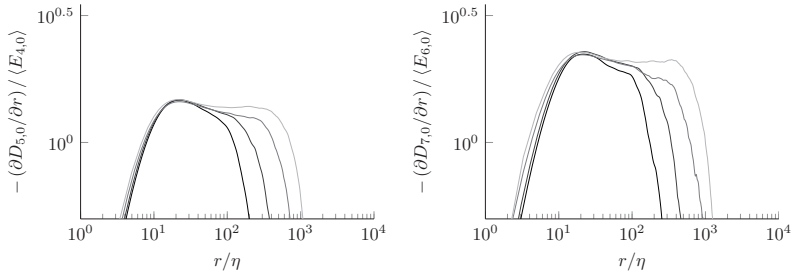

Figure 5.1: Ratio eq. (5.12) for $N = 4$ (a) and $N = 6$ (b) as evaluated from DNS for datasets R3, R4, R5 and R6. Higher Re_λ are indicated by lighter colours.

if eq. (5.11) is employed. In other words, if this ratio is constant in the inertial range, then RSH is compatible with the system of structure function equations. That is, RSH implies that (longitudinal) structure functions are determined by the (longitudinal) dissipation source terms. It should be stressed that $\partial D_{N+1,0}/\partial r \neq \nabla_r D_{N+1,0}$, but is only a part of the divergence, cf. eq. (5.6). This seems reasonable, because RSH has been postulated for longitudinal structure functions only, while the full transport term eq. (5.6) also contains mixed structure functions and cannot be integrated to solve for $D_{N+1,0}$ without $D_{N-1,2}$.

Both eq. (5.10) and eq. (5.12) are a-priori independent of any particular model for the statistics of ε_r. Nevertheless, a bad model for $\langle \varepsilon_r^{N/3} \rangle$ could theoretically still yield reasonable values for $\zeta_{N,0}$ if it sufficiently compensates deficiencies of eq. (5.12) and similarly a good model for $\langle \varepsilon_r^{N/3} \rangle$ may result in large deviations from measured $\zeta_{N,0}$ if eq. (5.12) does not hold. In the following, eq. (5.12) is numerically analysed using the dataset R3, R4, R5 and R6.

The ratio eq. (5.12) for even orders $N = 4$ and $N = 6$ are shown in fig. 5.1a and fig. 5.1b, respectively. While the lower Reynolds number cases show a clear r-dependence both for $N = 4$ and $N = 6$, $(\partial D_{5,0}/\partial r)/\langle E_{4,0}\rangle$ and $(\partial D_{7,0}/\partial r)/\langle E_{6,0}\rangle$ are constant for the highest Reynolds number $Re_\lambda = 754$ examined here. This is not that surprising considering that the dissipation source terms dominate the pressure source terms for even N, cf. section 3.2.1. While it is also found that the influence of $\langle T_{N,0}\rangle$ to the balance eq. (5.8) increases with increasing N, both $\langle T_{N,0}\rangle$ and $\langle E_{N,0}\rangle$ are found to have the same r-dependence

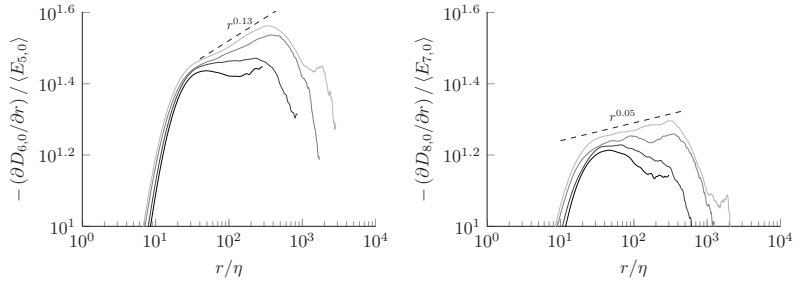

Figure 5.2: Ratio eq. (5.12) for $N = 5$ (a) and $N = 7$ (b) as evaluated from DNS for datasets R3, R4, R5 and R6. Higher Re_λ are indicated by lighter colours.

in the inertial range, cf. the figures 3.5a, 3.5b, 3.6a and 3.6b.

Compared to the even orders, the ratios eq. (5.12) for odd N are found to be slightly dependent on r in the inertial range, where we find a scaling $r^{0.13}$ for $N = 5$ and $r^{0.05}$ for $N = 7$. Noticeably, the r-dependence is smaller for $N = 7$ than for $N = 5$. The reason might be that while the pressure source terms are much larger than the dissipation source terms in the odd-order structure function equations (5.8) (cf. section 3.2.2 and Gotoh and Nakano 2003), the higher the order N the more similar is the scaling of $E_{N,0}$ and $T_{N,0}$ as function of r as is found for the even orders, cf. the figures 3.9a, 3.9b, 3.10a and 3.10b. Consequently, the assumption that the ratio $(\partial D_{N+1}/\partial r)/\langle E_{N,0}\rangle = const.$ is better satisfied at higher odd N. Moreover, it has been observed in section 3.2.2 that the odd-order dissipation source terms scale similarly as $\partial D_{N+1}/\partial r + 2D_{N+1}/r$.

A similar ratio as eq. (5.12) has been examined by Nakano et al. (2003) (their fig. 8), which in the notation used here is given by $(D_{N+1,0}/r)/\langle E_{N,0}\rangle$. They found that this ratio is constant in the inertial range for even N, while the ratio depends on r for small odd N with *decreasing* r-dependence for increasing odd N. This is consistent with the figures 5.2a and 5.2b if one assumes a power-law $D_{N+1,0} \sim r^{\zeta_{N+1,0}}$, which implies $\partial D_{N+1,0}/\partial r = \zeta_{N+1,0} D_{N+1,0}/r$, cf. eq. (3.37). Thus, we find that RSH works very well because it is a good approximation for the longitudinal dissipation source terms, which are found to scale similarly as the longitudinal structure functions. However, the question remains how the dissipation source terms depend on the higher moments of the pseudo-dissipation, $\langle(\epsilon_{11} + \epsilon'_{11})^N\rangle$ and whether and how they connect to RSH. We look at this in

more detail in section 5.3 below.

Finally, let us briefly discuss the different underlying assumptions of K41 and K62. As discussed in section 3.1.1, K41 theory eq. (5.1) implies

$$\frac{\partial D_{(N+1),0}}{\partial r} = \frac{N+1}{3}\frac{A_{N+1}}{A_{N-2}}\left\langle (\Delta u_1)^{N-2}\right\rangle \langle\varepsilon\rangle\,, \tag{5.13}$$

cf. eq. (3.27). This should be compared to

$$\frac{N+1}{3}\frac{\langle V^{N+1}\rangle}{\langle V^{N-2}\rangle}\left\langle (\Delta u_1)^{N-2}\,\varepsilon\right\rangle = \frac{N+1}{3}\frac{\langle V^{N+1}\rangle}{\langle V^{N-2}\rangle}B_N(r)\left\langle (\Delta u_1)^{N-2}\right\rangle \langle\varepsilon\rangle\,, \tag{5.14}$$

where $B_N(r)$ is the correlation of $(\Delta u_1)^{N-2}$ and ε and depends on r. Note that isotropy implies that $\langle\varepsilon\rangle = 3\langle\epsilon_{11}\rangle$, i.e. choosing eq. (5.11) instead of eq. (5.3) is consistent with the following analysis. Thus, K41 implies that the correlation of $(\Delta u_1)^{N-2}$ and ε does not depend on r, while anomalous scaling in the K62 framework is due to the r-dependence of $B_N(r)$. This is clearly seen by integrating eq. (5.10), from which one obtains

$$D_{N+1,0} = C_N\langle\varepsilon\rangle\int B_N(r)D_{N-2,0}\mathrm{d}r. \tag{5.15}$$

Together with $D_{3,0} = C_2\langle\varepsilon\rangle r$, this results in a hierarchy coupling every third structure function. For instance,

$$\begin{aligned} D_{6,0} &= C_5C_2\langle\varepsilon\rangle^2\int B_5(r)r\mathrm{d}r,\\ D_{9,0} &= C_8C_5C_2\langle\varepsilon\rangle^3\int B_8(r)\left(\int B_5(r)r\mathrm{d}r\right)\mathrm{d}r \end{aligned} \tag{5.16}$$

and so on. A similar hierarchy would also hold for the other longitudinal structure functions such as $D_{5,0}, D_{8,0}, ...$ and $D_{7,0}, D_{10,0}, ...$ and so on; however, because neither $D_{2,0}$ nor $D_{4,0}$ can be obtained from eq. (5.10) or, more precisely, because no exact solutions for $N = 1$ and $N = 3$ are known, the start of the consecutive iteration is missing. If one assumes a power-law scaling of $B_N(r)$ in the inertial range, $B_N(r) \sim r^{\beta_N}$, one obtains e.g. $D_{6,0} \sim r^{2+\beta_5}$, $D_{9,0} \sim r^{3+\beta_5+\beta_8}$ and so on. Thus, $\gamma_2 = \beta_6$ and all other $\gamma_{N/3}$ are related to the β_N as well. Moreover,

$\beta_N < 0$ for all $N \geq 4$, if $\zeta_{N,0} = f(N)$ is concave and vice versa.

5.2 Scaling of the normalised dissipation

In this section, we relate the longitudinal structure function scaling exponents to the Reynolds number scaling of the normalised moments of the dissipation $\langle\varepsilon^{N/2}\rangle/\langle\varepsilon\rangle^{N/2}$.

With the definition of the scales $\eta_{C,N}$ given in eq. (4.81), it is natural to write

$$\frac{\left\langle\varepsilon^{N/2}\right\rangle}{\left\langle\varepsilon\right\rangle^{N/2}} \sim \left.\frac{\left\langle\varepsilon_r^{N/2}\right\rangle}{\left\langle\varepsilon\right\rangle^{N/2}}\right|_{r\to\eta_{C,N}} \sim \left(\frac{\eta_{C,N}}{\eta}\right)^{\gamma_{N/2}} \left(\frac{\eta}{L}\right)^{\gamma_{N/2}}, \tag{5.17}$$

where ε_r is the volume-averaged dissipation as proposed by Obukhov (1962), cf. eq. (5.3) as well as section 5.1, and where $\gamma_{N/2}$ is the scaling exponent of the normalised dissipation

$$\frac{\left\langle\varepsilon_r^{N/2}\right\rangle}{\left\langle\varepsilon\right\rangle^{N/2}} \sim \left(\frac{r}{L}\right)^{\gamma_{N/2}}. \tag{5.18}$$

With eq. (4.87) and (4.88), we then find with $\eta/L \sim Re_\lambda^{-3/2}$ that

$$\alpha_{N/2} = -\frac{3}{2}\left(\frac{\gamma_{N/2}}{1+\gamma_{N/2}/(2N)}\right), \tag{5.19}$$

and consequently any model specifying $\gamma_{N/2}$ can be used to determine $\alpha_{N/2}$. If one assumes together with Kolmogorov (1962) the ansatz

$$D_{N,0} \sim \left\langle\varepsilon_r^{N/3}\right\rangle r^{N/3} \sim r^{\zeta_{N,0}} \tag{5.20}$$

as is widely accepted (cf. eq. (3.34)), also $\gamma_{N/2} = \zeta_{3(N/2),0} - N/2$ and therefore any theory predicting the structure function scaling exponents $\zeta_{3(N/2),0}$ predicts $\alpha_{N/2}$. One could also look at α in a different way: *Given* α, e.g. by some theory or measurements, one can solve for γ and then use $\gamma_{N/2} = \zeta_{3(N/2),0} - N/2$ to compute the scaling exponents

$$\zeta_{3(N/2),0} = \frac{N}{2}\left(1 - 4\frac{\alpha_{N/2}}{\alpha_{N/2}+3N}\right) \tag{5.21}$$

and the larger $\alpha_{N/2}$, the larger the deviations from K41 scaling $\zeta_{3(N/2),0} = N/2$ for a given N. As larger values of $\alpha_{N/2}$ imply larger higher moments of the dissipation, this is consonant with the notion that anomalous scaling is connected to the intermittency of the dissipation. From this point of view, K41 scaling implies $\alpha_{N/2} = 0$, i.e. $\langle\varepsilon^{N/2}\rangle/\langle\varepsilon\rangle^{N/2} = const.^*$. Hence, K41 scaling assumes that there is no intermittency of the flow.

Since $\zeta_{3(N/2),0} > 0$ for all N, we find from eq. (5.21) an upper limit for the scaling of the normalised dissipation as well as the ratio of the order-dependent scales

$$\alpha_{N/2} \leq N, \quad \frac{\alpha_{N/2}}{2N} \leq \frac{1}{2}. \tag{5.22}$$

Because $\alpha_{N/2}$ increases with increasing $N/2$ and $\alpha_1 = 0$, this implies that $\alpha_{N/2}/(2N)$ is concave and that $\alpha_{N/2}$ increases linearly for large N. Together with eq. (5.19) this then implies that $0 \leq \gamma_{N/2} \leq -N/2$.

Let us now briefly look at some well-known theories found in the literature and compare their predictions with our DNS[†]. For the rest of this section, we consider even N, i.e. $N/2 = M = 1, 2, 3, \ldots$[‡].

As described in section 3.1.1, Kolmogorov (1962) assumed a log-normal distribution for the dissipation which gives with eq. (3.29)

$$\alpha_{M,\mathrm{LN}} = \frac{6\mu M(M-1)}{8 + \mu(1-M)}. \tag{5.23}$$

where μ is a coefficient parametrising the intermittency. Sreenivasan and Kailasnath (1993) concluded that $\mu = 0.25 \pm 0.05$ from a comparison of different datasets in the literature. From eq. (5.23), $\alpha_{1,\mathrm{LN}} = 0$ as required. However, the log-normal model gives $\alpha_{M,\mathrm{LN}} \to \infty$ for $M \to 8/\mu + 1$ and negative $\alpha_{M,\mathrm{LN2}}$ for $M > 8/\mu + 1$. Similarly, the ratio $\eta_{C,N}/\eta \to 0$ for $M \to 8/\mu + 1$, while $\eta_{C,N} > \eta$ for $M > 8/\mu + 1$. This is at odds with the observation that the normalised moments $\langle\varepsilon^M\rangle/\langle\varepsilon\rangle^M$ increase with increasing Reynolds number for $M > 1$, i.e. $\alpha_M > 0$ for all $M > 1$. When using the log-normal model, at first the moments $\langle\varepsilon^M\rangle$ strongly increase with Re_λ and then strongly *decrease* when M is increased further. Similarly, the order-dependent scales $\eta_{C,N}$ become smaller and smaller than the Kolmogorov scale and then jump to $\eta_{C,N} > \eta$ after a critical threshold. With $\mu = 0.25$, we find the singularity for the 33th moment of the normalised

[*] Note that K41 makes no statement regarding the *shape* of the pdf $P(\varepsilon)$, since the constants may depend on N.

[†] Predictions of $\alpha_{N/2}$ for other models or theories can be derived easily by inverting eq. (5.21).

[‡] I.e. eq. (5.22) is now $\alpha_M \leq 2M$, $\alpha_M/(4M) \leq 1/2$.

dissipation and a reduced intermittency for $M > 33$.

Multi-fractality of the dissipation eq. (5.18) has been examined in detail by Meneveau and Sreenivasan (1991). An example for such a multi-fractal model is e.g. the p-model (see Meneveau and Sreenivasan (1987) and cf. (3.31)), which assumes that an eddy breaks up in two smaller eddies receiving a fraction p and $1-p$ of energy. The p-model then yields

$$\alpha_{M,\mathrm{p}} = 6\frac{M - \left\{1 - \log_2\left[p^M + \left(1-p^M\right)\right]\right\}}{3 + \frac{1}{M}\left\{1 - \log_2\left[p^M + (1-p^M)\right]\right\}}. \tag{5.24}$$

The p-model then gives $\alpha_{1,\mathrm{p}} = 0$ while for $M \to \infty$, $\alpha_{M,\mathrm{p}} \to 2M$ because the parameter $p \leq 1$.

Different to the (multi-)fractal framework, She and Leveque (1994) proposed a hierarchy of powers of the dissipation moments $\langle \varepsilon_r^{M+1}\rangle / \langle \varepsilon_r^M \rangle$. The She-Leveque model yields with eq. (3.32)

$$\alpha_{M,\mathrm{SL}} = 6\frac{M - 3\left[1 - \left(\frac{2}{3}\right)^M\right]}{5 + \frac{3}{M}\left[1 - \left(\frac{2}{3}\right)^M\right]}, \tag{5.25}$$

which contains no parameters, different to the two other models examined here. The She-Leveque model has been found to be in excellent agreement with structure function exponents obtained by measurements and DNS (see e.g. Anselmet et al. (1984), Benzi et al. (1995), and Gotoh et al. (2002)). Similarly to the log-normal and the p-model, the She-Leveque model gives $\alpha_{1,\mathrm{SL}} = 0$ and for $M \to \infty$, $\alpha_{M,\mathrm{SL}} \to 6M/5$, i.e. for very large M, $\langle \varepsilon^M \rangle / \langle \varepsilon \rangle^M$ scales linearly. Therefore, the order-dependent cut-off scales $\eta_{C,N}/\eta$ scale as $\alpha_M/(4M) \to 3/10$ for large M and the She-Leveque model satisfies eq. (5.22), i.e. the cut-off scales remain bounded at finite Reynolds numbers.

The α_M as computed from the three models above are shown in fig. 4.12b. While the log-normal model overpredicts α_M as expected, both the p-model and the She-Leveque model are in very good agreement with our DNS*. Structure function exponents as computed with eq. (5.21) using the α_M from our DNS are shown in table 5.1, together with the measurements of Anselmet et al. (1984) and Gotoh et al. (2002), which we have averaged when more than one value was reported. Moreover, there is good agreement with the data reported in table 3.3

*It should be emphasised though that they differ for larger M and the She-Leveque model is likely better suited for higher orders, cf. figure 3.3b and figure 4.12b, although no definitive conclusion can be drawn here.

Table 5.1: Comparison of $\zeta_{3M,0}$ computed with eq. (5.21) using α_M from our DNS and values from the literature.

M	eq. (5.21)	Anselmet et. al.	Gotoh et. al.
1	$\zeta_{3,0} = 1$	$\zeta_{3,0} = 1$	$\zeta_{3,0} = 1.015$
2	$\zeta_{6,0} = 1.7871$	$\zeta_{6,0} = 1.8$	$\zeta_{6,0} = 1.78$
3	$\zeta_{9,0} = 2.3904$	$\zeta_{9,0} = 2.465$	$\zeta_{9,0} = 2.35$
4	$\zeta_{12,0} = 2.8696$	$\zeta_{12,0} = 2.84$	-

as computed from the datasets R5 and R6. While we find very good agreement, it should be kept in mind that the higher orders (both for the measurements of Anselmet et al. (1984) and the DNS of Gotoh et al. (2002) as well as the ones computed from our data) might be subject to significant error bands. It is also worth mentioning that numerical errors in α_M translate to smaller errors in $\zeta_{3M,0}$, at least up to $M = 4$. This error decreases with increasing M: For instance, $\alpha_2 \pm 10\%$ yields $\zeta_{6,0} \pm 3.77\%$ while $\alpha_4 \pm 10\%$ yields $\zeta_{12,0} \pm 1.16\%$.

5.3 Relation between dissipation fluctuations and inertial range scaling exponents

In the inertial range, Kolmogorov (1962) included dissipation fluctuations by using a locally averaged dissipation ε_r as structure function scaling parameter instead of only the mean value $\langle\varepsilon\rangle$, as discussed in section 5.1. One would therefore think that ε_r must appear in the system of equations of section 3.3.1*. That is, we look for a connection between $\langle\varepsilon_r^{N/3}\rangle$ and the dissipative fluctuations such as $\langle(\epsilon_{11} + \epsilon'_{11})^{N/2}\rangle$ contained in the structure function equations. For that reason, we examine in this section a connection between the ε^2-term and the second moment of ε_r. Therefore, in order to analyse the effect of the dissipation parameter $\varepsilon^2_{[4]}$ on the inertial range scaling exponent $\zeta_{[5]}$, we must consider the dissipation source term equation. In a first step, we will integrate eq. (3.79) in the inertial range in order to calculate the fifth-order scaling exponent $\zeta_{[5]}$ implicitly defined by assuming a power-law $D_{[5]} \sim r^{\zeta_{[5]}}$. The idea is that because there are

*In section 5.1, it was shown that RSH implicitly assumes that longitudinal structure functions depend on the longitudinal dissipation source terms. This is *not* the same as finding ε_r in the system of equations. For eq. (5.10) to hold, one has to assume eq. (5.4).

equations for the structure functions as well as equations for their source terms, the scaling exponent has to be contained in the system of equations.

In the two-point equations derived systematically from the Navier-Stokes equations in the Archive material (`http://arxiv.org/abs/1504.07490`), from which we derived eq. (3.87), we have identified the terms describing dissipation fluctuations as ε^2-terms. They contain moments of the sum of components of the dissipation at two points, for instance, the moments $\langle(\epsilon+\epsilon')^M\rangle$. An integral expression such as

$$\widetilde{\varepsilon}_r = \frac{1}{V}\int \epsilon(\boldsymbol{x})\mathrm{d}\boldsymbol{x}, \tag{5.26}$$

where $V \sim \mathcal{O}(r^3)$ is a volume of dimension r^3, or the corresponding one-dimensional expression

$$\varepsilon_r = \frac{1}{r}\int \epsilon(x)\mathrm{d}x, \tag{5.27}$$

where the integral is over any length r, does not appear directly in these equations.

On the other hand, properties such as inertial range scaling exponents should, as a matter of principle, result from the two-point equations. If a power-law scaling can be assumed for the source terms in the structure function equations, the scaling exponents would follow from equations like eq. (5.32) below, to which both the pressure source term and the dissipation source term contribute. For even-order scaling exponents resulting from the odd-order structure function equations, Yakhot (2003) has argued that the dissipation source terms can be neglected and has proposed an algebraic closure relating the pressure source terms of arbitrary order to the structure functions. A similar closure could conceivably be developed for the odd-order scaling exponents in the even-order structure function equations. In these equations, the closure would be between the dissipation source terms and structure functions, while the pressure source terms can be neglected. The two-point equations show that dissipation fluctuations are represented by the dissipation parameters appearing in the successive source term equations and not by the source terms in the structure function equations.

It can be shown that the second moment of ε_r is related to the dissipation correlation $\langle\epsilon\epsilon'\rangle$ under the assumption of homogeneity by

$$\langle\epsilon\epsilon'\rangle = \frac{1}{2}\frac{\partial^2}{\partial r^2}\left[r^2\left\langle\varepsilon_r^2\right\rangle\right], \tag{5.28}$$

cf. Nelkin (1994), and similar relations can be found for the higher moments of ε_r. We only discuss the second moment, because we examine here the fourth-order

structure function equations. Particularly, we only look at the trace eq. (3.87), but our findings carry over to the individual equations for longitudinal, mixed, and transverse dissipation source terms as well. If one assumes a power-law for $\langle \varepsilon_r^2 \rangle \sim r^\gamma$, cf. eq. (5.18) where the scaling exponent and the prefactor are independent of r, as one is apt to do and which is at the very core of RSH and similar theories, one also finds by virtue of eq. (5.28) that $\langle \epsilon\epsilon' \rangle \sim r^\gamma$ and hence has the same r-scaling. The first term of the ε^2-term in eq. (3.96) can be written as the sum of constants and correlations; i.e.,

$$\left\langle (\epsilon + \epsilon')^2 \right\rangle = 2 \left\langle \epsilon^2 \right\rangle + 2 \left\langle \epsilon\epsilon' \right\rangle . \tag{5.29}$$

In other words, the r-dependence of ε_r is manifested in the ε^2-terms in the dissipation source terms by virtue of eq. (5.28) and eq. (5.29).

We begin with the integration of eq. (3.79) to link the structure function exponent to the source terms. We will neglect the diffusive and unsteady terms in eq. (3.79) and eq. (3.87) and perform an order of magnitude estimate of the source terms. If we assume in eq. (3.79) a power-law scaling for the source terms of the form*

$$\left\langle T_{[4]} \right\rangle = A^T_{[4]} r^{\xi^T_{[4]}} \tag{5.30}$$

$$\left\langle E_{[4]} \right\rangle = A^E_{[4]} r^{\xi^E_{[4]}} \tag{5.31}$$

which is consistent with Fig. 3.12, the trace of the fifth-order structure functions $D_{[5]}$ can be determined from eq. (3.79) by integration. Of course, eq. (5.30) and eq. (5.31) are approximations. However, without these assumptions, a power-law of the form $D_{[5]} = C_{[5]} r^{\zeta_{[5]}}$ is not compatible with eq. (3.79) as discussed in section 3.1.1. In other words, only if the source terms follow a power-law in the inertial range, so do the structure functions. The range of integration will be divided into two parts. The first part ranges from $r = 0$ to $r^* \approx 30\eta$, where the power-law in the inertial range starts to be valid. The second part ranges from there on to the value r of interest in the inertial range. The integration then

*In the following, $\xi^T_{[4]}$ and $\xi^E_{[4]}$ are scaling exponents of the traces of the fourth-order source terms and should not be confused with the $\xi_{m,n}$ of section 3.1.1.

yields

$$
\begin{aligned}
-D_{[5]} = \frac{1}{r^2}\int_0^{r^*} r^2 \left(\left\langle T_{[4]}\right\rangle + \left\langle E_{[4]}\right\rangle\right) \mathrm{d}r \\
- \frac{1}{r^2}\left\{ \frac{A^T_{[4]} r^{3+\xi^T_{[4]}}}{3+\xi^T_{[4]}} + \frac{A^E_{[4]} r^{3+\xi^E_{[4]}}}{3+\xi^E_{[4]}} \right\}_{r=r^*} \\
+ \frac{A^T_{[4]} r^{1+\xi^T_{[4]}}}{3+\xi^T_{[4]}} + \frac{A^E_{[4]} r^{1+\xi^E_{[4]}}}{3+\xi^E_{[4]}}.
\end{aligned}
\tag{5.32}
$$

Since the diffusion terms have been neglected from the very beginning, the first integral is incomplete, cf. eq. (3.70). The purpose here is to show that this and the second term on the right-hand side of eq. (5.32) can be neglected for large $r \gg r^*$ because of the term r^{-2} in front of them. Then, only the last two terms on the right-hand side of eq. (5.32) remain, and we find the trace of the structure functions to be given as a weighted sum of the two power-laws eq. (5.30) and eq. (5.31). More specifically, there are several possible contributions to the inertial range which have been neglected: The integral from 0 to r over the viscous term might not be negligible in the inertial range at r; the integral of the dissipation and pressure source terms over 0 to r^* might not be negligible in the inertial range at some r; the value of the transport term at $r = r^*$ might not be small compared to its inertial range value. Additionally, because η is not the correct dissipative length scale for the fourth-order equations (cf. section 4.4), r^*/η is dependent on the Reynolds number and this dependence is required to be small. While the importance of some of these contributions may already be estimated from the balance Fig. 3.12, it is more advantageous to look at the integrated balance, in the spirit of eq. (5.32) and the present section. For that reason, the numerical integration of eq. (3.79) over r is presented in Fig. 5.3. The integrated balance for the datasets R0 ($Re_\lambda = 88$) and R5 ($Re_\lambda = 529$) normalised by $\langle\varepsilon^2\rangle$ and ν are plotted over r/η. Indeed, the integrated viscous terms are negligible compared to all other integrated terms in the inertial range after $r/\eta = 30$. Also, the integrated dissipation source term, pressure source term and transport term are much smaller in the viscous range than in the inertial range. This holds for all datasets and not only the cases R0 and R5 shown in Fig. 5.3a. Lastly as shown in Fig. 5.3b, both the integrated dissipation source terms as well as the integrated viscous terms cross over to the inertial

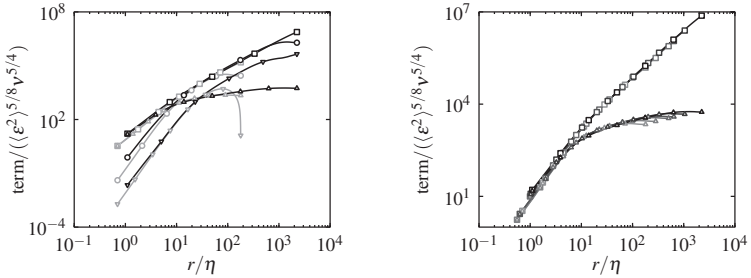

Figure 5.3: Terms of eq. (3.79) numerically integrated over r for cases R0 (grey) and R5 (black), where ∘: transport term, □: dissipation source term, ▽: pressure source term and △: viscous term (a). Integrated dissipation source term □ and integrated viscous terms △ for all cases $R0$ to $R5$ (from light grey to black) are shown in (b).

range at approximately the same value of r/η for the datasets analysed here, i.e. the true viscous cut-off length scale depends only weakly on the Reynolds number. Therefore, the simplifications with regard to the integration carried out in eq. (5.32) as described above seem justifiable.

The sum of two power-laws with constant prefactor and exponent does not give a power-law with constant prefactor and exponent. Only if $\xi^T_{[4]} = \xi^E_{[4]}$ or if one of the two terms is much smaller than the other one, the scaling of $D_{[5]}$ will result in an (approximate) power-law. We will explore the second possibility by approximating the scaling exponent $\zeta_{[5]}$ by neglecting the pressure source term (cf. Fig. 3.12, where the pressure source term is smaller than the dissipation source terms by a factor of four and also Fig. 5.3), resulting in

$$\zeta_{[5]} = 1 + \xi^E_{[4]}. \tag{5.33}$$

This relationship between $\zeta_{[5]}$ and $\xi^E_{[4]}$ is consistent with fusion rules, cf. Benzi et al. (1998) and L'vov and Procaccia (1996a), where the same relation for the fifth-order structure function is provided for the case when one of the two separation distances is in the viscous and the other in the inertial range. Here, eq. (5.33) follows directly from neglecting the pressure source term. We have calculated the scaling exponent $\xi^E_{[4]}$ of $\langle E_{[4]} \rangle$ already introduced in eq. (5.31) for

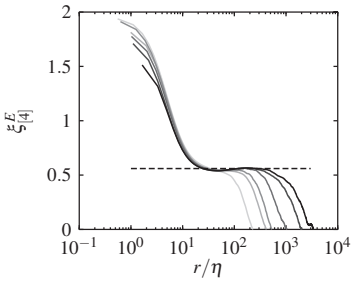

Figure 5.4: Scaling exponent $\xi^E_{[4]}$ for the cases R1-R6 with Re_λ ranging from 119 to 754 (higher Reynolds numbers indicated by darker shading). Dashed black horizontal line: $\xi^E_{[4]} = 0.56$.

all our DNS cases by using

$$\xi^E_{[4]} = \frac{r}{\langle E_{[4]} \rangle} \frac{\partial \langle E_{[4]} \rangle}{\partial r}. \tag{5.34}$$

As seen from Fig. 5.4, $\xi^E_{[4]} = 0.56$ in the inertial range for our datasets R1 to R6. The trace of the fifth-order structure functions $D_{[5]}$ is shown in Fig. 5.5 in compensated form; i.e., divided by $(r/\eta)^{1.56}$ and normalized by ν and $\langle \varepsilon^2 \rangle$. Since $\langle \varepsilon^2 \rangle$ represents the dissipation parameters at the fourth-order level, $\langle \varepsilon^2 \rangle$ provides indeed a better scaling than $\langle \varepsilon \rangle$ for quantities at that level. We plot the scaling exponents $\zeta_{[5]}$ in Fig. 5.5, as computed by

$$\zeta_{[5]} = \frac{r}{D_{[5]}} \frac{\partial D_{[5]}}{\partial r}, \tag{5.35}$$

where again implicitly a power-law for $D_{[5]}$ with constant prefactors and exponents is assumed. The dashed black horizontal line indicates the value $\zeta_{[5]} = 1.56$.

In the next step, a relation between $\xi^E_{[4]}$ and the ε^2-term is needed. Therefore, we need to look at the transport equation of the dissipation source term $\langle E_{[4]} \rangle$ in more detail. However, under the assumption of stationarity, there is no term containing $\langle E_{[4]} \rangle$ in its transport equation when the inertial range assumptions are invoked, as both the unsteady and the viscous terms are neglected. That is,

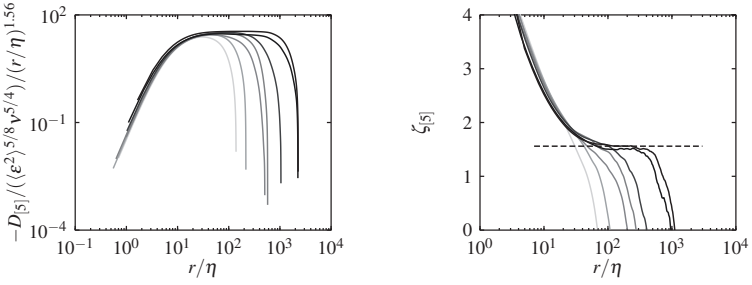

(a) **(b)**

Figure 5.5: Compensated structure function $D_{[5]}$ in the inertial range for the cases R0-R6 with Re_λ ranging from 88 to 754 (a) and scaling exponent $\zeta_{[5]}$ (b). Higher Reynolds numbers are indicated by darker shading. Horizontal dashed black line in (b): $\zeta_{[5]} = 1.56$.

information is lost by averaging, and hence, additional assumptions and closures are needed. The situation is similar to the second-order structure function equations, where one finds in the inertial range a solution for the *third*-order structure functions (i.e. the 4/5-law), but all connections to the second order are lost. If one is interested in the solution of the second order in the inertial range, one has to make additional assumptions such as Kolmogorov's constant skewness assumption*.

That is, we would now need a relation between $\langle \Delta u_1 E_{[4]} \rangle$ and $\langle E_{[4]} \rangle$, e.g. by employing a gradient flux ansatz. In the following, we rather use a slightly different approach. In analogy to K41 and K62 theory, one might postulate that fluctuations of the dissipation are the relevant scaling parameter in the inertial range. Since the transport equation for $\langle E_{[4]} \rangle$ contains the ε^2-term, which represents dissipation fluctuations, it seems reasonable to scale the dissipation source term with $\varepsilon_{[4]}^2$ and r. It should be mentioned that the r-dependence of the ε^2-term is cancelled out by the $\mathcal{D}$-term in the sum of the source terms. However, neither of the other terms combined with only r is sufficient to provide a scaling of the dissipation source term without an additional parameter like

*Defining a velocity difference skewness $S = D_{3,0}/(D_{2,0})^{3/2}$, one can write together with eq. (1.31)

$$D_{2,0} = \left(-\frac{4/5}{S}\right)^{2/3} \langle\varepsilon\rangle^{2/3}\, r^{2/3},$$

which gives K41 scaling for $D_{2,0}$ in the inertial range provided $S \neq f(r)$.

$\delta^E_{[4]}$ and the same holds for the cancellations of $\mathcal{D}_{[4]} + \varepsilon^2_{[4]}$ and $F_{[4]} + Q_{[4]}$. This indicates that some combination of the source terms in eq. (4.69) is needed to scale the dissipation source term and ultimately $D_{[5]}$. Consequently, not only the dissipation fluctuations characterised by the ε^2-term are relevant, but also the other source terms in eq. (4.69). However, the necessary combination of source terms cannot be determined by scaling arguments alone, because there are only two dimensions [m] and [s] and more than two scaling quantities. Furthermore, all terms are needed if the prefactor is also of interest.

In the following, we proceed to look only at the dissipation fluctuations, because they remain a quantity of high interest. We generalize the scaling of $\langle E_{[4]} \rangle$ with $\varepsilon^2_{[4]}$ and r by adding a prefactor $(r/r^*)^{\delta^E_{[4]}}$, i.e. use the ansatz

$$\left\langle E_{[4]} \right\rangle = c^E_{[4]} \left(\varepsilon^2_{[4]} \right)^{5/6} r^{2/3+\delta^E_{[4]}} \tag{5.36}$$

Here, $r^{*\delta^E_{[4]}}$ is contained in $c^E_{[4]}$. Of course, this is an ad-hoc ansatz and only one of many possibilities. We do not want to claim that this is the best or only way to close the equations; rather, we use it for its simplicity. We use this closure for analytical purposes only, i.e. do not want to make predictions regarding higher orders, other datasets or flows. Because there are other source terms in eq. (3.87) which contribute to the balance, one cannot expect that $\delta^E_{[4]}$ vanishes. Indeed from our DNS, we find that $\delta^E_{[4]} = -0.09$. The numerical values of $\delta^E_{[4]}$ for R1 to R6 are shown in Fig. 5.6a, where

$$\delta^E_{[4]} = r \left(\varepsilon^2_{[4]} \right)^{5/6} \left\langle E_{[4]} \right\rangle^{-1} \frac{\partial}{\partial r} \left(\left\langle E_{[4]} \right\rangle \left(\varepsilon^2_{[4]} \right)^{-5/6} \right) - \frac{2}{3} \tag{5.37}$$

and the dashed horizontal black line corresponds to $\delta^E_{[4]} = -0.09$. This value is empirically determined and not claimed to be universal or to carry over to other flows. Also, its exact value is not important in the present context. We will now insert eq. (5.36) into eq. (5.32) and integrate. That is, we now examine the scaling of the dissipation source term $\langle E_{[4]} \rangle$ compared to the scaling of the ε^2-term, $\varepsilon^2_{[4]}$, which contains $\langle \varepsilon^2_r \rangle$. Using the ansatz eq. (5.36), we find that this ratio should scale as $r^{2/3+\delta^E_{[4]}}$ in the inertial range, under the assumption that we may approximate the terms by power-laws in the inertial range. The ratio $\langle E_{[4]} \rangle / (\varepsilon^2_{[4]} r^{2/3+\delta^E_{[4]}})$ is shown in Fig. 5.6b for the cases R1 to R6. We find a scaling range in the inertial range. In short, we have now replaced the dissipation source terms with $\varepsilon^2_{[4]} r^{2/3+\delta^E_{[4]}}$, which has the same r-scaling in the inertial range.

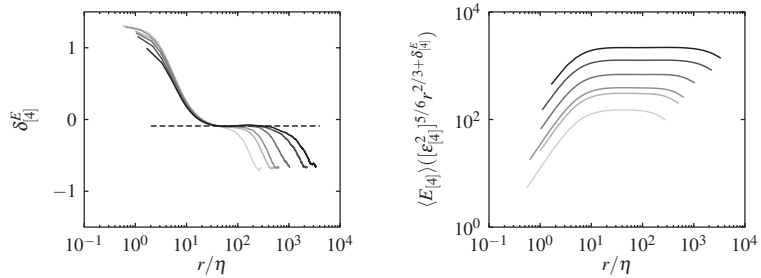

Figure 5.6: $\delta^E_{[4]}$ as evaluated by eq. (5.37) for $R1$ to $R6$ (a). Plot of the ratio $\langle E_{[4]}\rangle/(\varepsilon^2_{[4]}r^{2/3-\delta^E_{[4]}})$ with $\delta^E_{[4]} = -0.09$ (b). Higher Reynolds numbers are indicated by darker shading.

If the ε^2-term has a power-law scaling in the inertial range, we can now integrate to obtain for the structure function trace

$$D_{[5]} \sim r^{5/3+\delta^E_{[4]}} \left(\varepsilon^2_{[4]}\right)^{5/6}. \tag{5.38}$$

This should be compared to RSH, for which

$$D_{[5]} \sim r^{5/3}\langle\varepsilon_r^{5/3}\rangle. \tag{5.39}$$

That is, from the system of equations we would rather have a contribution from $\langle\varepsilon_r^2\rangle$, which is contained in $\varepsilon^2_{[4]}$, instead of $\langle\varepsilon_r^{5/3}\rangle$. As RSH gives satisfactory results when compared to experimental data, the differences have to be contained in the parameter $\delta^E_{[4]}$, which contains empirically the influence of the other source terms in eq. (4.69) on the dissipation source term $\langle E_{[4]}\rangle$. Note that eq. (5.39) implies $\langle E_{[4]}\rangle \sim r^{2/3}\langle\varepsilon_r^{5/3}\rangle$, if a power-law for ε_r can be assumed. However, there is no term containing $\langle\varepsilon_r^{5/3}\rangle$ in either the fourth- or the fifth-order equations.

We may conclude that the RSH assumption of using ε_r instead of the K41 ansatz using $\langle\varepsilon\rangle$ is compatible with the results of our approach here, in the sense that ε_r appears in the ε^2-term. However, we find in the system of equations a contribution to the fifth-order structure functions by $\langle\varepsilon_r^2\rangle$; i.e., the connection to $\langle\varepsilon_r^{N/3}\rangle$ is still missing. We expect similar results at higher orders, which should

then be related to higher moments of ε_r. However, the pressure source terms also might be important at higher orders (cf. the discussion and balances in chapter 3), which one would then need to close as well. Furthermore, we find that the r-scaling of the ε^2-term is cancelled out by the $\mathcal{D}$-term in the full system of equations. We are left with the fact that while we have found all higher moments of ε_r in the dissipation source term equations and further equations derived thereof, we cannot say why Nth-order structure functions should be determined by $\langle \varepsilon_r^{N/3} \rangle$, i.e. why the RSH assumption eq. (5.12) is valid. While the numerical values obtained either way agree fairly well (at least for the fourth order we examined here), such a connection cannot be obtained from the Navier-Stokes equations without additional, empirical closures.

The analysis can be carried to higher orders. It can easily be shown that the third successive equation for dissipation source terms in the trace of the eighth-order structure function equations contains a term $\langle(\epsilon_{ii} + \epsilon'_{ii})(\epsilon_{jj} + \epsilon'_{jj})(\epsilon_{kk} + \epsilon'_{kk})(\epsilon_{ll} + \epsilon'_{ll})\rangle$, which generates a dissipation parameter $\langle \epsilon^4 \rangle$. As one continues further, one will find all moments of the dissipation distribution function in the system of averaged equations. On the basis of the equations at the sixth-order structure function level, for instance, one could perform similar integrations as for the fourth-order level. For instance, in the Archive material at `http://arxiv.org/abs/1504.07490`, we have derived an equation for the dissipation source term $\langle E_{6,0} \rangle = 30\langle(\Delta u_1)^4(\epsilon_{11} + \epsilon'_{11})\rangle$ which appears in the sixth-order longitudinal structure function equation. In the equation for $\langle E_{6,0} \rangle$ a source term $\langle F_{6,0} \rangle = 60\langle(\Delta u_1)^2(\epsilon_{11} + \epsilon'_{11})^2\rangle$ appears. In the equation for $\langle F_{6,0} \rangle$, the term $120\langle(\epsilon_{11} + \epsilon'_{11})^3\rangle$ appears, which generates the new dissipation parameter $\langle \epsilon_{11}^3 \rangle$, and combined with the mixed and transverse equations, one finds a $\varepsilon_{[6]}^3$ term which contains $\langle(\epsilon + \epsilon')^3\rangle$, i.e. one would expect to find a contribution by $\langle \varepsilon_r^3 \rangle$ in the sixth-order equations. In order to calculate seventh-order inertial range scaling coefficients from the sixth-order structure function equations and their dissipation source terms, the trace of the structure function equations and two successive source term equations would have to be integrated. An ansatz similar to eq. (5.36) would provide at leading order the exponent 7/3. The deviation from this K41 scaling exponent would then involve more empirical terms. Similar arguments will hold for all other odd-order scaling exponents. Because there are no dissipation parameters in the odd-order source term equations, even-order scaling exponents cannot be determined this way.

5.4 Finite Reynolds number corrections of the 4/5-law for decaying turbulence

In this section, the finite Reynolds number influence of the unsteady and viscous terms in the inertial range are examined in more detail, as neglecting both the viscous and unsteady terms in the derivation of the eq. (3.40) as well as the 4/5-law eq. (3.40) amounts to assuming an infinite Reynolds number. The analysis is carried out for the second-order equations (3.38) and eq. (3.39), since they are easier to handle than the higher-order equations and the source terms are known. We use DNS data of decaying isotropic turbulence as described in section 2.2 rather than the forced isotropic datasets of section 2.1. Therefore, we have to include the unsteady terms $\partial D_{2,0}/\partial t$ and $\partial D_{0,2}/\partial t$ instead of a contribution $\langle \Delta u_i f_j \rangle$ by the large-scale forcing f_j. While both the unsteady and the forcing terms play similar roles, the former can be rewritten as function of r instead of t, while the latter depend on the forcing scheme and remain unclosed.

Noticeably, the range for which eq. (3.40) and eq. (3.41) are found to hold is rather small for experiments at finite Reynolds numbers (see e.g. Anselmet et al. (1984), Antonia and Burattini (2006), Gagne et al. (2004), and Zhou and Antonia (2000)). For that reason, modifications of the asymptotic results which include the finite Reynolds number effects were proposed for different kinds of flows. In the following, we use $\langle \varepsilon \rangle$ rather than $\langle \epsilon \rangle$ for convenience.

Lindborg (1999) considered the isotropic second-order equations of Kolmogorov and kept the unsteady term $\partial D_{2,0}/\partial t$. He then proceeded to express it using Kolmogorov's second similarity hypothesis, i.e. assumed that

$$\frac{\partial D_{2,0}}{\partial t} = C \frac{2}{3} \frac{\partial \langle \varepsilon \rangle}{\partial t} \langle \varepsilon \rangle^{-1/3} r^{2/3}, \tag{5.40}$$

where C is a constant. Employing the k-ε-model

$$\frac{\partial \langle \varepsilon \rangle}{\partial t} = -C_{\varepsilon 2} \frac{\langle \varepsilon \rangle^2}{\langle k \rangle} \tag{5.41}$$

to solve for $\partial \langle \varepsilon \rangle / \partial t$ and assuming a decay of the kinetic energy* $\langle k \rangle \sim t^{-n}$ enabled him to obtain solutions for different kind of flows and Reynolds numbers with good qualitative agreement of measurements and his model. Lundgren (2002, 2003) used asymptotic expansions to derive the longitudinal third-order structure function in the inertial range. He found the same Reynolds number

*For the remainder of this section, n denotes the decay exponent.

dependence as Lindborg.

Qian (1997, 1999) examined the approach of the 4/5-law in the inertial range using the energy spectrum equation. He found that the asymptotic results are approached rather slowly. Danaila et al. (1999) examined the inhomogeneous second-order structure function equations of Hill (1997) adapted for grid turbulence and looked at the balance of the respective terms. They found that the inhomogeneities contribute significantly for larger r. Similar conclusions were drawn by Zhou et al. (2000). Danaila et. al. measured the second-order structure function balance for channel flows (Danaila et al. (2001)) as well as homogeneous shear turbulence (Danaila et al. (2004)) and obtained similar results as for grid turbulence, in the sense that the inhomogeneities are important at large r and also in the inertial range.

Here, we will use the isotropic equations eq. (3.38) and eq. (3.39) and examine the influence of the unsteady and viscous terms, i.e. their contribution to the inertial range solutions for the third-order structure functions. While we keep the unsteady term as did Lindborg, our approach differs inasmuch that we transform eq. (3.38) and (3.39) into a self-preserving form depending only on a normalised length scale $\widetilde{r}$, similarly to the work of Schaefer et al. (2011) on the velocity correlation, and the unsteady term is reformulated assuming a decay of the kinetic energy $\langle k \rangle \sim t^{-n}$. Lundgren used the same coordinate transform, but neglected the unsteady term. Rather, he matched the leading-order terms of the asymptotic expansions of the structure functions for an outer and an inner region. Corrections to the 4/5-law eq. (3.41) then follow from the second-order terms of the expansion.

The (normalised) second-order structure function equations used here are derived in section 5.4.1. We then close the resulting system of equations using two different approaches as outlined in section 5.4.2. The second-order balances as computed using the DNS data of section 2.2 are presented in section 5.4.3. This allows a comparison with the closure results, which are used to examine both the Reynolds number scaling as well as to make predictions about large Reynolds number behaviour. This is discussed in more detail in section 5.4.4, were the balances of the (normalised) system of equations are examined using DNS data in order to check for the validity of the assumptions made in section 5.4.2.

5.4.1 Unsteady terms

To examine the influence of the unsteady terms $\partial D_{2,0}/\partial t$ and $\partial D_{0,2}/\partial t$, we use the identity

$$D_{2,0} = \left\langle (\Delta u_1)^2 \right\rangle = 2 \left\langle u_1^2 \right\rangle (1 - f(r,t)), \tag{5.42}$$

where $f(r,t)$ is the longitudinal correlation function

$$f(r,t) = \frac{\langle u_1(x_1+r,x_2,x_3,t)\ u_1(x_1,x_2,x_3,t)\rangle}{\langle u_1^2\rangle} \tag{5.43}$$

and similarly for the transverse structure function

$$D_{0,2} = \left\langle (\Delta u_2)^2 \right\rangle = 2\left\langle u_2^2\right\rangle (1-g(r,t)), \tag{5.44}$$

where $g(r,t)$ is the transverse correlation function

$$g(r,t) = \frac{\langle u_2(x_1+r,x_2,x_3,t)\ u_2(x_1,x_2,x_3,t)\rangle}{\langle u_2^2\rangle}. \tag{5.45}$$

Under the assumption of isotropy, $\left\langle u_1^2\right\rangle = \left\langle u_2^2\right\rangle \equiv U^2$. Taking the derivative of eq. (5.42) gives

$$\frac{\partial D_{2,0}}{\partial t} = 2\frac{\partial U^2}{\partial t}(1-f(r,t)) - 2U^2\frac{\partial f(r,t)}{\partial t} \tag{5.46}$$

and a similar expression for the transverse structure function eq. (5.44). In the following, r is normalised with a large scale in the spirit of Kármán and Howarth (1938), Lundgren (2003), and Schaefer et al. (2011), defined as

$$L(t) \equiv \frac{U^3}{\langle\varepsilon\rangle}, \tag{5.47}$$

where $U = \sqrt{\langle u_1^2\rangle}$. Then, the normalised length scale

$$\widetilde{r} = \frac{r}{L(t)}, \quad \widetilde{t} = t \tag{5.48}$$

and therefore

$$\frac{\partial \widetilde{r}}{\partial t} = -\frac{\widetilde{r}}{L(t)}\frac{\mathrm{d}L(t)}{\mathrm{d}t}. \tag{5.49}$$

Consequently,

$$\frac{\partial f(\widetilde{r},t)}{\partial t} = \frac{\partial f(\widetilde{r},\widetilde{t})}{\partial \widetilde{t}} - \frac{\widetilde{r}}{L(t)}\frac{\mathrm{d}L(t)}{\mathrm{d}t}\frac{\partial f(\widetilde{r},\widetilde{t})}{\partial \widetilde{r}} = -\frac{\widetilde{r}}{L(t)}\frac{\mathrm{d}L(t)}{\mathrm{d}t}\frac{\partial f}{\partial \widetilde{r}} \tag{5.50}$$

and

$$\frac{\partial g(\widetilde{r},t)}{\partial t} = \frac{\partial g(\widetilde{r},\widetilde{t})}{\partial \widetilde{t}} - \frac{\widetilde{r}}{L(t)}\frac{\mathrm{d}L(t)}{\mathrm{d}t}\frac{\partial g(\widetilde{r},\widetilde{t})}{\partial \widetilde{r}} = -\frac{\widetilde{r}}{L(t)}\frac{\mathrm{d}L(t)}{\mathrm{d}t}\frac{\partial g}{\partial \widetilde{r}} \tag{5.51}$$

where $\partial f(\widetilde{r},\widetilde{t})/\partial\widetilde{t}$ and $\partial g(\widetilde{r},\widetilde{t})/\partial\widetilde{t}$ vanish if $f(\widetilde{r},\widetilde{t})$ and $g(\widetilde{r},\widetilde{t})$ are self-similar. We will see in section 5.4.2 below that neglecting $\partial f/\partial\widetilde{t}$ and $\partial g/\partial\widetilde{t}$ has very little impact on the balance equations, i.e. that the assumption is well justified. From eqs. (5.42) and (5.44), we then have

$$\frac{\partial f(\widetilde{r},\widetilde{t})}{\partial \widetilde{r}} = -\frac{1}{2}\frac{\partial \widetilde{D}_{2,0}}{\partial \widetilde{r}}, \quad \frac{\partial g(\widetilde{r},\widetilde{t})}{\partial \widetilde{r}} = -\frac{1}{2}\frac{\partial \widetilde{D}_{0,2}}{\partial \widetilde{r}}, \tag{5.52}$$

as $\langle u_1^2 \rangle$ and $\langle u_2^2 \rangle$ do not depend on $\widetilde{r}$ and where $\widetilde{D}_{2,0} = D_{2,0}/U^2$ and $\widetilde{D}_{0,2} = D_{0,2}/U^2$ are the normalised second-order structure functions. Similarly for the third-order structure functions, $\widetilde{D}_{3,0} = D_{3,0}/U^3$ and $\widetilde{D}_{1,2} = D_{1,2}/U^3$.

For decaying homogeneous isotropic turbulence, the energy balance eq. (1.11) reduces after averaging to*

$$\frac{\partial U^2}{\partial t} = -\frac{2}{3}\langle\varepsilon\rangle\,. \tag{5.53}$$

In the self-similar decay state, $U^2 = U_0^2(t/t_0)^{-n}$, where n is a decay exponent (cf. fig. 2.1) and consequently $\langle\varepsilon\rangle = \langle\varepsilon_0\rangle(t/t_0)^{-n-1}$ in agreement with eq. (5.53).

Substituting eq. (5.53) and eq. (5.43) into eq. (5.46) and normalising with $\langle\varepsilon\rangle$ yields

$$\frac{1}{\langle\varepsilon\rangle}\frac{\partial D_{2,0}}{\partial t} = -\frac{2}{3}\widetilde{D}_{2,0} - \frac{\widetilde{r}}{U}\frac{\mathrm{d}L(t)}{\mathrm{d}t}\frac{\partial \widetilde{D}_{2,0}}{\partial \widetilde{r}} \tag{5.54}$$

and similarly,

$$\frac{1}{\langle\varepsilon\rangle}\frac{\partial D_{0,2}}{\partial t} = -\frac{2}{3}\widetilde{D}_{0,2} - \frac{\widetilde{r}}{U}\frac{\mathrm{d}L(t)}{\mathrm{d}t}\frac{\partial \widetilde{D}_{0,2}}{\partial \widetilde{r}}. \tag{5.55}$$

Finally, from eq. (5.47)

$$\frac{1}{U}\frac{\mathrm{d}L(t)}{\mathrm{d}t} = \frac{2}{3}\left(\frac{1}{n} - \frac{1}{2}\right). \tag{5.56}$$

*By definition, here $\langle k\rangle \equiv 3U^2/2$.

Dividing eq. (3.38) and eq. (3.39) by $\langle\varepsilon\rangle$ then gives the following equations

$$\overbrace{-\frac{2}{3}\widetilde{D}_{2,0}-\frac{2}{3}\left(\frac{1}{n}-\frac{1}{2}\right)\widetilde{r}\frac{\partial\widetilde{D}_{2,0}}{\partial\widetilde{r}}}^{\text{unsteady}}+\overbrace{\frac{1}{\widetilde{r}^2}\frac{\partial\widetilde{r}^2\widetilde{D}_{3,0}}{\partial\widetilde{r}}-\frac{4}{\widetilde{r}}\widetilde{D}_{1,2}}^{\text{transport}}=-\overbrace{\frac{4}{3}}^{\text{diss.}}$$
$$+\underbrace{\frac{2}{Re_L}\left[\frac{\partial^2\widetilde{D}_{2,0}}{\partial\widetilde{r}^2}+\frac{2}{\widetilde{r}}\frac{\partial\widetilde{D}_{2,0}}{\partial\widetilde{r}}+\frac{4}{\widetilde{r}^2}\left(\widetilde{D}_{0,2}-\widetilde{D}_{2,0}\right)\right]}_{\text{viscous}} \tag{5.57}$$

and

$$\overbrace{-\frac{2}{3}\widetilde{D}_{0,2}-\frac{2}{3}\left(\frac{1}{n}-\frac{1}{2}\right)\widetilde{r}\frac{\partial\widetilde{D}_{0,2}}{\partial\widetilde{r}}}^{\text{unsteady}}+\overbrace{\frac{1}{\widetilde{r}^4}\frac{\partial\widetilde{r}^4\widetilde{D}_{1,2}}{\partial\widetilde{r}}}^{\text{transport}}=-\overbrace{\frac{4}{3}}^{\text{diss.}}$$
$$+\underbrace{\frac{2}{Re_L}\left[\frac{\partial^2\widetilde{D}_{0,2}}{\partial\widetilde{r}^2}+\frac{2}{\widetilde{r}}\frac{\partial\widetilde{D}_{0,2}}{\partial\widetilde{r}}-\frac{2}{\widetilde{r}^2}\left(\widetilde{D}_{0,2}-\widetilde{D}_{2,0}\right)\right]}_{\text{viscous}} \tag{5.58}$$

where $Re_L = UL/\nu$ is a large scale Reynolds number. That is, the derivative with respect to t of the second-order structure functions has been reformulated in terms of spatial derivatives and the decay of kinetic energy expressed by the decay exponent n. Therefore, the partial differential equations are reduced to ordinary differential equations. This allows for an integration of eq. (5.57) and (5.58) in $\widetilde{r}$, if $\widetilde{D}_{2,0}$ and $\widetilde{D}_{0,2}$ are known as function of $\widetilde{r}$.

Equations eq. (5.57) and eq. (5.58) are also valid for grid turbulence, when invoking Taylor's hypothesis. Specifically, one obtains

$$\frac{\partial D_{2,0}}{\partial t}=\overline{U}_1\frac{\partial D_{2,0}}{\partial X_1},\quad \frac{\partial D_{0,2}}{\partial t}=\overline{U}_1\frac{\partial D_{0,2}}{\partial X_1} \tag{5.59}$$

with $\overline{U}_1$ as mean velocity and $X_1 = ((x_1 + r) + x_1)/2$ and where the x_1-coordinate corresponds to the streamwise direction. This leads to the equations also considered by Danaila et al. (1999), where the large scales are now determined by inhomogeneities in x_1-direction.

5.4.2 Description of possible closures

As eq. (5.57) and eq. (5.58) are unclosed, anything besides computing and comparing the individual terms from DNS requires additional closure assumptions. For this, we introduce two different approaches to close the system of equations in the following. First, we assume that the second-order structure functions follow a power-law, which allows us to directly integrate the two equations, finding explicit expressions for the third-order structure functions in the inertial range. The drawback of this approach is of course that the scaling range of the second-order structure functions is small at low Reynolds numbers and therefore the range for which the resulting third-order expressions hold is also quite limited. However interestingly enough, the same results derived differently by Lindborg (1999) and Lundgren (2003) are then recovered. Second, we close the equations by employing an eddy viscosity ansatz as presented by Oberlack and Peters (1993), which relates the second- and third-order structure functions. This allows us to also compare overall agreement and extrapolate the results to higher Reynolds numbers. We cannot rule out that the decay exponent has some influence on the parameters of the closures discussed in the following. However, we have varied the decay exponent while keeping all other parameters constant and have found no significant influence on the numerical solutions, as long as the decay exponent is not unrealistically large or small. Specifically, we compared $n = 1.4$, $n = 1.45$ and $n = 1.5$. For that reason, we are confident that the deviation from $n = 10/7$ is negligible.

Power-law closure

Here, we assume that the normalised second-order structure functions $\widetilde{D}_{0,2}$ and $\widetilde{D}_{2,0}$ follow a power-law of the form

$$\widetilde{D}_{2,0} = \widetilde{C}_{2,0}\widetilde{r}^{\zeta_{2,0}}, \quad \widetilde{D}_{0,2} = \widetilde{C}_{0,2}\widetilde{r}^{\zeta_{0,2}} \tag{5.60}$$

in the inertial range (cf. eq. (3.34)), where both the prefactors $\widetilde{C}_{2,0}$ and $\widetilde{C}_{0,2}$ as well as the exponents $\zeta_{2,0}$ and $\zeta_{0,2}$ are assumed to be independent of the separation distance $\widetilde{r}$. Power-laws for the second-order structure functions were introduced by Kolmogorov (1941a,b). In his theory (K41 theory), he assumed that in the inertial range the structure functions are only dependent on the mean dissipation $\langle\varepsilon\rangle$ and the scale r: Since the inertial range is situated in between the small scales and the large scales, the solution should not depend on either the viscosity ν, the dissipative length η or the integral length L. From dimensional

arguments, one then obtains power-laws with $\zeta_{2,0} = 2/3$ and $\zeta_{0,2} = 2/3$ as exponent. However, the use of the mean dissipation as scaling parameter has been questioned in an argument rooted in a remark of Landau (cf. e.g. the discussion in Frisch (1995)), namely that fluctuations of the dissipation may influence the scaling of the structure functions and consequently the scaling exponents may differ from 2/3. From experiments (see e.g. Antonia et al. (2000) and Attili and Bisetti (2012)) and DNS (e.g. Boratav and Pelz (1997) and Gotoh et al. (2002)), $\zeta_{2,0} > 2/3$ and $\zeta_{0,2} > 2/3$ have been found.

One of the advantages of the power-law ansatz is that it allows analytical integration of eq. (5.57) and eq. (5.58), i.e. the Reynolds number scaling of the respective terms can be examined explicitly. The exponents $\zeta_{2,0}$ and $\zeta_{0,2}$ are assumed to be Reynolds number independent, while the prefactors might vary slightly with the Reynolds number. Then, the exponents $\zeta_{2,0} = \zeta_{0,2} = \zeta_2$ are the same for both the longitudinal and transverse second-order structure functions, because they are linked via the continuity equation

$$\frac{\widetilde{r}}{2}\frac{\partial \widetilde{D}_{2,0}}{\partial \widetilde{r}} + \widetilde{D}_{2,0} - \widetilde{D}_{0,2} = 0, \tag{5.61}$$

i.e. the normalised eq. (3.23). Noticeably, the power-laws eq. (5.60) are solutions of eq. (5.61). We define $\mu = \zeta_2 - 2/3$ as deviation from the K41 value $\zeta_2 = 2/3$. Note that only for $\mu = 0$ the prefactors $\widetilde{C}_{2,0} = C_{2,0}$ and $\widetilde{C}_{0,2} = C_{0,2}$, i.e. equal the Kolmogorov constant(s) $C_{2,0} = D_{2,0}/(\langle\varepsilon\rangle r)^{2/3}$ and $C_{0,2} = D_{0,2}/(\langle\varepsilon\rangle r)^{2/3}$. For $\mu \neq 0$, the differences are probably small, as μ is small.

Substituting the power-laws eq. (5.60) into eq. (5.58) for the transverse second-order structure function then gives after integration

$$\frac{\widetilde{D}_{1,2}}{\widetilde{r}} = \frac{D_{1,2}}{\langle\varepsilon\rangle r} = -\frac{4}{15} + A_{1,2}Re_\lambda^{-1-3\mu/2}\left(\frac{r}{\eta}\right)^{2/3+\mu} + B_{1,2}Re_\lambda^{-3\mu/2}\left(\frac{r}{\eta}\right)^{\mu-4/3} \tag{5.62}$$

where $Re_\lambda = (15Re_L)^{1/2}$ is the Taylor-scale Reynolds number $Re_\lambda = u\lambda/\nu$ (the prefactor $\sqrt{15}$ is due to the definition $L = U^3/\langle\varepsilon\rangle$). The prefactors $A_{1,2}$ and $B_{1,2}$ are then constants and given by

$$A_{1,2} = \frac{2}{3}\frac{\widetilde{C}_{0,2}}{\mu + 17/3}\left(1 + \frac{2-n}{2n}\left(\mu + \frac{2}{3}\right)\right)\left(\frac{1}{15}\right)^{-3\mu/4-1/2} \tag{5.63}$$

$$B_{1,2} = \frac{2}{\mu + 11/3}\left[\widetilde{C}_{0,2}\left(\mu^2 + \frac{7}{3}\mu - \frac{8}{9}\right) + 2\widetilde{C}_{2,0}\right]\left(\frac{1}{15}\right)^{-3\mu/4} \tag{5.64}$$

Substituting the result for $D_{1,2}$ into eq. (5.57) yields then similarly after integration

$$\frac{\widetilde{D}_{3,0}}{\widetilde{r}} = \frac{D_{3,0}}{\langle\varepsilon\rangle\, r} = -\frac{4}{5} + A_{3,0} Re_\lambda^{-1-3\mu/2}\left(\frac{r}{\eta}\right)^{2/3+\mu} + B_{3,0} Re_\lambda^{-3\mu/2}\left(\frac{r}{\eta}\right)^{\mu-4/3} \tag{5.65}$$

with prefactors

$$A_{3,0} = \frac{2}{3}\frac{1}{\mu + 11/3}\left[1 + \frac{2-n}{2n}\left(\mu + \frac{2}{3}\right)\right]\left(\widetilde{C}_{2,0} + \frac{4\widetilde{C}_{0,2}}{\mu + 17/3}\right) \times \left(\frac{1}{15}\right)^{-3\mu/4-1/2} \tag{5.66}$$

$$B_{3,0} = \frac{2}{\mu + 5/3}\left[\frac{4\widetilde{C}_{0,2}}{\mu + 11/3}\left(\mu^2 + \frac{10}{3}\mu + \frac{25}{9}\right) + \widetilde{C}_{2,0}\left(\mu^2 + \frac{7}{3}\mu - \frac{26}{9} + \frac{8}{\mu + 11/3}\right)\right]\left(\frac{1}{15}\right)^{-3\mu/4} \tag{5.67}$$

The resulting equations (5.62) and (5.65) are very similar to the ones derived by Lindborg (1999). Combining eq. (5.40) and (5.41), one finds

$$\frac{\partial D_{2,0}}{\partial t} \sim \frac{\langle\varepsilon\rangle}{\langle k\rangle}\left(\langle\varepsilon\rangle\, r\right)^{2/3} \sim \frac{D_{2,0}}{\tau}, \tag{5.68}$$

with the integral time $\tau = \langle k\rangle/\langle\varepsilon\rangle$ and where K41 scaling $\zeta_2 = 2/3$ has been assumed in agreement with the ansatz eq. (5.40). A similar equation can be derived under the same assumptions for the transverse structure function $D_{0,2}$. Comparing with the unsteady term of eq. (5.57), it is readily seen that eq. (5.68) leads to the same results eq. (5.62) and (5.65) if $D_{2,0}$ and $D_{0,2}$ follow a power-law and $\mu = 0$.

The numerical values of $\widetilde{C}_{2,0}$, $\widetilde{C}_{0,2}$ and ζ_2 for the data we use here are shown

in table 5.2. Noticeably, there is a small trend for the prefactors to increase with the Reynolds number, although we cannot say whether they would approach a constant for very large Re_λ. As the Kolmogorov constant has been found to vary only slightly (if at all) with increasing Reynolds number, cf. Sreenivasan (1995), this might be due to the fact that $\mu \neq 0$.

Table 5.2: Numerical values of prefactors $\widetilde{C}_{2,0}$ and $\widetilde{C}_{0,2}$ and scaling exponent ζ_2 for datasets D_1 to D_4 of section 2.2.

	D_1	D_2	D_3	D_4
$\widetilde{C}_{2,0}$	1.68	1.72	1.75	1.81
$\widetilde{C}_{0,2}$	2.25	2.31	2.34	2.42
ζ_2	0.67	0.67	0.67	0.67

Eddy viscosity closure

Another approach to close the coupled system is to directly relate the second- and third-order structure functions, for which there are different approaches in the literature. One way to close the equations is to employ an eddy viscosity ansatz (see section 3.4), as e.g. discussed recently by Thiesset et al. (2013). Here, the formula of Oberlack and Peters (1993) is used. They proposed an eddy viscosity closure of the form

$$\widetilde{D}_{3,0} = -\widetilde{\nu}_{t,(3,0)} \frac{\partial \widetilde{D}_{2,0}}{\partial \widetilde{r}}, \quad \widetilde{D}_{1,2} = -\widetilde{\nu}_{t,(1,2)} \frac{\partial \widetilde{D}_{0,2}}{\partial \widetilde{r}} \tag{5.69}$$

with the eddy viscosities

$$\widetilde{\nu}_{t,(3,0)} = \kappa_1 \widetilde{r} \sqrt{\widetilde{D}_{2,0}}, \quad \widetilde{\nu}_{t,(1,2)} = \kappa_2 \widetilde{r} \sqrt{\widetilde{D}_{0,2}}. \tag{5.70}$$

Since both κ_1 and κ_2 as well as $\widetilde{D}_{2,0}$ and $\widetilde{D}_{0,2}$ are positive (and consequently also $\widetilde{\nu}_{t,(3,0)} \geq 0$ and $\widetilde{\nu}_{t,(1,2)} \geq 0$), the closure implies that $(\Delta u_1)^2$ and $(\Delta u_2)^2$ are transported towards smaller r, in agreement with the notion of the energy cascade towards smaller scales.

Together with eq. (5.57) and eq. (5.58) we then have a closed set of equations for $\widetilde{D}_{2,0}$ and $\widetilde{D}_{0,2}$, with the Reynolds number Re_L, the decay exponent n and

the coefficients κ_1 and κ_2 as parameters. The solution of $\widetilde{D}_{3,0}$ and $\widetilde{D}_{1,2}$ is then obtained by inserting the computed $\widetilde{D}_{2,0}$ and $\widetilde{D}_{0,2}$ into eq. (5.69) and eq. (5.70). It is readily checked that this closure gives $\zeta_2 = 2/3$ in the inertial range if the unsteady terms are neglected.

We need boundary conditions for $\widetilde{r} \to 0$ to solve the system of equations at hand. Specifically, four boundary conditions are needed as we have two second-order ODEs. For homogeneous isotropic turbulence, Kolmogorov (1941a) showed that for $\widetilde{r} \to 0$

$$\widetilde{D}_{2,0} = \frac{1}{15} Re_L \widetilde{r}^2, \quad \widetilde{D}_{0,2} = \frac{2}{15} Re_L \widetilde{r}^2, \tag{5.71}$$

see section 3.1.2, eq. (4.86) and the discussion in section 4.4.1 and therefore also

$$\frac{\partial \widetilde{D}_{2,0}}{\partial \widetilde{r}} = \frac{2}{15} Re_L \widetilde{r}, \quad \frac{\partial \widetilde{D}_{0,2}}{\partial \widetilde{r}} = \frac{4}{15} Re_L \widetilde{r} \tag{5.72}$$

for $\widetilde{r} \to 0$, which provides the four required boundary conditions. Consequently, $\widetilde{D}_{3,0} \sim \widetilde{r}^3$, $\widetilde{D}_{1,2} \sim \widetilde{r}^3$ in the viscous range, i.e. the model reproduces the correct $\widetilde{r}$-scaling for $\widetilde{r} \to 0$. Finally, the model parameters κ_1 and κ_2 have to be specified.

The values of κ_1 and κ_2 used here are shown in table 5.3. Noticeably, κ_1 and κ_2 do not vary much with the Reynolds number and no trend is observable, where it needs to be kept in mind that the considered range of Reynolds numbers is not that large. This observation is in line with the original formulation of Oberlack and Peters (1993), who related κ_1 to the Kolmogorov constant $C_{2,0}$. Here, κ_1 and κ_2 are rather directly computed from DNS via eq. (5.69) and eq. (5.70).

Combining both equations, one obtains

$$\frac{\kappa_1}{\kappa_2} = \frac{\widetilde{D}_{3,0}}{\widetilde{D}_{1,2}} \left(\frac{\widetilde{D}_{0,2}}{\widetilde{D}_{2,0}} \right)^{1/2} \frac{\partial \widetilde{D}_{0,2}/\partial \widetilde{r}}{\partial \widetilde{D}_{2,0}/\partial \widetilde{r}}. \tag{5.73}$$

Again assuming power-laws eq. (5.60) in the inertial range and writing $\widetilde{D}_{3,0} = -(4/5)\widetilde{r} + \Delta_{3,0}$ and $\widetilde{D}_{1,2} = -(4/15)\widetilde{r} + \Delta_{1,2}$, where $\Delta_{3,0}$ and $\Delta_{1,2}$ are corrections due to the unsteady and viscous terms, then

$$\frac{\kappa_1}{\kappa_2} = \frac{-(4/5)\widetilde{r} + \Delta_{3,0}}{-(4/15)\widetilde{r} + \Delta_{1,2}} \left(\frac{\widetilde{C}_{0,2}}{\widetilde{C}_{2,0}} \right)^{3/2} \approx 3 \left(\frac{\widetilde{C}_{0,2}}{\widetilde{C}_{2,0}} \right)^{3/2}, \tag{5.74}$$

if the corrections are small. Using the values of table 5.2 with eq. (5.74), one finds that $\kappa_1/\kappa_2 \approx 4.6$, which is close to the value $\kappa_1/\kappa_2 \approx 4.5$ from table 5.3. Consequently, κ_1 and κ_2 (and their ratio) weight the prefactors of the longitudinal and transverse structure functions. Noticeably, the continuity equation eq. (5.61) constrains the ratio $\widetilde{C}_{0,2}/\widetilde{C}_{2,0}$. Then,

$$\widetilde{C}_{0,2} = \widetilde{C}_{2,0}\left(1 + \frac{\zeta_2}{2}\right) \tag{5.75}$$

as function of the exponent ζ_2 only, which is thought to be independent of the Reynolds number (but not necessarily the flow configuration).

Table 5.3: Numerical values of model parameters κ_1 and κ_2 for datasets D_1 to D_4 of section 2.2.

	D_1	D_2	D_3	D_4
κ_1	0.3661	0.3697	0.3853	0.3817
κ_2	0.0784	0.0916	0.0867	0.0847

5.4.3 DNS results

To quantify the influence of the unsteady terms, the balance of eq. (5.57) and eq. (5.58) as evaluated from our DNS for the lowest and largest Reynolds number are shown in figure 5.7a and 5.7b ($Re_\lambda = 121.39$) and figure 5.8a and 5.8b ($Re_\lambda = 254.75$), respectively. The terms of the balances of both second-order structure function equations exhibit qualitatively the same behaviour. The first two terms on the l.h.s. of eq. (5.57) and eq. (5.58) are contributions by the unsteady terms, while the remaining term(s) are transport terms in r-space. On the r.h.s., the first term (the $-4/3$) is the dissipative term, as we normalised the equation by $\langle\varepsilon\rangle$, while the terms in square brackets are viscous terms.

For small $\widetilde{r}$ in the viscous range, the dissipative term is balanced by the viscous terms, while the transport and the unsteady terms are negligible. Solving eq. (5.57) and eq. (5.58) neglecting these terms then leads to eq. (5.71). The viscous terms are negligible for $\widetilde{r}$ outside the viscous range. At intermediate $\widetilde{r}$ in the inertial range, the largest terms are the transport terms, which give the leading-order solutions eq. (3.41) and eq. (3.40) after integration. However, the contribution of the unsteady terms is not negligible, as the transport terms alone

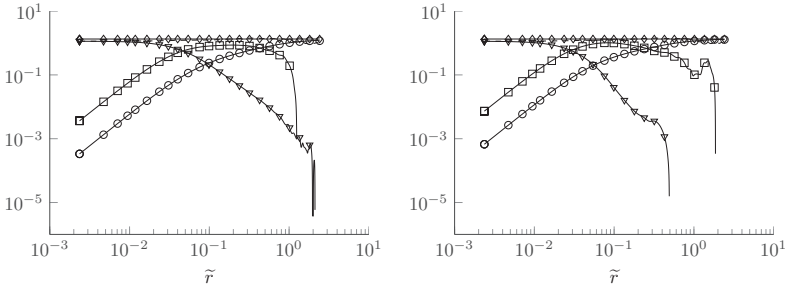

Figure 5.7: Balance of the longitudinal second-order structure function equation (5.57) (a) and of the transverse second-order structure function equation (5.58) (b) for $Re_\lambda = 121.39$. ∘ unsteady term, □ transport term, ◇ dissipation, ▽ viscous term.

are not sufficient to balance the dissipative term (the 4/3). For larger $\widetilde{r}$, the transport terms become smaller and the unsteady terms larger. For very large scales $\widetilde{r} > 1$ the unsteady terms are dominant and balance the dissipation. We also plot the sum of the unsteady, transport and viscous terms as indicated by the dashed black line and find that it balances the 4/3 very well (i.e. the dashed lines nearly coincide with the 4/3). In other words, the assumption that the temporal changes $\partial f/\partial\widetilde{t}$ and $\partial g/\partial\widetilde{t}$ in eq. (5.52) are negligible is well justified.

With increasing Reynolds number, the range of $\widetilde{r}$ for which the transport terms are larger than the viscous and the unsteady terms (i.e. the inertial range) increases (note that because of the normalisation with large scale quantities, the inertial range is shifted to smaller $\widetilde{r}$). Consequently, the scaling range of the transport terms for $Re_\lambda = 254.75$ is larger than at $Re_\lambda = 121.39$, but still very limited. Thus, the unsteady terms may not be neglected, as they contribute significantly at intermediate to large $\widetilde{r}$.

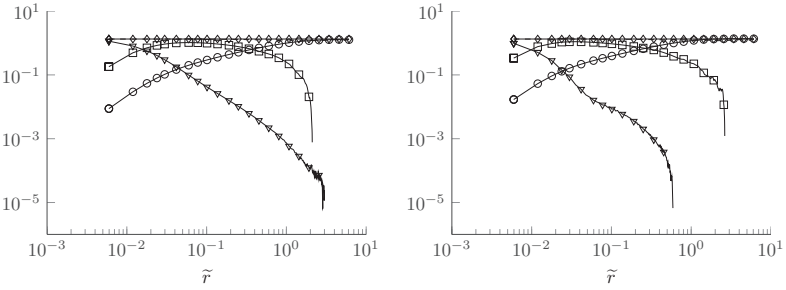

Figure 5.8: Balance of the longitudinal second-order structure function equation (5.57) (a) and of the transverse second-order structure function equation (5.58) (b) for $Re_\lambda = 254.75$. ∘ unsteady term, □ transport term, ◇ dissipation, ▽ viscous term.

5.4.4 Numerical results of the closures

Numerical results of the power-law closure

Let us first look at the power-law closure. The first term on the r.h.s. of eqs. (5.62) and (5.65) corresponds to Kolmogorov's asymptotic results in the inertial range for very large Reynolds numbers, while the second term on the r.h.s. is the contribution due to the unsteady term and the third term on the r.h.s. stems from the viscous terms. Indeed, the unsteady corrections (the second terms on the r.h.s.) become smaller with increasing Reynolds number. However, they increase with increasing r/η. As $A_{3,0}$ and $A_{1,2}$ are positive, $|\widetilde{D}_{3,0}|$ and $|\widetilde{D}_{1,2}|$ then become smaller than 4/5 and 4/15 at a fixed Reynolds number; the deviations are not negligible for r/η larger than a certain threshold and the higher the Reynolds number, the higher the threshold value of r/η. This behaviour is exactly the same as observed from our DNS data, cf. figures 5.7 and 5.8. Noticeably, the influence of μ, i.e. deviations from the K41 value $\zeta_2 = 2/3$ play only a marginal role, as μ is small. As μ is found to be positive (see table 5.2 for our DNS and e.g. Anselmet et al. (1984), Benzi et al. (1995), and Gotoh et al. (2002) in the literature) and small, $0 < \mu \ll 4/3$, the viscous terms decrease much faster with increasing r and are therefore negligible as expected ($r/\eta \gg 1$ in the inertial range). For K41 scaling, $\mu = 0$ and there is no Reynolds number dependence of the viscous terms. Physically, $\mu = 0$ corresponds to the statement

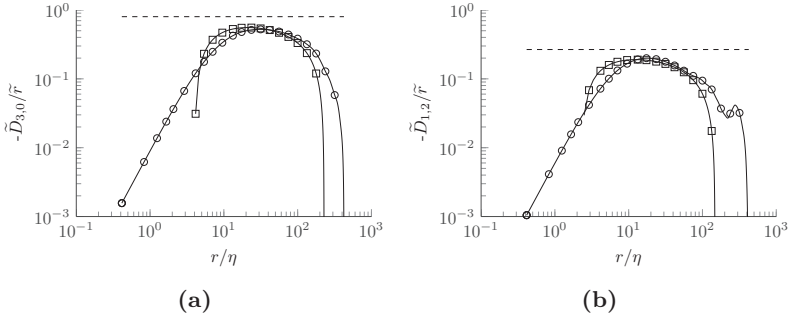

Figure 5.9: Third-order structure functions $\widetilde{D}_{3,0}$ (a) and $\widetilde{D}_{1,2}$ (b) for $Re_\lambda = 121.39$ as evaluated from DNS (○) and compared to the power-law closures eq. (5.65) and (5.62) (□) with parameters from table 5.4.

that the second-order structure functions are determined in the inertial range solely by the scale r (with dimension $[m]$) as well as another quantity with dimensions $[m^2/s^3]$ which is usually taken to equal the mean dissipation $\langle\varepsilon\rangle$, cf. K41 theory. In this spirit, $\mu \neq 0$ implies that there are more (albeit a-priori unknown) quantities which influence the second-order structure functions in the inertial range.

We compare eq. (5.65) and eq. (5.62) to our DNS for $Re_\lambda = 121.39$ (figures 5.9a and 5.9b) and $Re_\lambda = 254.75$ (figures 5.10a and 5.10b) as shown in figure 5.9 and figure 5.10. The values of the coefficients $A_{3,0}$, $A_{1,2}$, $B_{3,0}$ and $B_{1,2}$ as well as μ and n determined from the DNS are given in table 5.4. Because $\widetilde{C}_{2,0}$ and $\widetilde{C}_{0,2}$ vary with the Reynolds number, the coefficients A and B do so as well. The closure agrees better with the transverse $\widetilde{D}_{1,2}$ than the longitudinal $\widetilde{D}_{3,0}$. This is probably due to the fact that $\widetilde{D}_{1,2}$ feeds into $\widetilde{D}_{3,0}$, so that any errors of eq. (5.62) are carried over to eq. (5.65). Nevertheless, we find good qualitative agreement, also for the lower Reynolds number. As expected, the closure improves with increasing Reynolds number, because the scaling range of the second-order structure functions increases. However, the deviations from Kolmogorov's results eq. (3.40) and eq. (3.41) (the dashed black lines) are significant. At $Re_\lambda = 254.75$, the difference of $-\widetilde{D}_{3,0}$ and $-\widetilde{D}_{1,2}$ to 4/5 and 4/15 has only slightly decreased compared with $Re_\lambda = 121.39$. Also, the range for which $\widetilde{D}_{3,0}/\widetilde{r} \approx const.$ and

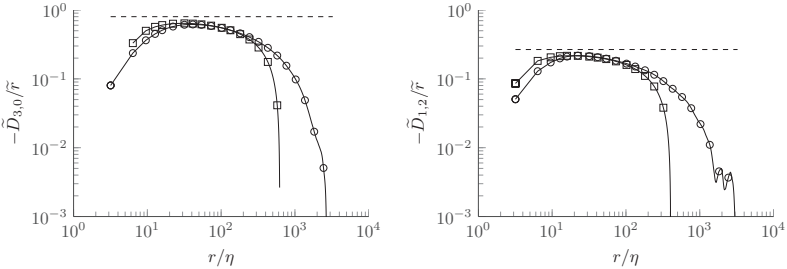

Figure 5.10: Third-order structure functions $\widetilde{D}_{3,0}$ (a) and $\widetilde{D}_{1,2}$ (b) for $Re_\lambda = 254.75$ as evaluated from DNS (○) and compared to the power-law closures eq. (5.65) and (5.62) (□) with parameters from table 5.4.

$\widetilde{D}_{1,2}/\widetilde{r} \approx const.$ is quite small.

Table 5.4: Numerical values of the power-law closure parameters for datasets D_1 to D_4 of section 2.2.

	D_1	D_2	D_3	D_4
$A_{3,0}$	2.61	2.67	2.71	2.81
$B_{3,0}$	4.84	4.98	5.04	5.21
$A_{1,2}$	1.16	1.19	1.21	1.25
$B_{1,2}$	0.76	0.77	0.79	0.82
n	1.45	1.45	1.45	1.45
μ	$3.34 \cdot 10^{-3}$	$3.34 \cdot 10^{-3}$	$3.34 \cdot 10^{-3}$	$3.34 \cdot 10^{-3}$

Numerical results of the eddy viscosity closure

The results of the eddy viscosity closure are shown in figures 5.11 and 5.12, where we compare the numerical solutions of $\widetilde{D}_{3,0}$ and $\widetilde{D}_{1,2}$ for the system of equations both with and without the unsteady terms to the DNS data. The model solution has been computed using an explicit Runge-Kutta solver. We use constant values of κ_1 and κ_2 throughout the numerical integration, which have been determined from DNS in the (presumed) inertial range. As the

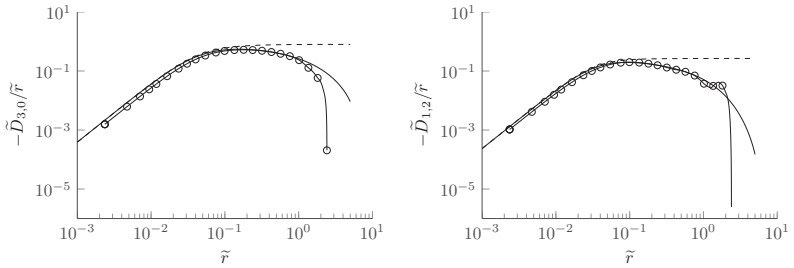

Figure 5.11: Third-order structure functions $\widetilde{D}_{3,0}$ (a) and $\widetilde{D}_{1,2}$ (b) for $Re_\lambda = 121.39$ as evaluated from DNS (∘) and compared to the eddy viscosity closure (solid line) with parameters from table 5.3. Dashed lines correspond to model solutions without the unsteady terms.

transport terms are small in the viscous range, the deviations of the constants κ_1 and κ_2 from their true viscous range values do not play a crucial role for the model performance, although they lead to small deviations in the viscous range. The model parameters used here are listed in table 5.3 where for our DNS the decay exponent $n = 1.45$. We observe striking agreement of the model with the DNS data when the unsteady terms are included for both $Re_\lambda = 121.39$ and $Re_\lambda = 254.75$. Without the unsteady terms, the difference between DNS and model increases with $\widetilde{r}$. This is not that surprising, because the contributions of the unsteady terms to the balances as seen by figure 5.7 and 5.8 increase with increasing $\widetilde{r}$. As discussed above, the model gives $\zeta_2 = 2/3$ and $\zeta_3 = 1$ (i.e. eq. (3.40) and eq. (3.41)) if the unsteady terms are neglected. Consequently, their absence at the intermediate and large scales then results in an infinitely long inertial range for the model, even at finite Reynolds numbers. This is in agreement with the observation that the unsteady term is the only term in the eqs. (5.57) and (5.58) which explicitly contains the large scales.

After having established that the eddy viscosity closure agrees very well with the DNS data when the unsteady corrections are included, we proceed to extrapolate towards higher Reynolds numbers. As κ_1 and κ_2 evaluated from our DNS (cf. table 5.3) do not show a clear Reynolds number dependence, we keep the values of κ_1 and κ_2 evaluated at $Re_\lambda = 254.75$ and increase the

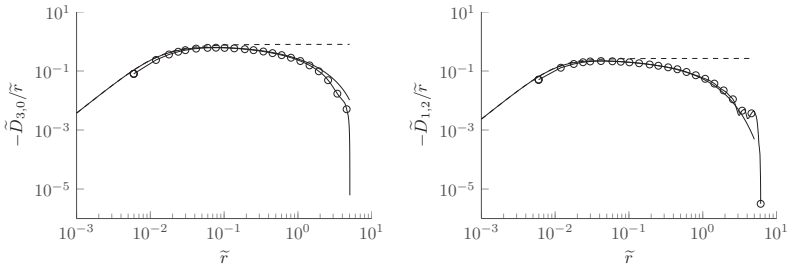

(a) **(b)**

Figure 5.12: Third-order structure functions $\widetilde{D}_{3,0}$ (a) and $\widetilde{D}_{1,2}$ (b) for $Re_\lambda = 254.75$ as evaluated from DNS (∘) and compared to the eddy viscosity closure (solid line) with parameters from table 5.3. Dashed lines correspond to model solutions without the unsteady terms.

Reynolds number. We have then computed the solution of the model for $Re_\lambda = 625, 1250, 2500, 5000, 10000$. The resulting $\widetilde{D}_{3,0}$ and $\widetilde{D}_{1,2}$ are shown in figure 5.13 and agree with the characteristics observed from DNS as described in section 5.4.2. As expected, the range for which $-\widetilde{D}_{3,0}$ and $-\widetilde{D}_{1,2}$ are approximately equal to 4/5 and 4/15 increases with increasing Reynolds number. However, the range one might call inertial range based on fig. 5.13 is quite small even at $Re_\lambda = 10000$. We show the unsteady and viscous terms of eq. (5.57) and eq. (5.58) computed using the modeled $\widetilde{D}_{2,0}$, $\widetilde{D}_{0,2}$, $\widetilde{D}_{3,0}$ and $\widetilde{D}_{1,2}$ in figure 5.14. We find that the range for which the transport terms dominate increases with increasing Reynolds number, in agreement with Kolmogorov's classical notion of the inertial range and fig. 5.13. The transport terms peak close to the intersection of the unsteady and viscous terms, which we briefly discuss in the following. We find that the intersection point $(\widetilde{r}_C, \widetilde{y}_C)$, i.e. the crossover after which the unsteady terms are larger than the viscous terms, scales with the Reynolds number as indicated with the dashed black line in figure 5.14a and figure 5.14b. We may thus write

$$\widetilde{r}_{C,\parallel} = A_{r,\parallel} Re_\lambda^{B_{r,\parallel}}, \quad \widetilde{y}_{C,\parallel} = A_{y,\parallel} Re_\lambda^{B_{y,\parallel}} \tag{5.76}$$

and

$$\widetilde{r}_{C,\perp} = A_{r,\perp} Re_\lambda^{B_{r,\perp}}, \quad \widetilde{y}_{C,\perp} = A_{y,\perp} Re_\lambda^{B_{y,\perp}}, \tag{5.77}$$

where $\parallel$ indicates the cross-over of the terms of eq. (5.57) and $\perp$ the cross-over of the terms of eq. (5.58). Using a least square fit, the model then gives the

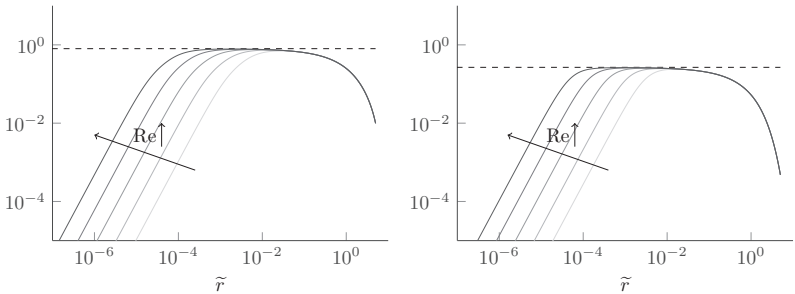

Figure 5.13: Normalised third-order structure functions $\widetilde{D}_{3,0}$ (a) and $\widetilde{D}_{1,2}$ (b) extrapolated towards higher Reynolds numbers $Re_\lambda = 625, 1250, 2500, 5000, 10000$ (lighter to darker colour) using the eddy viscosity closure.

parameters shown in table 5.5 and the longitudinal and transverse exponents are found to be approximately equal for both $\widetilde{r}_C$ and $\widetilde{y}_C$. Noticeably, only the prefactors of the cross-over length but not the corresponding values of the ordinate differ. That is, the inertial range of the longitudinal and transverse structure function is approached equally fast, but its location in $\widetilde{r}$ differs. Particularly, the inertial range of the transverse structure function $\widetilde{D}_{1,2}$ is shifted towards smaller $\widetilde{r}$ than the corresponding inertial range of $\widetilde{D}_{3,0}$ and we have $\widetilde{r}_{C,\parallel}/\widetilde{r}_{C,\perp} \approx 1.55$ and $\widetilde{y}_{C,\parallel}/\widetilde{y}_{C,\perp} \approx 1.15$ independent of the Reynolds number. We also find good agreement of the scaling as given by table 5.5 with the lower Reynolds numbers of our DNS.

As $\widetilde{r} = r/L$, for both the longitudinal and transverse non-normalised cross-over length

$$r_C \sim \lambda, \tag{5.78}$$

where the prefactor is $\mathcal{O}(1)$. In other words, the transport terms of eq. (5.57) and eq. (5.58) peak at the Taylor scale λ. That is, Kolmogorov's inertial range assumption that both the viscous and unsteady terms are small is best fulfilled at r on the order of the Taylor scale λ. This result is in agreement with the observation that λ is an intermediate length scale, smaller than the integral length L and larger than the dissipative scale η.

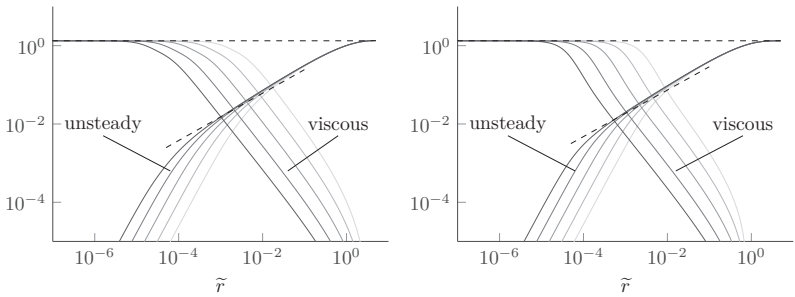

Figure 5.14: Unsteady and viscous terms of eq. (5.57) and eq. (5.58) as evaluated for the extrapolated Reynolds numbers $Re_\lambda = 625, 1250, 2500, 5000, 10000$ using the eddy viscosity closure. Reynolds numbers are indicated by the same colouring as in figure 5.13.

Table 5.5: Numerical values of the scaling of eq. (5.76) and eq. (5.77).

	A_r	B_r	A_y	B_y
$\parallel$	12.99	-1.02	4.63	-0.62
$\perp$	8.37	-1.05	4.04	-0.63

6 Streamline segment analysis

In this chapter, we will briefly look at the statistics of the velocity difference $\Delta u = u_{(2)} - u_{(1)}$ for streamline segments, where the subscripts indicate the segment endpoints and $u = \sqrt{u_i^2}$. In section 6.1, general properties of streamlines are presented. A brief overview of results found in the literature is given in section 6.1.2, where also the analogon to the structure function transport equations is derived. Since streamlines are tangent to the velocity field, they may not be Galilean invariant. This is briefly discussed in section 6.1.3.

Streamline segments were introduced by Wang (2010) and are described in more detail below. Different to longitudinal structure functions, where the velocity differences $\Delta u_1 = u_1 - u_1'$ and $\Delta u_2 = u_2 - u_2'$ are along fixed lines (r_i is aligned with x_1), the orientation of Δu depends on the local flow geometry. For that reason, the higher moments of Δu are of interest.

In a first step, we compare the segment statistics of the forced and the decaying isotropic datasets D1, D3, R5 and R6, i.e. two different Reynolds numbers for both flows types in section 6.2. Subsequently, streamline segments for anisotropic data are examined in section 6.3, based on Boschung et al. (2016b).

6.1 Properties of Streamlines

First, we briefly introduce the streamline coordinate system in section 6.1.1. We proceed to review known results found in the literature in section 6.1.2. Streamlines may not be Galilean invariant, the implications of which we discuss in section 6.1.3.

6.1.1 Streamline coordinate system

It is useful to describe curves with their intrinsic curvilinear coordinate system, as introduced below. For more details, see e.g. Kreyszig (1963) or Aris (1962).

In cartesian coordinates, a point can be uniquely identified by its position,

$$\boldsymbol{x} = (x_1, x_2, x_3). \tag{6.1}$$

The vector function

$$\boldsymbol{x} = \boldsymbol{x}(s) \tag{6.2}$$

can be thought of as the set of points which, if ordered by increasing s, forms a curve with $\boldsymbol{x}(s)$ being its parametric representation; s denotes the arc length of said curve. Then the tangent vector at any point of the curve is

$$t_i = \frac{\partial x_i}{\partial s} \tag{6.3}$$

and is a unit vector. Field lines (e.g. streamlines) of a vector field v_i are tangent to the unit vector $t_i = v_i/v$, where $v = \sqrt{v_i^2}$. For streamlines, v_i represents the components of the velocity field (i.e. $v_i = u_i$).

By the rules of partial differentiation, the derivative in direction of the arc length s is

$$\frac{\partial}{\partial s} = \frac{\partial x_i}{\partial s}\frac{\partial}{\partial x_i} = t_i \frac{\partial}{\partial x_i}, \tag{6.4}$$

i.e. the projection of the gradient onto the curve. Now, a new coordinate system may be found by choosing t_i as its first axis. As $t_i t_i = 1$,

$$t_i \frac{\partial t_i}{\partial s} = 0, \tag{6.5}$$

i.e. the vectors t_i and $\partial t_i/\partial s$ are orthogonal. Thus, the unit vector p_i can be defined as

$$p_i = \frac{\partial t_i/\partial s}{|\partial t_i/\partial s|} = \frac{\kappa_i}{\kappa}, \tag{6.6}$$

where $\kappa = \sqrt{{\kappa_i}^2} = \sqrt{(\partial t_i/\partial s)^2}$ denotes the curvature of the curve and its reciprocal $R = 1/\kappa$ is the local radius of the line. p_i is called the unit principal normal vector and, being perpendicular to t_i, may be chosen as the second unit vector of the curvilinear coordinate system. The curvature κ is a measure for the change of the unit vector t_i along the curve and can be interpreted as the deviation of the curve from its tangent vector.

A third unit vector which is orthogonal to t_i and p_i can be found from the vector product $b_i = \epsilon_{ijk} t_k p_j$ and is called the unit binormal vector. Both p_i and b_i lie in the plane normal to t_i (the so-called normal plane). From $b_i b_i = 1$, $b_i t_i = 0$ and the definition of p_i, it may be concluded that $-\partial b_i/\partial s \sim p_i$ and thus $\partial b_i/\partial s = -\tau p_i$, where τ is called the torsion of the curve. Figure 6.1 shows

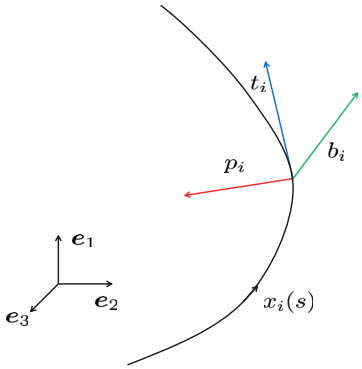

Figure 6.1: The curvilinear coordinate system, where $\boldsymbol{e}_1$, $\boldsymbol{e}_2$ and $\boldsymbol{e}_3$ are the Cartesian coordinate system unit vectors.

the curvilinear coordinate system with unit vectors t_i, p_i and b_i.

As κ relates p_i and $\partial t_i/\partial s$ and τ relates $\partial b_i/\partial s$ and p_i, the derivatives of t_i, p_i and b_i along the curve can be expressed as functions of t_i, p_i, b_i, κ and τ; these relations are known as the formulae of Frenet,

$$\frac{\partial t_i}{\partial s} = \kappa p_i, \quad \frac{\partial p_i}{\partial s} = -\kappa t_i + \tau b_i, \quad \frac{\partial b_i}{\partial s} = -\tau p_i. \tag{6.7}$$

6.1.2 Streamline segments

Definition and known results

Streamlines are in principle infinitely long, unless they hit a stagnation point where all three velocity components vanish. This is why Wang (2010) proposed to split streamlines into streamline segments which extend between local extreme points of u along the streamline. Streamline segments are bound by two extrema, i.e. points where the velocity derivative with respect to the arc length s vanishes. Wang further characterized streamline segments as positive or negative, depending on the sign of the gradient: within positive segments $\partial u/\partial s > 0$; within negative segments $\partial u/\partial s < 0$. Thus the flow along positive segments is accelerated, while it is decelerated along negative segments. Streamline segments are therefore characterised by the velocity difference Δu between two

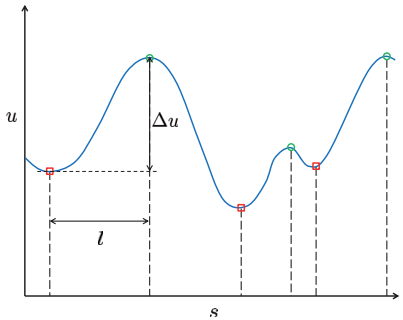

Figure 6.2: Projection of the velocity field u_i onto a streamline. Streamline segments are defined by the local minima □ and maxima ○ of the projected velocity $u = t_i u_i$ and characterised by their curvilinear length l along the streamline coordinate s and velocity difference Δu.

local extrema and the arc distance l between them, see figure 6.2, where $\Delta u > 0$ for positive segments and $\Delta u < 0$ for negative segments. Positive segments are stretched (on average) due to the positive velocity difference at their endpoints along the local streamline direction while negative segments are contracted. As a result stemming from this kinematic mechanism, positive segments are found to be longer than negative ones in agreement with the negative skewness of the longitudinal velocity derivative, cf. the discussion in Wang (2010). Because there are no segments with $\Delta u = 0$, the joint pdf $P(\Delta u, l)$ is wing-shaped, see section 6.2.1 below, where the jpdf for the datasets D1, D3, R5 and R6 are shown.

Wang (2012) then applied this method to vortex lines and vortex tubes, analogous to the streamline segmentation (i.e. choosing the extrema of the vorticity projected onto the vortex line for the segmentation). However, an inherent kinematic mechanism of stretching positive and compressing negative segments is missing and therefore both positive and negative segments are found to have the same mean length.

Schaefer et al. (2012a) pursued the ideas of Wang and adapted the stochastic model of Wang and Peters (2006, 2008) to model the length distribution of streamline segments, based on slow changes by diffusional and convective drift

in phase space as well as fast changes by cutting and reconnection of segments. The underlying physical process is that very small elements are determined by diffusion, medium-length segments are stretched by strain and large segments are cut. That is, the segment length can change due to slow processes (by diffusion) or very fast processes when a segment is either cut or reconnects with another segment. The model agrees well with results from direct numerical simulations (DNS). Based on dimensional grounds, Schaefer et al. (2012b) proposed that the mean segment length scales with the geometrical mean of the Taylor scale λ and the Kolmogorov scale η, i.e. $l_m \sim \sqrt{\lambda\eta}$.

Statistics of dissipation and vorticity conditioned on the curvature and torsion of streamlines have been reported by Braun et al. (2006). However, only a weak correlation between dissipation and curvature has been found. Schaefer (2012) examined the probability density function (pdf) of the curvature of streamlines and the mean curvature and derived a power-law scaling for the tails of both distributions.

Streamlines, transporting mass, belong to a larger family of field lines based on transport fields. Meyers and Meneveau (2013) proposed the use of momentum lines (tangent to the total flux of momentum in an arbitrary but fixed direction) and energy lines (tangent to the total flux of the kinetic energy) to visualize the momentum and energy flux in various flows, such as wind farms.

Boschung et al. (2014) introduced a general classification scheme for the local behaviour of field lines based on the first and second invariant

$$H = -\frac{\partial t_i}{\partial x_i}, \quad K = \frac{1}{2}\left(\frac{\partial t_i}{\partial x_i}\frac{\partial t_j}{\partial x_j} - \frac{\partial t_i}{\partial x_j}\frac{\partial t_j}{\partial x_i}\right) \tag{6.8}$$

of the tensor $\partial t_i/\partial x_j$. Noticeably, the third invariant $I = -\det|\partial t_i/\partial x_j| = 0$ for all vector fields v_i, because $t_i(\partial t_i/\partial s) = 0$.

This H-K-classification is somewhat similar to the P-Q-R flow topology classification scheme of Chong et al. (1990) based on the velocity gradient tensor $\partial u_i/\partial x_j$. While the latter describes the local topology of the flow around a point in space moving with its local velocity (and is therefore Galilean invariant), the former characterises the local behaviour of field lines based on the underlying vector field v_i and is therefore only Galilean invariant if v_i is.

Navier-Stokes equation projected onto streamlines

Following Wang (2010), one can derive an equation for the magnitude of the velocity u along streamlines by multiplying the Navier-Stokes equation eq. (1.5)

with the unit vector $t_i = u_i/u$. This results in

$$\frac{\partial u}{\partial t} + u\frac{\partial u}{\partial s} = -\frac{\partial p}{\partial s} + \nu\frac{\partial^2 u}{\partial x_j^2} - u\nu\frac{\partial t_i}{\partial x_j}\frac{\partial t_i}{\partial x_j}, \tag{6.9}$$

where the projection of the viscous term on the r.h.s. of the Navier-Stokes equations leads to the two terms $\nu(\partial^2 u/\partial x_j^2)$ and $u\nu(\partial t_i/\partial x_j)(\partial t_i/\partial x_j)$, where the latter term is always positive and can be interpreted as a dissipative quantity. Noticeably, eq. (6.9) does not depend on the arc length s only, due to the viscous term: Since the Laplace operator $\boldsymbol{\nabla}^2 = \partial^2/\partial x_i^2$ can be interpreted as a local averaging operator, it includes information in all directions and not only along t_i, but also in p_i- and b_i-direction. For stationary, inviscid flows, eq. (6.9) reduces after integration from $s_{(1)}$ to $s_{(2)}$ to Bernoulli's equation

$$\frac{1}{2}\Delta\left(u^2\right) + \Delta p = 0, \tag{6.10}$$

where Δ is the difference between two points $s_{(2)}$ and $s_{(1)}$ along the streamline*. One can also project the Navier-Stokes equation in the other two principal directions by multiplying with the unit vectors p_i and b_i, respectively†. However, the resulting equations are not examined here.

It is possible to derive an equation for Δu along s from eq. (6.9) in the spirit of section 3.1. Consider two points (2) and (1) with coordinates $s_{(2)}$ and $s_{(1)}$ along the line and define

$$S = \frac{1}{2}\left(s_{(2)} + s_{(1)}\right) \tag{6.11}$$

as middle position and

$$\Delta s = \left(s_{(2)} - s_{(1)}\right) \tag{6.12}$$

*Since body forces such as $g_i = ge_i$ where g is the gravitational acceleration and $e_i = (0, 0, 1)$, say, were neglected in the Navier-Stokes equation (1.5), the term $g\Delta x_3$ does not appear in eq. (6.10).

†For instance, multiplying the Navier-Stokes equations with the normal vector p_i gives

$$p_i\frac{\partial u_i}{\partial t} + u\kappa = -\frac{\partial p}{\partial n} + \nu p_i\frac{\partial^2 u_i}{\partial x_j^2},$$

where $\partial/\partial n$ is the derivative in p_i-direction. For stationary, inviscid flows this reduces to the well-known relation

$$u\kappa = -\frac{\partial p}{\partial n},$$

which relates the curvature κ of a streamline to the pressure gradient normal to it.

as arc length distance between the two points. This results in a coordinate transform equivalent to eq. (3.5),

$$\frac{\partial}{\partial s_1} = \frac{1}{2}\frac{\partial}{\partial S} - \frac{\partial}{\partial \Delta s}, \quad \frac{\partial}{\partial s_2} = \frac{1}{2}\frac{\partial}{\partial S} + \frac{\partial}{\partial \Delta s}. \tag{6.13}$$

Writing the projected Navier-Stokes equations (6.9) at $s_{(2)}$ and $s_{(1)}$ gives

$$\begin{aligned} \frac{\partial u_{(2)}}{\partial t} + u_{(2)}\frac{\partial u_{(2)}}{\partial s_{(2)}} &= -\frac{\partial p_{(2)}}{\partial s_{(2)}} + \nu D_{(2)} \\ \frac{\partial u_{(1)}}{\partial t} + u_{(1)}\frac{\partial u_{(1)}}{\partial s_{(1)}} &= -\frac{\partial p_{(1)}}{\partial s_{(1)}} + \nu D_{(1)} \end{aligned} \tag{6.14}$$

where the viscous term νD is defined as

$$\nu D = \nu t_i \frac{\partial^2 u_i}{\partial x_j^2}. \tag{6.15}$$

Introducing $\Delta u = u_{(2)} - u_{(1)}$, $\Delta p = p_{(2)} - p_{(1)}$, $\Delta D = D_{(2)} - D_{(1)}$ and noting that the derivative of quantities at $s_{(2)}$ with respect to $s_{(1)}$ vanish and vice versa then yields after subtracting both equations and using the coordinate transform

$$\frac{\partial \Delta u}{\partial t} + \Delta u \frac{\partial \Delta u}{\partial \Delta s} + U_S \frac{\partial \Delta u}{\partial S} = -\frac{\partial \Delta p}{\partial S} + \nu \Delta D, \tag{6.16}$$

where $U_S = (u_{(2)} + u_{(1)})/2$ has been used. Therefore, eq. (6.16) may be considered as analogon to eq. (3.10) for the velocity difference along streamlines. One would therefore hope that one could multiply eq. (6.16) by some power of $(\Delta u)^{N-1}$, average and then integrate in Δs to determine $\left\langle (\Delta u)^{N+1} \right\rangle$. However, eq. (6.16) is *not* suitable to examine streamline segments, because by definition $\partial u / \partial s = 0$ at the two segment endpoints. Consequently, the transport term(s) in eq. (6.14) vanish, if both equations are evaluated at the segment endpoints; one is left with an equation where Δu is only contained in the unsteady and viscous term, both of which cannot be integrated in Δs analytically.

6.1.3 Galilean invariance?

It is well known that the Navier-Stokes equations are Galilean-invariant, i.e. do not change under a continuous movement of the coordinate system. Also, all quantities derived from velocity gradients, such as the dissipation or the vorticity,

are Galilean-invariant as well. However, streamlines based on the instantaneous velocity field are clearly not. For instance, adding a very large uniform velocity in x_1-direction, say, leads to the streamlines being aligned with the x_1-axis, since the streamline unit vector approaches $t_i \to (1, 0, 0)$. If one is interested in analysing Galilean-invariant quantities such as the dissipation, streamlines based on the instantaneous velocity field seem not suited. However, one can choose the *fluctuating* velocity field, since adding a constant velocity changes only the mean velocity field; the fluctuating velocity field can be considered Galilean-invariant. In case of isotropic turbulence, the mean velocity vanishes by definition, i.e. there is no difference between the instantaneous and the fluctuating velocity*. This is not the case for other flows such as the fractal grid data used below. For that reason, we have subtracted the mean flow for the analysis in section 6.3. It should be mentioned that Hennig et al. (2016) compared streamline segment statistics based on the instantaneous velocity field for isotropic turbulence and a wavy channel flow and found very good agreement for the length and velocity difference pdfs after normalising with the mean segment length l_m and the standard deviation σ of the velocity difference Δu, although the non-normalised pdfs differed significantly. These findings are remarkable because the streamlines are orientated mostly in downstream direction in case of the wavy wall flow, i.e. have a preferred orientation while those for the isotropic turbulence do not. The reason might be that effects introduced by the curvature of the streamlines are not significant after normalisation for these specific cases; indeed, the mean segment length for the isotropic flow was found to be much shorter than for the wavy wall.

Finally, it should be mentioned that there are fields which are always Galilean-invariant, such as the vorticity field $\omega_i = \epsilon_{ijk}\partial u_k/\partial x_j$ or all other vector quantities based solely on velocity gradients. For that reason, examining statistics of vorticity segments (defined similarly to streamline segments, cf. section 6.1.2) seems very interesting. Vortex segments have been studied by Wang (2012) and Boschung et al. (2014). Further analysis is not carried out here, but remains for future studies.

*Adding a constant velocity would then lead to a non-zero mean velocity and would break the isotropy of the instantaneous velocity field, while the fluctuating velocity field would remain isotropic.

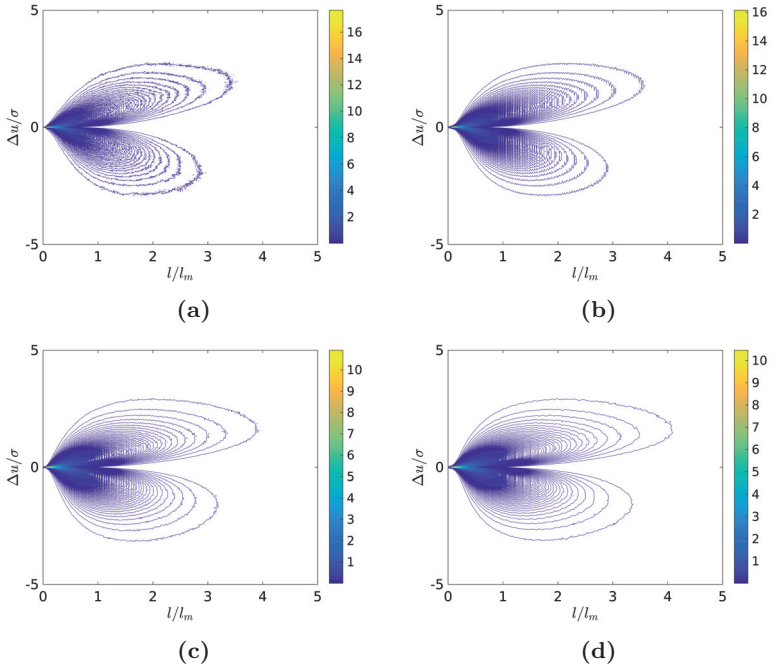

Figure 6.3: Normalised joint pdfs $P(\Delta u/\sigma, l/l_m)$. (a) decaying turbulence dataset D1, (b) decaying turbulence dataset D3, (c) forced turbulence dataset R5, (d) forced turbulence dataset R6.

6.2 Segment statistics for isotropic flows

6.2.1 Probability density functions

Joint pdfs

The normalised joint pdfs $P(\Delta u/\sigma, l/l_m)$ are shown in figure 6.3 for the isotropic datasets D1, D3, R5 and R6, where $\sigma = \sqrt{\langle(\Delta u - \langle\Delta u\rangle)^2\rangle}$ is the standard deviation of the velocity difference Δu of the segment endpoints and l_m is the mean segment length and are found to be in good agreement with the results of Wang (2010). For all four datasets, we find the same shape with two distinct

wings, since $\Delta u \neq 0$ by definition. Noticeably, positive segments with $\Delta u > 0$ are longer on average than negative segments $\Delta u < 0$. The notion is that positive segments are stretched because $\Delta u > 0$ while negative segments are compressed, $\Delta u < 0$. This is in agreement with the negative skewness of the velocity derivative as discussed by Wang (2010). Because positive and negative segments alternate along a streamline, this implies that $|\Delta u|$ is larger on average for negative segments compared to positive segments due to continuity (i.e. $\langle u \rangle = const.$ in isotropic turbulence).

As $|\Delta u| > 0$, both wings of the jpdf should be separated. This is not the case for the jpdfs in figure 6.3 due to finite binning. A model for the jpdf has been given by Schaefer et al. (2013a), which shows good qualitative agreement with data from DNS.

On first sight, the conditional means $\langle (\Delta u)^N | l \rangle$ appear to be similar to the longitudinal structure functions $D_{N,0} = \langle (\Delta u_1)^N | r \rangle$. However, they differ for several reasons:

1. Because $\langle (\Delta u)^N | l \rangle$ is computed along streamlines, the separation l which equals the arc length of the segment is not aligned with a fixed axis such as $r_i = (r, 0, 0)$ and differs in orientation for every segment, although it might be argued that there is also no preferred direction when averaging over multiple streamlines.

2. As a corollary to 1., the arc length l differs from the shortest distance in space between the two streamline endpoints. One could easily imagine a very curved segment with large l but short distance between its endpoints. On the other hand, the separation vector r_i is the shortest distance between the two points $\boldsymbol{x}$ and $\boldsymbol{x}'$ used to compute the structure functions $D_{N,0}$.

3. Streamlines may locally converge or diverge, so that not every part of the volume is equally weighted when averaging even when the streamlines are started at equidistant points. This is different to the structure functions which uniformly sample the volume.

4. Probably most important, streamline segments introduce an intrinsic local length scale l. In case of structure functions, on the other hand, the separation distance is not a random variable but can be rather thought of as a parameter. It might be argued that streamline segments are thus better suited to reflect the local flow structure. Moreover because of the segmentation, it follows that $|\Delta u| > 0$ always, while the difference $u_1 - u_1'$ can vanish.

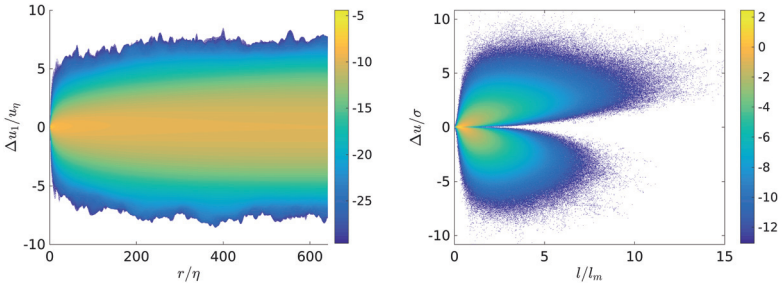

Figure 6.4: Joint pdfs $\log(P(\Delta u_1/u_\eta, r/\eta))$ (a) and $\log(P(\Delta u/\sigma, l/l_m))$ (b) for dataset R4.

These differences are best highlighted by comparing the jpdf $P(\Delta u_1/u_\eta, r/\eta)$ and the jpdf $P(\Delta u/\sigma, r/l_m)$, cf. figure 6.4 for dataset R4 where $P(\Delta u_1, r)$ has been normalised with u_η and η. While l can be thought of as a stochastic variable, $P(r) = const.$, i.e. every r is equally sampled by definition*, $P(\Delta u_1, r) = P(r)P(\Delta u_1|r) \sim P(\Delta u_1|r)$. Moreover, the maximal segment length l is bounded by intrinsic physical processes such as the cutting of large segments while the maximal separation distance r is determined by the experimental apparatus of the measurement in question. This is clearly seen in figure 6.4b, where there are hardly any segments with $l/l_m \geq 4$ while r is evenly distributed. Furthermore, there is no separation into two distinct regions for $\Delta u_1 > 0$ and $\Delta u_1 < 0$. Also note that because of the asymmetry of the jpdf $P(\Delta u, l)$, the conditional mean $\langle \Delta u|l \rangle$ does not vanish, different to the first-order structure function $D_{1,0} = \langle u_1 - u_1' \rangle$, which vanishes due to homogeneity. However, this does not imply that $P(\Delta u_1, r)$ is symmetric although one might think so at first glance, since odd-order structure functions do not vanish in general.

We look at $\langle (\Delta u)^N|l \rangle$ in more detail in section 6.2.2 and section 6.3.3.

*That is, $P(r) = 1/(r_{\max} - r_{\min})$ where $r_{\min}$ and $r_{\max}$ are the shortest and longest separation distance evaluated. For the DNS used here, $r_{\min} = 0$ and $r_{\max} = \pi$ as the periodic box has an edge length of 2π.

Marginal pdfs

Next, the normalised marginal pdfs $P(l/l_m)$ and $P(\Delta u/\sigma)$ are compared, again for the datasets D1, D3, R5 and R6. In figure 6.5a and figure 6.5b, $P(l/l_m)$ is shown, where D1 corresponds to the blue, D3 to the red, R5 to the black and R6 to the green lines, respectively. Here, the statistics were computed with all segments, i.e. positive and negative segments were not distinguished when calculating the pdfs.

For $l/l_m \to 0$, $P(l/l_m)$ increases linearly due to the viscous drift of small segments (cf. Schaefer et al. (2012a) and Schaefer et al. (2013b)) while for large l/l_m, the pdfs have an exponential tail characteristic for a random cutting process modeled by a poisson-distribution (see e.g. Wang and Peters (2006, 2008)).

Normalising the pdfs with the mean length l_m leads to collapsing cores of the pdfs, while the tails are longer the higher the Reynolds number. That is, the length distribution of small segments up to $l/l_m \sim 4$ seems to be independent of the Reynolds number and the flow type (here forced isotropic and decaying isotropic turbulence), while the large segments differ. This observation is in agreement with the notion of local isotropy, namely that the small scales should be universal, while large scales are determined by boundary conditions such as the flow geometry.

Similarly, $P(\Delta u/\sigma)$ is shown in figure 6.5c and figure 6.5d, where the same colouring for the different datasets is used. Again, the normalised pdfs collapse for small $\Delta u/\sigma$ and differ for $|\Delta u|/\sigma \gtrsim 4$. As larger $|\Delta u|$ are correlated with longer segments, cf. the jpdfs above, this is again consonant with local isotropy.

Note that the non-collapsing tails of the pdfs imply that also the jpdfs do not perfectly collapse when normalised with l_m and σ^*.

6.2.2 Scaling of $\left\langle (\Delta u)^N | l \right\rangle$

First conditional moment $\langle \Delta u | l \rangle$

As discussed above, $\langle \Delta u | l \rangle \neq 0$, different to the first-order longitudinal structure function. For that reason, we examine the first conditional moment here. $\langle \Delta u | l \rangle$ is shown in figure 6.6 for the datasets D1 (blue), D3 (red), R5 (black) and R6 (green). Again we do not discriminate between positive and negative segments.

*However, the statistics of positive and negative segments might collapse when normalised with their individual mean length l_m and standard deviation σ, i.e. when analysing the statistics of positive and negative segments separately (Lipo Wang, private communication).

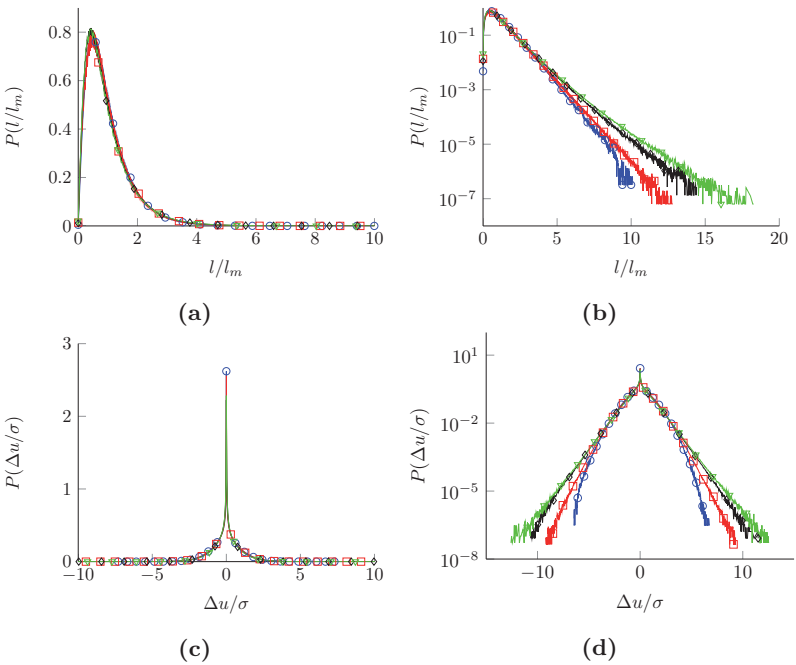

Figure 6.5: Normalised pdfs $P(l/l_m)$ (a) and (b) and $P(\Delta u/\sigma)$ (c) and (d) for datasets D1 (○), D3 (□), R5 (◇) and R6 (▽).

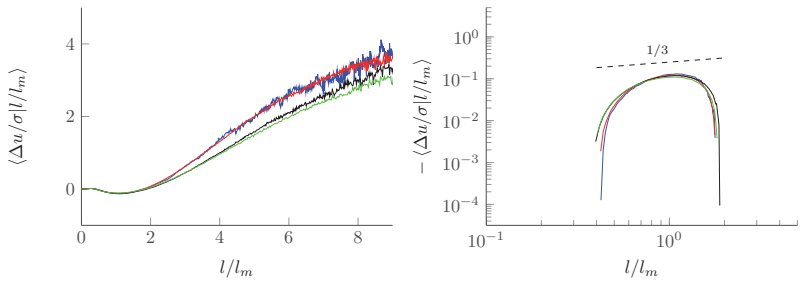

(a) **(b)**

Figure 6.6: Normalised conditional mean $\langle \Delta u/\sigma | l/l_m \rangle$ plotted as function of l/l_m for datasets D1, D3, R5 and R6.

The conditional mean $\langle \Delta u | l \rangle$ is small and positive for small l, where it is determined by viscous effects. At intermediate $l \sim l_m$, $\langle \Delta u | l \rangle < 0$, cf. figure 6.6b, because in this range more negative than positive segments are found (cf. also the jpdfs). In the range $3 \lesssim l/l_m \lesssim 5$, $\langle \Delta u | l \rangle$ is linear. At larger l/l_m, another linear range is found, but with different slope.

As was found for the normalised pdfs $P(l/l_m)$ and $P(\Delta u/\sigma)$, the conditional means collapse for small l/l_m, while they differ for larger l/l_m.

Let us now briefly look at the first linear range, $3 < l/l_m < 5$. Writing

$$\begin{aligned} u_{(2)} &= u_{(S)} + \left.\frac{\partial u}{\partial s}\right|_{s=S} \left(s_{(2)} - S\right) + \mathcal{O}\left(\left(s_{(2)} - S\right)^2\right), \\ u_{(1)} &= u_{(S)} - \left.\frac{\partial u}{\partial s}\right|_{s=S} \left(S - s_{(1)}\right) + \mathcal{O}\left(\left(S - s_{(1)}\right)^2\right) \end{aligned} \tag{6.17}$$

and subtracting yields

$$\Delta u = \left.\frac{\partial u}{\partial s}\right|_{s=S} \Delta s + \mathcal{O}((\Delta s)^3) \tag{6.18}$$

with $s_{(2)} - S = S - s_{(1)} = \Delta s/2$ and where $\partial u/\partial s$ is evaluated at the segment midpoint S. We drop the subscript in the following. Consequently,

$$\langle \Delta u | \Delta s = l \rangle = \left\langle \left.\frac{\partial u}{\partial s}\right| l \right\rangle l \sim a_\infty l. \tag{6.19}$$

On first glance, the expansion eq. (6.17) seems somewhat disheartening, since it is a Taylor series around the segment midpoint S for small Δs aimed at examining the conditional mean for large segments $l > l_m$. However as saving grace, one should keep in mind that because the segments are bound by extrema, the velocity u is monotonic and consequently the mean curvature* of u and the higher moments $\langle \partial^n u/\partial s^n \rangle$ are also highest at the segment endpoints but small inside the segment†. Indeed, eq. (6.17) is more accurate, the larger the length l of the segments, cf. figure 3 of Schaefer et al. (2013a) where the averaged non-dimensional profile of segments with $l/l_m > 1.5$ is approximately linear whereas the average non-dimensional profile of segments with $l/l_m < 0.25$ is sinusoidal.

Since a_∞ can be interpreted as strain induced by the large scales stretching intermediate segments (and should therefore not depend on the segment length l for the range under consideration), it can be expressed by the inverse of the integral timescale $\tau = \langle k \rangle / \langle \varepsilon \rangle$, i.e.

$$a_\infty \tau \sim const. \tag{6.20}$$

This is shown in figure 6.7, where indeed $a_\infty \tau$ becomes constant for the larger Reynolds numbers and where a_∞ was computed by fitting the linear range of $\langle \Delta u | l \rangle$ at intermediate $3 < l/l_m < 5$‡. That is, a_∞ is not evaluated at $l/l_m \to \infty$, although another linear scaling can be observed in that limit. This is because intermediate segments are stretched while large segments are cut, i.e. stretching as characterised by a_∞ does not determine the length of large segments. One would rather expect that for very large segments, $\Delta u/l \sim f_{\mathrm{cut}}$, where f_{cut} is the characteristic cutting frequency.

Higher-order conditional moments $\left\langle (\Delta u)^N | l \right\rangle, N = 2, 3, 4$

Next, the higher moments $\langle (\Delta u)^N | l \rangle$ normalised with σ and l_m for $N = 2, 3, 4$ are shown in figure 6.8, while the corresponding structure functions were shown in figure 4.10 and figure 4.11 in chapter 4. To better compare the plots, $\langle (\Delta u)^N | l \rangle$

*I.e. $\partial^2 u/\partial s^2$, not to be confused with the curvature κ of the streamline.

†Because the segments are not symmetric, the mean curvature $\langle \partial^2 u/\partial s^2 \rangle$ does not exactly vanish at S, but is small.

‡Noticeably, Gampert et al. (2011) were able to collapse the conditional mean $\langle \Delta u | l \rangle$ along dissipation elements for five different flow types (shear flow, forced turbulence, decaying turbulence, channel flow and Kolmogorov flow) also using the timescale $\tau = \langle k \rangle / \langle \varepsilon \rangle$ and the strain rate α_∞.

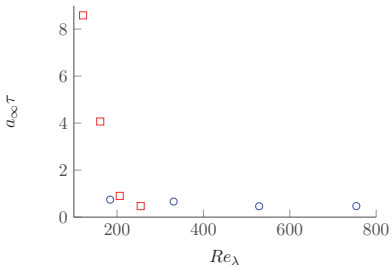

Figure 6.7: Plot of $a_\infty\tau$ over Re_λ for the forced datasets R4, R5 and R6 (○) and decaying datasets D1, D2, D3 and D4 (□).

are also shown logarithmically. The colours are the same as previously, i.e. D1 correspond to the blue lines, D3 to the red lines, R5 to the black lines and R6 to the green lines. As for the first conditional moment $\langle \Delta u|l\rangle$, we find similar qualitative behaviour for the higher orders for the different Reynolds numbers and flow cases examined here.

The second conditional moment $N = 2$ is shown in figure 6.8a and figure 6.8b, $\langle(\Delta u)^3|l\rangle$ in figure 6.8c and figure 6.8d and $\langle(\Delta u)^4|l\rangle$ in figure 6.8e and figure 6.8f. Noticeably, the conditional moments do not differ much at small l/l_m, which is in line with collapsing cores of the normalised pdfs $P(l/l_m)$ and $P(\Delta u/\sigma)$. Identifying power-law scaling is somewhat challenging, since corresponding scaling ranges are very short (if existent). If there is scaling, it differs significantly from K41 scaling $N/3$ as seen in figure 6.8b and figure 6.8f*.

While the even conditional moments are always positive by definition, the odd moments such as $\langle(\Delta u)^3|l\rangle$ are negative at $l \sim l_m$, due to the asymmetry of the jpdfs. However different to odd-order structure functions, the range for which $\langle(\Delta u)^N|l\rangle < 0$ with N odd is very limited and a scaling exponent can hardly be identified. While it can be seen from eq. (4.38) that $D_{3,0} < 0$ for $r \to 0$, an analogous result for $\langle(\Delta u)^3|l\rangle$ for $l \to 0$ is missing†. Similarly, $D_{3,0} < 0$ in the inertial range (cf. section 1.4) and $D_{3,0} \to 0$ for very large r, because the velocities u_1 and u_1' at the two points are then decorrelated. On the other hand, $\langle(\Delta u)^3|l\rangle > 0$ for large l, because there are many more positive than negative segments for large l. Moreover, this range seems to increase with increasing Reynolds number (albeit not much). From these observations, one might thus

*Of course, also $\zeta_2 \neq 2/3$ and $\zeta_4 \neq 4/3$, cf. e.g. table 3.3, but the differences are much smaller.

†Indeed as seen from figure 6.8d, $\langle(\Delta u)^3|l\rangle > 0$ for $l \to 0$.

muse whether the range at $l \sim l_m$ for which $\langle(\Delta u)^3|l\rangle < 0$ plays a similar role as the inertial range regarding cascades. This is briefly discussed in the next section, where streamline statistics of anisotropic, fractal-generated turbulence are examined.

6.3 Comparison with fractal flows

Lastly, streamline statistics in stationary homogeneous isotropic turbulence and in turbulence generated by a fractal square grid are compared. The fractal grid is described in more detail in section 2.3. We have split the domain of the fractal DNS into two equal subdomains, the first one called the production region directly behind the grid. The second subdomain is located further downstream and hereafter called decaying region*, where the flow is further away from the grid and more isotropic. The streamline segment statistics of these two subdomains are compared to those of the forced homogeneous isotropic dataset R2 (statistically stationary periodic turbulence), which has been chosen because of its similar Reynolds number Re_λ compared to the fractal flow. We also briefly look at streamline segment statistics calculated from an artificial dataset with vanishing skewness. This velocity field was obtained by randomising the phases of the Fourier-transformed velocity components of R2 while keeping the amplitude fixed. Continuity is then retained by projecting the Fourier-transformed velocity in the plane normal to the wave vector. The skewness of the longitudinal velocity gradient is then decreased to -0.00295 as compared to -0.54 for the original dataset R2.

We find close agreement between the stationary homogeneous isotropic turbulence and the decay region of the fractal-generated turbulence as well as the production region of the fractal flow for small segments. The statistics of larger segments are very similar for the isotropic turbulence and the decay region, but differ for the production region. Specifically, we examine the first, second and third conditional mean $\langle(\Delta u)^N|l\rangle$. Noticeably, non-vanishing $\langle(\Delta u)^N|l\rangle$ for $N = 1$ and $N = 3$ also found for the anisotropic flows and are due to the same asymmetry of positive and negative segments as for the isotropic datasets. This asymmetry is not only kinematic, but also due to dissipative effects and therefore $\langle(\Delta u)^N|l\rangle$ contains cascade information.

*Not to be confused with the decaying isotropic turbulence described in section 2.2.

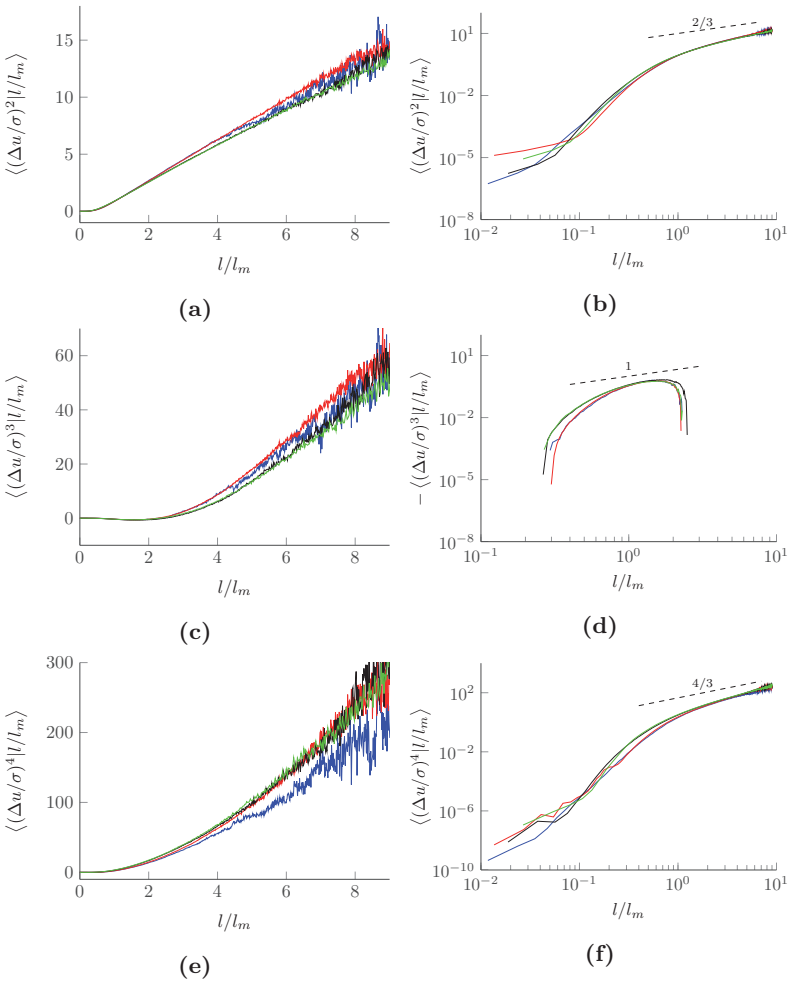

Figure 6.8: Normalised conditional moments $\langle(\Delta u)^N/\sigma|l/l_m\rangle$ for isotropic datasets D1, D3, R5 and R6. (a) and (b) $N = 2$, (c) and (d) $N = 3$, (e) and (f) $N = 4$.

6.3.1 Joint pdf

Figure 6.9 shows the joint probability density function (jpdf) $P(\Delta u, l)$ for the forced turbulence case R2 (figure 6.9a), the fractal flow in the production region close to the grid (figure 6.9b) and in the near-field decay region further downstream (figure 6.9c) normalised by their respective mean segment length l_m and standard deviation $\sigma = \langle(\Delta u - \langle\Delta u\rangle)^2\rangle^{1/2}$.

For dataset R2 (fig. 6.9a), we find the same shape as Wang (2010) and the other isotropic datasets D1, D3, R5 and R6 above, namely a noticeable asymmetry. Specifically, positive segments are longer on average than negative segments. This is consistent with their positive velocity difference $\Delta u > 0$ which stretches positive segments, while negative segments are compressed by their negative velocity difference $\Delta u < 0$. It follows that the absolute mean velocity difference of positive segments is necessarily smaller than that of negative segments, as positive and negative segments along a streamline alternate and the velocity u is finite. This is confirmed by the shape of the jpdf as also previously found for the isotropic datasets above.

The jpdf for the production region close to the fractal grid looks qualitatively similar compared to the isotropic case, albeit more symmetrical. Further downstream, in the near-field decay region where the turbulence is out of Richardson-Kolmogorov equilibrium, the jpdf (fig. 6.9c) approaches that of the statistically stationary periodic turbulence (i.e. R2) which is in equilibrium by virtue of the near-instantaneous balance between dissipation and power input required to keep it statistically stationary.

Finally, we show the jpdf of the artificial, vanishing velocity derivative skewness data in figure 6.9d. The shape of the jpdf is symmetric, i.e. positive and negative segments have the same statistics. As the energy cascade causes the velocity derivative skewness to be non-zero (and negative), this result suggests that the asymmetry of the jpdf in figures 6.9a, 6.9b and 6.9c is a reflection of the energy cascade at length-scales which are multiples/fractions but of the order of the mean segment length l_m. This is not a trivial result, in particular because l_m is a dissipative range length scale since $l_m = \sqrt{\eta\lambda}$, where η is the Kolmogorov length scale and λ is the Taylor length scale, see Schaefer et al. (2012b).

6.3.2 Marginal pdfs

The marginal probability density functions (pdfs) of l and Δu normalised by l_m and σ are shown in figure 6.10 both plotted linearly and semi-logarithmically.

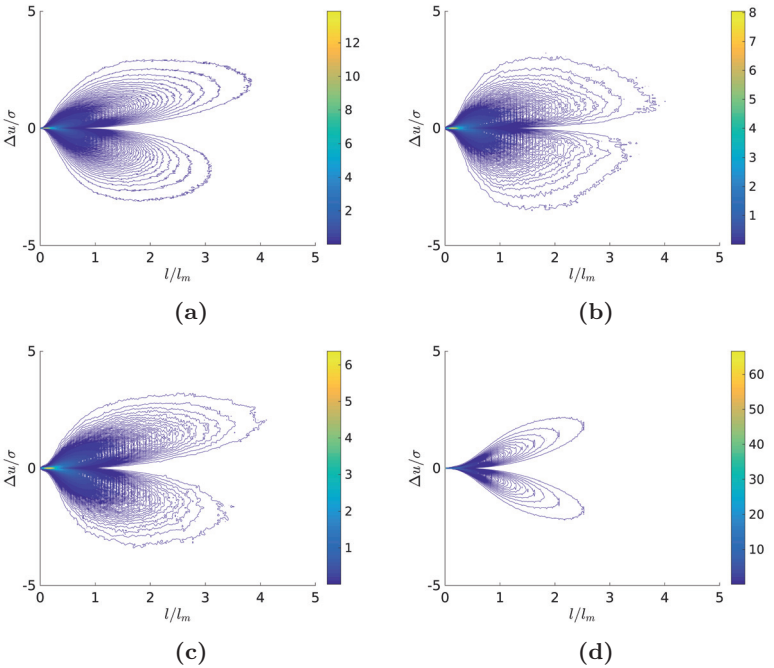

Figure 6.9: Joint pdf $P(\Delta u/\sigma, l/l_m)$. (a) Periodic dataset, (b) production region, (c) decay region, (d) vanishing skewness.

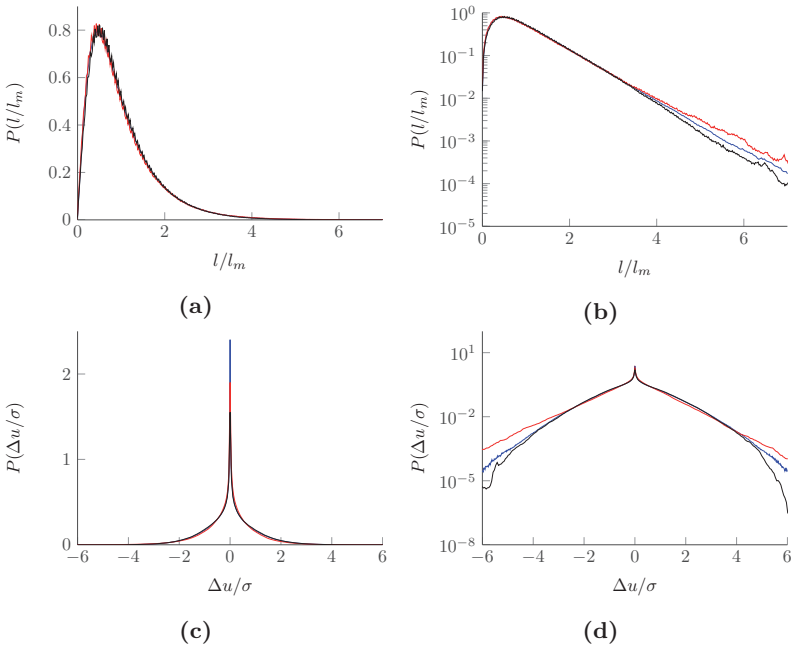

Figure 6.10: Normalised marginal pdfs. (a) and (b) $P(l)$, (c) and (d) $P(\Delta u)$. Blue: Periodic isotropic dataset, red: production region, black: decay region.

The vanishing velocity skewness data has been used to make the connection between turbulence cascade and the streamline segment statistics and is not needed any longer. It is therefore not included in the figures and discussion of this and the next subsection.

Noticeably, the normalised pdf of the segment length collapses for the three cases of homogeneous isotropic turbulence and the production and decay region of the fractal flow. The pdfs peak at $l/l_m \sim 0.6$ and show a linear behaviour for $l/l_m \to 0$ and an exponential tail for $l/l_m \to \infty$. This exponential tail is especially highlighted in figure 6.10b and corresponds to a random cutting-/reconnection process acting on large segments, cf. Schaefer et al. (2012a). Small segments $l/l_m \to 0$ are dominated by a drift towards smaller l due to molecular diffusion, in agreement with the linear rise observed in figure 6.10a, cf. Schaefer et al. (2012a). Schaefer et al. (2012a) derived a model for the pdf of l, which agrees very well with DNS data. Noticeably, their model includes a small Reynolds number dependence of the cutting-/reconnection process. Note that there are not that many segments with very high l and that their number is even less in the case of the fractal dataset. We can therefore not rule out that the tails may not be converged and that they would collapse if we had more data. Hence, we can not conclude whether the production and the non-equilibrium decay regions have same or different marginal distributions for segment lengths $l/l_m > 3$ when normalised with l_m. Comparing to $P(l/l_m)$ for the isotropic datasets D1, D3, R5 and R6, the pdfs for the periodic dataset, production region and decay region seem to better collapse. This is likely due to their very similar Re_λ.

The marginal pdf of the velocity difference Δu at the end points of the segments normalised by σ is shown in figure 6.10c and 6.10d. We find that the normalised $P(\Delta u)$ significantly deviate from a normal distribution and that they collapse for small velocity differences Δu as observed for D1, D3, R5 and R6 in section 6.2.1 above. Also, the tails of the pdfs do not collapse; especially negative segments differ. We find the production region pdf to be more symmetric than for both the statistically stationary periodic turbulence and the near-field decaying turbulence, in agreement with their joint pdfs in figure 6.9. It should be mentioned that the non-normalised pdfs $P(\Delta u)$ and $P(l)$ of all three cases differ wildly (not shown) and that they are only similar when normalised with l_m and σ, respectively.

6.3.3 Conditional means

Finally, we consider the conditional means $\langle (\Delta u)^N | l \rangle$ for $N = 1, 2, 3$ for the fractal flow. As discussed above, the separation vector r_i is fixed in space when evaluating structure functions, independent the local flow topology. This is

obviously not the case for $\langle(\Delta u)^N|l\rangle$, where the separation is equal to the segment length and orientated along the streamline. We may thus expect that $\langle(\Delta u)^N|l\rangle$ takes the local flow into account and that the velocity along the streamline is more correlated than along the arbitrary separation vector r_i. However, we must keep in mind that the separation vector r_i is arbitrarily large whereas the streamline length l has a maximum value. Hence we should not expect the range of l to be comparable to an inertial range. The streamline segment statistics mostly explore the dissipation range.

The first moment $\langle\Delta u|l\rangle$ is shown in both figure 6.11a and figure 6.11b. Note that, unlike structure functions, the first moment does not vanish even in statistically stationary periodic turbulence due to the characteristic differences between positive and negative segments as highlighted by the asymmetry of the jpdfs, cf. section 6.2.1 and section 6.3.1. For statistically stationary periodic turbulence and near-field grid-generated decaying turbulence, we find that for very small segments $l/l_m \lesssim 0.5$, $\langle\Delta u|l\rangle \sim 0$. Intermediate segments $0.5 \lesssim l/l_m \lesssim 2$ have a negative mean velocity difference, while $\langle\Delta u|l\rangle > 0$ for large segments $2 \lesssim l/l_m$. In agreement with section 6.2.2 and the findings of Wang (2009) and Wang and Peters (2010), we find a linear relation of the form $\langle\Delta u/\sigma|l/l_m\rangle \sim (l/l_m)$ for large l/l_m also for the fractal flow. Wang (2009) showed that the velocity difference along scalar trajectories (i.e. dissipation elements) does scale linearly with l when l is large. As dissipation elements and streamline segments are conceptually related inasmuch as that they depend on the flow structure, the linear increase as seen in figure 6.11a is not completely surprising, although the theory can not be carried over straightforwardly. Thus, figure 6.11a implies that intermediate segments are compressed while larger segments are stretched, in agreement with the jpdfs figure 6.9c above and section 6.2.2. In fact, there is very good agreement between the isotropic data and the downstream fractal flow. The production region data show qualitatively similar behaviour, but with a wider range of segment lengths with negative mean velocity difference and a smaller slope for large segments. This might indicate in conjunction with figure 6.7 that it could be possible to collapse all three plots at intermediate l/l_m in the first linear range if normalised with suitable quantities such as the integral timescale τ. Figure 6.11b highlights the region for which $\langle\Delta u|l\rangle < 0$. We find a remarkably good agreement between all our data for intermediate segment lengths.

The second moment $\langle(\Delta u)^2|l\rangle$ is shown in figure 6.11c and figure 6.11d. Similarly to the first moment, the statistically stationary periodic turbulence data and the grid-generated turbulence decay data agree very well, while the produc-

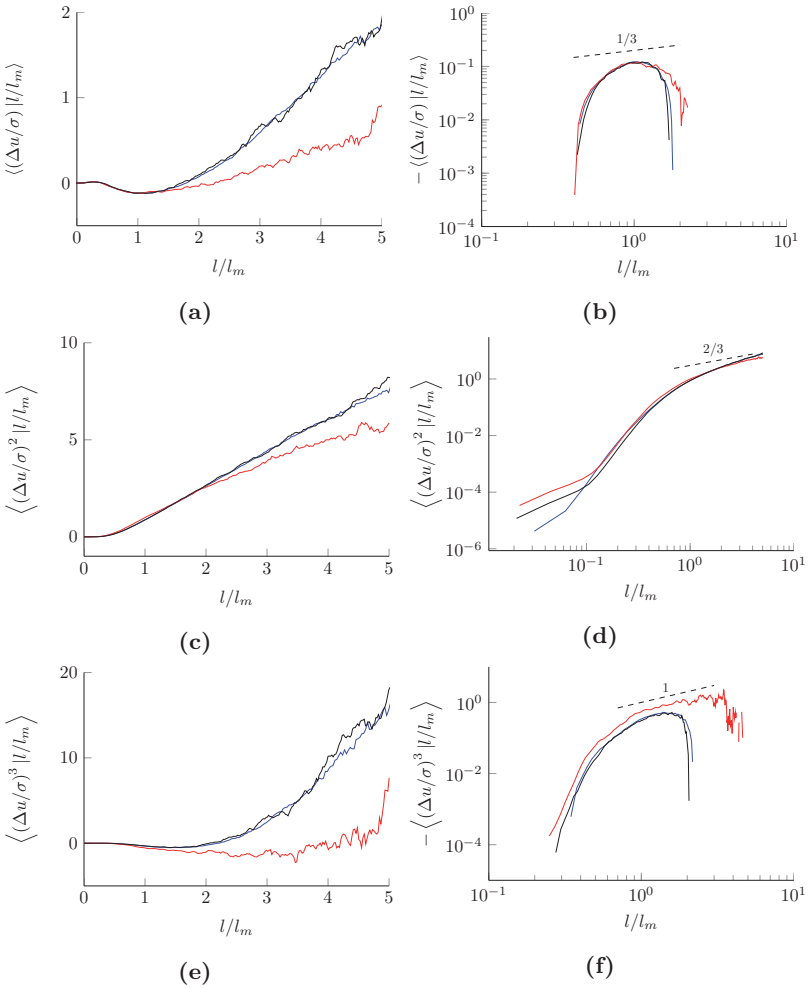

Figure 6.11: Conditional moments $\langle(\Delta u)^N|l\rangle$ normalised with σ and the mean length l_m. (a) and (b) $N = 1$, (c) and (d) $N = 2$, (e) and (f) $N = 3$. Blue: Periodic isotropic dataset, red: production region, black: decay region.

tion region data close to the grid exhibits a different slope for large segments. Curiously, for small l/l_m, the periodic turbulence data agrees better with the production region data than with the decay region data. However, for $l/l_m \gtrsim 0.5$, the periodic and the decay data agree very well, cf. figure 6.11d. For large l, we find a linear increase of $\langle(\Delta u)^2|l\rangle$ with l. If there is power-law scaling, it differs significantly from the scaling of the second-order structure function $D_{2,0}$, $\zeta_2 \approx 2/3$, cf. also figure 6.8a.

The third moment $\langle(\Delta u)^3|l\rangle$ is presented in figure 6.11e and figure 6.11f. As expected, we find a similar behaviour as in case of the first moment. However, the range of l/l_m for which $\langle(\Delta u)^3|l\rangle < 0$ is larger than the corresponding range for the first moment. This agrees with the jpdfs inasmuch as large values of Δu for a certain l are now higher weighted and that $|\Delta u|$ was found to be higher for negative segments than for positive segments. Again, we find that the statistically stationary periodic turbulence and the grid-generated decaying turbulence data agree very well and collapse for all l/l_m, while the production region data shows qualitatively similar behaviour.

The range $\langle(\Delta u)^3|l\rangle < 0$ is of particular interest, as the asymmetry in the joint PDF of figure 6.9 is related to the turbulence cascade process (see end of section 6.3.1) and one might ask whether the negative sign of $\langle(\Delta u)^3|l\rangle$ reflects the forward nature of this process at dissipative scales in the same way that the negative sign in Kolmogorov's 4/5-law $D_{3,0} = -4/5\langle\varepsilon\rangle r$ reflects the forward nature of the cascade process in inertial scales. The scaling with l of $-\langle\Delta u)^3|l\rangle$ is shown in figure 6.11f. There is no such power-law scaling range for the periodic and the decaying turbulence data, but there may be a very short one with exponent 1 for the highly non-Gaussian data in the production region of the grid-generated turbulence exhibits. This observation is consonant with the finding of Laizet et al. (2013), Gomes-Fernandes et al. (2015) and Laizet et al. (2015a) that the best $-5/3$ power-law spectrum over the entire grid-generated turbulence is found in the production region. It may be that the non-Gaussianity in the production region has the same cause as these well-defined power-laws, namely the sharp interfaces between alternating potential and vortical flow patches. The cause of these well-defined power-laws has nothing to do with Kolmogorov's theory as already noted by Laizet et al. (2013), Gomes-Fernandes et al. (2015) and Laizet et al. (2015a).

The asymmetry in Figure 6.9 which shows that there are longer streamline segments with positive than with negative velocity difference Δu is a dynamic effect reflecting inertial cascade processes at dissipative scales. The turbulence cascade mechanism is expressed in terms of structure functions and their power-law dependence on two-point separation distance in the so-called inertial range

of length-scales. The statistical quantities $\langle(\Delta u)^N|l\rangle$ studied here are defined over a range of streamline segment lengths which extends up to no more than an order of magnitude higher than $l_m = \sqrt{\eta\lambda}$. Hence, the range of scales sampled by the streamline segments statistics $\langle(\Delta u)^N|l\rangle$ is mostly dissipative. Nevertheless, the asymmetry in the jpdf underlying these statistics is an asymmetry between strain and compression and can only reflect the time-irreversible energy cascade from large to small scales. Hence, the streamline segment statistics $\langle(\Delta u)^N|l\rangle$ are capable of picking up cascade information but at the dissipation range level. They are also capable of displaying approximate linear dependencies on l if l is not much smaller than one or two l_m.

The comparison we have made suggests that, even if sensitive to the average direction of the cascade, streamline statistics are not very sensitive to the difference between equilibrium and non-equilibrium cascades. Indeed, the grid-generated decaying turbulence and the statistically stationary periodic turbulence have very similar such statistics.

The similarities of streamline segment statistics between isotropic and anisotropic datasets are very promising, although they differ significantly from longitudinal structure functions $D_{N,0}$. As the analysis presented in this chapter is rather brief and only qualitative, more research regarding the streamline segments and their conditional moments $\langle(\Delta u)^N|l\rangle$ would be very welcome.

7 Summary

Hereinafter, the most important findings of the main body are summarised.

As detailed in chapter 3, transport equations for structure functions $\boldsymbol{D}_N$ of arbitrary order as well as their trace can be derived from the Navier-Stokes equations. The structure functions are then solutions of the coupled system of equations, where the boundary conditions for $r \to 0$ are known. The coupling of the system is two-fold: First, there is a coupling via the transport term in the equations which stems from the non-linear term in the Navier-Stokes equations. These terms couple structure functions of the next higher order $N+1$ to the Nth order. Therefore, the system is unclosed and closure needs to be introduced if one is interested in solving the complete system. Second, there is an inter-order coupling between longitudinal, mixed and transverse structure functions of the same order N in the Nth-order equations; this coupling is due to the viscous terms stemming form the Laplacian of the Navier-Stokes equations. Noticeably, the boundary conditions of $\boldsymbol{D}_N$ for $r \to 0$ are known. It has been shown that all longitudinal, even-order structure functions collapse for $r \to 0$ when normalised with $\langle \varepsilon^{N/2} \rangle$ and ν with known, exact prefactors. Similarly, it has been empirically found that also mixed and transverse structure functions as well as odd-order structure functions collapse with $\langle \varepsilon^{N/2} \rangle$ and ν for $r \to 0$, albeit with empirical prefactors. That is, the pdf of the dissipation $P(\varepsilon)$ and the viscosity ν provide the boundary conditions $r \to 0$ for the system of equations.

Furthermore, there are two kind of source terms found in the system of equations: The first called dissipation source terms $\langle \boldsymbol{E}_N \rangle$ correspond to correlations of velocity differences of order $N-2$ and components of the pseudo-dissipation tensor ϵ_{ij}. The second called pressure source terms $\langle \boldsymbol{T}_N \rangle$ are given by correlations of velocity differences of order $N-1$ and pressure gradient differences. The source terms $\langle \boldsymbol{E}_N \rangle$ and $\langle \boldsymbol{T}_N \rangle$ are a-priori unknown and need to be closed. They are important since they determine the solution of the system and one can derive transport equations for $\langle \boldsymbol{E}_N \rangle$ and $\langle \boldsymbol{T}_N \rangle$ to further analyse them. This has been done exemplarily for the fourth-order source terms $\langle \boldsymbol{E}_4 \rangle$ and their trace.

In this framework, the inertial range assumptions correspond to a special truncation of the system. Indeed, all terms containing structure functions of order N are then neglected in the Nth-order equations and one obtains balances

for $\boldsymbol{D}_{N+1}$ as function of the Nth-order source terms. Noticeably, only for even orders there are enough equations to solve for $\boldsymbol{D}_{N+1}$ even if the source terms are known. In the viscous range for $r \to 0$, the Laplacian of the Nth-order structure functions is balanced by the dissipation source term $\langle \boldsymbol{E}_N \rangle$, while all other terms can be neglected. However, it is not possible to solve for $\boldsymbol{D}_N$ in general, because the resulting equations are linearly dependent. Only the second and third order can be completely solved, because the continuity equation provides an additional equation for $N = 2$ and $N = 3$.

Furthermore, balances of structure function equations and their traces up to the seventh order using DNS of homogeneous isotropic flow with Reynolds number up to $Re_\lambda = 754$ were computed and analysed. For even orders, the dissipation source terms $\langle \boldsymbol{E}_N \rangle$, which are related to correlations between velocity differences and the pseudo-dissipation, were found to be the dominant source terms. In the viscous range, they balance the viscous terms, while they balance the transport terms in the inertial range to leading order. Interestingly, there are as many equations as unknown structure functions in the inertial range at even orders, similarly to the K41 result for the second-order equations leading to the 4/5-law. That is, one can integrate the even-order equations under the inertial range assumptions and could solve for all odd orders, if the source terms were known. Again, the second order is very special, since the pressure source terms vanish due to isotropy and the dissipation source terms can be written as $\langle \epsilon \rangle$, i.e. become a one-point quantity independent of r, thus facilitating the integration resulting in the 4/5-law. There are no analogous results for higher even orders, since the pressure source terms do not vanish (but may be negligible at not too high orders) and the dissipation source terms remain two-point quantities depending on r, thus immediately prohibiting simple phenomenology such as K41. Noticeably, the coupling in the mixed and longitudinal equations contributes significantly to the balance, to the effect that one could neglect also the dissipation source term in these equations for the orders examined here. However, the ratio of pressure source terms to the dissipation source terms $T_{N,0}/E_{N,0}$ in the longitudinal equations increases with increasing order, so that these approximations may not be warranted at higher-order N. On the other hand, odd orders are different inasmuch that there is one less equation than unknown structure functions $\boldsymbol{D}_{N+1}$ under the inertial range assumptions, even if the source terms were known. Noticeably, the pressure source terms are dominant in the odd-order equations and balance the transport terms nearly perfectly. Remarkably, this seems to hold even in the viscous range, where still the dissipation source terms balance the viscous terms as in the even-order equations.

The balances of the traces of the structure function equations up to the seventh order were also examined. The trace equations are of interest, because they contain the higher moments of the pseudo-dissipation in equations for the trace of te dissipation source terms. For instance, the dissipation source term of the second-order trace equation equals the mean of the pseudo-dissipation $\langle\epsilon\rangle$. Similarly, one finds the second moment $\langle\epsilon^2\rangle$ in the transport equation of the trace of fourth-order dissipation source terms, $\langle\epsilon^3\rangle$ in the transport equation of one of the source terms of the trace of sixth-order dissipation source terms and so on. Since the trace is either a scalar for even orders or the 1-component of a vector for odd orders, one can always solve the trace equation in the inertial and viscous range if the source terms are known, as there is one equation for one unknown. However, there is no coupling via the transport terms between trace equations of $N+1$ and N for N odd. That is, there is no system of trace equations as compared to the individual equations analogous to figure 3.1 in the sense that one cannot compute the trace $D_{[N+1]}$ for odd N and insert them into the transport term of the even-order trace equations. Since the trace is the sum of the longitudinal, mixed and transverse structure functions, the trace balances are qualitatively similar to the individual balances. For even orders, the trace of dissipation source terms balance the trace of viscous terms in the viscous range and to leading order the trace of transport terms in the inertial range, while the pressure source terms are negligible. For odd orders, the dissipation source terms are negligible, while still balancing the trace of viscous terms for $r \to 0$. However, the trace of pressure source terms balance the trace of transport terms nearly perfectly both in the viscous and inertial range.

After having discussed the system of equations, the viscous range was examined more closely in chapter 4. Since components of the pseudo-dissipation are found in the system of equations, the Reynolds number scaling of the ratios of the moments of pseudo-dissipation to the dissipation, $\langle\epsilon^M\rangle/\langle\varepsilon^M\rangle$, the ratio of their components to $\langle\varepsilon^M\rangle$ and the ratio of the velocity gradients $G_{p,q}/\langle\varepsilon^M\rangle$ for $M = 1, ..., 4$ with $M = p + q$ have been examined. All these ratios become constant when the Reynolds number is large enough. This implies that one can use the moments of the pseudo-dissipation and the kinetic energy dissipation interchangeably, although their ratio needs to be determined empirically (except for the mean $\langle\epsilon\rangle = \langle\varepsilon\rangle$). Similarly, all components of the moments of the pseudo-dissipation have the same Reynolds number scaling as the moments of the dissipation $\langle\varepsilon^M\rangle$. This is comforting, since their sum appears in the system of structure function equations in the viscous range, which may then be replaced by the invariant quantity $\langle\varepsilon^M\rangle$. Again, the numerical values of the ratios need to be determined empirically. The same conclusion is drawn for the

ratio of moments of velocity gradients and dissipation, $G_{p,q}/\langle\varepsilon^M\rangle$. Indeed, it has been shown analytically that the ratio of longitudinal velocity gradients and dissipation $G_{M,0}/\langle\varepsilon^M\rangle$ is independent of the Reynolds number and can be derived exactly under the assumptions of homogeneity and isotropy. Empirically, this also holds for mixed and transverse velocity gradients. Moreover, there are exact result for the third-order structure functions $D_{3,0}$ and $D_{1,2}$ in the viscous range.

Using the relations between the moments of the longitudinal velocity gradient and the moments of the dissipation, exact solutions of longitudinal structure functions in the viscous range were determined without ambiguity or any free parameters for arbitrary even orders, where the prefactors are known universal (Reynolds number independent) constants. The only required assumptions are (local) isotropy, (local) homogeneity and incompressibility. From this, generalised cut-off scales $\eta_{C,N}$ and $u_{C,N}$ as given by eq. (4.81) and eq. (4.82) were defined. These scales are exact under the above assumptions and can be interpreted as a generalisation of the Kolmogorov scales η and u_η; they are determined by dissipative quantities (the moments of the dissipation and the kinematic viscosity) only. The question then becomes whether the same results hold for mixed and transversal structure functions as well as odd orders. As found empirically from the DNS data, this is indeed the case for the mixed and transversal structure functions, because the ratio of the velocity gradients $\langle(\partial u_2/\partial x_1)^{p+q}\rangle$ and $\langle(\partial u_1/\partial x_1)^p(\partial u_2/\partial x_1)^q\rangle$ to $\langle(\partial u_1/\partial x_1)^{p+q}\rangle$ is constant at sufficiently high Reynolds number. Also, it has been found that using moments $\langle\varepsilon^{N/2}\rangle$ with odd N collapses the odd-order structure functions, although the required connectors again cannot be derived and remain empirical. As the normalised moments of the dissipation increase with increasing Reynolds number and order, the cut-off length scales $\eta_{C,N}$ decrease. This implies that K41 scaling is only correct for the second order (and for the third order in the inertial range), while for higher orders the new scales $\eta_{C,N}$ and $u_{C,N}$ should be used, which were defined without any ambiguity or additional assumptions.

As there is a myriad of order (and Reynolds number) dependent cut-off length scales, the grid needs to be finer with increasing order and Reynolds number, an effect well-known in the literature, which is not captured by K41. The exact cut-off lengths $\eta_{C,N}$ and the DNS data were used to estimate the grid resolution at a given order, which gives satisfactory agreement with previous results in the literature. Thus when carrying out DNS studies, one should consider the desired Reynolds number one is aiming at as well as the order which needs to be fully resolved. Resolving the (K41) Kolmogorov scale η is sufficient to resolve the transport of kinetic energy down the cascade and its dissipation.

Higher resolution is required if one is interested in higher-order statistics, which consequently need higher orders fully resolved. This is evident inasmuch that the moments of the velocity gradient pdf can be obtained from the limit of $D_{m,n}/r^{m+n}$ for $r \to 0$.

In chapter 5, the inertial range was examined more closely. It has been shown that Kolmogorov's refined similarity hypothesis (RSH) predicts that the longitudinal $N+1$th-order structure functions $D_{N+1,0} = \langle(\Delta u_1)^{N+1}\rangle$ are determined by the longitudinal dissipation source terms $\langle E_{N,0}\rangle \sim \langle(\Delta u_1)^{N-2}\epsilon_{11}\rangle$ of order N in the inertial range, for all $N \geq 4$. Therefore, RSH is consistent with the structure function equations if $(\partial D_{N+1,0}/\partial r)$ (but not necessarily the full transport terms $\nabla_r D_{N+1,0}$) and $\langle E_{N,0}\rangle$ have the same r-dependency in the inertial range. Anomalous scaling, i.e. deviations from K41 scaling $\zeta = N/3$ can then be interpreted to stem from the correlations of $(\Delta u_1)^{N-2}$ and ϵ_{11}, which depend on r. Indeed from DNS, the ratio $(\partial D_{N+1,0}/\partial r)/\langle E_{N,0}\rangle$ is found to be constant in the inertial range for even N. On the other hand, the ratios for odd-order N exhibit a slight r-dependence, which decreases with increasing N, consistent with fig. 8 of Nakano et al. 2003. This is probably due to the observation that the dominant source terms in the odd-order equations, the pressure source terms $\langle T_{N,0}\rangle$, scale differently from $\langle E_{N,0}\rangle$ in the inertial range for lower N; the differences in scaling (but not necessarily in magnitude) are found to decrease with increasing N in agreement with the balances of section 3.2. Thus, one may conclude that the RSH prediction $(\partial D_{N+1,0}/\partial r)/\langle E_{N,0}\rangle = const.$ is in good agreement with the even-order balances for all N; for the odd orders, the agreement increases with increasing N.

At scales $r \sim \mathcal{O}(\eta_{C,N})$, the normalised moments of the dissipation cross over to the volume-averaged dissipation ε_r. Consequently, any theory predicting the scaling of ε_r or the structure function exponents in the inertial range can be used to determine the scaling of $\eta_{C,N}$. It is found that the log-normal model makes unphysical predictions, while both the multi-fractal p-model as well as the She-Leveque model agree very well with the DNS. Similarly, one can compute inertial range scaling exponents from the Reynolds number scaling of the moments of the dissipation. It is then seen that anomalous scaling is due to internal intermittency.

In addition to ν and $\langle\varepsilon\rangle$, all higher-order moments of the dissipation distribution function appear as dissipation parameters in the extended system of two-point equations for small-scale turbulence. The effect of the higher-order dissipation parameters on the solutions of these equations is demonstrated for the trace of the fourth-order structure function equations, which are invariant, independent of the coordinate system. The procedure can also be carried over to

the individual structure function equations at higher even orders; for example, in the sixth-order equations, the third-order dissipation parameters $\langle(\epsilon_{11}+\epsilon'_{11})^3\rangle$ etc. are found. The analysis uses exact equations, but because of the inherent closure problem needs to apply empirical closure assumptions between some of the terms. It can be concluded that the trace of the dissipation parameters in the system of equations contains the moments of ε_r. However, the relation of $\langle\varepsilon_r^{N/3}\rangle$ for the Nth-order structure functions in the inertial range to the dissipation parameters such as $\langle(\epsilon_{11}+\epsilon'_{11})^{N/2}\rangle$ derived from the Navier-Stokes equations is missing.

Under the inertial range assumptions, the unsteady and viscous terms are neglected. However at finite Reynolds numbers, they contribute to the structure function equation balances in the inertial range. These contributions were examined for the second order and one might expect similar contributions at higher orders. After normalising the unsteady terms in the second-order equations of Hill (2002) with the large scale L, they can be written as function of $\widetilde{r} = r/L$ only. Evaluating the balance of the second order using DNS, the unsteady terms contribute significantly to the inertial range solution of the third-order structure functions $D_{3,0}$ and $D_{1,2}$ in agreement with previous results in the literature. Using a power-law closure, it is seen that the contribution of the unsteady terms increases with increasing r/η, but decreases with increasing Reynolds number in agreement with the notion of an inertial range. If the second-order structure functions follow K41 scaling, the same result as previously reported by Lundgren (2002) and Lindborg (1999) is recovered. Closing the system of equations by directly coupling the second- and third-order structure functions using an eddy-viscosity ansatz gives very good agreement with the DNS when the unsteady terms are included. This model also allows for solving the equations for higher Reynolds numbers for which no DNS is available while retaining the influence of the unsteady and viscous terms. From the model, it is found that the intersection of these two terms scales with the Taylor scale λ, i.e. λ is situated in the inertial range.

Finally, streamline segment statistics were briefly examind in chapter 6. The endpoints of streamline segments are defined by local minima and maxima of u along the streamlines and are characterised by the velocity difference Δu of the endpoints as well as the arclength l. Conceptually, the conditional means $\langle(\Delta u)^N|l\rangle$ are somewhat similar to the longitudinal structure functions $D_{N,0}$ because $u = t_i u_i$ is the projection of the velocity u_i onto the streamline. Whereas the separation vector r_i of structure functions can be considered as a parameter, the streamlines depend on the local flow field and consequently their length l

is an intrinsic quantity linked to the flow; thus, they might be a more suitable candidate to examine turbulent structures and explore the multi-scale behaviour of turbulent flows.

It is found that streamline segment statistics differ from longitudinal structure functions for several reasons. Most importantly, the segment length l is a stochastic variable while the separation vector can be thought of as a parameter with uniform distribution. Additionally, streamline segments may locally converge or diverge, so that the segment statistics do not sample the volume uniformly. Moreover, the velocity difference $|\Delta u| > 0$ always, whereas $u_1(\boldsymbol{x} + \boldsymbol{r}) - u_1(\boldsymbol{x})$ may vanish. Thus, the joint pdf $P(\Delta u, l)$ is separated into two distinct regions for positive ($\Delta u > 0$) and negative ($\Delta u < 0$) segments. Positive segments are found to be longer on average than negative segments. As a result, one finds an asymmetric wing-shaped jpdf $P(\Delta u, l)$ which differs significantly from $P(\Delta u_1, r)$. Remarkably enough, the shape of $P(\Delta u, l)$ is quantitatively similar for both the homogeneous isotropic datasets with different Reynolds numbers as well as for an anisotropic fractal grid flow also examined and is linked to the negative skewness of the velocity gradients. Indeed, for an artificial flow with vanishing skewness the jpdf $P(\Delta u, l)$ was found to be symmetric.

The normalised marginal pdfs $P(l/l_m)$ and $P(\Delta u/\sigma)$ (where l_m is the mean segment length and σ the standard deviation of u) were found to collapse for small l and u but exhibit Reynolds number dependent tails.

Considering the conditional means $\langle(\Delta u)^N|l\rangle$, it is found that odd-order moments are negative in a limited range close to $l/l_m \sim 1$ due to the asymmetry of the jpdf $P(\Delta u, l)$. This is reminiscent of the odd-order structure functions $D_{N,0}$, which are also negative. However, power-law scaling of $\langle(\Delta u)^N|l\rangle$ is not evident. Rather, $\langle(\Delta u)^N|l\rangle$ are found to increase linearly for larger l. Remarkably enough, it has been found that streamline segment statistics of isotropic and anisotropic flows are qualitatively very similar, which is very promising for future research.

Appendix A

Isotropic tensors

In the following, isotropic tensors are briefly discussed. For an overview, see Kearsley and Fong (1975) and Robertson (1940) as well as the books by Aris (1962) and Schade and Neemann (2009).

Formally, the components of an isotropic tensor remain unchanged under a rotation of the frame of reference. It can be shown that the only fundamental isotropic tensors are the Kronecker delta δ_{ij},

$$\delta_{ij} = \begin{cases} 1, & \text{if } i = j, \\ 0, & \text{if } i \neq j. \end{cases} \tag{A.1}$$

and the ϵ-tensor ϵ_{ijk}[†], where

$$\epsilon_{ijk} = \begin{cases} 1, & \text{if } (i,j,k) \text{ is } (1,2,3),(2,3,1) \text{ or } (3,1,2), \\ -1, & \text{if } (i,j,k) \text{ is } (3,2,1),(1,3,2) \text{ or } (2,1,3), \\ 0, & \text{otherwise,} \end{cases} \tag{A.2}$$

i.e. $\epsilon_{ijk} = 1$ for even permutations of $(1,2,3)$, $\epsilon_{ijk} = -1$ for odd permutations of $(1,2,3)$ and $\epsilon_{ijk} = 0$ if an index is repeated.

In case of isotropic turbulence, statistics should also be invariant with respect to reflections of the coordinate system, which is a stronger constraint than solely invariance with respect to rotations of the coordinate system. Then, the statistics do not depend on linear combinations of ϵ_{ijk}, because after reflection e.g. $\epsilon_{123} = 1 \neq \epsilon_{132} = -1$, say; the statistics depend only on linear combinations of $\delta_{ij} = \delta_{ji}$.

Thus, the one-point tensor $A_{ijkl...}$ can be written assuming isotropic turbulence

$$A_{ijkl...} = A_1 \delta_{ij}\delta_{kl}... + A_2 \delta_{ik}\delta_{jl}... + A_3 \delta_{il}\delta_{jk}... + ..., \tag{A.3}$$

[†]Here, ϵ_{ijk} should not be confused with the pseudo-dissipation tensor ϵ_{ij}.

i.e. by writing down all possible combinations of $\delta_{ij}\delta_{kl}...$ multiplied by scalar functions A_m. This implies that there are no odd-order one-point tensors when assuming isotropic turbulence.

Following Robertson (1940), two-point tensors which depend on the separation distance r can be similarly written as combinations of δ_{ij} and the separation vector r_k/r multiplied with scalar functions $A_l(r)$. For instance assuming isotropic turbulence,

$$\begin{aligned} A_{ijkl...}(r) = {} & A_1(r)\frac{r_i}{r}\frac{r_j}{r}\frac{r_k}{r}\frac{r_l}{r}... + A_2(r)\frac{r_i}{r}\frac{r_j}{r}\delta_{kl}... + A_3(r)\frac{r_i}{r}\frac{r_k}{r}\delta_{jl}... \\ & + A_4(r)\frac{r_i}{r}\frac{r_l}{r}\delta_{jk}... + A_5(r)\frac{r_j}{r}\frac{r_k}{r}\delta_{il}... + A_6(r)\frac{r_j}{r}\frac{r_l}{r}\delta_{ik}... \\ & + A_7(r)\frac{r_k}{r}\frac{r_l}{r}\delta_{ij}... + A_8(r)\delta_{ij}\delta_{kl}... + A_9(r)\delta_{ik}\delta_{jl}... \\ & + A_{10}(r)\delta_{il}\delta_{jk}... + ... \end{aligned} \tag{A.4}$$

In the following, the explicit notation (r) is dropped but implied for two-point tensors. Noticeably, two-point tensors are determined by more scalar functions than same-order one-point tensors. Furthermore, odd-order two-point tensors do not vanish. For instance the third-order tensor

$$A_{ijk} = A_1\frac{r_i}{r}\frac{r_j}{r}\frac{r_k}{r} + A_2\frac{r_i}{r}\delta_{kl} + A_3\frac{r_j}{r}\delta_{ik} + A_4\frac{r_k}{r}\delta_{ij} \tag{A.5}$$

is completely determined by the four scalar functions A_1, A_2, A_3 and A_4, which depend on r.

One can proceed and derive the gradient and Laplacian of any isotropic tensor by taking derivatives of eq. (A.4) with respect to r_i and specifying the scalar functions A_j. When taking the derivatives, the following relations are helpful:

$$\begin{aligned} \frac{r_n r_n}{r^2} &= 1 \\ \frac{\partial}{\partial r_n}\left(\frac{r_i}{r}\right) &= \left(\delta_{in} - \frac{r_i r_n}{r^2}\right)\frac{1}{r} \\ \frac{\partial}{\partial r_n}\left(\frac{r_n}{r}\right) &= \left(\delta_{nn} - \frac{r_n r_n}{r^2}\right)\frac{1}{r} = \frac{2}{r} \\ \frac{\partial A(r)}{\partial r_n} &= \frac{r_n}{r}\frac{\partial A(r)}{\partial r} \\ \frac{\partial}{\partial r_n}\left(\frac{1}{r}\right) &= -\frac{1}{r^2}\frac{\partial\sqrt{r_i^2}}{\partial r_n} = -\frac{1}{r^2}\frac{r_i}{\sqrt{r_i^2}}\frac{\partial r_i}{\partial r_n} = -\frac{1}{r^2}\frac{r_i}{r}\delta_{in} = -\frac{r_n}{r^3} \end{aligned} \tag{A.6}$$

Consequently, also

$$\frac{r_n}{r}\frac{\partial}{\partial r_n}\left(\frac{r_i}{r}\right) = \left(r_n\delta_{in} - \frac{r_n r_i r_n}{r^2}\right)\frac{1}{r^2} = (r_i - r_i)\frac{1}{r^2} = 0, \tag{A.7}$$

which simplifies the derivation.

Without loss of generality, one may choose $r_i = (r, 0, 0)$, i.e. align the separation vector with the x_1-axis. Further simplifications occur when the tensor $\langle A_{ijkl...}\rangle$ is symmetrical under interchange of some or all of its indices.

Next, the Laplacian of the fourth-order structure function tensor $\boldsymbol{D}_4 = \langle \Delta u_i \Delta u_j \Delta u_k \Delta u_l\rangle$ and the gradient of the fifth-order structure function tensor $\boldsymbol{D}_5$ which are found in the fourth-order structure function equations as discussed in section 3.1.2 are exemplary derived.

A.1 Laplacian of the fourth-order structure function tensor

Here, we give the derivation of the isotropic form of the Laplacian of a fourth-order tensor, specifically the fourth-order structure function tensor. The same procedure can be applied to tensors of higher (or lower) order. From eq. (A.4), a fourth-order tensor of two-point type which is invariant to rotation and reflection of the coordinate system (as is the case for isotropic turbulence) is given by

$$\begin{aligned} A_{ijkl} = {} & A_1\frac{r_i r_j r_k r_l}{r^4} + A_2\delta_{ij}\frac{r_k r_l}{r^2} + A_3\delta_{ik}\frac{r_j r_l}{r^2} + A_4\delta_{il}\frac{r_j r_k}{r^2} + A_5\delta_{jk}\frac{r_i r_l}{r^2} \\ & + A_6\delta_{jl}\frac{r_i r_k}{r^2} + A_7\delta_{kl}\frac{r_i r_j}{r^2} + A_8\delta_{ij}\delta_{kl} + A_9\delta_{ik}\delta_{jl} + A_{10}\delta_{jk}\delta_{il}, \end{aligned} \tag{A.8}$$

where A_i are scalar functions depending on the separation distance r, δ_{ij} is the Kronecker delta, i.e. $\delta_{ij} = 1$ for $i = j$ and $\delta_{ij} = 0$ for $i \neq j$ and r_i a separation vector with magnitude r.

In the following, let $A_{ijkl} = \boldsymbol{D}_4 = D_{ijkl} = \langle \Delta u_i \Delta u_j \Delta u_k \Delta u_l\rangle$, i.e the fourth-order structure function tensor. As the tensor is symmetrical under interchange of all indices, $D_{ijkl} = D_{jikl} = D_{ijlk} = D_{jlik} = ...$, one finds from eq. (A.8) that

$A_1 = \widetilde{A}_1$, $A_2 = A_3 = ... = A_7 = \widetilde{A}_2$ and $A_8 = A_9 = A_{10} = \widetilde{A}_3$, and we then have

$$\begin{aligned} D_{ijkl} = & \widetilde{A}_1 \frac{r_i r_j r_k r_l}{r^4} \\ & + \widetilde{A}_2 \left(\delta_{ij} \frac{r_k r_l}{r^2} + \delta_{ik} \frac{r_j r_l}{r^2} + \delta_{il} \frac{r_j r_k}{r^2} + \delta_{jk} \frac{r_i r_l}{r^2} \delta_{jl} \frac{r_i r_k}{r^2} + \delta_{kl} \frac{r_i r_j}{r^2} \right) \\ & + \widetilde{A}_3 \left(\delta_{ij}\delta_{kl} + \delta_{ik}\delta_{jl} + \delta_{jk}\delta_{il} \right). \end{aligned} \tag{A.9}$$

That is, the number of scalar functions needed to fully describe the complete tensor is reduced significantly because of the symmetries of the tensor.

Next, the scalar functions $\widetilde{A}_1$, $\widetilde{A}_2$, $\widetilde{A}_3$ need to be determined. Without loss of generality, let $r_1 = r$, $r_2 = r_3 = 0$, i.e. the separation vector is aligned with the x_1-axis. Choosing $D_{4,0} = D_{1111}$, eq. (A.9) then yields

$$D_{1111} = \widetilde{A}_1 + \widetilde{A}_2 + 3\widetilde{A}_3, \tag{A.10}$$

while $D_{2,2} = D_{1122}$ gives

$$D_{1122} = \widetilde{A}_2 + \widetilde{A}_3 \tag{A.11}$$

and $D_{0,4} = D_{2222}$ yields

$$D_{2222} = 3\widetilde{A}_3. \tag{A.12}$$

Thus, the three scalar functions $\widetilde{A}_1$, $\widetilde{A}_2$ and $\widetilde{A}_3$ are determined by the three tensor components D_{1111}, D_{1122} and D_{2222} and solving for them gives

$$\begin{aligned} \widetilde{A}_1 &= D_{1111} - 6D_{1122} + D_{2222}, \\ \widetilde{A}_2 &= D_{1122} - \frac{1}{3} D_{2222}, \\ \widetilde{A}_3 &= \frac{1}{3} D_{2222}. \end{aligned} \tag{A.13}$$

Next, $\partial^2 D_{ijkl} / \partial r_n^2$ depending on the scalar functions $\widetilde{A}_1$, $\widetilde{A}_2$, $\widetilde{A}_3$ and the separation vector r_i is derived. Thus, taking the derivative of the first term on

the r.h.s. of eq. (A.9),

$$\begin{aligned}\frac{\partial}{\partial r_n}\left(\widetilde{A}_1\frac{r_ir_jr_kr_l}{r^4}\right) &= \frac{r_ir_jr_kr_l}{r^4}\frac{\partial\widetilde{A}_1}{\partial r_n}\\ &+\widetilde{A}_1\left[\frac{r_ir_jr_k}{r^3}\left(\delta_{ln}-\frac{r_lr_n}{r^2}\right)\frac{1}{r}+\frac{r_ir_jr_l}{r^3}\left(\delta_{kn}-\frac{r_kr_n}{r^2}\right)\frac{1}{r}\right.\\ &\left.+\frac{r_ir_kr_l}{r^3}\left(\delta_{jn}-\frac{r_jr_n}{r^2}\right)\frac{1}{r}+\frac{r_jr_kr_l}{r^3}\left(\delta_{in}-\frac{r_ir_n}{r^2}\right)\frac{1}{r}\right]\\ &=\frac{r_ir_jr_kr_lr_n}{r^5}\frac{\partial D_1}{\partial r}\\ &+\frac{\widetilde{A}_1}{r}\left[\frac{r_ir_jr_k}{r^3}\left(\delta_{ln}-\frac{r_lr_n}{r^2}\right)+\frac{r_ir_jr_l}{r^3}\left(\delta_{kn}-\frac{r_kr_n}{r^2}\right)\right.\\ &\left.+\frac{r_ir_kr_l}{r^3}\left(\delta_{jn}-\frac{r_jr_n}{r^2}\right)+\frac{r_jr_kr_l}{r^3}\left(\delta_{in}-\frac{r_ir_n}{r^2}\right)\right].\end{aligned} \tag{A.14}$$

Taking the second derivative with respect to r_n and using eq. (A.6) and eq. (A.7) then results in

$$\begin{aligned}\frac{\partial^2}{\partial r_n^2}\left(\widetilde{A}_1\frac{r_ir_jr_kr_l}{r^4}\right) &= \frac{r_ir_jr_kr_l}{r^4}\left(\frac{\partial^2\widetilde{A}_1}{\partial r^2}+\frac{2}{r}\frac{\partial\widetilde{A}_1}{\partial r}\right)\\ &+\frac{2}{r^2}\widetilde{A}_1\left[\frac{r_kr_l}{r^2}\left(\delta_{ij}-\frac{r_ir_j}{r^2}\right)+\frac{r_jr_l}{r^2}\left(\delta_{ik}-\frac{r_ir_k}{r^2}\right)\right.\\ &+\frac{r_jr_k}{r^2}\left(\delta_{il}-\frac{r_ir_l}{r^2}\right)\\ &\left.+\frac{r_ir_l}{r^2}\left(\delta_{jk}-\frac{r_jr_k}{r^2}\right)+\frac{r_ir_k}{r^2}\left(\delta_{jl}-\frac{r_jr_l}{r^2}\right)\right.\\ &\left.+\frac{r_ir_j}{r^2}\left(\delta_{kl}-\frac{r_kr_l}{r^2}\right)\right]\\ &-\frac{8}{r^2}\widetilde{A}_1\frac{r_ir_jr_kr_l}{r^4}.\end{aligned} \tag{A.15}$$

Similarly, one finds for the second line of eq. (A.9)

$$\begin{aligned}
\frac{\partial^2}{\partial r_n^2}\Big[\widetilde{A}_2\Big(\delta_{ij}\frac{r_k r_l}{r^2} \;+\; \delta_{ik}\frac{r_j r_l}{r^2}+\delta_{il}\frac{r_j r_k}{r^2}+\delta_{jk}\frac{r_i r_l}{r^2}+\delta_{jl}\frac{r_i r_k}{r^2}+\delta_{kl}\frac{r_i r_j}{r^2}\Big)\Big] \\
= \Big(\delta_{ij}\frac{r_k r_l}{r^2}+\delta_{ik}\frac{r_j r_l}{r^2}+\delta_{il}\frac{r_j r_k}{r^2}+\delta_{jk}\frac{r_i r_l}{r^2} \\
+\;\delta_{jl}\frac{r_i r_k}{r^2}+\delta_{kl}\frac{r_i r_j}{r^2}\Big)\left(\frac{\partial^2 D_2}{\partial r^2}+\frac{2}{r}\frac{\partial \widetilde{A}_2}{\partial r}\right) \\
+\,2\frac{\widetilde{A}_2}{r^2}\Big[\delta_{ij}\left(\left(\delta_{kl}-\frac{r_k r_l}{r^2}\right)-2\frac{r_k r_l}{r^2}\right) \\
+\delta_{ik}\left(\left(\delta_{jl}-\frac{r_j r_l}{r^2}\right)-2\frac{r_j r_l}{r^2}\right) \\
+\;\delta_{il}\left(\left(\delta_{jk}-\frac{r_j r_k}{r^2}\right)-2\frac{r_j r_k}{r^2}\right) \\
+\delta_{jk}\left(\left(\delta_{il}-\frac{r_i r_l}{r^2}\right)-2\frac{r_j r_l}{r^2}\right) \\
+\;\delta_{jl}\left(\left(\delta_{ik}-\frac{r_i r_k}{r^2}\right)-2\frac{r_i r_k}{r^2}\right) \\
+\delta_{kl}\left(\left(\delta_{ij}-\frac{r_i r_j}{r^2}\right)-2\frac{r_i r_j}{r^2}.\right)\Big]
\end{aligned} \tag{A.16}$$

Finally, the third line of eq. (A.9) gives

$$\begin{aligned}
\frac{\partial^2}{\partial r_n^2}\Big[\widetilde{A}_3\left(\delta_{ij}\delta_{kl} \;+\delta_{ik}\delta_{jl}+\delta_{jk}\delta_{il}\right)\Big] \\
= \left(\delta_{ij}\delta_{kl}+\delta_{ik}\delta_{jl}+\delta_{jk}\delta_{il}\right)\left(\frac{\partial^2 \widetilde{A}_3}{\partial r^2}+\frac{2}{r}\frac{\partial \widetilde{A}_3}{\partial r}\right).
\end{aligned} \tag{A.17}$$

Now, adding eq. (A.15), eq. (A.16) and eq. (A.17) and substituting $i = j =$

$k = l = 1$ gives

$$\begin{aligned}\frac{\partial^2 D_{1111}}{\partial r_n^2} = &\left(\frac{\partial^2 \widetilde{A}_1}{\partial r^2} + \frac{2}{r}\frac{\partial D_1}{\partial r}\right) - \frac{8}{r^2}\widetilde{A}_1 \\ &+ 6\left(\frac{\partial^2 \widetilde{A}_2}{\partial r^2} + \frac{2}{r}\frac{\partial \widetilde{A}_2}{\partial r}\right) - \frac{24}{r^2}D_2 \\ &+ 3\left(\frac{\partial^2 \widetilde{A}_3}{\partial r^2} + \frac{2}{r}\frac{\partial \widetilde{A}_3}{\partial r}\right).\end{aligned} \tag{A.18}$$

Using the relations eq. (A.13) yields

$$\frac{\partial^2 D_{1111}}{\partial r_n^2} = \left(\frac{\partial^2 D_{1111}}{\partial r^2} + \frac{2}{r}\frac{\partial D_{1111}}{\partial r}\right) - \frac{8}{r^2}D_{1111} + \frac{24}{r^2}D_{1122}. \tag{A.19}$$

Setting $i = j = 1$, $k = l = 2$ in the summation of eq. (A.15), eq. (A.16) and eq. (A.17) yields

$$\begin{aligned}\frac{\partial^2 D_{1122}}{\partial r_n^2} = &\frac{2}{r^2}\widetilde{A}_1 + \left(\frac{\partial^2 \widetilde{A}_2}{\partial r^2} + \frac{2}{r}\frac{\partial D_2}{\partial r}\right) - \frac{2}{r^2}D_2 \\ &+ \left(\frac{\partial^2 \widetilde{A}_3}{\partial r^2} + \frac{2}{r}\frac{\partial \widetilde{A}_3}{\partial r}\right)\end{aligned} \tag{A.20}$$

and with the relations eq. (A.13)

$$\begin{aligned}\frac{\partial^2 D_{1122}}{\partial r_n^2} = &\left(\frac{\partial^2 D_{1122}}{\partial r^2} + \frac{2}{r}\frac{\partial D_{1122}}{\partial r}\right) + \frac{2}{r^2}D_{1111} - \frac{14}{r^2}D_{1122} \\ &+ \frac{8}{3r^2}D_{2222}.\end{aligned} \tag{A.21}$$

In the same way, setting $i = j = k = l = 2$ gives

$$\frac{\partial^2 D_{2222}}{\partial r_n^2} = \frac{12}{r^2}\widetilde{A}_2 + 3\left(\frac{\partial^2 \widetilde{A}_3}{\partial r^2} + \frac{2}{r}\frac{\partial \widetilde{A}_3}{\partial r}\right), \tag{A.22}$$

i.e. using eq. (A.13)

$$\frac{\partial^2 D_{2222}}{\partial r_n^2} = \left(\frac{\partial^2 D_{2222}}{\partial r^2} + \frac{2}{r}\frac{\partial D_{2222}}{\partial r} \right) + \frac{12}{r^2} D_{1122} - \frac{4}{r^2} D_{2222}. \tag{A.23}$$

We therefore have the Laplacian of the structure functions $D_{4,0} = D_{1111}$, $D_{2,2} = D_{1122}$ and $D_{0,4} = D_{2222}$ in agreement with table 3.2 and the matrix algorithm by Hill (2001).

The longitudinal (eq. (A.19)) and transverse equations (eq. (A.23)) have been compared and checked against DNS data. Specifically, the r.h.s. $\partial^2 D_{ijkl}/\partial r_n^2$ has been computed by rewriting

$$\begin{aligned} \frac{\partial^2 D_{1111}}{\partial r_n^2} = \frac{\partial^2 \left\langle (\Delta u_1)^4 \right\rangle}{\partial r_n^2} &= \frac{1}{2} \left\langle \left(\frac{\partial^2 (\Delta u_1)^4}{\partial x_n^2} + \frac{\partial^2 (\Delta u_1)^4}{\partial x_n'^2} \right) \right\rangle \\ &= 2 \left\langle (\Delta u_1)^3 \left(\frac{\partial^2 u_1}{\partial x_n^2} - \frac{\partial^2 u_1'}{\partial x_n'^2} \right) \right\rangle \\ &\quad + 6 \left\langle (\Delta u_1)^2 \left(\frac{\partial u_1}{\partial x_n}\frac{\partial u_1}{\partial x_n} + \frac{\partial u_1'}{\partial x_n'}\frac{\partial u_1'}{\partial x_n'} \right) \right\rangle, \end{aligned} \tag{A.24}$$

$$\begin{aligned} \frac{\partial^2 D_{2222}}{\partial r_n^2} &= 2 \left\langle (\Delta u_2)^3 \left(\frac{\partial^2 u_2}{\partial x_n^2} - \frac{\partial^2 u_2'}{\partial x_n'^2} \right) \right\rangle \\ &\quad + 6 \left\langle (\Delta u_2)^2 \left(\frac{\partial u_2}{\partial x_n}\frac{\partial u_2}{\partial x_n} + \frac{\partial u_2'}{\partial x_n'}\frac{\partial u_2'}{\partial x_n'} \right) \right\rangle, \end{aligned} \tag{A.25}$$

and compared with the results one obtains by taking the respective combination of derivatives of the structure functions with respect to r. Specifically, the l.h.s. of eq. (A.19) and eq. (A.23) have been evaluated by computing $D_{4,0} = \langle (\Delta u_1)^4 \rangle$, $D_{2,2} = \langle (\Delta u_1)^2 (\Delta u_2)^2 \rangle$ and $D_{0,4} = \langle (\Delta u_2)^4 \rangle$ as function of r from DNS and then using a finite difference scheme to calculate the first and second derivative $\partial D_{4,0}/\partial r$, $\partial^2 D_{4,0}/\partial r^2$ and so forth. Eq. (A.19) and eq. (A.24) are plotted in figure A.1, while eq. (A.23) and eq. (A.25) are plotted in figure A.2. We find very good agreement, also at larger r. It should be stressed that all derivatives and terms evaluated in chapters 3 to chapter 6 were computed similarly to the calculation of eq. (A.24) and eq. (A.25) where the derivatives computed using FFT and only the dashed red lines in figure A.1 and figure A.2 were produced employing a finite difference scheme.

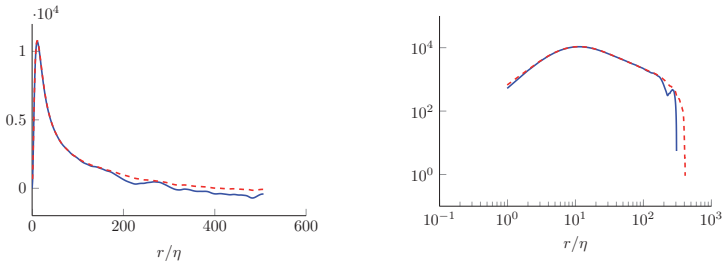

Figure A.1: Eq. (A.19) computed with a finite difference scheme (dashed red line) and eq. (A.24) computed using FFT from DNS (solid blue line) as function of r/η.

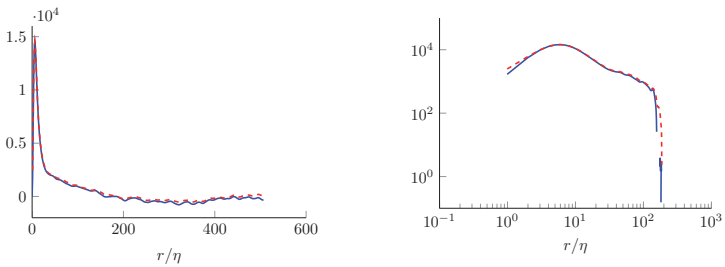

Figure A.2: Eq. (A.23) computed with a finite difference scheme (dashed red line) and eq. (A.25) computed using FFT from DNS (solid blue line) as function of r/η.

A.2 Fifth-order gradient

Here, we give the isotropic form for the gradient of a tensor of fifth order, first with interchangeable indices and second where only some of the indices may be interchanged. The first case corresponds to the transport terms in the fourth-order structure function equations as discussed in section 3.1.2; the second kind of tensor appears for the gradient of the structure function source terms when deriving the higher-order source term equations, cf section 3.1.3. Again, the same steps can be carried out for higher-order tensors.

Consider the general form of a fifth-order tensor A_{nijkl} of two-point type, cf. eq. (A.4),

$$\begin{aligned}
A_{nijkl} = {} & A_1 \frac{r_n}{r}\frac{r_i}{r}\frac{r_j}{r}\frac{r_k}{r}\frac{r_l}{r} + A_2\delta_{ni}\frac{r_j}{r}\frac{r_k}{r}\frac{r_l}{r} + A_3\delta_{nj}\frac{r_i}{r}\frac{r_k}{r}\frac{r_l}{r} \\
& + A_4\delta_{nk}\frac{r_i}{r}\frac{r_j}{r}\frac{r_l}{r} + A_5\delta_{nl}\frac{r_i}{r}\frac{r_j}{r}\frac{r_k}{r} \\
& + A_6\delta_{ij}\frac{r_n}{r}\frac{r_k}{r}\frac{r_l}{r} + A_7\delta_{ik}\frac{r_n}{r}\frac{r_j}{r}\frac{r_l}{r} \\
& + A_8\delta_{il}\frac{r_n}{r}\frac{r_j}{r}\frac{r_k}{r} + A_9\delta_{jk}\frac{r_n}{r}\frac{r_i}{r}\frac{r_l}{r} \\
& + A_{10}\delta_{jl}\frac{r_n}{r}\frac{r_i}{r}\frac{r_k}{r} + A_{11}\delta_{kl}\frac{r_n}{r}\frac{r_i}{r}\frac{r_j}{r} \\
& + A_{12}\delta_{ni}\delta_{jk}\frac{r_l}{r} + A_{13}\delta_{ni}\delta_{jl}\frac{r_k}{r} + A_{14}\delta_{ni}\delta_{kl}\frac{r_j}{r} \\
& + A_{15}\delta_{nj}\delta_{kl}\frac{r_i}{r} + A_{16}\delta_{nj}\delta_{ik}\frac{r_l}{r} + A_{17}\delta_{nj}\delta_{il}\frac{r_k}{r} \\
& + A_{18}\delta_{nk}\delta_{ij}\frac{r_l}{r} + A_{19}\delta_{nk}\delta_{il}\frac{r_j}{r} + A_{20}\delta_{nk}\delta_{jl}\frac{r_i}{r} \\
& + A_{21}\delta_{nl}\delta_{ij}\frac{r_k}{r} + A_{22}\delta_{nl}\delta_{ik}\frac{r_j}{r} + A_{23}\delta_{nl}\delta_{jk}\frac{r_i}{r} \\
& + A_{24}\delta_{ij}\delta_{kl}\frac{r_n}{r} + A_{25}\delta_{ik}\delta_{jl}\frac{r_n}{r} + A_{26}\delta_{il}\delta_{jk}\frac{r_n}{r}
\end{aligned} \tag{A.26}$$

where again A_i are scalar functions of the separation distance r.

A.2.1 Fourth-order structure function equation transport term

If $A_{nijkl} = \boldsymbol{D}_{[5]} = \langle \Delta u_n \Delta u_i \Delta u_j \Delta u_k \Delta u_l \rangle$, all indices are interchangeable and

$$\begin{aligned} A_1 &= \widetilde{A}_1 \\ A_2 = A_3 = A_4 = A_5 = A_6 = A_7 = A_8 = A_9 = A_{10} = A_{11} &= \widetilde{A}_2 \\ A_{12} = A_{13} = A_{14} = A_{15} = A_{16} = A_{17} = A_{18} = A_{19} &= A_{20} \\ = A_{21} = A_{22} = A_{23} = A_{24} = A_{25} = A_{26} &= \widetilde{A}_3. \end{aligned} \tag{A.27}$$

Inserting $D_{5,0} = D_{11111}$, $D_{3,2} = D_{11122}$ and $D_{1,4} = D_{12222}$ into eq. (A.26), one finds that the scalar functions

$$\begin{aligned} \widetilde{A}_1 &= D_{5,0} - 10D_{3,2} + 5D_{1,4} \\ \widetilde{A}_2 &= D_{3,2} - D_{1,4} \\ \widetilde{A}_3 &= \frac{1}{3} D_{1,4}, \end{aligned} \tag{A.28}$$

where again $r_i = (r, 0, 0)$ without loss of generality.

Inserting eq. (A.27) into eq. (A.26) and taking the derivative with respect to

r_n results in

$$\begin{aligned}
\frac{\partial A_{nijkl}}{\partial r_n} &= \left(\frac{\partial \widetilde{A}_1}{\partial r} + \frac{2}{r}\widetilde{A}_1 + 4\frac{\partial \widetilde{A}_2}{\partial r} - \frac{12}{r}\widetilde{A}_2\right)\frac{r_i r_j r_k r_l}{r^4} \\
&+ \left(\frac{\partial \widetilde{A}_2}{\partial r} + \frac{4}{r}\widetilde{A}_2 + 2\frac{\partial \widetilde{A}_3}{\partial r} - \frac{2}{r}\widetilde{A}_3\right)\delta_{ij}\frac{r_k r_l}{r^2} \\
&+ \left(\frac{\partial \widetilde{A}_2}{\partial r} + \frac{4}{r}\widetilde{A}_2 + 2\frac{\partial \widetilde{A}_3}{\partial r} - \frac{2}{r}\widetilde{A}_3\right)\delta_{ik}\frac{r_j r_l}{r^2} \\
&+ \left(\frac{\partial \widetilde{A}_2}{\partial r} + \frac{4}{r}\widetilde{A}_2 + 2\frac{\partial \widetilde{A}_3}{\partial r} - \frac{2}{r}\widetilde{A}_3\right)\delta_{il}\frac{r_j r_l}{r^2} \\
&+ \left(\frac{\partial \widetilde{A}_2}{\partial r} + \frac{4}{r}\widetilde{A}_2 + 2\frac{\partial \widetilde{A}_3}{\partial r} - \frac{2}{r}\widetilde{A}_3\right)\delta_{jk}\frac{r_i r_l}{r^2} \\
&+ \left(\frac{\partial \widetilde{A}_2}{\partial r} + \frac{4}{r}\widetilde{A}_2 + 2\frac{\partial \widetilde{A}_3}{\partial r} - \frac{2}{r}\widetilde{A}_3\right)\delta_{jl}\frac{r_i r_k}{r^2} \\
&+ \left(\frac{\partial \widetilde{A}_2}{\partial r} + \frac{4}{r}\widetilde{A}_2 + 2\frac{\partial \widetilde{A}_3}{\partial r} - \frac{2}{r}\widetilde{A}_3\right)\delta_{kl}\frac{r_i r_j}{r^2} \\
&+ \left(\frac{\partial \widetilde{A}_3}{\partial r} + \frac{6}{r}\widetilde{A}_3\right)\delta_{ij}\delta_{kl} + \left(\frac{\partial \widetilde{A}_3}{\partial r} + \frac{6}{r}\widetilde{A}_3\right)\delta_{ik}\delta_{jl} \\
&+ \left(\frac{\partial \widetilde{A}_3}{\partial r} + \frac{6}{r}\widetilde{A}_3\right)\delta_{il}\delta_{jk}.
\end{aligned} \tag{A.29}$$

where eq. (A.6) and eq. (A.7) were used. Then, setting $i = j = k = l = 1$, $i = j = 1, k = l = 2$ and $i = j = k = l = 2$ with the relations eq. (A.28), one has

$$\frac{\partial D_{n1111}}{\partial r_n} = \frac{\partial D_{5,0}}{\partial r} + \frac{2}{r}D_{5,0} - \frac{8}{r}D_{3,2} \tag{A.30}$$

$$\frac{\partial D_{n1122}}{\partial r_n} = \frac{\partial D_{3,2}}{\partial r} + \frac{4}{r}D_{3,2} - \frac{8}{3r}D_{1,4} \tag{A.31}$$

$$\frac{\partial D_{n2222}}{\partial r_n} = \frac{\partial D_{1,4}}{\partial r} + \frac{6}{r}D_{1,4}, \tag{A.32}$$

for the gradient $\boldsymbol{\nabla} \cdot \boldsymbol{D}_5$ in agreement with table 3.2 and the matrix algorithm

by Hill (2001).

A.2.2 Fourth-order dissipation source term equation transport term

Now, let the indices i, j, k, l be interchangeable, while n may *not* be interchanged with any other index, i.e. $A_{nijkl} = \langle \Delta u_n E_{ijkl} \rangle$, cf. section 3.1.3. This implies that

$$\begin{aligned} A_1 &= \widetilde{A}_1 \\ A_2 &= A_3 = A_4 = A_5 = \widetilde{A}_2 \\ A_6 &= A_7 = A_8 = A_9 = A_{10} = A_{11} = \widetilde{A}_3 \\ A_{12} &= A_{13} = A_{14} = A_{15} = A_{16} = A_{17} = A_{18} = A_{19} = A_{20} \\ &= A_{21} = A_{22} = A_{23} = \widetilde{A}_4 \\ A_{24} &= A_{25} = A_{26} = \widetilde{A}_5, \end{aligned} \tag{A.33}$$

i.e. the tensor is determined by five scalar functions (if n could be interchanged as well, there would be only three scalar functions, cf. eq. (A.27) above resulting in eq. (A.30) to eq. (A.32)).

In the next step, the scalar functions have to be chosen. Let again $r_1 = r$, $r_2 = r_3 = 0$ without loss of generality. Then,

$$\begin{aligned} A_{11111} &= \widetilde{A}_1 + 4\widetilde{A}_2 + 6\widetilde{A}_3 + 12\widetilde{A}_4 + 3\widetilde{A}_5 \\ A_{11122} &= \widetilde{A}_3 + 2\widetilde{A}_4 + 1\widetilde{A}_5 \\ A_{12222} &= 3\widetilde{A}_5 \\ A_{22111} &= \widetilde{A}_1 + 3\widetilde{A}_4 \\ A_{21222} &= 3\widetilde{A}_4 \end{aligned} \tag{A.34}$$

Other choices of components of A_{nijkl} would also be viable, leading to different

scalar functions. Solving for $\widetilde{A}_i$ then gives

$$\begin{aligned}
\widetilde{A}_1 &= A_{11111} - 6A_{11122} + A_{12222} - 4A_{22111} + 4A_{21222} \\
\widetilde{A}_2 &= A_{22111} - A_{21222} \\
\widetilde{A}_3 &= A_{11122} - \frac{2}{3}A_{21222} - \frac{1}{3}A_{12222} \\
\widetilde{A}_4 &= \frac{1}{3}A_{21222} \\
\widetilde{A}_5 &= \frac{1}{3}A_{12222}.
\end{aligned} \tag{A.35}$$

Here, $A_{11111} = \langle \Delta u_1 E_{4,0} \rangle$, $A_{11122} = \langle \Delta u_1 E_{2,2} \rangle$, $A_{1222} = \langle \Delta u_1 E_{0,4} \rangle$, $A_{22111} = \langle \Delta u_2 E_{3,1} \rangle$ and $A_{21222} = \langle \Delta u_2 E_{1,3} \rangle$.

Next, the derivative of the tensor with respect to r_n is computed resulting in

$$\begin{aligned}
\frac{\partial}{\partial r_n}\left(\widetilde{A}_1 \frac{r_n}{r}\frac{r_i}{r}\frac{r_j}{r}\frac{r_k}{r}\frac{r_l}{r}\right) &= \frac{r_n}{r}\frac{r_i}{r}\frac{r_j}{r}\frac{r_k}{r}\frac{r_l}{r}\left(\frac{\partial \widetilde{A}_1}{\partial r} + \frac{2}{r}\widetilde{A}_1\right) \\
\frac{\partial}{\partial r_n}\left(\widetilde{A}_2 \delta_{ni} r \frac{r_j}{r}\frac{r_k}{r}\frac{r_l}{r}\right) &= \frac{r_i}{r}\frac{r_j}{r}\frac{r_k}{r}\frac{r_l}{r}\frac{\partial \widetilde{A}_2}{\partial r} \\
&\quad + \widetilde{A}_2\left(\frac{r_k}{r}\frac{r_l}{r}\left(\delta_{ij} - \frac{r_i r_j}{r^2}\right)\frac{1}{r}\right. \\
&\quad + \frac{r_j}{r}\frac{r_l}{r}\left(\delta_{ik} - \frac{r_i r_k}{r^2}\right)\frac{1}{r} \\
&\quad \left. + \frac{r_j}{r}\frac{r_k}{r}\left(\delta_{il} - \frac{r_i r_l}{r^2}\right)\frac{1}{r}\right) \\
\frac{\partial}{\partial r_n}\left(\widetilde{A}_3 \delta_{ij}\frac{r_n}{r}\frac{r_k}{r}\frac{r_l}{r}\right) &= \delta_{ij}\frac{r_k}{r}\frac{r_l}{r}\frac{\partial \widetilde{A}_3}{\partial r} + \delta_{ij}\frac{r_k}{r}\frac{r_l}{r}\frac{2}{r}\widetilde{A}_3 \\
\frac{\partial}{\partial r_n}\left(\widetilde{A}_4 \delta_{ni}\delta_{jk}\frac{r_l}{r}\right) &= \delta_{jk}\frac{r_l}{r}\frac{r_i}{r}\frac{\partial \widetilde{A}_4}{\partial r} + \delta_{jk}\widetilde{A}_4\left(\delta_{il} - \frac{r_i r_l}{r^2}\right)\frac{1}{r} \\
\frac{\partial}{\partial r_n}\left(\widetilde{A}_5 \delta_{ij}\delta_{kl}\frac{r_n}{r}\right) &= \delta_{ij}\delta_{kl}\frac{\partial \widetilde{A}_5}{\partial r} + \delta_{ij}\delta_{kl}\frac{2}{r}\widetilde{A}_5
\end{aligned} \tag{A.36}$$

and similarly for the other terms, resulting in

$$\begin{aligned}
\frac{\partial A_{nijkl}}{\partial r_n} = &\left(\frac{\partial \widetilde{A}_1}{\partial r} + \frac{2}{r}\widetilde{A}_1 + 4\frac{\partial \widetilde{A}_2}{\partial r} - \frac{12}{r}\widetilde{A}_2\right)\frac{r_i r_j r_k r_l}{r^4} \\
&+ \left(\frac{2}{r}\widetilde{A}_2 + \frac{\partial \widetilde{A}_3}{\partial r} + \frac{2}{r}\widetilde{A}_3 + 2\frac{\partial \widetilde{A}_4}{\partial r} - \frac{2}{r}\widetilde{A}_4\right)\delta_{ij}\frac{r_k r_l}{r^2} \\
&+ \left(\frac{2}{r}\widetilde{A}_2 + \frac{\partial \widetilde{A}_3}{\partial r} + \frac{2}{r}\widetilde{A}_3 + 2\frac{\partial \widetilde{A}_4}{\partial r} - \frac{2}{r}\widetilde{A}_4\right)\delta_{ik}\frac{r_j r_l}{r^2} \\
&+ \left(\frac{2}{r}\widetilde{A}_2 + \frac{\partial \widetilde{A}_3}{\partial r} + \frac{2}{r}\widetilde{A}_3 + 2\frac{\partial \widetilde{A}_4}{\partial r} - \frac{2}{r}\widetilde{A}_4\right)\delta_{il}\frac{r_j r_l}{r^2} \\
&+ \left(\frac{2}{r}\widetilde{A}_2 + \frac{\partial \widetilde{A}_3}{\partial r} + \frac{2}{r}\widetilde{A}_3 + 2\frac{\partial \widetilde{A}_4}{\partial r} - \frac{2}{r}\widetilde{A}_4\right)\delta_{jk}\frac{r_i r_l}{r^2} \\
&+ \left(\frac{2}{r}\widetilde{A}_2 + \frac{\partial \widetilde{A}_3}{\partial r} + \frac{2}{r}\widetilde{A}_3 + 2\frac{\partial \widetilde{A}_4}{\partial r} - \frac{2}{r}\widetilde{A}_4\right)\delta_{jl}\frac{r_i r_k}{r^2} \\
&+ \left(\frac{2}{r}\widetilde{A}_2 + \frac{\partial \widetilde{A}_3}{\partial r} + \frac{2}{r}\widetilde{A}_3 + 2\frac{\partial \widetilde{A}_4}{\partial r} - \frac{2}{r}\widetilde{A}_4\right)\delta_{kl}\frac{r_i r_j}{r^2} \\
&+ \left(\frac{4}{r}\widetilde{A}_4 + \frac{\partial \widetilde{A}_5}{\partial r} + \frac{2}{r}\widetilde{A}_5\right)\delta_{ij}\delta_{kl} \\
&+ \left(\frac{4}{r}\widetilde{A}_4 + \frac{\partial \widetilde{A}_5}{\partial r} + \frac{2}{r}\widetilde{A}_5\right)\delta_{ik}\delta_{jl} \\
&+ \left(\frac{4}{r}\widetilde{A}_4 + \frac{\partial \widetilde{A}_5}{\partial r} + \frac{2}{r}\widetilde{A}_5\right)\delta_{il}\delta_{jk}.
\end{aligned} \tag{A.37}$$

Therefore,

$$\begin{aligned}
\frac{\partial A_{n1111}}{\partial r_n} = &\frac{\partial \widetilde{A}_1}{\partial r} + \frac{2}{r}\widetilde{A}_1 + 4\frac{\partial \widetilde{A}_2}{\partial r} + 6\frac{\partial \widetilde{A}_3}{\partial r} + \frac{12}{r}\widetilde{A}_3 + 12\frac{\partial \widetilde{A}_4}{\partial r} + 3\frac{\partial \widetilde{A}_5}{\partial r} \\
&+ \frac{6}{r}\widetilde{A}_5
\end{aligned} \tag{A.38}$$

and inserting $\widetilde{A_i}$

$$\frac{\partial \langle \Delta u_n E_{4,0} \rangle}{\partial r_n} = \frac{\partial \langle \Delta u_1 E_{4,0} \rangle}{\partial r} + \frac{2}{r} \langle \Delta u_1 E_{4,0} \rangle - \frac{8}{r} \langle \Delta u_2 E_{3,1} \rangle . \tag{A.39}$$

Similarly,

$$\frac{\partial A_{n1122}}{\partial r_n} = \frac{2}{r}\widetilde{A}_2 + \frac{\partial \widetilde{A}_3}{\partial r} + \frac{2}{r}\widetilde{A}_3 + 2\frac{\partial \widetilde{A}_4}{\partial r} + \frac{2}{r}\widetilde{A}_4 + \frac{\partial \widetilde{A}_5}{\partial r} + \frac{2}{r}\widetilde{A}_5 \tag{A.40}$$

i.e.

$$\frac{\partial \langle \Delta u_n E_{2,2} \rangle}{\partial r_n} = \frac{\partial \langle \Delta u_1 E_{2,2} \rangle}{\partial r} + \frac{2}{r} \langle \Delta u_1 E_{2,2} \rangle + \frac{2}{r} \langle \Delta u_2 E_{3,1} \rangle - \frac{8}{3r} \langle \Delta u_2 E_{1,3} \rangle \tag{A.41}$$

and

$$\frac{\partial A_{n1122}}{\partial r_n} = 3\left(\frac{4}{r}\widetilde{A}_4 + \frac{\partial \widetilde{A}_5}{\partial r} + \frac{2}{r}\widetilde{A}_5\right) \tag{A.42}$$

resulting in

$$\frac{\partial \langle \Delta u_n E_{0,4} \rangle}{\partial r_n} = \frac{\partial \langle \Delta u_1 E_{0,4} \rangle}{\partial r} + \frac{2}{r} \langle \Delta u_1 E_{0,4} \rangle + \frac{4}{r} \langle \Delta u_2 E_{1,3} \rangle . \tag{A.43}$$

A.3 Divergence and Laplacian of the odd-order trace equations

Here, the divergence and the Laplacian of the trace equations are briefly discussed. Note that for odd N, a more general equation is

$$\frac{\partial}{\partial t}\left\langle \Delta u_j \left[(\Delta u_k)^2\right]^{(N-1)/2} \right\rangle + \frac{\partial}{\partial r_i}\left\langle \Delta u_i \Delta u_j \left[(\Delta u_k)^2\right]^{(N-1)/2} \right\rangle = \dots \tag{A.44}$$

which is a transport equation for the two-point vector $\langle \Delta u_j [(\Delta u_k)^2]^{(N-1)/2} \rangle$ and contracting with r_j/r then yields a transport equation for

$$\frac{r_j}{r}\left\langle \Delta u_j \left[(\Delta u_k)^2\right]^{(N-1)/2} \right\rangle = D_{[N]}. \tag{A.45}$$

This is equivalent to multiplying the odd-order longitudinal, mixed and transverse equations with the respective prefactors given in table 3.6 and summing up, e.g. for $N = 5$

$$\frac{\partial D_{[5]}}{\partial t} = \frac{\partial}{\partial t}\left\langle \Delta u_1 \left[(\Delta u_j)^2\right]^2 \right\rangle = \frac{\partial D_{5,0}}{\partial t} + 4\frac{\partial D_{3,2}}{\partial t} + \frac{8}{3}\frac{\partial D_{1,4}}{\partial t} = \frac{r_i}{r}\frac{\partial}{\partial t}\left\langle \Delta u_i \left[(\Delta u_j)^2\right]^2 \right\rangle, \quad \text{(A.46)}$$

because we have chosen $r_i = (r, 0, 0)$ without loss of generality.

A.3.1 Divergence

In the odd-order trace equations, the transport term is a component of the more general tensor $\partial(\langle \Delta u_i \Delta u_j [(\Delta u_k)^2]^{(N-1)/2}\rangle)/\partial r_i$, i.e. corresponds to the divergence of a two-point tensor

$$A_{ij} = C_1 \frac{r_i}{r}\frac{r_j}{r} + C_2 \delta_{ij}, \quad \text{(A.47)}$$

where isotropy is assumed, C_1 and C_2 are scalar functions depending on r and δ_{ij} is the Kronecker symbol, $\delta_{ij} = 1$ if $i = j$ and $\delta_{ij} = 0$ otherwise. Thus,

$$\frac{\partial A_{ij}}{\partial r_i} = \frac{\partial}{\partial r_i}\left(C_1 \frac{r_i}{r}\frac{r_j}{r} + C_2 \delta_{ij}\right) = \frac{r_j}{r}\left(\frac{\partial C_1}{\partial r} + \frac{2}{r}C_1 + \frac{\partial C_2}{\partial r}\right), \quad \text{(A.48)}$$

where the relations

$$\frac{\partial}{\partial r_i}\left(\frac{r_j}{r}\right) = \frac{1}{r}\left(\delta_{ij} - \frac{r_i}{r}\frac{r_j}{r}\right), \quad \frac{\partial}{\partial r_i}\left(\frac{r_i}{r}\right) = \frac{2}{r}, \quad \frac{\partial C}{\partial r_i} = \frac{r_i}{r}\frac{\partial C}{\partial r} \quad \text{(A.49)}$$

were used. Contracting with r_j/r then gives

$$\frac{r_j}{r}\frac{\partial A_{ij}}{\partial r_i} = \frac{\partial C_1}{\partial r} + \frac{2}{r}C_1 + \frac{\partial C_2}{\partial r}. \quad \text{(A.50)}$$

From eq. (A.47),

$$\begin{aligned} A_{11} &= \langle (\Delta u_1)^2 [(\Delta u_k)^2]^{(N-1)/2}\rangle = C_1 + C_2, \\ A_{22} &= \langle (\Delta u_2)^2 [(\Delta u_k)^2]^{(N-1)/2}\rangle = C_2 \end{aligned} \quad \text{(A.51)}$$

and therefore

$$\frac{r_j}{r}\frac{\partial A_{ij}}{\partial r_i} = \frac{\partial A_{11}}{\partial r} + \frac{2}{r}\left(A_{11} - A_{22}\right), \tag{A.52}$$

which has the same form as the second-order structure function relation stemming from continuity as expected. Consequently,

$$\begin{aligned}\frac{r_j}{r}\frac{\partial}{\partial r_i}\left\langle \Delta u_i \Delta u_j \left[(\Delta u_k)^2\right]^{(N-1)/2}\right\rangle &= \frac{\partial}{\partial r}\left\langle (\Delta u_1)^2 \left[(\Delta u_k)^2\right]^{(N-1)/2}\right\rangle \\ &+ \frac{2}{r}\left\langle (\Delta u_1)^2 \left[(\Delta u_k)^2\right]^{(N-1)/2}\right\rangle \\ &- \frac{2}{r}\left\langle (\Delta u_2)^2 \left[(\Delta u_k)^2\right]^{(N-1)/2}\right\rangle. \end{aligned} \tag{A.53}$$

A.3.2 Laplacian

The Laplacian in the odd-order structure function trace equations is given by $\partial\langle \Delta u_i (\Delta u_k)^{N-1}\rangle/\partial r_n^2$ which is the Laplacian of a two-point vector. Assuming isotropy, this vector can be written as

$$A_i = C_1 \frac{r_i}{r}, \tag{A.54}$$

where again C_1 is a scalar function. Therefore using the relations given in eq. (A.49),

$$\begin{aligned}\frac{\partial}{\partial r_n^2}\left\langle \Delta u_i \left[(\Delta u_k)^2\right]^{(N-1)/2}\right\rangle &= \frac{\partial^2}{\partial r_n^2}\left(C_1 \frac{r_i}{r}\right) \\ &= \frac{r_i}{r}\left(\frac{\partial^2 C_1}{\partial r^2} + \frac{2}{r}\frac{\partial C_1}{\partial r} - \frac{2}{r^2}C_1\right) \end{aligned} \tag{A.55}$$

and contracting with r_i/r then yields

$$\begin{aligned}\frac{r_i}{r}\frac{\partial}{\partial r_n^2}\left\langle \Delta u_i \left[(\Delta u_k)^2\right]^{(N-1)/2}\right\rangle &= \frac{\partial^2 C_1}{\partial r^2} + \frac{2}{r}\frac{\partial C_1}{\partial r} - \frac{2}{r^2}C_1 \\ &= \frac{1}{r^2}\left[\frac{\partial}{\partial r}\left(r^2 \frac{\partial C_1}{\partial r}\right) - 2C_1\right] \end{aligned} \tag{A.56}$$

where due to eq. (A.54)

$$C_1 = \left\langle \Delta u_1 \left[(\Delta u_k)^2 \right]^{(N-1)/2} \right\rangle = D_{[N]} \tag{A.57}$$

for odd N.

Appendix B

Source term closures

Here, we briefly sketch possible closures for the dissipation source terms and the pressure source terms. Of course, the approaches presented here are only two of many possible and viable closures and remain qualitative. In the following, $\langle \widehat{E}_N \rangle$ and $\langle \widehat{T}_N \rangle$ are not necessarily the full source terms $\langle \boldsymbol{E}_N \rangle$ and $\langle \boldsymbol{T}_N \rangle$ but may be some of their components. Similarly, $\widehat{\Delta u}$ and $\widehat{D}_N$ may refer to any suitable velocity difference or structure function of order N.

B.1 dissipation source term

From eq. (3.14), the dissipation source terms have the form

$$\left\langle \widehat{E}_N \right\rangle \sim \left\langle \left(\widehat{\Delta u} \right)^{N-2} (\varepsilon + \varepsilon') \right\rangle . \tag{B.1}$$

In the viscous range $r \to 0$, $\langle \widehat{E}_N \rangle \sim \langle \varepsilon^{N/2} \rangle \nu^{1-N/2} r^{N-2}$ and one would have

$$\left\langle \widehat{E}_N \right\rangle \sim \frac{\widehat{D}_N}{\widehat{D}_2} \langle \varepsilon \rangle . \tag{B.2}$$

This gives the correct result $\widehat{D}_N \sim \langle \varepsilon^{N/2} \rangle \nu^{-N/2} r^N$ for the structure functions after integrating twice as seen from the balance $\nu \nabla^2 \widehat{D}_N \sim \widehat{E}_N$ for $r \to 0$, cf. eq. (4.86)[†].

On the other hand, it has been found by Nakano et al. (2003), that in the inertial range the ratio

$$\frac{r \left\langle \widehat{E}_N \right\rangle}{\widehat{D}_{N+1}} \sim const. \tag{B.3}$$

[†]I.e. $\langle \varepsilon \rangle$ is cancelled out in eq. (B.2) by $\widehat{D}_2 \sim (\langle \varepsilon \rangle / \nu) r^2$.

is constant, see also section 5.1. From eq. (B.2), in the viscous range $r \to 0$, one has

$$\frac{r\left\langle \widehat{E}_N \right\rangle}{\widehat{D}_{N+1}} \sim \frac{\widehat{D}_N}{\widehat{D}_2} \frac{r\left\langle \varepsilon \right\rangle}{\widehat{D}_{N+1}} \tag{B.4}$$

and inserting the results eq. (4.86) for $r \to 0$ yields

$$\frac{r\left\langle \widehat{E}_N \right\rangle}{\widehat{D}_{N+1}} \sim \frac{\nu^{3/2}\left\langle \varepsilon^{N/2} \right\rangle}{\left\langle \varepsilon^{(N+1)/2} \right\rangle} r^{-2}. \tag{B.5}$$

Thus merging both eq. (B.3) and eq. (B.5),

$$\frac{r\left\langle \widehat{E}_N \right\rangle}{\widehat{D}_{N+1}} \sim A_N \left(\frac{\nu^{3/2}\left\langle \varepsilon^{N/2} \right\rangle}{\left\langle \varepsilon^{(N+1)/2} \right\rangle} r^{-2} + \delta_N \right) \tag{B.6}$$

where A_N and δ_N are model parameters. This closure captures the viscous and inertial range behaviour of $\langle \widehat{E}_N \rangle$, but may not be accurate in the transitional region between the two regimes.

B.2 Pressure source term

From eq. (3.13), the pressure source terms are given by

$$\begin{aligned}
\left\langle \widehat{T}_N \right\rangle &\sim \left\langle \left(\widehat{\Delta u} \right)^{N-1} \left(\frac{\partial p}{\partial x_{(k)}} - \frac{\partial p'}{\partial x'_{(k)}} \right) \right\rangle \\
&\sim \mathcal{A}_N(r) \widehat{D}_{N-1} \left\langle \left(\frac{\partial p}{\partial x_{(k)}} - \frac{\partial p'}{\partial x'_{(k)}} \right)^2 \right\rangle^{1/2} \\
&\sim \mathcal{A}_N(r) \widehat{D}_{N-1} \left[\left\langle \left(\frac{\partial p}{\partial x_{(k)}} \right)^2 \right\rangle - \left\langle \left(\frac{\partial p}{\partial x_{(k)}} \frac{\partial p'}{\partial x'_{(k)}} \right) \right\rangle \right]^{1/2} \\
&\sim \mathcal{A}_N(r) \widehat{D}_{N-1} \left(C_\chi \chi - A_{(kk)} \right)^{1/2},
\end{aligned} \tag{B.7}$$

where C_χ is a constant and $\mathcal{A}_N(r)$ depends on r and possibly the Reynolds number. Here, there is no summation over (k) and (kk) as indicated by the brackets, i.e. $\partial p/\partial x_{(k)}$ is a suitable pressure gradient. As shown by Hill and

Wilczak (1995), χ is given by

$$\chi = 4 \int_0^\infty r^{-3} \left[D_{4,0} + D_{0,4} - 6D_{2,2} \right] \mathrm{d}r \tag{B.8}$$

and $A_{(kk)}$ by

$$\begin{aligned} A_{11} = \frac{\chi}{3} &- \frac{1}{6} \frac{\partial^2 D_{4,0}}{\partial r^2} - \frac{2}{3r} \frac{\partial}{\partial r} \left(D_{4,0} - 3D_{2,2} \right) \\ &- \frac{2}{3r^2} \left(D_{4,0} + 2D_{0,4} - 9D_{2,2} \right) \\ &- \frac{4}{3} \int_0^r y^{-3} \left(D_{4,0} + D_{0,4} - 6D_{2,2} \right) \mathrm{d}y \end{aligned} \tag{B.9}$$

and

$$\begin{aligned} A_{22} = A_{33} = \frac{\chi}{3} &- \frac{1}{6r} \frac{\partial D_{4,0}}{\partial r} - \frac{2}{3r^2} \left(D_{4,0} - 3D_{2,2} \right) \\ &- \frac{4}{3} \int_0^r y^{-3} \left(D_{4,0} + D_{0,4} - 6D_{2,2} \right) \mathrm{d}y. \end{aligned} \tag{B.10}$$

Thus, the pressure difference is determined by the fourth-order structure functions and the pressure source terms are closed if the prefactors $\mathcal{A}_N(r)$ and the constants C_χ are given. Noticeably, inserting this closure in the system of structure function equations then results in a set of integro-differential equations. The appearance of the integrals from 0 to r and from 0 to ∞ in eq. (B.8), eq. (B.9) and eq. (B.10) is not that surprising considering the nature of pressure in incompressible flows, cf. eq. (1.7). Nevertheless, numerically solving coupled integro-differential equations is expensive and cumbersome and a different closure for the pressure source terms seems desirable.

References

Anselmet, F., Gagne, Y., Hopfinger, E. J., and Antonia, R. A. (1984). "High-order velocity structure functions in turbulent shear flows". *J. Fluid Mech* 140 (63), pp. 63–89.

Antonia, R. A. and Burattini, P. (2006). "Approach to the 4/5 law in homogeneous isotropic turbulence". *Journal of Fluid Mechanics* 550 (1), pp. 175–184.

Antonia, R. A., Pearson, B., and Zhou, T. (2000). "Reynolds number dependence of second-order velocity structure functions". *Physics of Fluids* 12 (11), pp. 3000–3006.

Aris, R. (1962). *Vectors, tensors, and the basic equations of fluid mechanics*. Prentice-Hall (Englewood Cliffs, NJ).

Attili, A. and Bisetti, F. (2012). "Statistics and scaling of turbulence in a spatially developing mixing layer at $Re_\lambda = 250$". *Physics of Fluids (1994-present)* 24 (3), p. 035109.

Batchelor, G. K. (1959). "Small-scale variation of convected quantities like temperature in turbulent fluid Part 1. General discussion and the case of small conductivity". *Journal of Fluid Mechanics* 5 (1), pp. 113–133.

Batchelor, G. K., Howells, I. D., and Townsend, A. A. (1959). "Small-scale variation of convected quantities like temperature in turbulent fluid Part 2. The case of large conductivity". *Journal of Fluid Mechanics* 5 (1), pp. 134–139.

Batchelor, G. K. (1967). *An introduction to fluid dynamics*. Cambridge University Press.

Benzi, R., Ciliberto, S., Tripiccione, R., Baudet, C., Massaioli, F., and Succi, S. (1993). "Extended self-similarity in turbulent flows". *Physical Review E* 48 (1), R29–R32.

Benzi, R., Biferale, L., and Toschi, F. (1998). "Multiscale velocity correlations in turbulence". *Physical Review Letters* 80 (15), pp. 3244–3247.

Benzi, R., Ciliberto, S., Baudet, C., and Chavarria, G. R. (1995). "On the scaling of three-dimensional homogeneous and isotropic turbulence". *Physica D: Nonlinear Phenomena* 80 (4), pp. 385–398.

Betchov, R. (1956). "An inequality concerning the production of vorticity in isotropic turbulence". *Journal of Fluid Mechanics* 1 (5), pp. 497–504.

Boratav, O. N. and Pelz, R. B. (1997). "Structures and structure functions in the inertial range of turbulence". *Physics of Fluids (1994-present)* 9 (5), pp. 1400–1415.

Boschung, J., Gauding, M., Hennig, F., Denker, D., and Pitsch, H. (2016a). "Finite Reynolds number corrections of the 4/5 law for decaying turbulence". *Physical Review Fluids* 1 (6), p. 064403.

Boschung, J., Peters, N., Laizet, S., and Vassilicos, J. (2016b). "Streamlines in stationary homogeneous isotropic turbulence and fractal-generated turbulence". *Fluid Dynamics Research* 48 (2), p. 021403.

Boschung, J., Schaefer, P., Peters, N., and Meneveau, C. (2014). "The local topology of stream- and vortex lines in turbulent flows". *Physics of Fluids (1994-present)* 26 (4), p. 045107.

Boschung, J. (2015). "Exact relations between the moments of dissipation and longitudinal velocity derivatives in turbulent flows". *Physical Review E* 92 (4), p. 043013.

Boschung, J., Hennig, F., Denker, D., Pitsch, H., and Hill, R. J. (2017a). "Analysis of structure function equations up to the seventh order". *Journal of Turbulence*. DOI: 10.1080/14685248.2017.1346377.

Boschung, J., Hennig, F., Denker, D., Pitsch, H., and Hill, R. J. (2017b). "Ratios of same-order moments of dissipation, pseudo-dissipation and dissipation surrogates in homogeneous isotropic turbulence". *submitted to Journal of Turbulence*.

Boschung, J., Hennig, F., Gauding, M., Pitsch, H., and Peters, N. (2016c). "Generalised higher-order Kolmogorov scales". *Journal of Fluid Mechanics* 794, pp. 233–251.

Boschung, J., Pitsch, H., and Hill, R. J. (2017c). "Balances of structure function equations and their traces for the second to seventh order for homogeneous, isotropic turbulence". *will be uploaded to arXive.org*.

Braun, W., De Lillo, F., and Eckhardt, B. (2006). "Geometry of particle paths in turbulent flows". *Journal of Turbulence* 7, N62.

Chen, S., Doolen, G. D., Kraichnan, R. H., and She, Z.-S. (1993). "On statistical correlations between velocity increments and locally averaged dissipation in homogeneous turbulence". *Physics of Fluids A: Fluid Dynamics (1989-1993)* 5.2, pp. 458–463.

Chen, S., Doolen, G. D., Kraichnan, R. H., and Wang, L.-P. (1995). "Is the Kolmogorov refined similarity relation dynamic or kinematic?" *Physical review letters* 74.10, p. 1755.

Chen, S., Sreenivasan, K. R., Nelkin, M., and Cao, N. (1997). "Refined similarity hypothesis for transverse structure functions in fluid turbulence". *Physical Review Letters* 79 (12), pp. 2253–2256.

Chong, M. S., Perry, A. E., and Cantwell, B. J. (1990). "A general classification of three-dimensional flow fields". *Physics of Fluids* 2 (5), pp. 408–420.

Danaila, L., Anselmet, F., Zhou, T., and Antonia, R. A. (1999). "A generalization of Yaglom's equation which accounts for the large-scale forcing in heated decaying turbulence". *Journal of Fluid Mechanics* 391, pp. 359–372.

Danaila, L., Anselmet, F., Zhou, T., and Antonia, R. A. (2001). "Turbulent energy scale budget equations in a fully developed channel flow". *Journal of Fluid Mechanics* 430, pp. 87–109.

Danaila, L., Anselmet, F., and Zhou, T. (2004). "Turbulent energy scale-budget equations for nearly homogeneous sheared turbulence". *Flow, Turbulence and Combustion* 72 (2), pp. 287–310.

Davidson, P. A. (2004). *Turbulence: An Introduction for Scientists and Engineers*. Oxford University Press.

Donzis, D. A., Yeung, P. K., and Sreenivasan, K. R. (2008). "Dissipation and enstrophy in isotropic turbulence: Resolution effects and scaling in direct numerical simulations". *Physics of Fluids (1994-present)* 20 (4), p. 045108.

Dubrulle, B. (1994). "Intermittency in fully developed turbulence: Log-Poisson statistics and generalized scale covariance". *Physical Review Letters* 73 (7), pp. 959–962.

Eswaran, V. and Pope, S. B. (1988). "Direct numerical simulations of the turbulent mixing of a passive scalar". *Physics of Fluids* 31 (3), pp. 506–520.

Falkovich, G., Fouxon, I., and Oz, Y. (2010). "New relations for correlation functions in Navier–Stokes turbulence". *Journal of Fluid Mechanics* 644, pp. 465–472.

Frisch, U. and Vergassola, M. (1991). "A prediction of the multifratal model: the intermediate dissipation range". *EPL (Europhyics Letters)* 14 (5), pp. 439–444.

Frisch, U. (1995). *Turbulence: the legacy of A. N. Kolmogorov*. Cambridge university press.

Frisch, U., Sulem, P.-L., and Nelkin, M. (1978). "A simple dynamical model of intermittent fully developed turbulence". *Journal of Fluid Mechanics* 87 (04), pp. 719–736.

Gagne, Y., Castaing, B., Baudet, C., and Malécot, Y. (2004). "Reynolds dependence of third-order velocity structure functions". *Physics of Fluids (1994-present)* 16 (2), pp. 482–485.

Gampert, M., Boschung, J., Hennig, F., Gauding, M., and Peters, N. (2014). "The vorticity versus the scalar criterion for the detection of the turbulent/non-turbulent interface". *Journal of Fluid Mechanics* 750, pp. 578–596.

Gampert, M., Goebbert, J. H., Schaefer, P., Gauding, M., Peters, N., Aldudak, F., and Oberlack, M. (2011). "Extensive strain along gradient trajectories in the turbulent kinetic energy field". *New Journal of Physics* 13 (4), p. 043012.

Gauding, M. (2014). "Statistics and Scaling Laws of Turbulent Scalar Mixing at High Reynolds Numbers". PhD thesis. RWTH Aachen University.

Gomes-Fernandes, R., Ganapathisubramani, B., and Vassilicos, J. C. (2015). "The energy cascade in near-field non-homogeneous non-isotropic turbulence". *Journal of Fluid Mechanics* 771, pp. 676–705.

Gotoh, T. and Nakano, T. (2003). "Role of pressure in turbulence". *Journal of Statistical Physics* 113 (5), pp. 855–874.

Gotoh, T., Fukayama, D., and Nakano, T. (2002). "Velocity field statistics in homogeneous steady turbulence obtained using a high-resolution direct numerical simulation". *Physics of Fluids* 14 (3), pp. 1065–1081.

Grauer, R., Homann, H., and Pinton, J.-F. (2012). "Longitudinal and transverse structure functions in high-Reynolds-number turbulence". *New Journal of Physics* 14 (6), p. 063016.

Grossmann, S., Lohse, D., and Reeh, A. (1997). "Application of extended self-similarity in turbulence". *Physical Review E* 56 (5), pp. 5473–5478.

Gylfason, A., Ayyalasomayajula, S., and Warhaft, Z. (2004). "Intermittency, pressure and acceleration statistics from hot-wire measurements in wind-tunnel turbulence". *Journal of Fluid Mechanics* 501, pp. 213–229.

Hennig, F., Boschung, J., and Peters, N. (2016). "Statistical Description of Streamline Segments in a Turbulent Channel Flow with a Wavy Wall". *New Results in Numerical and Experimental Fluid Mechanics X*. Ed. by A. Dillmann, G. Heller, E. Krämer, C. Wagner, and C. Breitsamter. Springer International Publishing, pp. 135–143.

Hierro, J. and Dopazo, C. (2003). "Fourth-order statistical moments of the velocity gradient tensor in homogeneous, isotropic turbulence". *Physics of Fluids (1994-present)* 15 (11), pp. 3434–3442.

Hill, R. J. (1997). "Applicability of Kolmogorov's and Monin's equations of turbulence". *Journal of Fluid Mechanics* 353, pp. 67–81.

Hill, R. J. (2001). "Equations relating structure functions of all orders". *Journal of Fluid Mechanics* 434, pp. 379–388.

Hill, R. J. (2002). "Exact second-order structure-function relationships". *Journal of Fluid Mechanics* 468, pp. 317–326.

Hill, R. J. (2006). “Opportunities for use of exact statistical equations”. *Journal of Turbulence* 7, N43.
Hill, R. J. and Boratav, O. N. (2001). “Next-order structure-function equations”. *Physics of Fluids* 13 (1), pp. 276–283.
Hill, R. J. and Wilczak, J. M. (1995). “Pressure structure functions and spectra for locally isotropic turbulence”. *Journal of Fluid Mechanics* 296, pp. 247–269.
Hinze, J. O. (1975). *Turbulence*. McGraw-Hill.
Hosokawa, I. (2007). “A paradox concerning the refined similarity hypothesis of Kolmogorov for isotropic turbulence”. *Progress of Theoretical Physics* 118.1, pp. 169–173.
Hou, T. Y. and Li, R. (2007). “Computing nearly singular solutions using pseudo-spectral methods”. *Journal of Computational Physics* 226 (1), pp. 379–397.
Hurst, D. and Vassilicos, J. C. (2007). “Scalings and decay of fractal-generated turbulence”. *Physics of Fluids (1994-present)* 19 (3), p. 035103.
Ishida, T., Davidson, P. A., and Kaneda, Y. (2006). “On the decay of isotropic turbulence”. *Journal of Fluid Mechanics* 564, pp. 455–475.
Ishihara, T., Kaneda, Y., Yokokawa, M., Itakura, K., and Uno, A. (2007). “Small-scale statistics in high-resolution direct numerical simulation of turbulence: Reynolds number dependence of one-point velocity gradient statistics”. *Journal of Fluid Mechanics* 592, pp. 335–366.
Ishihara, T., Gotoh, T., and Kaneda, Y. (2009). “Study of high-Reynolds number isotropic turbulence by direct numerical simulation”. *Annual Review of Fluid Mechanics* 41, pp. 165–180.
Ishihara, T., Morishita, K., Yokokawa, M., Uno, A., and Kaneda, Y. (2016). “Energy spectrum in high-resolution direct numerical simulations of turbulence”. *Physical Review Fluids* 1 (8), p. 082403.
Jiménez, J., Wray, A., Saffman, P., and Rogallo, R. (1993). “The structure of intense vorticity in isotropic turbulence”. *Journal of Fluid Mechanics* 255, pp. 65–90.
Kaneda, Y. and Morishita, K. (2013). “Small-scale Statistics and Structure of Turbulence - in the Light of High Resolution Direct Numerical Simulation”. *Ten Chapters in Turbulence*. Ed. by P. A. Davidson, Y. Kaneda, and K. R. Sreenivasan. Cambridge University Press, pp. 1–42.
Kármán, T. de and Howarth, L. (1938). “On the Statistical Theory of Isotropic Turbulence”. *Proceedings of the Royal Society of London. Series A-Mathematical and Physical Sciences* 164 (917), pp. 192–215.

Kearsley, E. A. and Fong, J. (1975). "Linearly independent sets of isotropic Cartesian tensors of ranks up to eight". *Journal of Research of the National Bureau of Standards B: Mathematical Sciences* 79, pp. 49–58.

Kolmogorov, A. N. (1941a). "Dissipation of energy in locally isotropic turbulence". *Dokl. Akad. Nauk SSSR* 32.1, pp. 16–18. reprinted in A. N. Kolmogorov. "Dissipation of Energy in the Locally Isotropic Turbulence". *Proceedings: Mathematical and Physical Sciences* 434 (1890), pp. 15–17.

Kolmogorov, A. N. (1941b). "The local structure of turbulence in incompressible viscous fluid for very large Reynolds numbers". *Dokl. Akad. Nauk SSSR* 30.4, pp. 299–303. reprinted in A. N. Kolmogorov. "The Local Structure of Turbulence in Incompressible Viscous Fluid for Very Large Reynolds Numbers". *Proceedings: Mathematical and Physical Sciences* 434 (1890), pp. 9–13.

Kolmogorov, A. N. (1962). "A refinement of previous hypotheses concerning the local structure of turbulence in a viscous incompressible fluid at high Reynolds number". *Journal of Fluid Mechanics* 13, pp. 82–85.

Kreyszig, E. (1963). *Differential geometry*. Toronto Press, Toronto.

Kurien, S. and Sreenivasan, K. R. (2001). "Dynamical equations for high-order structure functions, and a comparison of a mean-field theory with experiments in three-dimensional turbulence". *Physical Review E* 64 (5), p. 056302.

Laizet, S., Nedić, J., and Vassilicos, J. C. (2015a). "The spatial origin of -5/3 spectra in grid-generated turbulence". *Physics of Fluids (1994-present)* 27 (6), p. 065115.

Laizet, S., Vassilicos, J. C., and Cambon, C. (2013). "Interscale energy transfer in decaying turbulence and vorticity–strain-rate dynamics in grid-generated turbulence". *Fluid Dynamics Research* 45 (6), p. 061408.

Laizet, S. and Lamballais, E. (2009). "High-order compact schemes for incompressible flows: A simple and efficient method with quasi-spectral accuracy". *Journal of Computational Physics* 228.16, pp. 5989–6015.

Laizet, S. and Li, N. (2011). "Incompact3d: A powerful tool to tackle turbulence problems with up to $O(10^5)$ computational cores". *International Journal for Numerical Methods in Fluids* 67 (11), pp. 1735–1757.

Laizet, S., Nedić, J., and Vassilicos, C. (2015b). "Influence of the spatial resolution on fine-scale features in DNS of turbulence generated by a single square grid". *International Journal of Computational Fluid Dynamics* 29.3-5, pp. 286–302.

Laizet, S. and Vassilicos, J. C. (2011). "DNS of fractal-generated turbulence". *Flow, Turbulence and Combustion* 87 (4), pp. 673–705.

Landau, L. D. and Lifshitz, E. M. (1959). *Fluid Mechanics*. Vol. 6. Course of Theoretical Physics. Pergamon Press.

Lele, S. K. (1992). "Compact finite difference schemes with spectral-like resolution". *Journal of Computational Physics* 103 (1), pp. 16–42.
Lesieur, M. (1997). *Turbulence in Fluids*. Kluwer Academic Publishers.
Li, N. and Laizet, S. (2010). "2DECOMP & FFT-A Highly Scalable 2D Decomposition Library and FFT Interface". *Cray User Group 2010 conference*, pp. 1–13.
Lindborg, E. (1999). "Correction to the four-fifths law due to variations of the dissipation". *Physics of Fluids* 11 (3), pp. 510–512.
Lundgren, T. S. (2002). "Kolmogorov two-thirds law by matched asymptotic expansion". *Physics of Fluids* 14 (2), pp. 638–642.
Lundgren, T. S. (2003). "Kolmogorov turbulence by matched asymptotic expansions". *Physics of fluids* 15 (4), pp. 1074–1081.
L'vov, V. and Procaccia, I. (1995). ""Intermittency" in hydrodynamic turbulence as intermediate asymptotics to Kolmogorov scaling". *Physical Review Letters* 74 (14), pp. 2690–2693.
L'vov, V. and Procaccia, I. (1996a). "Fusion rules in turbulent systems with flux equilibrium". *Physical Review Letters* 76 (16), pp. 2898–2891.
L'vov, V. and Procaccia, I. (1996b). "Towards a nonperturbative theory of hydrodynamic turbulence: Fusion rules, exact bridge relations, and anomalous viscous scaling functions". *Physical Review E* 54 (6), pp. 6268–6284.
Mazellier, N. and Vassilicos, J. C. (2008). "The turbulence dissipation constant is not universal because of its universal dependence on large-scale flow topology". *Physics of Fluids* 20 (1), p. 015101.
Meneveau, C. and Sreenivasan, K. R. (1987). "Simple multifractal cascade model for fully developed turbulence". *Physical review letters* 59 (13), pp. 1424–1427.
Meneveau, C. (1996). "Transition between viscous and inertial-range scaling of turbulence structure functions". *Physical Review E* 54 (4), pp. 3657–3663.
Meneveau, C. and Sreenivasan, K. R. (1989). "Measurement of $f(\alpha)$ from scaling of histograms, and applications to dynamical systems and fully developed turbulence". *Physics Letters A* 137 (3), pp. 103–112.
Meneveau, C. and Sreenivasan, K. R. (1991). "The multifractal nature of turbulent energy dissipation". *Journal of Fluid Mechanics* 224.429-484, p. 180.
Meyers, J. and Meneveau, C. (2013). "Flow visualization using momentum and energy transport tubes and applications to turbulent flow in wind farms". *Journal of Fluid Mechanics* 715, pp. 335–358.
Monin, A. S. and Yaglom, A. M. (1975). *Statistical Fluid Mechanics II*. MIT Press, Cambridge.
Mydlarski, L. and Warhaft, Z. (1998). "Passive scalar statistics in high-Péclet-number grid turbulence". *Journal of Fluid Mechanics* 358, pp. 135–175.

Nakano, T., Gotoh, T., and Fukayama, D. (2003). "Roles of convection, pressure, and dissipation in three-dimensional turbulence". *Physical Review E* 67 (2), p. 026316.

Nelkin, M. (1994). "Universality and scaling in fully developed turbulence". *Advances in Physics* 43 (2), pp. 143–181.

Nie, Q. and Tanveer, S. (1999). "A note on third–order structure functions in turbulence". *Proceedings of the Royal Society of London. Series A: Mathematical, Physical and Engineering Sciences* 455 (1985), pp. 1615–1635.

Oberlack, M. and Peters, N. (1993). "Closure of the two-point correlation equation as a basis for Reynolds stress models". *Applied Scientific Research* 51.1-2, pp. 533–538.

Obukhov, A. M. (1962). "Some specific features of atmospheric turbulence". *Journal of Fluid Mechanics* 13 (1), pp. 77–81.

Orszag, S. A. and Patterson Jr, G. S. (1972). "Numerical simulation of three-dimensional homogeneous isotropic turbulence". *Physical Review Letters* 28 (2), pp. 76–79.

Paladin, G. and Vulpiani, A. (1987a). "Anomalous scaling laws in multifractal objects". *Physics Reports* 156 (4), pp. 147–225.

Paladin, G. and Vulpiani, A. (1987b). "Degrees of freedom of turbulence". *Physical Review A* 35 (4), pp. 1971–1973.

Papoulis, A. (1991). *Probability, Random Variables, and Stochastic Processes*. McGraw Hill.

Peters, N., Boschung, J., Gauding, M., Göbbert, J. H., and Pitsch, H. (2015). "Exact equations for structure functions and equations for source terms up to the sixth order". *arXiv preprint arXiv:1504.07490*.

Peters, N., Boschung, J., Gauding, M., Goebbert, J. H., Hill, R. J., and Pitsch, H. (2016). "Higher-order dissipation in the theory of homogeneous isotropic turbulence". *Journal of Fluid Mechanics* 803, pp. 250–274.

Polyakov, A. M. (1995). "Turbulence without pressure". *Physical Review E* 52 (6), pp. 6183–6188.

Pope, S. B. (2000). *Turbulent flows*. Cambridge University Press.

Qian, J. (1997). "Inertial range and the finite Reynolds number effect of turbulence". *Physical Review E* 55 (1), pp. 337–342.

Qian, J. (1999). "Slow decay of the finite Reynolds number effect of turbulence". *Physical Review E* 60 (3), pp. 3409–3412.

Richardson, L. F. (1922). *Weather Prediction by Numerical Process*. Cambridge University.

Robertson, H. P. (1940). "The invariant theory of isotropic turbulence". *Mathematical Proceedings of the Cambridge Philosophical Society*. Vol. 36. Cambridge Univ Press, pp. 209–223.

Rotta, J. C. (1972). *Turbulente Strömungen: eine Einführung in die Theorie und ihre Anwendung*. Vol. 8. B. G. Teubner.

Schade, H. and Neemann, K. (2009). *Tensoranalysis*. Walter de Gruyter.

Schaefer, P. (2012). "Curvature statistics of streamlines in various turbulent flows". *Journal of Turbulence* 13 (4), pp. 1–22.

Schaefer, P., Gampert, M., Goebbert, J., Gauding, M., and Peters, N. (2011). "Asymptotic analysis of homogeneous isotropic decaying turbulence with unknown initial conditions". *Journal of Turbulence* 12, N30.

Schaefer, P., Gampert, M., and Peters, N. (2012a). "The length distribution of streamline segments in homogeneous isotropic decaying turbulence". *Physics of Fluids* 24 (4), p. 045104.

Schaefer, P., Gampert, M., and Peters, N. (2013a). "A model equation for the joint distribution of the length and velocity difference of streamline segments in turbulent flows". *Physics of Fluids (1994-present)* 25 (11), p. 115107.

Schaefer, P., Gampert, M., and Peters, N. (2013b). "Joint statistics and conditional mean strain rates of streamline segments". *Physica Scripta* 2013 (T155), p. 014004.

Schaefer, P., Gampert, M., and Peters, N. (2012b). "On the scaling of the mean length of streamline segments in various turbulent flows". *Comptes Rendus Mécanique* 340.11-12, pp. 859–866.

Schumacher, J., Scheel, J. D., Krasnov, D., Donzis, D. A., Yakhot, V., and Sreenivasan, K. R. (2014). "Small-scale universality in fluid turbulence". *Proceedings of the National Academy of Sciences* 111 (30), pp. 10961–10965.

Schumacher, J., Sreenivasan, K. R., and Yakhot, V. (2007). "Asymptotic exponents from low-Reynolds-number flows". *New Journal of Physics* 9 (4), p. 89.

She, Z.-S. and Leveque, E. (1994). "Universal scaling laws in fully developed turbulence". *Physical review letters* 72 (3), pp. 336–339.

She, Z.-S. and Waymire, E. C. (1995). "Quantized energy cascade and log-Poisson statistics in fully developed turbulence". *Physical Review Letters* 74 (2), pp. 262–265.

Shen, X. and Warhaft, Z. (2002). "Longitudinal and transverse structure functions in sheared and unsheared wind-tunnel turbulence". *Physics of fluids* 14 (1), pp. 370–381.

Siggia, E. D. (1981). "Invariants for the one-point vorticity and strain rate correlation functions". *Physics of Fluids (1958-1988)* 24 (11), pp. 1934–1936.

Sreenivasan, K. R. (1991). "On local isotropy of passive scalars in turbulent shear flows". *Proceedings of the Royal Society of London A: Mathematical, Physical and Engineering Sciences*. Vol. 434. The Royal Society, pp. 165–182.

Sreenivasan, K. R. (1998). "An update on the energy dissipation rate in isotropic turbulence". *Physics of Fluids* 10 (2), pp. 528–529.

Sreenivasan, K. R. and Antonia, R. A. (1997). "The phenomenology of small-scale turbulence". *Annual Review of Fluid Mechanics* 29 (1), pp. 435–472.

Sreenivasan, K. R. and Kailasnath, P. (1993). "An update on the intermittency exponent in turbulence". *Physics of Fluids A: Fluid Dynamics (1989-1993)* 5 (2), pp. 512–514.

Sreenivasan, K. R. (1995). "On the universality of the Kolmogorov constant". *Physics of Fluids (1994-present)* 7 (11), pp. 2778–2784.

Stolovitzky, G., Kailasnath, P., and Sreenivasan, K. R. (1992). "Kolmogorov's refined similarity hypotheses". *Physical Review Letters* 69 (8), pp. 1178–1181.

Taylor, G. I. (1935). "Statistical theory of turbulence". *Proceedings of the Royal Society of London. Series A, Mathematical and Physical Sciences* 151 (873), pp. 421–444.

Tennekes, H. and Lumley, J. L. (1972). *A first course in turbulence*. MIT press.

Thiesset, F., Antonia, R. A., Danaila, L., and Djenidi, L. (2013). "Kármán-Howarth closure equation on the basis of a universal eddy viscosity". *Physical Review E* 88 (1), p. 011003.

Thoroddsen, S. (1995). "Reevaluation of the experimental support for the Kolmogorov refined similarity hypothesis". *Physics of Fluids* 7.4, pp. 691–693.

Thoroddsen, S. and Van Atta, C. (1992). "Experimental evidence supporting Kolmogorov's refined similarity hypothesis". *Physics of Fluids A: Fluid Dynamics (1989-1993)* 4.12, pp. 2592–2594.

Tong, C. and Warhaft, Z. (1994). "On passive scalar derivative statistics in grid turbulence". *Physics of Fluids (1994-present)* 6 (6), pp. 2165–2176.

Townsend, A. A. (1951). "On the fine-scale structure of turbulence". *Proceedings of the Royal Society of London. Series A. Mathematical and Physical Sciences* 208 (1095), pp. 534–542.

Tsinober, A. (2009). *An Informal Conceptual Introduction to Turbulence*. Springer Science & Business Media.

Vassilicos, J. C. (2015). "Dissipation in Turbulent Flows". *Annual Review of Fluid Mechanics* 47, pp. 95–114.

Wang, L. (2009). "Scaling of the two-point velocity difference along scalar gradient trajectories in fluid turbulence". *Physical Review E* 79 (4), p. 046325.

Wang, L. (2010). "On properties of fluid turbulence along streamlines". *Journal of Fluid Mechanics* 648, pp. 183–203.

Wang, L. (2012). "Structures of the vorticity tube segment in turbulence". *Physics of Fluids* 24 (4), p. 045101.
Wang, L. and Peters, N. (2006). "The length-scale distribution function of the distance between extremal points in passive scalar turbulence". *Journal of Fluid Mechanics* 554, pp. 457–476.
Wang, L. and Peters, N. (2008). "Length-scale distribution functions and conditional means for various fields in turbulence". *Journal of Fluid Mechanics* 608, pp. 113–138.
Wang, L. and Peters, N. (2010). "Mean velocity increment conditioned on gradient trajectories of various scalar variables in turbulence". *Physica Scripta* 2010 (T142), p. 014004.
Warhaft, Z. (2000). "Passive scalars in turbulent flows". *Annual Review of Fluid Mechanics* 32 (1), pp. 203–240.
Yakhot, V. (2001). "Mean-field approximation and a small parameter in turbulence theory". *Physical Review E* 63 (2), p. 026307.
Yakhot, V. (2003). "Pressure-velocity correlations and scaling exponents in turbulence". *Journal of Fluid Mechanics* 495, pp. 135–143.
Yakhot, V. (2006). "Probability densities in strong turbulence". *Physica D: Nonlinear Phenomena* 215 (2), pp. 166–174.
Yakhot, V. and Sreenivasan, K. R. (2005). "Anomalous scaling of structure functions and dynamic constraints on turbulence simulations". *Journal of Statistical Physics* 121.5-6, pp. 823–841.
Yeung, P. K., Donzis, D. A., and Sreenivasan, K. R. (2012). "Dissipation, enstrophy and pressure statistics in turbulence simulations at high Reynolds numbers". *Journal of Fluid Mechanics* 700, p. 5.
Yeung, P. K. and Pope, S. B. (1989). "Lagrangian statistics from direct numerical simulations of isotropic turbulence". *Journal of Fluid Mechanics* 207 (1), pp. 531–586.
Zhou, T. and Antonia, R. A. (2000). "Reynolds number dependence of the small-scale structure of grid turbulence". *Journal of Fluid Mechanics* 406, pp. 81–107.
Zhou, T., Antonia, R. A., Danaila, L., and Anselmet, F. (2000). "Approach to the four-fifths 'law' for grid turbulence". *Journal of Turbulence* 1, N5.